Development of a Two-Gas Atmosphere Sensor System (Mass Spectrometer)

Contract NAS 1-5679
SDS Data Systems Register No. 1-3006

Prepared For
National Aeronautics and Space Administration
Langley Research Center
Hampton, Virginia 23365

31 March 1966

Book I of III
Phase I - Final Study Report

SDS
DATA SYSTEMS

TABLE OF CONTENTS

LIST OF ILLUSTRATIONS

LIST OF ILLUSTRATIONS (Continued)

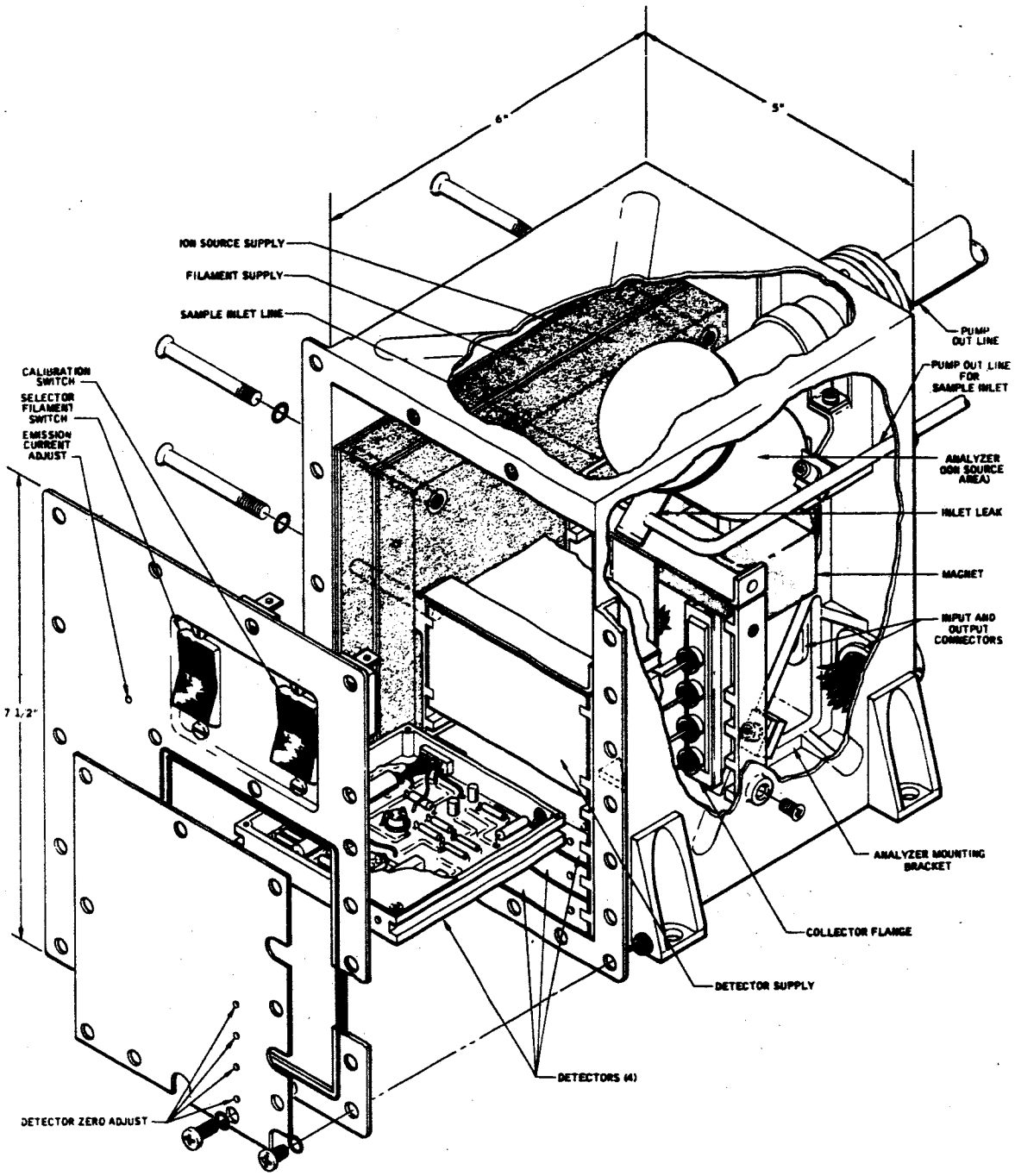
6"
5"
ION SOURCE SUPPLY
FILAMENT SUPPLY
SAMPLE INLET LINE
CALIBRATION SWITCH
SELECTOR FILAMENT SWITCH
EMISSION CURRENT ADJUST
7 1/2"
PUMP OUT LINE
PUMP OUT LINE FOR SAMPLE INLET
ANALYZER (ION SOURCE AREA)
INLET LEAK
MAGNET
INPUT AND OUTPUT CONNECTORS
ANALYZER MOUNTING BRACKET
COLLECTOR FLANGE
DETECTOR SUPPLY
DETECTORS (4)
DETECTOR ZERO ADJUST

1. INTRODUCTION

Future space programs involving the Apollo spacecraft are being considered with mission durations of from 45 to 120 days. For these extended flight periods it is expected that a two gas cabin atmosphere will be used in lieu of the present single gas O_2 atmosphere. This will be necessary due to the uncertainty of the long term physiological effects of a pure oxygen atmosphere.

The adaption of existing atmosphere control systems to a two gas atmosphere presents the problem of sensing the two major constituents independently. In the past a total pressure sensor was adequate whereas now a partial pressure analyzer is required. This type of instrumentation does not exist in a form qualified for flight application and therefore a development program is necessary.

Since instrumentation has to be developed, it is logical to require that the principal products of human metabolism, ie., carbon dioxide and water vapor, also be monitored. The present plans call for the use of nitrogen as the diluent gas. The specific requirement is then for a sensor system which monitors the partial pressures of O_2, N_2, CO_2 and H_2O. This system must be compatible with the Apollo cabin environment and must present outputs which are suitable for input to existing types of atmosphere control devices and for telemetry and visual display.

This report presents the results of a study of a mass spectrometer sensor system for the above application. Two types of mass spectrometer analyzers were investigated with the object of finding the one best suited for this task. The optimization of the entire sensor system was sought with respect to performance, environmental, and reliability goals. Simultaneously it was required that the resulting instrument place realistic power, weight, and size demands upon the spacecraft.

As a result of detailed investigations of the sensor subsystems in conjunction with careful interface analysis a conceptual design evolved which lead finally to the definition of a preferred reference system. This system formed the basis for a proposed design and development program.

d. Demand Factors - This category is comprised of a special set of factors which determine the demands that the instrument package places upon the environment. These are power consumption, weight, and volume of the instrument. These factors may also be considered as specifying the gross physical characteristics of the instrument. Demand factors could be thought of as environmental factors since they are constrained by the environment. Their uniqueness results from the thought process which is applied to the optimization of all the design factors. This will become apparent in Section 2.3.

2.2 WEIGHTING OF DESIGN FACTORS

The classification of design factors is useful in that it allows the designer to assign priorities to them based upon a logical analysis of the overall program goals. In most instances the design factors are intimately related so that emphasis upon one group will have marked consequences upon the others. Therefore it is necessary to have a clear understanding of their interrelations in addition to their relative importance.

The object of any type of instrumentation is to perform a defined function. In this instance the sensor system is required to deliver specified information to the atmosphere control modules, as well as to the crew and ground observers. Since this function satisfies the need for the instrument it is clear that the "performance factors" must assume first rank over the other design factors. All of the other design factors assume at least a partially dependent role. With this importance goes a certain degree of responsibility. It is exercised by not requiring more information from the instrument than is necessary to satisfy the needs of the receiving elements. The primary function of the sensor system is to act as the error detecting element in the atmosphere control system. The initial assumption was made that the other control system elements are largely developed and therefore their characteristics are defined. Then the information demands upon the sensor system need only be compatible with the requirements of the control elements. For example it appears that the control system including the cabin will have a time response which is relatively slow compared with typical mass spectrometer capabilities. As a result the sensor should not be required to have speed simply for the sake of speed. When it is considered that time response is directly tradeable for sensitivity and sensitivity for size (and weight) it becomes clear that limiting demands in this area will be rewarding.

Once the performance factors have been determined, attention must be given to the environmental factors. The instrument must not only perform a given task, but it must perform it in the operating environment. The environmental constraints must be carefully considered and then the corresponding design factors adjusted to meet them.

The reliability factors are no less important. The instrumention can only be considered to be fulfilling its task if it meets the performance objectives over the duration of the mission. Reliability must be considered as an integral part of the overall design. Perhaps the most important single reliability factor is the simplicity of the approach to the instrumentation. This will be seen to be fundamental in the approach to this design problem.

After satisfying the other objectives of the instrument design one is finally left with the demand factors. These are typically the most dependent variables in the system. Therefore, when stating specific goals it is more reasonable to specify performance, environmental, and reliability constraints than to begin with the specification of power, weight, and size. If constraints are given in all areas, it is likely that the system will be overconstrained and a dilema will result.

SDS Data Systems experience has shown that allowing the demand factors to take on an essentially dependent role results in the most acceptable instrumentation as long as the other design constraints are carefully chosen. It is of interest to note that the statement of work to which this contract is being performed (L-5908-B) conforms with this type of thinking since power, weight, and size goals are not specified.

At the same time it must be emphasized that every effort should be made to reduce the demand factors to the lowest possible levels consistent with the other design factors. This was accomplished by the selection of the type of analyzer, in the analyzer optimization as well as in the circuit, and mechanical design areas.

2.3 LOGIC OF SOLUTION

A mass spectrometer system consists of several functional modules which combine to determine total system characteristics. If an optimum mass spectrometer system is to be found, it is essential that a logical approach be taken to the investigation of each of the modules with maximum attention being paid to the module interfaces. These considerations may be put in focus by the use of a mass spectrometer system logic diagram. Figure 2-1 is a diagram of the two gas sensor.

This diagram shows the functional elements of the mass spectrometer sensor system and the most important relationship between them as well as to the design factors. The principal sensor system components are the sample inlet system, ion source, analyzer, pump system, detector, support electronics, filament, and system packaging. The interrelations between these elements will not be discussed in detail at this time; however there are a few points worth noting. First, a large number of the performance factors and reliability goals directly affect the detector system. Furthermore, the detector limitations impose direct requirements upon the output current from the analyzer which are in turn related to the demand factors. Thus a clear design philosophy in the detector area is essential. Two approaches are possible.* A maximum sensitivity electrometer could be designed with the goal of minimizing the ion current demands upon the analyzer. This would allow a minimum size and weight analyzer to be designed. This approach entails the use of an electrometer amplifier with an electrometer tube input since this device has superior signal-to-noise characteristics. However, a

*An electron multiplier is immediately dismissed because of its complexity and instability in addition to its support electronics requirements.

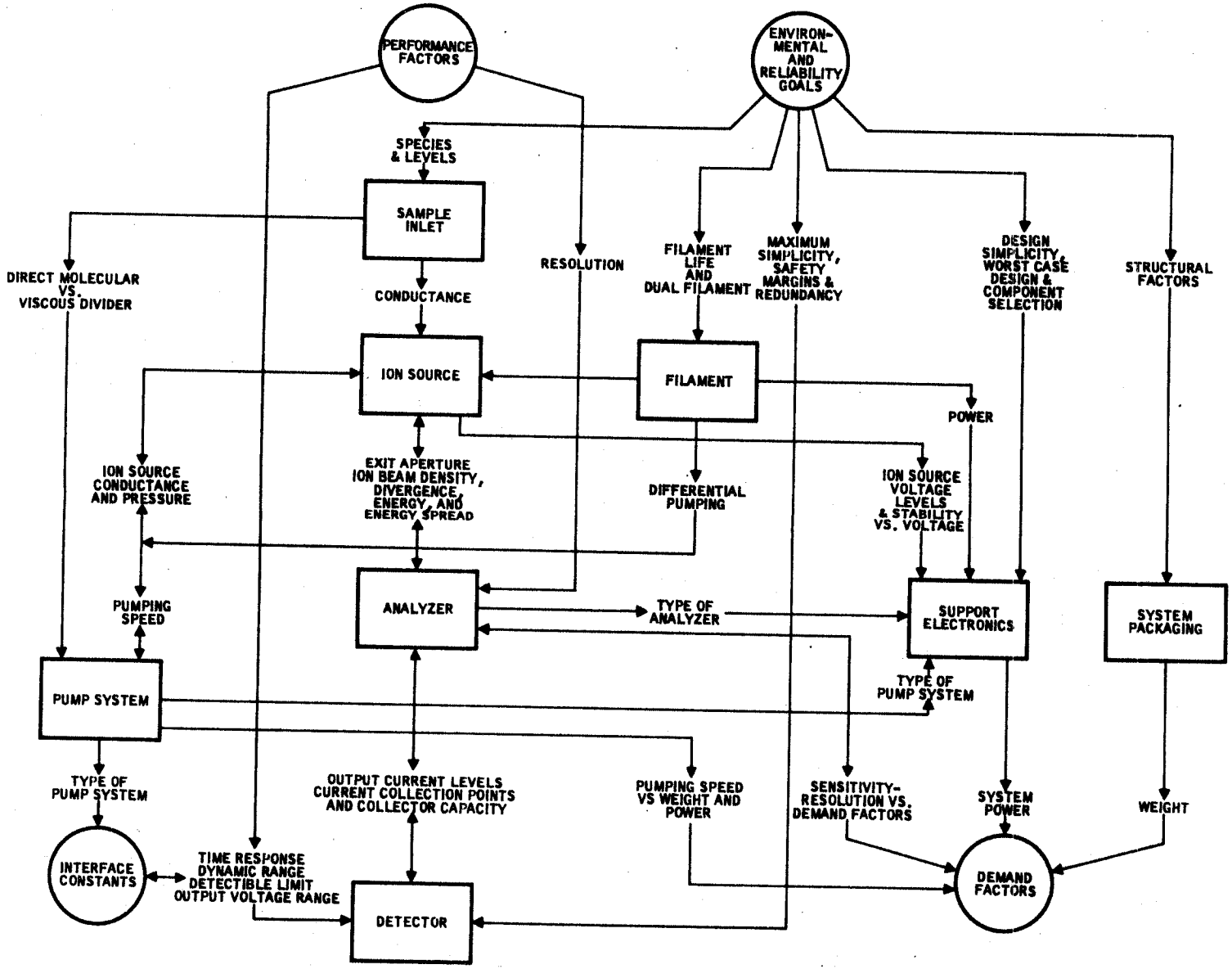

FIGURE 2-1
System Block Diagram

rezeroing circuit would be required in order to continually compensate the amplifier drift at the low current levels. The other approach is to use a less sensitive electrometer which is also less complex. The use of a solid-state input device is suited to this type of design. Most devices have sufficiently high input impedances for such application; however, their noise figure is higher so that signal currents cannot be resolved at the same levels as with electrometer tubes (the difference is roughly a factor of five). At the same time, drifts are less so that no rezeroing circuitry is necessary. A further simplification results from the fact that no voltage need be supplied to a tube filament, consequently eliminating a transformer secondary winding, a bridge rectifier, and a voltage regulator circuit.

It was decided that the second approach would be the most in line with the weighting of the design factors prescribed in Section 2.2. Further it can be shown that the increase in the demand factors due to the solid-state detector approach are small, when the weight and power of the eliminated electronics is balanced against the analyzer increases. Once the approach is selected, a minimum detectable signal level can be determined based upon a consideration of the expected detector noise level and drift. This of course is dependent upon the desired system response time which is controlled largely by the bandwidth of the detector noise filter. The minimum detectable signal can then be translated into an analyzer sensitivity requirement.

The analyzer sensitivity is determined primarily by the product of the ion source exit slit dimensions and the ion current density per unit pressure. This results from the fact that the mass resolving section is usually designed with a transmission efficiency as close to 100% as possible in order to minimize inaccuracies due to variations in the transmission factor.

It becomes apparent that the ion source is the key to an optimized analyzer design. Not only is sensitivity determined by the ion source, but its other characteristics including ion beam divergence angle, ion energy, and ion energy spread are important in determining the characteristics of the mass resolver. Other ion source properties such as mass discrimination, gas conductance, and volume are also important to the overall instrument operation.

The optimization of the analyzer is achieved by minimizing its associated demand factors for a given resolution and sensitivity. This process combines the ion source and analyzer characteristic equations and expressing the result in terms of power, weight, and volume demands.

The first variable to be exercised is the type of analyzer* which is chosen. There are a great many analyzer types from which an optimum can be selected. A preliminary examination of all types led to the selection of two analyzers for further study. The considerations governing their selection are covered in Section 3.3. Once the type of analyzer has been selected a detailed optimization process is conducted.

*The term analyzer may refer to the entire analyzer tube (including the ion source) or it may be applied to the mass resolving section of the mass spectrometer excluding the ion source.

In this path of logic the analyzer design assumes a somewhat dependent role, but is largely justified because of the flexibility of analyzer configurations. Furthermore the analyzer plays only a partial role in the determination of the overall demand factors. For example, the system electronics generally weigh more than the analyzer (sometimes by more than a factor of two). Also a large portion of the system power is consumed by the ion source filament which is invariant in the analyzer design.

Similar logic paths are found with respect to the other system elements. The support electronics also assume a largely dependent role. The ion source, analyzer, detector, and pump system combine with the environmental and reliability constraints to determine the support electronics requirements. Here too flexibility in component selection and circuit design techniques allows a significant degree of optimization. The conceptual design of the electronics package was carried out using a compromise between simplicity and power requirements. Some feedback to the other elements was allowed in the form of the specification of reasonable voltage tolerances.

The other subsystem dependencies are fairly straightforward, the principal ones being covered by the logic diagram. Further discussion of these considerations is given in Section 4.

3. INITIAL INFORMATION

3.1 BOUNDARY CONDITIONS

The boundary conditions for this problem were specified in the LRC Statement of Work L-5908-B. In addition a few other constraints were established in verbal communications between LRC and SDS Data Systems. This information is reproduced below for convenience and clarity.

3.1.1 DEFINITIONS

3.1.1.1 Flight Prototype

A hardware design embodying inherent ruggedness, operational simplicity, reliability, minimum power requirements, optimum size and weight compatible with flight environment. The unit to be developed in this contract will not be required to undergo flight qualification, but should possess inherent characteristics which would be required if both flight and reliability qualifications were to be imposed.

3.1.1.2 Sensor System

A system for measuring, either directly or indirectly, the partial pressures of O_2, N_2, CO_2, and H_2O, and integrating these measurements into signals suitable for monitoring and controlling the basic two gas atmosphere within acceptable limits. The physical control devices and ancillary electronics are not a part of this contract. However, attention must be paid to these spacecraft interfaces.

3.1.1.3 Two Gas Atmosphere

Basically a mixture of O_2 and N_2 with small quantities of CO_2 and H_2O released by the crew. Additional trace gases, present in the spacecraft atmosphere shall not be considered in this study.

3.1.1.4 Apollo Type Spacecrafts

See Spacecraft Models, Sections 3.1.2.1 and 3.1.2.2. Two spacecraft models are presented to define the maximum possible ranges in the Apollo extension activity. The contractor shall design and develop the sensor system for the most stringent requirements.

3.1.2 RESTRAINTS

3.1.2.1 Spacecraft Model

Maximum duration 45 days:

a. Type: Apollo Command Module, with or without the Lunar Excursion Module.

b. Volume: Apollo Command Module 138 ft^3
Lunar Excursion Module 180 ft^3

c. Power Penalty: Fixed - 450 #/KW
Variable - 1.51 #/KW hour

d. Location of Sensor Unit: Apollo CM

e. Operational Temperature Range: +40°F to 90°F

f. Cabin Leakage Rate: 0.3 pounds/hr

g. Subsystem Types:

1. Power: H_2/O_2 Fuel Cells, 28 ±0.5 VDC

2. Life Support:

O_2 supply, supercritical cryogenic

N_2 supply, supercritical cryogenic

CO_2 removal by chemical absorbers or by regenerative zeolite beds

Humidity control; condenser/separator

Thermal control; coolant/space radiator

3.1.2.2 Spacecraft Model

Maximum duration 120 days:

a. Type: Apollo Command Module, with dependent laboratory module

b. Volume: Apollo Command Module 138 ft^3
Laboratory Module 1500 ft^3

c. Power Penalty: Fixed - 500 #/KW
Variable - 0.0 #/KW hour

d. Location of Sensor Unit: Apollo CM

e. Operational Temperature Range: +40°F to +90°F

f. Cabin Leakage Rate: 0.3 pounds/hour

g. Subsystem Types:

1. Power: Solar cells or isotope dynamic, 28 ±0.5 VDC

2. Life Support:

O_2 supply, supercritical or subcritical cryogenic, or reclamation from CO_2 and H_2O

N_2 supply, supercritical or subcritical cryogenic

CO_2 removal by regenerative zeolite beds, or other means

Humidity control; condenser/separator

Thermal control; coolant/space radiator

3.1.2.3 Cabin Atmosphere Requirements

Parameter	Nominal Design Point
Total pressure	362 ±11 mm H_g
O_2 partial pressure	181 ±5.5 mm H_g
N_2 partial pressure	diluent, to provide total pressure
CO_2 partial pressure	($\leq$7.6 mm H_g; brief excursions to 15 mm H_g)
H_2O partial pressure	(5 to 16.5 mm H_g)*
Temperature	70° ±5°F
Minimum detectible partial pressure change	±.38 mm H_g

NOTE:

* Corresponds to relative humidity variations from 35% to 75% relative over the stated temperature range.

3.1.2.4 Crew Safety Limits

Parameter	Deviation
O_2 partial pressure	140 to 200 mm H_g (one hour limit)
CO_2 partial pressure	8 to 15 mm H_g. (one hour limit)

3.1.2.5 Sensor Type

The sensor type and techniques to be investigated during Phase I of this contract shall include quadrupole and single focusing mass spectrometers.

3.1.3 SPECIAL DESIGN REQUIREMENTS

The two-gas atmosphere sensor system shall have as a design goal an operational life of not less than 120 days. Replacement of sensor elements by the crew will be permitted; however, this technique should be avoided wherever possible and limited to plug-in units. A maximum time of 2 minutes/day will be allowed for calibration, maintenance, and replacement activities performed by the crew. In addition, as a design goal, the system shall have a shelf life of one year.

The selection of the basic sensors and components which comprise the sensor system shall be designed so as to be compatible with the launch load and dynamic spectrum (acceleration, vibration,and acoustic) established in "Supporting Technical Information" previously furnished to the Contractor, a copy of which is in possession of the Contracting Officer.

The sensor system repeatability, accuracy of measurement, and redundant features are to represent best practices commensurate with mission constraints.

The sensor system signals are to be suitable for further conditioning (if required) to provide automatic control, visual and audible displays, and/or data recording and transmitting equipment. The output voltage range shall be zero to five volts.

The sensor system shall incorporate sensing techniques which will inherently provide a reliable design over the expected time of use. Future requirements for flight qualification shall be considered in the design of the sensors.

3.2 DETERMINATION OF PERFORMANCE PARAMETERS

The required performance parameters were determined from the logic of the solution process and the boundary conditions given in the Statement of Work. The following five basic performance parameters were considered:

a. Time response

b. Detectable limit

c. Analyzer sensitivity

d. Resoltuion

e. Accuracy

3.2.1 TIME RESPONSE

The analysis is begun with some considerations given to the complete control loop. It is emphasized that the following analysis is not complete in that it does not consider the optimization of the control system. This was not possible due to a lack of detailed information of the cabin characteristics and associated control equipment. Furthermore, a NASA/LRC directive requested that the analysis be limited in this area. Therefore, only an approximate representation was used which could be solved fairly rapidly.

A block diagram of a possible control system is shown in Figure 3-1.

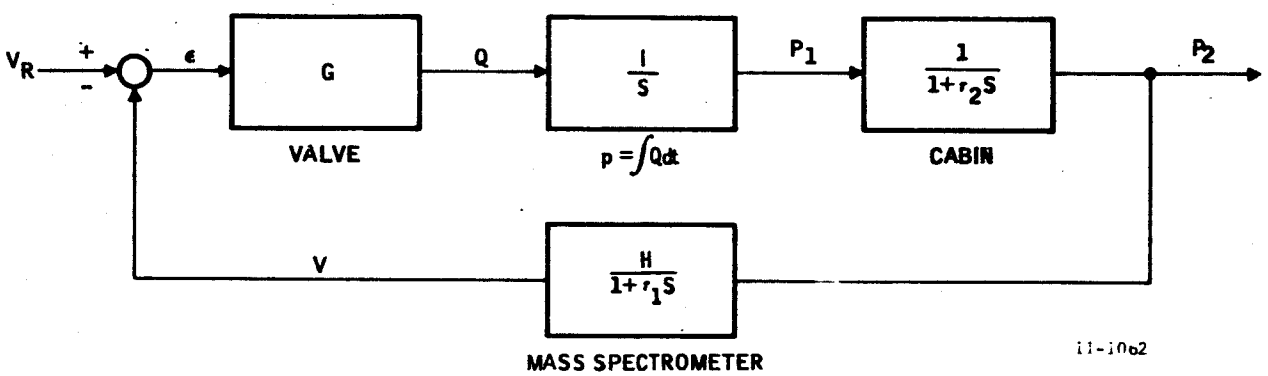

V_R = REFERENCE VOLTAGE LEVEL CORRESPONDING TO A REFERENCE PRESSURE LEVEL

ϵ = ERROR SIGNAL

V = MASS SPECTROMETER OUTPUT VOLTAGE

P_1 = PARTIAL PRESSURE NEAR VALVE

τ_2 = CABIN TIME CONSTANT

P_2 = PRESSURE NEAR MASS SPECTROMETER SAMPLE POINT

H = MASS SPECTROMETER GAIN

τ_1 = MASS SPECTROMETER TIME CONSTANT

G = FLOW PER UNIT ERROR VOLTAGE

FIGURE 3-1
Control Loop Block Diagram

The salient features of this control system are the reference level, summing junction, and servo controlled valve with gain G allowing a flow Q which gives rise to a partial pressure change P_1 near the valve. The cabin transmits this change to the mass spectrometer sample point where a partial pressure change p_2 is read. Using Laplace transform notation, the transfer function for this system is:

$$p_2(s) = \frac{G\left(s + \omega_1\right)}{\tau_2\left(s^3 + \omega_o s^2 + \omega'^2 s + G'\right)} V_R(s) \qquad (1)$$

where

$$\omega_o = \frac{\tau_1 + \tau_2}{\tau_1 \tau_2}, \quad (\omega')^2 = \frac{1}{\tau_1 \tau_2}, \quad G' = \frac{GH}{\tau_1 \tau_2}$$

The first case considered is the one for which the mass spectrometer is infinitely fast. The $\tau_1 = 0$ and

$$p_2(s)\Big|_{\tau_1=0} = \frac{G}{\tau_2} \frac{1}{\left(s^2 + \omega_2 s + \omega_2 GH\right)} V_R(s) \qquad (2)$$

For a step change in the reference level $V_R(s) = V_o/s$ then

$$p_2(s)\Big|_{\tau_1=0} = \frac{G}{\tau_2} \cdot \frac{1}{s\left(s^2 + \omega_2 s + \omega_2 GH\right)} \qquad (3)$$

By considering the probable magnitudes of the quantities involved, the gain of the mass spectrometer is the full scale output divided by the full scale input. Hence

$$H = \frac{5 \text{ volts}}{3 \text{ pounds}} = 1.66 \text{ volts/pound}$$

where the partial pressure is measured in pounds instead of torr for convenience. The O_2 partial pressure is under consideration. The maximum gain of the valve is the maximum flow rate divided by the maximum error signal

$$G\Big|_{max} = \frac{200 \text{ pounds/hour}}{5 \text{ volts}} = \frac{40 \text{ pounds/hour}}{\text{volt}}$$

The number 200 pounds/hour comes from information on the requirements for a flowmeter to monitor oxygen flow in the Apollo spacecraft. Then $GH\Big|_{max} = .0185 \text{ sec}^{-1}$.

The time constant for the cabin is roughly determined from the maximum atmosphere flow rate and a nominal flow distance:

$$T = \frac{10 \text{ feet}}{40 \text{ feet/minute}} = .25 \text{ minute} = 15 \text{ seconds}$$

where

10 feet is the nominal circulating distance and 40 feet/second is the maximum circulation rate.

It is assumed that $T = 3\ \tau_2$ since when the flow has reached the sensor most of the partial pressure change should be evident. Then $\tau_2 = 5$ seconds. An interesting case is that of critical damping. Then from Equation (3):

$$GH = \frac{1}{4}\omega_2 \tag{4}$$

Hence

$$GH = .05 \text{ sec}^{-1}$$

It should be noted that this gain is somewhat higher than the maximum allowable value for earlier calculations. This might be expected due to the crudeness of the calculations. It is interesting to note that either a higher flow rate or a longer cabin time constant is implied. For lack of a better choice higher flow rate will be allowed in order to give the required value for GH (Note that if GH $<.05$ the system will be over damped which implies a longer stabilizing time.) For critical damping:

$$p_2(s) = \frac{GV_o}{\tau_2} \quad \frac{1}{s(s + \omega_2/2)} \tag{5}$$

which gives the following expression for the monitored pressure as a function of time:

$$p_2(t) = p_o \left[u(t) - \left(1 + \frac{\omega_2}{2} t\right)_{\exp} \left(\frac{-\omega_2 t}{2}\right)\right] \tag{6}$$

Evaluating Equation (6) gives the following numerical expression for the normalized time function:

$$\frac{p_2(t)}{p_o} = 1 - (1 + 0.1t)\ e^{-0.1t} \tag{7}$$

Now consider the case in which $\tau_1 = 0$ and is equal to $0.2\ \tau_2$ or 1 second.

Then from Equation (1):

$$p_2(s) = \frac{GV_o}{\tau_2} \quad \frac{s + 1}{s\left(s^3 + 1.25\ s^2 + .2s + .01\right)} \tag{9}$$

In calculating the inverse transform of the above expression it can be shown that the pole at -1.072 is approximately cancelled by the zero at -1 hence, the $e^{-1.072t}$ term may be neglected. Then from measurements on the pole-zero plot the normalized time function is found to be:

$$\frac{p_2(t)}{p_o} = 1 + 2.68\ e^{-.089t} \cos\ (.0355t + 4.32) \tag{10}$$

Equations (7) and (10) are plotted in Figure 3-2. It is seen that the system with τ_1=1 sec is actually faster than the system with τ_1=0.

Of course this may not be true for higher values of loop gain, but it must be remembered that limitations appear to exist on the upper value which GH can have.

In view of the preceding calculation it is believed that a value of one second for τ_1 is a reasonable choice upon which to base the study of this instrument. This is further substantiated by the relatively slow expected rates of change of CO_2, O_2, and H_2O as discussed in Section 6.1.

3.2.2 DETECTABLE LIMIT

The minimum detectable signal, set by NASA/LRC at .38 torr, was considered next The consideration leading to this was that .38 torr is one tenth of the difference between the nominal CO_2 partial pressure and the maximum CO_2 partial pressure. The minimum detectable level is related to the noise plus drift levels expected at the mass spectrometer output. From experience a more conservative relationship was chosen. First, it was decided to reduce the minimum detectable signal to 0.20 torr. Second, it was decided to make the drift plus noise equal to one fifth of the minimum detectable signal. In order to gain interchangeability between amplifiers (and thereby some functional redundancy) the H_2O and CO_2 detectors and the O_2 and N_2 detectors were made identical. Then the full scale outputs (of 5 volts as specified) correspond to 20 torr for the high sensitivity detectors and 200 torr for the low sensitivity detectors. Experience with the type of detector which was being proposed indicated that no less than ±10 millivolts noise plus drift was to be expected with a 10^{12} ohm feedback resistor, thus a minimum detectable signal of 50 millivolts output or 5×10^{-14} amperes input is implied on the high sensitivity detectors. (This assumption is verified in Section 4.5)

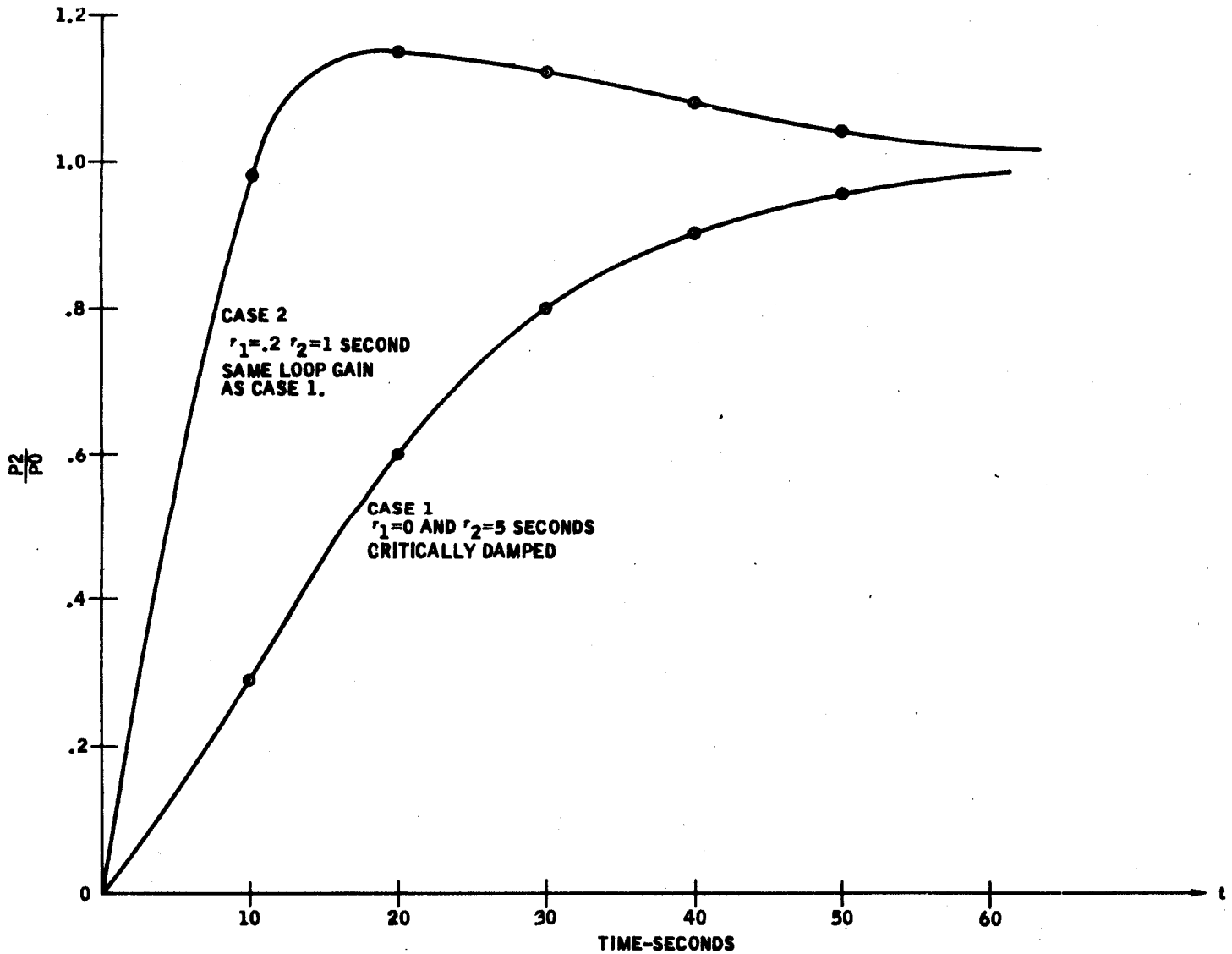

FIGURE 3-2
Atmosphere Control System Response
to a Step Change in the Reference Level

On the low sensitivity detectors for the O_2 and N_2 ion currents a 10^{11} ohm feedback resistor is implied. This should reduce the noise level but this is required since the minimum detectable pressure change of ±.20 torr is now equivalent to .1% of full scale, or 5 millivolts. The detailed analysis of the detector given in Section 4.5, indicated that this level could not be met due to drift. In this case, the minimum detectable pressure change was increased to .40 torr. This sets the minimum detectible signal equal to the expected drift plus noise. Therefore no safety margin exists on the major components.

What does a particular noise and drift level imply in terms of the controlled partial pressure p_2? The drift level will simply appear as percentage fluctuation in p_2. Then a drift of ±10 millivolts on the O_2 output (see Section 4.5) would give a variation of ±.4 torr in p_2 or ±.2% of the maximum O_2 partial pressure. A noise level of ±10 millivolts on the O_2 output would probably imply a reduced pressure variation due to the additional bandwidth limitations of the cabin transfer function.

While there is no safety margin between the minimum detectible signal and the drift plus noise on the major components, it is believed that a required minimum detectible signal of 0.2% is excessive. This value should be carefully reviewed. If it were relaxed somewhat, a reduction in the system demand factors could be realized.

3.2.3 ANALYZER SENSITIVITY

The required analyzer sensitivity was then found using the detector current of the previous section. It was determined that a maximum ion source pressure of 2×10^{-4} torr would be reasonable. (This assumption is verified in Section 4.2.) This was set to correspond to a maximum external pressure of 400 torr. Then the minimum detectable pressure change of 0.2 torr corresponds to

$$\frac{.2}{400} \times 2 \times 10^{-4} = 10^{-7} \text{ torr in the ionizing region.}$$

The required ion source sensitivity is then:

$$S = \frac{5 \times 10^{-14}}{10^{-7} \text{ torr}} \text{ amps} = 5 \times 10^{-7} \text{ amps/torr}$$

Due to the difficulty in obtaining a highly accurate ion source sensitivity equation, it was decided to aim for 1×10^{-6} amps/torr. Experience with small non-magnetic ion sources indicated that this was a reasonable target value to aim for in view of the size of the instrument that was envisioned.

3.2.4 RESOLUTION

From the masses to be investigated three resolution requirements were identified for the required resolution:

Separation of m/e 17 and m/e 18	$\Delta m/m = 1/17.5$
Separation of m/e 28 and m/e 32	$\Delta m/m = 1/7.5$
Separation of m/e 40 and m/e 44	$\Delta m/m = 1/9.5$

The m/e 17 peak arises from OH^+ which is a product of the ionization of H_2O. This peak is then proportional to H_2O with an amplitude of about 30% of m/e 18. These peaks must be resolved since an incomplete resolution would result in a variable amount of m/e 17 ion current being collected as the ion beam position shifts due to voltage instability. It might be possible to collect m/e 17 and m/e 18 together since they come from the same source, but then they would have to be resolved from m/e 16 (O_2^{++} and O^+). Here the situation would be much more critical since m/e 16 does not arise from the same source as m/e 17 and m/e 18 and furthermore it has a higher amplitude (m/e 16 = 21% of 200 torr maximum compared to m/e 17 = 30% of 20 torr maximum). Therefore, it was decided to resolve m/e 17 from m/e 18.

The m/e 28 (N_2^+) and m/e 32 (O_2^+) peaks must be resolved for obvious reasons. The resolution of m/e 40 (A^+) and m/e 44 (CO_2^+) is necessary primarily for testing convenience since it might be desirable to use air samples. It should be pointed out that the above resolutions are half peak height values which implies that while all of the desired ion beam is falling in its collector that none of the unwanted ion beam is being received.

If a constant resolving power analyzer is designed then a $\Delta m/m$ of 1/17.5 would be required. This would give substantially higher resolution than required for resolution of the high masses. The accurate measurement of H_2O is probably the least important requirement, then a reduction in resolving power by almost a factor of two would result only in a decrease in the accuracy of this relatively unimportant component. The implications of an analyzer with non-constant resolving power are discussed in a later section.

3.2.5 ACCURACY

Since the major partial pressures are to be controlled within ±3%, the sensor system must have an accuracy equal to or greater than this value. The error due to time lag should be relatively small when considering the slow rate of partial pressures change under normal conditions when compared to the expected system time response. Furthermore the error due to noise and drift in the mass spectrometer has been shown to be very small. The bulk of the error can be then attributed to variations in the gains of the control system elements. Considering Equation (1) and seeking the steady state value for p_2 the result is:

$$p_2(t)\Big|_{t=\infty} = \lim_{s \to o} sp_2(s) \qquad (11)$$

For $V_R(s) = V_o/s$ the result is

$$p_2\Big|_{ss} = \frac{V_o}{H} \tag{12}$$

Differentiating this expression gives:

$$\frac{dp_2}{p_2} = \frac{dV_o}{V_o} - \frac{dH}{H} \tag{13}$$

V_o is simply a reference voltage level and can be held very closely so that essentially

$$\frac{dp_2}{p_2} = \frac{-dH}{H} \tag{14}$$

This means that for $dp/p = \pm 3\%$, $dH/H = \pm 3\%$

It should be realized that Equation (14) depends upon a particular control loop characteristic. For example if the integrator in the forward loop is eliminated than it can be shown that:

$$\frac{dp_2}{p_2} = \frac{1}{1 + G'H}\frac{dG'}{G'} - \frac{G'}{1 + G'H}\frac{dH}{H} \tag{15}$$

where G' is the forward loop gain and is different than G. It is seen that the stability considerations may be quite different in this case depending upon the exact values of G' and H. Due to the uncertainty in the control loop design the allowable value of dH/H should be less than ±3%. An initial target value of 1% accuracy was assumed with the possibility that this could be relaxed if the proper control loop design was instituted. This was believed to be a reasonable value in view of the complexity of the instrument which was contemplated.

It is evident from the preceding analyses and discussions that the requirements placed upon the mass spectrometer are intimately associated with the fundamental control requirements and the details of the control loop characteristics. Therefore, the design of an optimized sensor system must be predicated on an accurate and complete knowledge of these factors. To the extent that this knowledge is lacking, the sensor system may exceed or fall short of the necessary operation. It is believed that in order to meet the objectives of a relatively undefined task it is best to allow a limited amount of overdesign. This is what has been done in the specification of the performance parameters, and at the same time the expected demand factors were held within reason.

3.3 CHOICE OF ANALYZERS TO BE INVESTIGATED

One of the advantages of the mass spectrometer is its design flexibility. The chief reason for this is the large number of mass separation techniques which are available. All of these techniques have one thing in common. They rely on the use of magnetic or electrodynamic fields to resolve ions according to their mass to charge ratios.

Many mass analyzers can be considered. The most well known of these are the following:

a. Single focusing magnetic sector

b. Double focusing magnetic sector (electrostatic sector preceding the magnetic sector)

c. Cycloidal (combined use of magnetic and electrostatic field)

d. Omegatron (based upon cyclotron principal)

e. Radio frequency types such as the Bennett tube and Bode types

f. Time of flight (including the coincidence type)

g. Quadrupole mass filter

h. Monopole mass filter (variation on the quadrupole)

While a logical approach might imply a detailed analysis of all of these types this would be time consuming and costly. Therefore it was necessary to narrow the field by the use of some basic arguments and cursory analysis. A detailed discussion of how these were applied to the above list of mass analyzers will not be given here. The considerations which were applied to these analyzers include such things as analyzer complexity, stability dependence upon analyzer electronics (this is related to 100% transmission), support electronics requirements, implication regarding the detector system (such as the necessity of an electron multiplier), rough comparisons of sensitivity, and general state of development for space flight use.

An examination of these types indicates that the single focusing magnetic sector, because of its simplicity, reliability and relatively high sensitivity; and the quadrupole mass filter, because of its degree of development, are the best suited instruments for this task. The quadrupole mass filter was first used as a mass spectrometer by Paul and Ruether in 1955. Since that time, it has undergone a rapid development in this country as well as in Germany. Its flexibility and non-magnetic nature have led to wide applications in the analytical field. This analyzer obtains its mass separation by the action of a continuous rf field and therefore does not require either shaped pulses or a magnetic field. The analyzer can be operated in a 100% transmission mode so that the output sensitivity is independent of the analyzer conditions.

The flat topped peaks thus produced are important in providing stable analysis. This type of instrument is operated with an ion current collector and an electrometer amplifier detector and therefore does not require an electron multiplier, which would add increased complexity and instability. The quadrupole mass filter is extremely versatile. Power, size, and sensitivity are interdependent variables which can be optimized for a given problem. In addition, resolution may be easily adjusted by a voltage control allowing rapid selection of the required value. Quadrupole mass spectrometers have been designed and built for space application with power and weight requirements which fall in the desired range for this application. Therefore this analyzer type had to be given consideration.

While the quadrupole mass filter has been successfully miniaturized for space use, this was done primarily for applications which prohibit an external magnetic field. There was a strong possibility that an instrument based upon the single focusing magnetic sector would prove capable of lower weight and reduced complexity. Although it does require a magnet, its inherently higher sensitivity will allow an analyzer of very small size to be utilized. This type of analyzer requires fewer components than the quadrupole, which should increase its reliability. In a miniaturized mass spectrometer, the electronics system accounts for a major portion of the weight. It is here that the magnetic sector instrument has an edge over the quadrupole. The analyzer (mass separator) itself does not require any electronics for its operation, since the mass separation is obtained entirely from the action of the magnetic field. At the same time, the elimination of the requirement of analyzer electronics also reduces the total power consumption of the instrument. These combined advantages make the magnetic sector type extremely competitive.

It is believed that a mass spectrometer sensing system based upon one of these concepts offers the optimum solution to the task. This study offered an excellent opportunity to accurately compare the two instruments which appeared closest to the optimum for the two gas atmosphere sensor system.

As a further confirmation of these choices it should be noted that the majority of successful rocket and satellite mass spectrometer flights have employed quadrupole or sector type analyzers.

4. STUDY OF SYSTEM COMPONENTS

4.1 ANALYZER

4.1.1 INTRODUCTION

The analyzer is that section of the sensor system which performs the mass resolving function. The operation of the quadrupole and single focusing mass analyzers are based upon two widely different principles. A discussion of their operational concepts is not given in this report. Several references are footnoted below[1, 2] which give this type of general information. The following analysis assumes some familiarity with the fundamentals of these instruments.

The primary operational parameter controlled by the analyzer is the resolution. This depends in turn upon ion beam parameters and upon the particular resolving properties of the analyzer. For this reason the following analyzer analysis are begun with discussions of the ion beam properties.

The analysis of the single focusing magnetic sector is carried out to find an optimum design in terms of size and weight. The analysis of the quadrupole mass filter was partially based upon the parameters of an existing system which is close to an optimum for this task. The justification for this less rigorous approach is the fact that in order to compare the magnetic and quadrupole analyzers it is not necessary to have fully optimized analyzers. This is shown in Section 4.1.3.

4.1.2 DETERMINATION OF AN OPTIMUM MAGNETIC SECTOR

In optimizing the magnetic sector analyzer, several factors must be considered. These include magnetic sector angle, magnet radius, magnet gap, magnet flux density, normal versus non-normal entry and exit, object slit and collector placement, and ion source trade-offs between the object slit width, beam divergence, and ion beam energy. All of these factors and others are considered in the analysis.

If a true optimization process were followed, extremely difficult equations would result and take a great deal of time to solve. Even with the aid of a computer the problem would still be imposing since a complicated program would be required to perform the optimization. Therefore, a more straight forward approach was taken which reduced the complexity of the problem. By this process a matrix of parameter values were examined with the best result being chosen from them. At the same time some restriction of the number of

---

1. Design and Construction of a Mass Spectrometer for the Study of Basic Processes in Plasma Physics by M. Mosharrata and H. J. Oskam, ASTIA - AD-274Z49.
2. Mass Spectrometry by Charles A. McDowell, McGraw-Hill.

parameter points which were investigated was required. This was necessary in order to limit the computer time to a reasonable level as well as to keep the quantity of the resulting data within tolerable limits. One of the parameter limitations which resulted was that only 60°, 90°, and 180° sector instruments were examined. The results of this limitation are discussed later in this section.

The analysis logically begins with the ion source as discussed earlier. It was decided to assume that a thermal focus would be examined since this type of focus gives a maximum sensitivity. Furthermore, it is assumed that a one dimensional focal system would be considered since the expected length of the object slit may prohibit adequate focusing in the other plane. It is found that Louiville's Theorem[3] gives the required relationship for ion beam divergence, density, and energy:

$$j_m = j_o \left[\frac{2}{\pi}^{\frac{1}{2}} \Phi^{\frac{1}{2}} + \Phi (1 - \text{erf } \Phi^{\frac{1}{2}})\right] \sin \alpha \qquad (1)$$

where:

j_m = maximum ion current density at the focus (at the ion source exit slit)

j_o = ion current density in the ionizing region

α = maximum ion trajectory angle at the focus with respect to the axis

$\Phi = \frac{eV}{kT_s}$

V = ion kinetic energy at focus (injection energy into magnetic sector)

T_s = ion source temperature $\approx 330°K$

The second term in Equation (1) can be neglected for large values of Φ giving:

$$\frac{j_m}{j_o} = 1.128 \, \Phi^{\frac{1}{2}} \sin \alpha \qquad (2)$$

Since Equation (2) is for a maximum theoretical exit current density a slight safety margin can be allowed by letting the coefficient be unity. The expression for j_o is:

$$j_o = \frac{6.5 I_e P}{W_{cm}} \qquad (3)$$

3. Theory and Design of Electron Beams, J. R. Pierce, Van Nostrand

where:

I_e = ionizing current = 5×10^{-5} amps

p = ion source pressure in torr

W_{cm} = electron beam width in centimeters = .2 cm

This expression is readily derived from ionization probability considerations. The numbers are for 70 V electrons and N_2 sample gas.

Further, the expression for ion source current is:

$$I^+ = j_m h S_o \tag{4}$$

where

h = exit slit height

S_o = exit slit width (object width)

Combining equations: (2), (3) and (4) gives:

$$\frac{I^+}{p_{torr}} = 1.625 \times 10^{-3}\, h S_o\, \Phi^{\frac{1}{2}} \sin\alpha \quad \frac{\text{amps}}{\text{torr}} = \text{sensitivity} = S \tag{5}$$

Since the density distribution falling on the exit slit is a transformed Maxwell - Boltzman distribution having a maximum value of j_m, it can be assumed that a reduction in the coefficient of Equation (5) to 1.5 will represent the integration over the slit. Then substituting for Φ

$$h\, S_o V^{\frac{1}{2}} \sin\alpha = 1.125 \times 10^{-4} \tag{6}$$

Relating S_o and h by the parameter η the final expression relating the ion source parameters is:

$$\frac{S_o^2}{\eta}\, V^{\frac{1}{2}} \sin\alpha = 1.125 \times 10^{-4} \tag{7}$$

Where

$$\eta = \frac{S_o}{h} \tag{8}$$

The next step is to relate the ion source parameters to the analyzer properties. Two approaches are possible. The first is to use the fundamental equation for ion motion in a uniform magnetic field. This relationship is given as Equation (20). It shows that the ion trajectories are circles of radius r_o which depend upon the ion mass m, the ion energy V, and the magnetic field strength, B. Then, by the use of geometrical construction,

ion paths can be traced through any magnetic field and their focal properties can be examined. In this way a minimum ion beam cross section might be determined and such a point could be considered as an ion collection point. This approach was examined and found to lead to rather complicated results. Therefore a second approach was considered. It made use of the Johnson-Nier Equation [4] which gives the expression for the displacement of a ray from the central ray due to small variations in initial displacement, velocity, mass, or angle:

$$y = d\{\cos\phi - n_i \sin\phi\} + r_o\delta\{1 - \cos\phi + n_i \sin\phi\} \quad (9)$$
$$+ r_o\alpha\{(1 - n_o n_i)\sin\phi + (n_o + n_i)\cos\phi\}$$
$$-\tfrac{1}{2} r_o\alpha^2 \{g^2 + \frac{1}{g}\}$$

and

$$\delta = \beta + \gamma$$

where:

ϕ = angle of deflection in the magnetic field

d = initial displacement from the central ray

r_o = radius of curvature in the magnetic field

β = velocity dispersion = $\Delta v/v$

γ = mass dispersion = $\Delta m/m$

$n_o = \frac{\ell_o}{r_o}$

$n_i = \frac{x}{r_o}$

ℓ_o = object-magnet boundary distance

x = image magnet boundary distance

$g = \cos(\tan^{-1} n_i) / \cos(\tan^{-1} n_o)$

These relationships are found in Figure 4-1. It can be shown that the biggest aberration is the α aberration and therefore, the first step

4. "Angular Aberrations in Sector Shapped Electromagnetic Lenses for Focusing Beams of Charged Particles" Physical Review Vol. 91, No. 1, July 1, 1953 by E. G. Johnson and A. O. Nier.

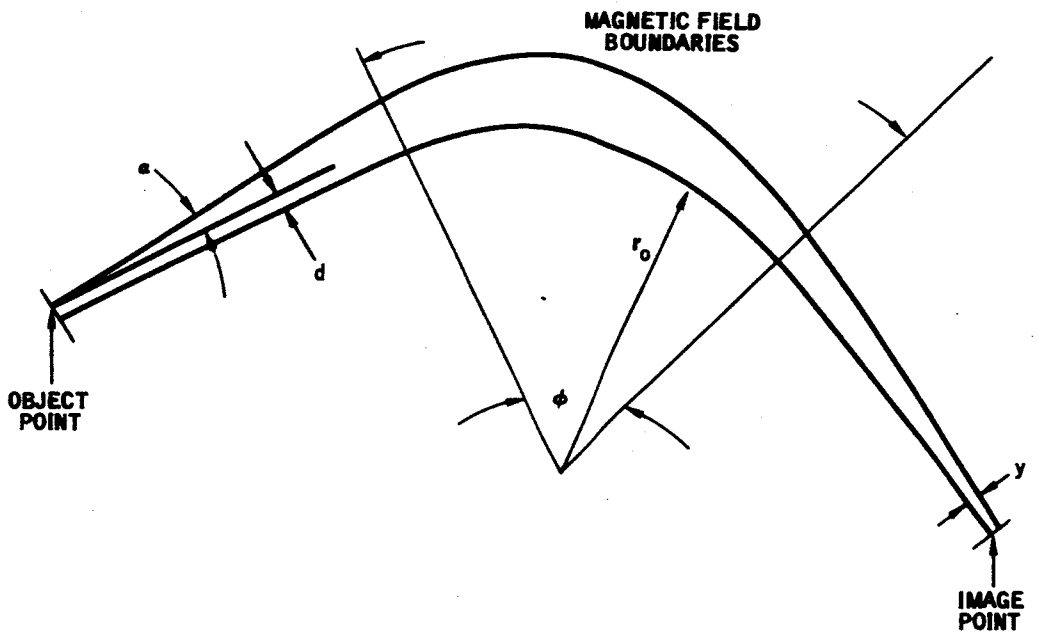

FIGURE 4-1
Magnetic Focusing Relations

is to locate at the first-order focus by making the a coefficient zero. This can be translated into the following relationships for $\phi = 60°$, 90°, and 180°:

$$\phi = 60° \qquad n_i = \frac{1 + .577\ n_o}{n_o - .577}$$

$$\phi = 90° \qquad n_i = \frac{1}{n_o}$$

$$\phi = 180° \qquad n_i = 0 \quad n_o = 0$$

From this point on, unless otherwise stipulated, it will be assumed that these equations apply.

In optimizing a mass spectrometer design it is important to think in terms of beam width instead of single ray displacement. Positive and negative variations must be considered simultaneously. From Equation (3) the beam width can be expressed:

$$B = MS_o + \tfrac{1}{2}K_2\ r_o\ \frac{\Delta V}{V} + K_4\ r_o\ a^2 \qquad (10)$$

where:

$S_o = 2d$ = object slit width

ΔV = total ion energy spread (positive and negative)

$\frac{1}{2}\frac{\Delta V}{V} = 2\beta$ and $\gamma = 0$ since a single mass is under consideration

$M = \cos\phi - n_i \sin\phi$ = object magnification

$K_2 = 1 - \cos\phi + n_i \sin\phi$ = energy aberration coefficient

$K_4 = \frac{1}{2}\left(g^2 + \frac{1}{g}\right) = r_o\ a^2$ aberration coefficient

There are two other aberrations which should be included. One is the image curvature due to the fringe field. This is given in McDowell[5] as $\frac{Z^2}{r_o}$ where Z is the half gap width of the magnet.

The other aberration which should be included is due to those rays which have an angle out of the central plane of the magnet. This is a second order aberration and is approximately $r_o\ \xi^2$ where ξ is the initial angle of the ray with respect to the central plane. The beam with equation becomes:

5. Mass Spectrometry by C. A. McDowell, McGraw-Hill

$$B = MS_o + \tfrac{1}{2}K_2\, r_o \frac{\Delta V}{V} + K_4\, r_o\, a^2 + r_o\, \xi^2 + \frac{z^2}{r_o} \qquad (11)$$

The next consideration is determining mass dispersion and its relation to resolution and beam width. The variation of the final position of a ray with mass is the same as its variation with voltage. While this is not clear from the relation for β, γ and δ, it must be remembered that when considering mass variation the ion energy is held constant. Then for $\Delta V = 0$ $\beta = \tfrac{1}{2}\gamma$ and then $\delta = \tfrac{1}{2}\gamma$. Hence from Equation (9):

$$D = \tfrac{1}{2}\, r_o K_2\, \Delta m/m = \text{beam displacement with mass change or mass dispersion} \qquad (12)$$

If a mass scan is considered and it is asked that two adjacent mass peaks at mass m be completely resolved, then

$$D = B + S_I$$

where S_I is the image slit width (collector width). In the case at hand it is only required that there be no contribution of m/e 17 to m/e 18. This amounts to half peak height resolution in which case

$$D = S_I \qquad (13)$$

The other considerations which enter into the determination of the beam and slit dimensions are the stability of the ion energy and the possibility of misalignment of the exit slit. The top width of a mass peak is determined by

$$T = S_I - B = 2\Delta y \qquad (14)$$

but

$$\Delta y = \tfrac{1}{2}\, K_2 r_o \frac{\Delta V_I}{V_I} + \Delta Y \qquad (15)$$

where

ΔY = slit misalignment

$\frac{\Delta V_I}{V_I} = \psi$ = voltage instability

Then from Equations (12), (13), (14), and (15):

$$B = r_o K_2 \left(\tfrac{1}{2}\frac{\Delta m}{m} - \psi\right) - 2\Delta Y \qquad (16)$$

In this case the required resolution is 1/18. It appears that the ion energy can be regulated to .5% but a safety factor of 50% will be allowed. Hence $\psi = .0075$. It is assumed that the collector slit position can be placed within .005 inch of the theoretical point normal to the beam. Then:

$$B = .02\ r_o K_2 - .0254 \text{ cm} \tag{17}$$

Referring to Equation (11) let it be assumed that the major contributions to the beam width are the MS_o, $\frac{1}{2}K_2 r_o \frac{\Delta V}{V}$ and $\frac{Z^2}{r_o}$ terms. Then let a 33% factor be assumed to include the effects of the other minor aberrations. This can be stated:

$$MS_o + \tfrac{1}{2}K_2 r_o \frac{\Delta V}{V} + \frac{Z^2}{r_o} = .75B \tag{18}$$

The half magnet gap width must now be related to other parameters. It will be assumed that the ion beam diverges from the ion source with the angle ξ equal to α. Then:

$$\begin{aligned} Z &= t + \tfrac{1}{2}\frac{S_o}{\eta} + (\ell_o + r_o\phi + x)\tan\alpha \\ &= t + .5\frac{S_o}{\eta} + r_o\,(n_o + n_i + \phi)\tan\alpha \end{aligned} \tag{19}$$

where

t = thickness of the envelope wall. Let t = .030 inch = .0763 cm

The angle of entry of the ion beam to the magnet boundary can be adjusted to give some Z axis focusing so that this should be a fairly conservative estimate of the required half gap width.

The desired goal of this investigation is to minimize the analyzer demand factors. The principal demand factor which has any degree of flexibility is the weight of the analyzer magnet. Then for a given magnet material, the parameter to be optimized is the magnet volume. To aid in this process a magnet volume parameter is defined which is approximately proportional to the magnet volume:

$$V_m = r_o^2\, Z\phi\, G$$

where

G = field strength in gauss

In order to procede further it is necessary to evaluate the expressions for M, K_2 and K_4 for $\phi = 60°$, 90°, and 180°. They are found to be:

$\phi = 60°$:

$$M = \left|.5 - .866\ n_i\right|$$

$$K_2 = .5 + .866\ n_i$$

$$g = 1/(.866\ n_i - .5)$$

$$K_4 = .5\ (g^2 + \frac{1}{g})$$

$\phi = 90°$ $\quad M = n_i$

$$K_2 = 1 + n_i$$

$$K_4 = .5\left(\frac{1}{n_i^2} + n_i\right)$$

$\phi = 180°$ $\quad M = 1$

$$K_2 = 2$$

$$K_4 = 1$$

Using these equations it is now possible to find an optimum magnet volume parameter. Of the parameters which have been considered some are dependent variables while others are independent. It is desirable to reduce the number of independent variables to a minimum. Three of them which can be related are the radius r_o, energy V and magnetic flux strength G. The defining relation is:

$$r_o = \frac{1.4395 \times 10^2 \sqrt{mV}}{G} \qquad (20)$$

where

m is the mass of the ion being considered. By considering the maximum mass of interest which is m/e 44. Then

$$r_o = 955\sqrt{V}/G$$

The ion energy was allowed to vary from 125 to 225 V, and G from 3 to 4 kg. These appeared to cover the acceptable ranges based on past experience.

The next parameter which must be chosen is the value of n_o. Two factors govern this choice. First, which value tends to minimize the beam width and second, which values are acceptable in view of the size limiatations of the instrument. The size limitation comes about due to the relation between n_o and n_i which exists for a zero α aberration condition. Some of these are tabulated in Table 4-1.

TABLE 4-1
Object and Image Distance Relations

ϕ	n_o	n_i	
60°	1.0	3.73	
	1.5	2.02	← minimum
	2.0	1.51	
	2.5	1.27	
	3.0	1.127	
	3.5	1.032	

TABLE 4.1 (Continued)

90°	0.25	4.00
	0.50	2.00
	1.00	1.00 ← minimum
	2.00	0.50
	4.00	0.25

It is seen that as n_o approaches zero n_i goes to infinity and vice versa. The tabulated values are felt to give the largest acceptable range of values in view of the range of values for r_o. Insofar as minimizing beam width is concerned it can be shown that the largest contributor to beam width is the energy aberation. In the expressions for K_2 for $\phi = 60°$ and 90° it is seen that a minimum value occurs for a minimum value of n_i. On the other hand mass dispersion varies in the same manner as the energy aberation, and then, it is possible that a minimum in magnification, M, is desirable. Again, within the range of values which have been given above a minimum in n_i is desirable. A third possibility is that the Z^2/R aberation is of such importance that it should be minimized relative to the dispersion in which case the latter should be made as large as possible. In view of this complexity it was necessary to test the full range of values for n_o and n_i given above.

A computer program was employed to perform the optimization of V_m. The following ranges of independent variable were assumed:

ϕ = 60°, 90°, 180°

n_o = as given above for $\phi = 60°$ and 90° and $n_i = 0$, $n_o = 0$ for 180°

G = 3000, 4000 gauss

ΔV = 2, 3 V

V = 125, 150, 175, 200, 225 V

η = .03125, .0625, .125, .25, .5

Z = .126, .189, .252, .315, .378 cm

The significant results of the computer investigation are shown in Table 4-2. Only the minimum magnet volume is tabulated for each value of n_o. Actually over 6000 configurations were examined.

It is evident from the results that the magnet weight can be minimized by reducing the magnet angle. However there is a limitation on how small ϕ can go since the smaller ϕ is the larger are the values of n_o and n_i and, hence, the larger are the overall instrument dimensions. It was clear from the data in Table 4-2 that the 180° case can be ruled out due to an excessively large magnet volume parameter. In the case of the 60° sector it was decided to consider the most nearly optimum case which put the ion source the

Magnet Volume	Beam Width	α^2 Aberration	S_o	Z Actual	Z Set	V Ion Energy	ΔV	η	G	n_o	Z^z/r_o	Solution Number	ϕ
7400	.1927	.0001	.0184	.207	.252	150	2	3	4000	1.0	.0147	363	60°
7125	.1167	.0000	.0285	.171	.189	175	2	4	4000	1.5	.0093	922	60°
7125	.0890	.0000	.0281	.171	.189	175	2	4	4000	2.0	.0093	1422	60°
7250	.0757	.0001	.0276	.174	.189	175	2	4	4000	2.5	.0096	1922	60°
7420	.0678	.0001	.0272	.178	.189	175	2	4	4000	3.0	.0100	2422	60°
7590	.0627	.0001	.0267	.182	.189	175	2	4	4000	3.5	.0105	2922	60°
7590	.0688	.0001	.0442	.159	.189	200	2	5	4000	3.5	.0075	2982	60°
11125	.2415	.0005	.0125	.249	.252	125	2	3	4000	0.25	.0232	3353	90°
9710	.1500	.0002	.0209	.181	.189	150	2	4	4000	0.5	.0112	3912	90°
9920	.0916	.0001	.0175	.185	.189	150	2	3	4000	1.0	.0118	4362	90°
10520	.0694	.0001	.0273	.168	.189	175	2	4	4000	2.0	.0089	4922	90°
11780	.0536	.0003	.0252	.188	.189	175	2	4	4000	4.0	.0112	5422	90°
19320	.0916	.0003	.0175	.180	.189	150	2	4	4000	0	.0111	5912	180°
9600	.2417	.0000	.0301	.179	.189	225	3	4	4000	1.0	.0090	447	60°
8780	.1266	.0001	.0219	.184	.189	200	3	4	4000	1.5	.0100	937	60°
9115	.1043	.0000	.0309	.170	.189	225	3	4	4000	2.0	.0081	1447	60°
9230	.0892	.0000	.0312	.172	.189	225	3	4	4000	2.5	.0083	1947	60°
9340	.0803	.0000	.0316	.174	.189	225	3	4	4000	3.0	.0085	2447	60°
10070	.0745	.0001	.0310	.117	.189	225	3	4	4000	3.5	.0087	2947	60°
13700	.2904	.0002	.0156	.219	.252	175	3	3	4000	0.25	.0152	3378	90°
12470	.1772	.0001	.0232	.174	.189	200	3	4	4000	0.5	.0089	3937	90°
12730	.1178	.0001	.0307	.158	.189	225	3	5	4000	1.0	.0070	4497	90°
13130	.0820	.0002	.0315	.163	.189	225	3	5	4000	2.0	.0074	4997	90°
14340	.0641	.0001	.0331	.178	.189	225	3	4	4000	4.0	.0089	5447	90°
23800	.1097	.0001	.0210	.166	.189	200	3	4	4000	0	.0082	5937	180°

TABLE 4-2
Optimum Magnetic Analysis as Determined
by Digital Computer

farthest from the magnet and the collectors closest. This has several advantages including minimizing the magnetic field disturbance in the ion source and minimizing the length of the collector flange. The optimum 60° and 90° cases for ΔV = 3v. were geometrically constructed and the following information was compared:

	Optimum 90°	Optimum 60°
Magnet Volume Parameter (corrected)	12730	9115
Analyzer Area Parameter	4.52 $in.^2$	5.53 $in.^2$
Maximum Analyzer Dimension (Object slit to m/e 44 collector)	5.39 in.	7.16 in.

Examination of these numbers in conjunction with the estimation of magnet weight indicates that the 90° magnet would weigh approximately 1/4 of a pound more than the 60° magnet. On the other hand the dimensional considerations favor the 90° sector instrument from a structural and packaging point of view. A significant portion of the 1/4 pound of additional magnet weight is offset by reduced structural weight due to the greater compactness of the analyzer and therefore of the overall package.

Another factor which is of some importance is that the 60° sector analyzer gives a smaller angle between the ion rays and the focal plane than does the 90° sector. This increases the difficulty in designing movable ion current collectors, especially for m/e 28 and m/e 32.

Taking all of these factors into account there is little to choose between the 60° and 90° cases. This also leads to the conclusion that there is no other magnet angle that would lead to a significantly greater optimization. Weighing all factors it was decided that the 90° sector would give the most satisfactory results.

The parameters of the chosen configuration are:

ϕ = 90°

V = 225v

r_o = 3.589 cm for m/e 44

B = 4000 gauss

ΔV = 3v

S_o = 0.0307 cm

h = 0.0614 cm

n_o = 1

$n_i = 1$

$Z = .158$ cm

$\psi = .0075$

The more detailed calculations in Section 4.1.5 caused some of these numbers to change slightly.

Sufficient information was available at this time to allow a comparison of the quadrupole and magnetic sector analysis. This is discussed in Section 4.1.4.

4.1.3 QUADRUPOLE ANALYZER DESIGN FOR THE TWO GAS ATMOSPHERE SENSOR SYSTEM

In the design of a quadrupole mass spectrometer, two types of operation must be considered. The first is the 100% transmission case which leads to flat topped mass peaks, and the second is the pointed peak mode of operation. For the type of operation which is required in a cabin monitoring system, the first type of operation is dictated. There are two reasons for this. First, a stepped mode mass scan can be employed since there is a finite range of voltage or frequency for which the output of the analyzer is a constant. In the case of pointed peak operation, a scan mode of operation would have to be employed, at least in the region of each mass peak of interest, in order to ensure that an accurate result was being obtained. This would lead to complications in the quadrupole electronics. Second, there must be a small restriction between the ionizing region and the analyzer in order to achieve a high value differential pressure ratio. This, in turn, restricts the amount of ion current which is available for transmission into the analyzer. Therefore, not much can be gained by opening up the entrance aperture. For these reasons, it is possible to restrict the design effort to the 100% transmission case.

This is a fortunate restriction since this case lends itself more readily to an analytical solution. Hall and Ruecker[6] have derived the transmission equations for a quadrupole mass filter operating in the 100% transmission mode and have coupled them with a perfect imaging ion source to obtain Equations (1), (2), and (4) below:

$$\left(\frac{r_e}{r_o}\right) = 0.0346 \frac{dm}{m} \left[1 - \frac{T}{B}\right] \qquad (1)$$

r_e = analyzer entrance aperture radius for ion current

r_o = quadrupole rod spacing parameter (distance from the axis of the quadrupole to the edge of each rod)

$\frac{dm}{m} = \frac{1}{R_o}$ = fundamental resolution (excluding peak tails)

$\frac{T}{B}$ = peak top width to base width ratio (with no tails)

This equation gives the $\frac{r_e}{r_o}$ ratio for maximum sensitivity for some given analyzer conditions. For the value of $\frac{r_e}{r_o}$ given in Equation (1), the required ion source characteristics may be related to the analyzer characteristics by the following relation:

---

6. Appendix D-Quadrupole Mass Spectrometer for Energetic Particle Measurements.

$$V_I \sin^2 \alpha \leq 0.00955\ V_{ac} \frac{dm}{m} \left[1 - \frac{T}{B}\right] \quad (2)$$

V_I = ion injection energy into analyzer

α = maximum entrance half angle

V_{ac} = zero to peak amplitude of the rf voltage on the quadrupole rods.

In the derivation of this equation, Abbe's Law[7] for a worst case initial angle of 90° is employed. The relating equation is:

$$\sin \alpha_{max} = \frac{1}{M} \sqrt{\frac{V_o}{V_I}} \quad (3)$$

M = linear magnification of the ion source focal system

V_o = initial ion energy

Abbe's Law is valid only in the case of a perfect imaging ion source. In the present optimization it is desired to consider a thermal imaging focus in which all of the rays are focused at a single point. By the use of Louiville's Theorem[8] it can be shown that the maximum current density which can be obtained at a point focus is given by:

$$j_m = j_o (1 + \Phi) \sin^2 \theta \quad (4)$$

for an axially symmetrical system where

j_o = initial current per unit area in ionizing region

Φ = maximum permissible half angle at the focus =

$\theta = eV_I/kT$

T = ion source temperature

V_I = final ion energy

In this case a two dimensional focusing system can be considered due to the symmetry of the quadrupole. In the case of interest $\phi \gg 1$, then Equation (4) takes on the appearance of Equation (3) with $V_o = kT/e$. Consequently, it is seen that the equations which have been derived for a perfect imaging source are also valid for a thermal imaging source provided that the proper substitution for V_o is made.

7. Electron Optics by O. Klemperer, Cambridge Press pp 12-14
8. Theory and Design of Electron Beams by J. R. Pierce, Van Nostrand.

The ion source current can be expressed:

$$I^+ = \pi r_e^2 j_m \tag{5}$$

Under the conditions of Equations (1), (2) and (4) the ion source current is:

$$I^+ = 3.305 \times 10^{-4} \frac{V_{ac}}{V_o} \pi r_o^2 j_o \left(\frac{dm}{m}\right)^2 \left(1 - \frac{T}{B}\right)^2 \tag{6}$$

As used before in Section 4.1.2

$$J_o^+ = \frac{6.5\, I_e\, p}{w} \quad (\text{amps/cm}^2) \tag{7}$$

where

I_e = ionizing current in amperes

p = partial pressure in torr in the ionizing region

Then from Equations (6) and (7)

$$S_{N_2} = \frac{6.75 \times 10^{-3}\, V_{ac}}{w_{cm}} \; r_o^2 \left(\frac{dm}{m}\right)^2 \left(1 - \frac{T}{B}\right)^2 \tag{8}$$

S = analyzer sensitivity for N_2 in amps/torr-amp

This gives the analyzer sensitivity in terms of the important quadrupole parameters V_{ac}, r_o, dm/m, and T/B. The next question of importance is how long must the quadrupole rods be. This is dependent upon the magnitude of the peak tails which can be tolerated.

The width of a mass peak is controlled by two independent phenomena. The fundamental base width is controlled by the point at which the scan line cuts through the stability diagram (See Figure 2 of Appendix D) which determines the width of the bandpass. This is a function of the V_{dc}/V_{ac} voltage ratio. In addition to the fundamental base width, the mass peak will also exhibit tails. These arise due to unstable ions which do not grow in amplitude rapidly enough to strike the rods. As a result, there is transmission in the unstable region. As the operating point approaches the stability boundary, the degree of instability is reduced, and the amount of transmission is increased.

No adequate treatment of the relationship between peak tails and the quadrupole parameters exists in the literature. Von Zahn has given an expression for the relationship between resolution and the number of cycles which the ion must spend in the rf field. Close examination of his work indicates that his expression is not valid for any case other than the one for which it was empirically derived. Appendix K gives an approximate mathematical solution to the transmission efficiency outside the stable region.

With reference to the application of equation (13) in Appendix K, it should be noted that there is a quadrupole bias voltage which is applied between the entrance aperture and the quadrupole region to slow the ions down in order to reduce the tails. Due to this bias voltage V_Z is different from V_I . The V_Z appearing in the exponential is the value after deceleration since this is the value which the ions have during most of their travel down the axis. On the other hand, V_I which appears in the y'_o coefficient is the full ion energy before deceleration.

With these equations, it is possible to calculate the magnitude of a peak tail once numbers are plugged in. While this derivation has been carried out for the y tail, essentially the same results hold for the x tail with a different multiplier.

One of the primary constraints on a quadrupole mass spectrometer is the power which is required to maintain the rf voltage field. If only the power in the load is considered, the power is given by:

$$P = \frac{2V_{ac}^2 \quad \omega C}{Q} \qquad \text{(watts)} \qquad (9)$$

where

C = quadrupole capacity (farads)

Q = quality factor of tank circuit

$\omega = 2\pi f$ where f = frequency of rf voltage

Generally, either V_{ac} or ω is eliminated from this expression depending upon which parameter is to be varied in the mass scan. It has been shown that the voltage scan is unsatisfactory for a stepped scan where the peak top width must be maintained to accept fluctuations in the ratio of V_{ac}/ω^2. [9] Therefore, a frequency scan mode is considered in which case, the frequency variable is eliminated by the use of:

$$V_{ac} = 7.25\, m r_o^2 f^2 \qquad \text{(volts)} \qquad (10)$$

where

m = mass in amu

r_o = rod spacing parameter in cm

f = frequency in megacycles

---

[9] Appendix F Quadrupole Stability Requirements

This is the alternate form of Equation (13). Substitution of Equation (11) into Equation (22) gives:

$$P = \frac{4.6 \times 10^{-6} \, V_{ac}^{5/2} C_{pf}}{m^{\frac{1}{2}} \, r_o \, Q} \quad \text{watts} \tag{12}$$

Where C_{pf} = the quadrupole capacity in picofarads.

Frequency scanning can be accomplished either by varying the capacity or the inductance of the tank circuit. It can be shown that using shunt inductors is the cheapest technique in terms of power. In this case, the capacity C_{pf} is equal to the quadrupole capacity of C_Q. It has been empirically shown that

$$C_Q \approx \ell_{cm} + C_R \tag{13}$$

where ℓ_{cm} = rod length in centimeters and C_R is equal to the end capacity and header capacity. For the size instrument which is being considered, $C_R \approx 5$ pf. With Equations (12) and (13), the quadrupole power can be related to the other quadrupole parameters.

In order to compare the quadrupole and magnetic analyzers, it is necessary to make use of the power penalty. The least severe penalty which is imposed on the 120 day mission is 0.5 pounds/watt. Using this value, a weight equivalent can be given to the quadrupole power.

With the equations which have been derived numerical results can now be obtained. Before applying the sensitivity equation it should be checked by application to an existing instrument. This instrument has the following parameter values:

V_{ac} = 250 V

r_o = 0.508 cm

$\frac{dm}{m}$ = 1/20

$\frac{T}{B}$ = 0.5

V_o = 0.03 V

w_{cm} = 0.2 cm

Substitution of these values into Equation (8) gives a predicted sensitivity of 2.265×10^{-6} amperes/torr with 50 microamperes ionizing current. The measured value is 1.6×10^{-6} amperes/torr. There have been some problems in the analyzer configuration which have limited the resolution and top to base ratio. Indications are that the existing instrument is capable of a higher resolution which would bring the numbers into better agreement. For the present a 25% safety factor will be used.

Before applying Equation (8) to the present problem it is useful to express the required $\frac{T}{B}$ ratio in terms of a stability requirement. Stability requirements for the quadrupole analyzer have been worked out [10] and can be expressed:

$$\frac{\Delta q}{q_o} = \pm \frac{T}{B} \frac{\Delta m}{m} \quad \text{for constant } V_{dc} \tag{14}$$

where

$$\frac{\Delta q}{q_o} = \left| \frac{\Delta V_{ac}}{V_{ac}} \right| + 2 \left| \frac{\Delta f}{f} \right| \tag{15}$$

Since the quadrupole voltage supply is an rf and dc supply it is difficult to maintain extremely tight regulation without very complex electronics. Experience has shown the following variations to be expected:

$$\Delta\left(V_{dc}/V_{ac}\right) / \left(V_{dc}/V_{ac}\right) = 0.5\%, \quad \Delta V_{ac}/V_{ac} = 1\%, \quad \Delta f/f = 0.5\%$$

then from Figure 3 of the referenced Appendix the allowable $\Delta q/q_o$ is approximately 0.50 of the value given in Equation (14).

At this point a restrictive step is in order. If an optimum quadrupole analyzer were sought a range of values for r_o would be substituted into Equation (8) and values for V_{ac} determined. Then Equation (13)K would be applied to determine the required quadrupole rod length. Then from Equations (12) and (13) the quadrupole power could be determined. Now by application of the power penalty factor an optimum effective weight can be found.

This is a rather lengthy process to carry out for a large number of r_o values. Consideration of past designs indicates that the curve of effective weight as a function of r_o does not change rapidly and therefore a single value of r_o equal to 0.508 centimeters was chosen. This is the same as for an existing instrument and is believed to be close to an optimum. Then for a fundamental resolution of 1/20, an ionizing current of 50 microamperes with an electron beam width of 0.2 centimeters, an initial ion energy of 0.03 volts, a value of T/B as determined by the preceding considerations, and a sensitivity of 1.25×10^{-6} amperes/torr the required value of V_{ac} is 138 volts. Then from

---

10. Appendix F - Quadrupole Stability Requirements

Equation (2) $V_I \sin^2 \alpha \leq .0329$. Experience has indicated that a value of V_I larger than 300 volts should not be assumed giving $\alpha = 0.6°$. It does not appear reasonable to assume α values less than 0.8° so this was used as the maximum angle. The next step in the specification of the quadrupole is to determine the required rod length. This is done by evaluating Equation (13)K over a range of initial conditions. The following ranges were used with uniform distributions:

$$y_o = o \text{ to } r_e$$

$$\alpha = -0.8° \text{ to } +0.8°$$

$$\omega t_o = 0 \text{ to } 360°$$

$$V_z = 2 \text{ to } 5 \text{ volts}$$

In determining V_z a 3 V ion energy spread was assumed with the quadrupole bias set 2 V below the minimum ion energy to allow for voltage variations. In order to evaluate Equation(13)K, values must be given for L and R_t. L was assumed to have the values of 30 r_o, 15 r_o, 7.5 r_o, and 3.75 r_o. The maximum value corresponds to an existing quadrupole mass filter for which the properties are known. R_t was chosen based upon a fundamental resolving power of $r_o = 20$, and allowing a tail width to the point where contribution to the m/e 18 peak occurs.

Using a computer program to evaluate the transmission efficiency a value of L/r_o was found to be approximately equal to 11. By adding 2 r_o at each end to allow for the regions at the ends of the rods where the ions are traveling much faster, the total required rod length of 15 r_o or 3 inches. This is a reasonable value based on past designs.

Now a calculation of the required quadrupole power can be carried out. From Equation (13) the quadrupole capacity is 12.6 picofarads. Experience has shown that the loaded Q of the type of rf oscillator which is required is about 20. From Equation (24) the power is 0.302 watts. The associated control electronics which operate with the quadrupole oscillator are generally about 50% efficient so that the total power is approximately 0.6 watts. It is furthermore likely that due to the reduced load power the efficiency of the control electronics would be further reduced so that a more realistic value for required power is about 1 watt. This is equivalent to an effective weight of 0.5 pounds using the power penalty.

4.1.4 COMPARISON OF THE SINGLE FOCUSING MAGNETIC AND QUADRUPOLE ANALYZERS

Now that the initial analyses of the magnetic and quadrupole analyzers have been completed, a comparison of their relative merits can be made. The analysis of each of these mass separating techniques was based upon the same sensitivity and resolution and similar ion source requirements. The comparison must be made based upon the support electronics requirements, reliability, environmental, and demand factors.

First consider the weight demand of the two analyzers. Using known weight information for a small quadrupole analyzer with the same r_o (taking into account the reduction in rod length from 6 inches to 3 inches) and comparing this against the estimated magnetic analyzer weight, it was found that the quadrupole analyzer would weigh approximately 0.25 pounds more than the magnetic analyzer. This difference is due primarily to the quadrupole rods and rod supporting structure. The magnet weight for the magnetic sector analyzer is calculated to be 0.9 pounds (See Section 4.1.6), and this is paired off against the quadrupole power of 1 watt using the 0.5 pound/watt power penalty so that the total effective analyzer weight difference is 0.15 pounds in favor of the quadrupole analyzer.

Next the analyzer electronics must be compared. The magnetic sector requires no electronics for its operation. The mass resolution is obtained solely by the action of the permanent magnet. On the other hand, the quadrupole analyzer requires an rf oscillator and V_{dc} supply. Both the frequency and voltage of the oscillator output must be tightly controlled as shown in Section 4.1.3. This necessitates the use of a feedback control loop and voltage regulator to supply a controlled B+ to the oscillator which maintains V_{ac} constant.

Since there are four masses of interest, the frequency of the oscillator must be variable to four values. This is most efficiently done by switching in inductance and capacitance to vary the tank circuit resonating frequency. Each of these tank circuits must be capable of fine tuning. A sequential stepping logic circuit is required to switch the tank circuits. This circuit has the form of a clock pulse and shift register with relay drivers to drive the reed relays. This total system would be very similar to the one used on an existing miniaturized quadrupole mass spectrometer system. It has been weighed at 1 pound 11 1/2 ounces. It is doubtful that this number could be reduced by more than 25% and so a weight value for the quadrupole electronics of 1.3 pounds will be used for comparative purposes. Adding this weight difference to the value for the analyzers gives a total weight difference of 1.15 pounds in favor of the magnetic sector analyzer. The magnetic sector instrument will use four detectors with an additional weight of 0.4 pounds and a minor increase in power. Subtracting this from the previous difference value gives a 0.75 pound advantage to the magnetic sector. From the standpoint of demand factors, the magnetic sector has a clear advantage over the quadrupole analyzer.

Next, the relative reliabilities of the two approaches must be considered. The quadrupole electronics require over 200 electronic components of all types. This would represent a 50% increase in the number of electronic components in the sensor system based upon a magnetic analyzer. On a component count basis alone, a quadrupole sensor system would be considerably less reliable than the magnetic sector instrument. Experience has shown that more problems are encountered with the quadrupole electronics than with the other support electronics areas so that the net result is a much less reliable instrument.

In addition, the single ion current detector used with the quadrupole analyzer must have two sensitivity ranges, necessitating a range switch driven by the logic. This is one further unreliability in series with the output. On the other hand, the multiple detectors employed by the magnetic sector analyzer offer a degree of functional redundancy since the two high level and two low level detectors are interchangeable.

It is also of interest to look at the operational features of the two instruments. The quadrupole analyzer must operate in a serial mode looking at each mass one after the other. On the other hand, the magnetic sector sensor would use a multiple collector system with separate output channels. This gives a time response advantage to the magnetic sector instrument since it will give continuous parallel outputs. Parallel outputs should also make the instrument more compatible with the control system since no serial to parallel switching or signal holding circuits will be required.

A further possible disadvantage of the quadrupole analyzer lies in the increased difficulty in meeting a tight RFI specification which would probably be imposed on a flight instrument. This difficulty arises not only from the presence of the rf signal but also from wideband noise transients caused by the switching of the tank circuits.

In summary, it must be concluded that the single focusing magnetic sector analyzer has significant advantages over the quadrupole analyzer in terms of power and weight demands, performance, reliability, and interface compatibility. Therefore, the single focusing magnetic sector analyzer was selected as the basis for the sensor system, and all further discussion relates only to this analyzer.

4.1.5 DETAILED MAGNETIC SECTOR CONSIDERATIONS

Having selected an analyzer configuration, a more detailed analysis is in order. First a check on the required magnet angle was made. From Equation (7) of Section 4.1.2

$$\sin \alpha = 1.125 \times 10^{-4} \frac{\eta}{S_o^{\,2} V^{\frac{1}{2}}}$$

$$\eta = 0.5\, S_o = 0.0307 \text{ cm}, \quad V = 225 \text{ volts}$$

The result is $\sin \alpha = 0.0040$ or $\alpha = 0.29°$.

It has been anticipated thus far that a thermal imaging ion source be employed for this task. In this type of ion source, the exit angle is limited primarily by geometrical means. Two defining apertures a distance ℓ apart, limit the angle to $\alpha = \tan^{-1} h/\ell$ where h is the slit height. In the case at hand, $h = 2\, S_o = 0.0614$ cm. Then for $\alpha = 0.29°$, $\ell = 15.4$ cm. This distance is clearly excessive.

If the numbers obtained so far are substituted into Equation (2) of Section 4.1.2, it is found that $j_m < j_o$ implies a defocusing lens system. This is indeed the best way of reducing the ion source exit angles. On the other hand, if one considers a simple immersion lens as the most direct method of obtaining this type of focusing, the governing equation is:[7]

$$f = \frac{4V}{E_2 - E_1} \tag{1}$$

where

V = ion energy, and $E_2 - E_1$ = gradient difference across the lens plane.

A very long and negative focal length is required which means that the gradients E_2 and E_1 are approximately equal. But E_1 is the gradient in the ionizing region which is limited to about 40 volts per cm by ion energy spread considerations.

This implies that in order for the ions to acquire the necessary 225 volts of energy, they must travel approximately 6 centimeters. This ion path length is also considered to be excessive.

Even if twice as large a value of α were allowed, the above considerations would still lead to excessive focal distances. Faced with this problem, it was decided to examine the situation from a different direction. First, a perfect imaging ion source was considered. In this type of focal system, ions were considered which have an initial velocity parallel to the axis of

---

[7]See Electron Optics by O. Klemperer, Cambridge Press, 1953.

the ion source and a final velocity which is also parallel to the ion source axis. An optical representation of this type of focusing is shown in Figure 4-2. In this type of system, the ion parameters are related to initial parameters by Abbe's Law:

$$y_o V_o^{\frac{1}{2}} \sin \theta_o = y_i V_i^{\frac{1}{2}} \sin \theta_i \qquad (2)$$

where 'o' subscripts denote object parameters and 'i' subscripts denote image parameters. Letting $M = y_i/y_o$ = the linear magnification of the focal system and choosing a worst case value of 90° for θ_o (normal to axis) then

$$\sin \theta_i = \frac{1}{M}\left(\frac{V_o}{V_I}\right)^{\frac{1}{2}} = \sin \alpha \qquad (3)$$

where α is the worst case of θ_i, and V_I is the ion source injection energy.

In order to obtain a numerical value for α, values for M, V_o, and V_I must be assigned. The required value of M is determined by sensitivity considerations. In Equation (2) of Section 4.1.2, only one dimensional focusing was assumed due to the large expected ratio of h to S_o. It has been shown that a smaller ratio of h to S_o is more optimum; therefore, it is now logical to think in terms of focusing in both transverse planes. In this case

$$j_i = \frac{j_o}{M^2} \qquad (4)$$

where j_i is the ion current density at the image plane and j_o is the ion current density in the ionizing region.

The expression for ion source sensitivity is found to be:

$$S = \frac{6.5\ h\ S_o\ I_e}{W\ M^2}$$

With the following numbers:

$S = 1 \times 10^{-6}$ amperes/torr

$I_e = 5 \times 10^{-5}$ amperes

$S_o = 0.0307$ cm

$h = 0.0614$ cm

$W = 0.200$ cm

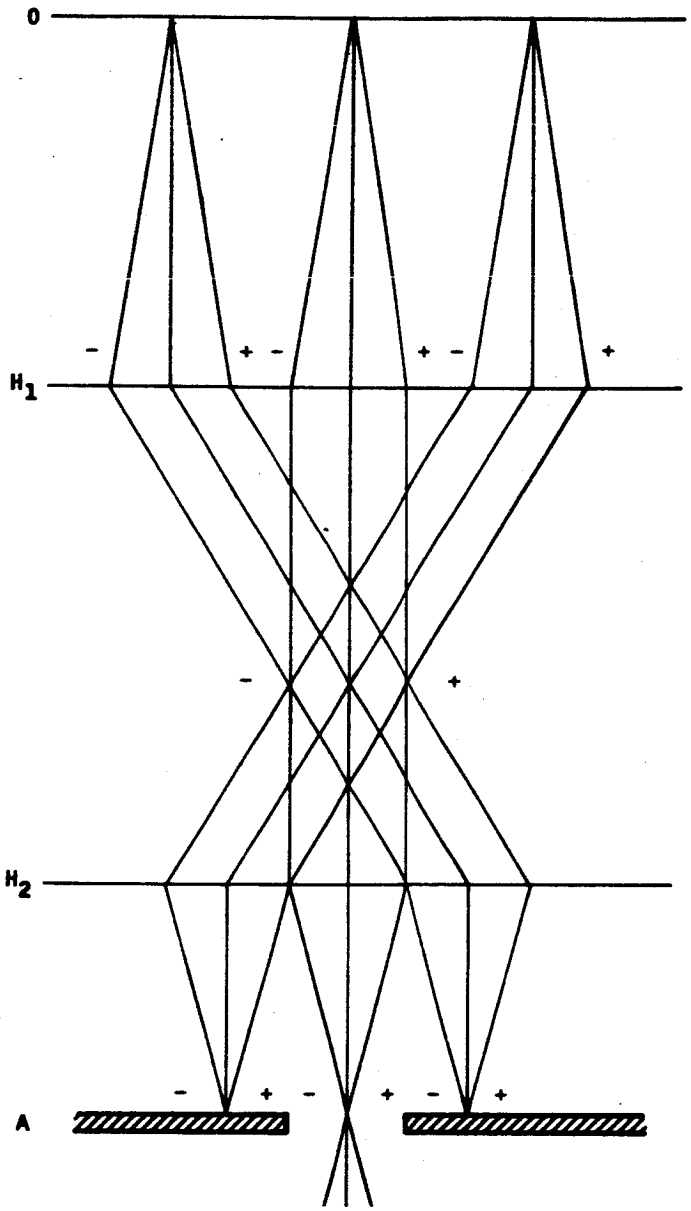

FIGURE 4-2
Perfect Imaging Focusing

the necessary magnification is found to be 1.75. Since the desired ion source injection energy is 225 v, it only remains to determine V_o. It was decided to choose $V_o = 3kt/e$, which for the expected ion source temperature, is 0.1 V. By looking at the form of Abbe's Law, it can be seen that we are asking that the radial component of energy is less than 3kt/e. It can be shown that the density distribution for the radial velocity component is given by:*

$$\frac{dn}{dv_r} = N \frac{m}{kt} v_r \exp\left(-\frac{mvr^2}{2kt}\right) \tag{5}$$

When this is integrated over v_r, the result is:

$$\frac{N\left(\frac{1}{2} mvr^2 < \frac{xkt}{e}\right)}{N_{total}} = (1 - e^{-x}) \tag{6}$$

For x = 3, the value of the righthand term is 0.95 which says that 95% of the ions arriving at the ion source image plane have radial energies less than 3kt. Part of the remaining five percent will represent some transmission loss in the analyzer due to increased α ; however, this loss will be fairly constant so that the resulting inaccuracy will be small.

Solving Equation (3) for α gives:

$$\alpha = 1/3.06 \sqrt{\frac{0.1}{225}} = 0.00688 \text{ or } \alpha = 0.40°.$$

While a theoretical design of a perfect imaging ion source would give this angle, aberrations in the ion optics cause an increase in the angle. Experience has shown the sum of these distortions is approximately a factor of 2, so a maximum α equal to 0.8° will be used. The details of the perfect imaging focal system are discussed in Section 4.2.2.

The $r_o\alpha^2$ aberration for the instrument being considered was shown to be quite small so no problem is expected from this source for the increased α. Next, the effect of α on the required magnet gap width must be determined. Equation (19) of Section 4.1.2 can be used, but it is assumed that the envelope thickness may be increased after the magnetic sector is traversed and therefore Z does not depend upon the distance from the magnet boundary to the collector. Consequently, the x term is dropped.

Then, the half magnet gap,

$$Z = t + \frac{h}{2} + r_o (n_o + \phi) \tan \alpha \tag{7}$$

*See Appendix N.

For

$t = 0.0763$ cm = envelope wall thickness

$\frac{h}{2} = 0.0307$ cm = ½ exit slit lenght

$r_o = 3.59$ cm = ion radius of curvature

$n_o = 1.0$ = source magnet distance/r_o

$\phi = 1.57$

$\tan \alpha = 0.00688$

$Z = 0.1705$ cm = half gap width

It is possible that such a thin envelope wall will experience some deflection due to the pressure of the external environment. This possibility was checked roughly, and it was found that allowing an additional 0.0254 cm for this would be more than sufficient. Then another safety factor, about 10%, was applied to account for possible fabrication problems to bring the total gap requirement to a little over 4 mm or 0.160 inches. The previous gap requirement was about 0.125 inches so a slightly larger magnet will be required. This result was taken into account in the magnet weight value used in comparing the quadrupole and magnetic sector analyzers.

The analysis in Section 4.1.2 considered only a single ion beam of m/e 44. This was chosen since it represents the maximum ion beam radius and therefore gives a better measure of the magnet requirements. In the contemplated design, multiple collectors are considered so that the m/e 18, 28, and 32 beam widths must also be considered. A normal entry magnet is being used. Analysis of other configurations did not indicate any significant improvements and only increased the complexity of the calculations. With this type of magnet, ions of all masses will enter the magnet normal to the magnet boundary, but only one mass can be selected to leave the magnetic field normal to the boundary. It was decided to choose m/e 28 as the normal ray since it is nearly the geometric mean between the extreme rays (m/e 18 and m/e 44). In this way, the average effects due to non-normal exit can be minimized.

Not only is the m/e 28 ray the only one with normal exit, it is also the only one that travels through 90° in the magnetic field. This is apparent from geometrical construction, and the new values for ϕ are readily calculated. The new values for ϕ lead to new values for n_i. One must be careful to note also that while $n_o = 1$ for m/e 28, it is different for the other masses since

while ℓ_o remains fixed r_o changes. Both of these changes lead to new values for n_i. By setting the a aberration coefficient in Equation (9) of Section 4.1.2 equal to zero, the general relation between n_o and n_i is found to be:

$$n_i = \frac{1 + n_o \cot \phi}{n_o - \cot \phi} \tag{8}$$

Evaluation of this expression with the new ϕ and n_o values gives the new n_i values.

The smaller aberrations were not calculated in detail in Section 4.1.2. In order to have a higher degree of assurance that the design parameters given thus far represent a feasible analyzer, these calculations must be carried out in detail. In order to account for all higher order aberrations, it is necessary to investigate the effects of misalignment. Even though the a aberration is zero, small misalignments can lead to a significant $r_o a$ term. Assuming a $\Delta\ell_o$ and Δx in the a aberration term of Equation (9) of Section 4.1.2, the result is:

$$a\left\{(\Delta\ell_o + \Delta x)\cos\phi - (n_o\Delta x + n_i\Delta\ell_o)\sin\phi\right\} \tag{9}$$

There is also the possibility of a misalignment in the magnet angle ϕ applied to the a aberration term:

$$a r_o\,\Delta\phi\left\{(1 - n_o n_i)\cos\phi - (n_o + n_i)\sin\phi\right\} \tag{10}$$

Equation (18) of Section 4.1.2 also allows for a misalignment of the collector in a direction normal to the beam. It should be pointed out that this also can include a misalignment of the object slit in a direction normal to the beam. Hence

$$\Delta Y = \Delta C + M\Delta S$$

where

ΔC = collector misalignment normal to beam

ΔS = object slit misalignment normal to beam

M = magnification as defined in Section 4.1.2

Insofar as misalignment in the Z direction is concerned (normal to magnet plane) it is assumed that margins in the magnet gap and collector height are sufficient to handle these. A summary of misalignments is given in Figure 4-3.

The complete aberration equations including misalignments are:

1) Magnification $M(S_o + \frac{1}{2} h \Delta\omega_{xo})$

2) Energy aberration $0.5\, K_2 r_o \Delta V/V$

3) Image curvature Z^2/r_o

4) Alpha aberration $2(\alpha + \Delta\alpha)\left\{(\Delta\ell_o + \Delta x)\cos\phi - (n_o \Delta x + n_i \ell_o)\sin\phi\right\}$

$2(\Delta + \Delta\alpha) r_o \Delta\phi\left\{(1 - n_o n_i)\cos\phi - (n_o + n_i)\sin\phi\right\}$

$$\Delta\ell_o = \Delta x_o + \Delta x_m + r_o \Delta\omega_{Zm} + \frac{1}{4} h\,(\Delta\omega_{yo})^2 + \frac{1}{4} S_o\,(\Delta\omega_{zo})^2$$

$$X = \Delta_{yc} + \Delta_{ym} + r_o \Delta\omega_{Zm} + \frac{1}{4} h_c\,(\Delta\omega_{xc})^2 + \frac{1}{4} S_I\,(\Delta\omega_{Zc})^2$$

5) Alpha squared aberration: $\frac{r_o}{2}\,(g^2 + \frac{1}{g})\,(\alpha + \Delta\alpha)^2$

6) Aberration due to angle out of plane: $r_o(\xi + \Delta\xi)^2$

The beam width is the sum of the above terms 1) through 6) plus an undetermined quantity for the $\alpha\beta$ aberration.

The required beam width is:

$$B_{req} = r_o K_2 \left(\frac{1}{2}\frac{\Delta m}{m} - \psi\right) - 2\Delta y$$

where:

$$\Delta y = M\Delta_{yo} + \Delta c + \frac{1}{2} h_c \Delta\omega_{yc} + \frac{1}{4} h_c\,(\Delta\omega_{yo})^2$$

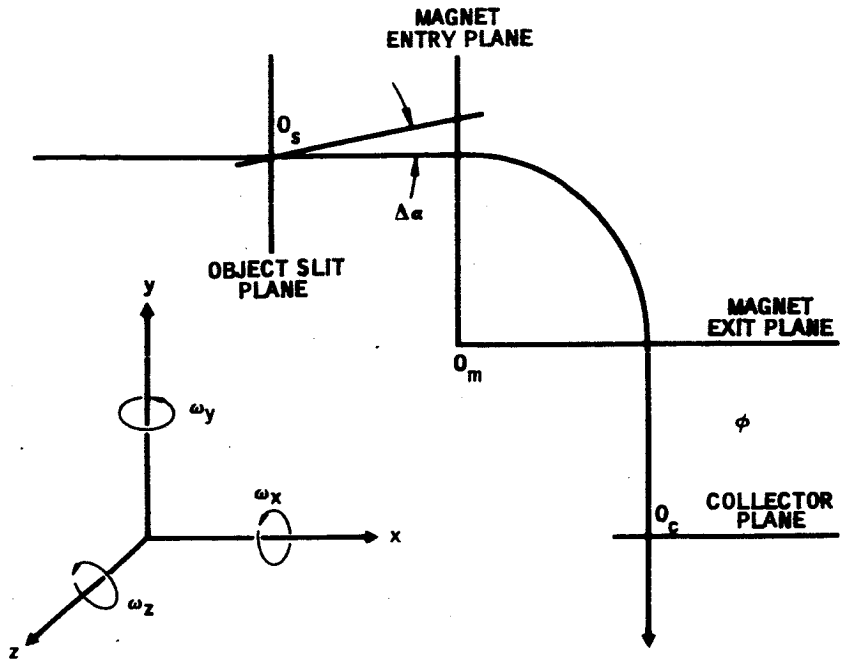

$\Delta x_0 \rightarrow$	$\Delta \ell_0$	CAUSES α ABERRATION
$\Delta y_0 \rightarrow$	MΔS	CONTRIBUTES TO Δy
$\Delta z_0 \rightarrow$		INCREASED GAP AND COLLECTOR HEIGHTS MARGIN ALLOWED
$\Delta\omega_{x0} \rightarrow$	$\Delta S = \frac{1}{2} h\omega_x$	INCREASES EFFECTIVE OBJECT SLIT WIDTH
$\Delta\omega_{y0} \rightarrow$	$\Delta \ell_0 = \frac{h(\Delta\omega_{y0})^2}{4}$	CAUSES A $\Delta \ell_0$ AND SMALLER SLIT AREA (LESS SENSITIVITY, NO PROBLEM)
$\Delta\omega_{z0} \rightarrow$	$\Delta \ell_0 = \frac{h(\Delta\omega_{z0})^2}{4}$	CAUSES A $\Delta \ell_0$ AND SMALLER SLIT AREA (LESS SENSITIVITY, NO PROBLEM)
$\Delta X_c \rightarrow$	ΔC	CONTRIBUTES TO Δy
$\Delta Y_c \rightarrow$	ΔX	CAUSES α ABERRATION
$\Delta Z_c \rightarrow$		SAME AS ΔZ_0
$\Delta\omega_{xc} \rightarrow$	ΔX	CAUSES A ΔX AND SMALLER COLLECTOR AREA (LATTER NO PROBLEM)
$\Delta\omega_{yc} \rightarrow$	$\Delta C = h\Delta\omega_{yc}$	DECREASES COLLECTOR WIDTH (ADD TO Δy)
$\Delta\omega_{zc}$	$\Delta C = S_1 \frac{\Delta\omega_{zc}^2}{2}$	DECREASES COLLECTOR WIDTH (ADD TO Δy)
ΔX_m		ALREADY INCLUDED BY ΔX_0
ΔY_m		ALREADY INCLUDED BY ΔY_c
ΔZ_m		SAME AS ΔZ_0 AND ΔZ_c
$\Delta\omega_{xm}$		CAUSES A ΔZ_{in} AND ΔZ_c NO PROBLEM
$\Delta\omega_{ym}$		SAME AS $\Delta\xi$
$\Delta\omega_{zm} \rightarrow$		CONTRIBUTES TO NON NORMAL ENTRY AND EXIT (ALSO SAME AS $\Delta\alpha$)
$\Delta\alpha$		DUE TO ION SOURCE AXIS MISALIGNMENT ADD TO α IN ABERRATION EQUATIONS WHICH INCLUDE α
$\Delta\xi$		DUE TO ION SOURCE AXIS MISALIGNMENT ADD TO ξ IN ABERRATION EQUATIONS WHICH INCLUDE ξ. ALSO ADDS TO GAP REQUIREMENT. MUST BE HELD TIGHT.
$\Delta\phi$		

FIGURE 4-3
Summary of Misalignments

In order to evaluate the above expressions, the following relations are used:

$$M = \left|\cos\phi - n_i \sin\phi\right|$$

$$K_2 = \left|1 - \cos\phi + n_i \sin\phi\right|$$

$$n_i = \frac{1 + n_o \cot\phi}{n_o - \cot\phi}$$

$$g = \cos(\tan^{-1} n_i) / \cos(\tan^{-1} n_o)$$

The numbers required to evaluate the above equations are:

S_o = 0.0307 cm, $\Delta V/V$ = 3/225 $\approx$ 0.0133

Z = 0.203 cm, h = 0.0614 cm $h_c \approx$ 0.250 cm

(Note: h_c is actually the beam width at the collector)

ψ = 0.0075

$\Delta m/m$ = 1/18 for m/e 18 (resolve m/e 17 and 18)

= 1/10 for m/e 28 and m/e 32 (resolve m/e 28 and 32)

= 1/10 for m/e 44 (resolve m/e 40 and 44)

α = 0.80°, $\Delta\alpha$ = 0.1°, ξ = 0.8°, $\Delta\xi$ = 0.1°

All analyzer Δx, Δy and Δz = 0.002" $\approx$ 0.005 cm

Δx_m and Δy_m = 0.005" $\approx$ 0.012 cm

All analyzer $\Delta\omega$ = 1°.

Do not assume that $\Delta\omega_{zm}$ causes an additional displacement of the magnet boundary.

It was felt that the image distance for m/e 44 was excessive, and therefore in order to fit in with the desired configuration x was reduced from the optimum value of 7.10 cm to the desired value of 4.50 cm which makes n_1 = 1.257. The primary result of doing this is to create an α aberration.[1] The contribution to beam width due to this aberration is 0.0530 cm.

The results of the numberical evaluation of the above parameters are given in Table 4-3. It is seen that in all cases, the actual beam width is less than the required beam width and therefore the design is adequate.

TABLE 4-3

Mass to Charge Ratio	m/e	18	28	32	44
Angle through Magnetic Sector	ϕ	104.5°	90°		78.3°
Radius in Magnetic Sector	r_o	2.30 cm	2.86 cm	3.06 cm	3.59 cm
Object distance/radius	n_o	1.247	1.000	0.935	0.796
Image distance/radius	n_i	0.450	1.000	**	1.257*
Image distance	X		2.86 cm		4.50 cm*
Magnification	M	0.685	1.000		1.027‡
Energy aberration factor	K_2	1.685	2.000		2.2027‡
Image Width	MS_o	0.0214 cm	0.0312		0.0321‡
Energy Aberration	A_β	0.0258	0.0381		0.0486‡
Image Curvature aberration	Z^2/r_o	0.0180	0.0145		0.1115
$r_o \alpha^2$ aberration	A_α	0.0008	0.0007		0.0008
$r_o \xi^2$ aberration	A_ξ	0.0002	0.0003		0.0004
Alpha Aberration due to misalignment		0.0060	0.0074		0.0530†
$\alpha\beta$ Aberration (Estimate)		0.0020	0.0020		0.0020
Beam width		0.0742 cm	0.0942 cm		0.1484cm
Required beam width	β	0.0761 cm	0.2143 cm		0.3193cm
Magnet gap (Total)	2Z	0.4000 cm	0.4000 cm		0.4000cm

*Not optimum value

‡For non-optimum value of n_i

†$r_o \alpha$ aberration due to non-optimum n_i

**Values were not calculated for m/e 32 because they are similar to m/e 28

There are some other less important effects such as aberration due to non-normal exit of the ion beam, Z axis focusing due to non-normal exit of the ion beam, and pre-bending and post-bending of the ion beam due to the action of the fringe field which have also been considered. In addition, the improvements associated with a normal circle magnet design were investigated. This information is given in Appendices G, H, I, and J.

In conclusion, it can be stated that the proposed design parameters given in Table 4-3 lead to an acceptable solution.

4.1.6 ANALYZER MAGNET DESIGN

An appreciable portion of the analyzer weight is accounted for by the permanent magnet. Therefore it is necessary to do a preliminary magnet design in order to determine an approximate weight. This was accomplished using the best available design equations. These equations were checked by applying them to an existing magnet and found to be reasonably accurate. In addition, an approximate weight was obtained by scaling the same existing magnet. These two techniques gave results within about 12%. The highest value was then used for the magnet weight. This was 0.9 pound. The magnet material used for this calculation was Alnico V. Other materials were examined, but were found to be unacceptable for one reason or another. The calculations and discussion of other magnet materials are given in Appendix A. The final magnet design is shown in Figure 4-4.

A parallel effort was required on the magnet design and therefore the magnet gap of .537 cm which was used for the magnet calculations is not in agreement with the required value of .400 cm. Reducing the gap to this value will give a weight reduction. This improvement was not reflected in the weight breakdown in Table 5-2.

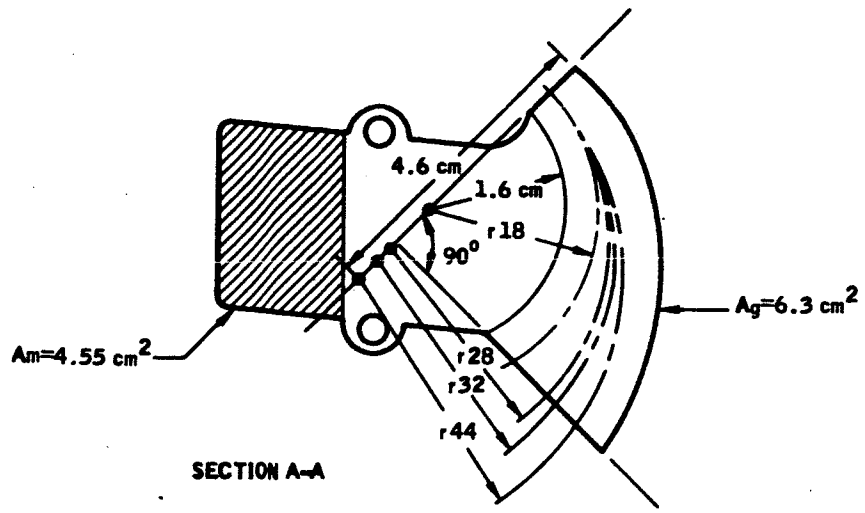

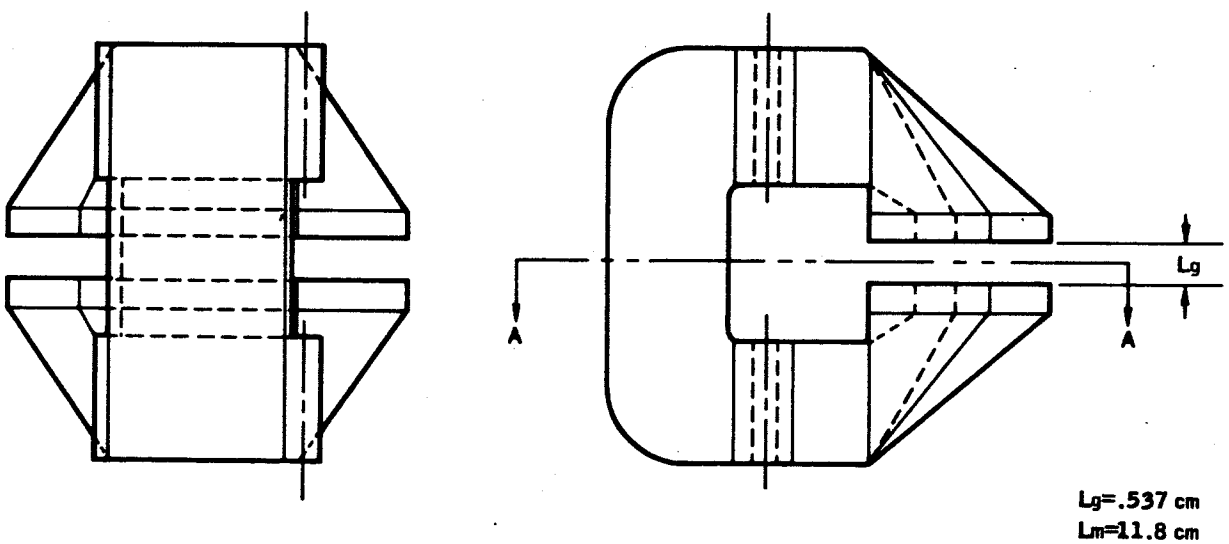

FIGURE 4-4
Analyzer Magnet Design

4.2 ION SOURCE

4.2.1 ELECTRON GUN AND IONIZING REGION

The ion source performs the important function of ionizing the sample gas, focusing the resulting ions, and transmitting an ion beam with narrowly defined properties to the analyzer. The ion beam consists of positively charged particles, which are directly proportional to the admitted sample gas pressure. The mass resolving analyzer separates the ion beam by the mass-to-charge ratios which are consequently proportional to the partial pressures of their corresponding sample constituents.

The most common technique of ionization used in mass spectrometry is electron bombardment. Other techniques such as alpha bombardment or photo ionization are not acceptable due to a low cross section for ionization.

The most common source of electrons for an electron bombardment ion source is a hot wire filament. Other techniques such as an indirectly heated cathode, cold cathode, field emission, electron multiplier, radioactive sources, and tunnel emission have been or might be employed; however, they are found to be unsatisfactory for a variety of reasons. Attention is therefore restricted to the hot filament emitter.

In the hot filament emission system, an electron beam is formed from thermionically emitted electrons off a heated filament. The types of filament materials are constantly under investigation, and this is covered in Section 4.7 of this report. The electrons in the beam collide with the neutral gas particles, and some collisions produce positive ions which are extracted from the ionizing region by an electrostatic field, focused, and transmitted to the analyzer region.

That part of the ion source, and, in fact, of the entire analyzer, which has the least reliability is the filament. This results from the fact that efforts to reduce the filament power have pushed filament wire diameters down to smaller and smaller values. Filaments as small as 0.001 inch in diameter have been used.

Rather than go back to larger diameters in order to gain reliability, it seems that a better method is to add a second filament to gain redundancy. It is believed in this way that a reasonable compromise can be achieved between filament power and reliability. The possibility of in-flight replacement of filaments is ruled out for several reasons. First, it requires venting the analyzer which can lead to contamination and pump down problems. Second, alignment is very critical and it would be difficult to locate the second filament in exactly the same position as the first. In this case, retuning the electron gun would be necessary which would be very time consuming and possibly not within the capability of the astronauts.

Considering various types of dual filament ion sources has led to three types which appear to be the most promising. These are:

a. Movable filaments mounted with a detent so that a new filament can be moved into the position occupied by the old one.

b. Two filaments mounted very closely together and utilizing the same focusing structure to form the electron beam.

c. Two orthogonal electron guns. This system would have not only dual filaments but dual focusing structures.

The approach which is selected will necessarily have an effect upon the ion source design and therefore these alternates must be discussed in detail before the ion source configuration can be determined.

The movable filament technique would require two filaments to be mounted on a movable structure within the ion source housing. The linear motion required to replace the filament is transferred through the ion source housing by a shaft mounted on a flexible bellows. The filament assemblies will have to be tightly constrained so that only the prescribed translational motion results. Three problems are discussed below:

a. The bellows does provide an additional seal or weld point with the possibility of a leak.

b. The connections to the filament may have to be made with OFHC copper wire. The bending of the wire when the filament is moved will cause hardening of the wire which ultimately leads to fracture. This problem has been experienced in the past, along with the fact that the failure rate of electrical connections is much higher for wires which are moved after original seating due to increased stress on the spot welded connections. Obviously, this type of connection would be involved with the filament shield and electron focus electrodes.

c. Lubrication between the movable filament assembly and the confining structure could be a problem. Otherwise a more complex and bulky structure utilizing rolling sapphire or ruby balls might be used.

It is very difficult to mount filaments in exact locations and have them stay permanent. Typically, a spring is required to take up the slack in the filament as the wire expands upon heating. The use of the spring increases the difficulty of making an accurate location. Therefore, it becomes apparent that the electron beam focal structure will have to be varied in some way to compensate for the change in position. This implies a change in voltages of the focal electrodes.

Another factor to be considered is that in some instances when the filament burns out, insulating oxide deposits are left on the surrounding electrodes. These can cause instability in the electron gun operation if subsequent electrons strike these surfaces and charge them. In order to avoid this, each filament should be surrounded by its own surfaces. This implies that the electrodes nearest the filament be duplicated. This also aids in minimizing the problems of compensating for filament position, since all electrodes can be connected and switching of voltages is not required. On the other hand it becomes clear that a great deal of duplication is being required.

Since this is the case, it seems logical to extend this philosophy to its obvious conclusion. This is to have two complete electron guns mounted in fixed positions, thus eliminating the problems associated with moving the filament. The type of ionizing region which is considered for use in this system is ideally suited for two electron guns mounted at right angles. A conceptual design of this configuration is shown in Figure 4-5. A cross-section of the ionizing region is shown in Figure 4-6. This figure shows a design which is being studied on another contract. It is likely that a less complex structure will be acceptable for this task.

It should be noted that the filament mounting alternative (b) can be dispensed with, as implied in the discussion concerning charge up of surface deposits and the importance of exact location which have already been given.

Electron bombardment ion sources utilizing filaments can generally be classified into two categories; magnetic and nonmagnetic. In the magnetic ion source the magnetic field is employed to constrain the electron beam against the force of the ion extraction field. A magnetic ion source would not be compatible with the proposed dual filament approach since it would be difficult to design a magnetic field to constrain two orthogonal beams. A second problem with magnetic ion sources is that they cause mass discrimination in the ion source which causes loss of sensitivity on the low mass ions. This effect will be pronounced in an ion source with small focusing apertures such as the one which must be used (This will be discussed later in this Section.). Also if helium were used as the diluent gas in the cabin, the problem would become severe.

A third problem with the magnetic ion source is that while the magnetic field constrains the electron beam it does not actually focus it. As will be shown, the ion source conductance must be made relatively small in order to achieve a high differential pumping ratio. Therefore the slot through which the electron beam must pass is necessarily small. This implies a degree of focusing which is not possible with the use of a magnetic field.

For these reasons a non-magnetic ion source is the best choice for this instrument. Non-magnetic ion sources have been successfully used in applications where low ion source conductances were required. An existing ion source has been capable of delivering 50 μa of ionizing current through a rectangular slot 0.010 inch by 0.080 inch.

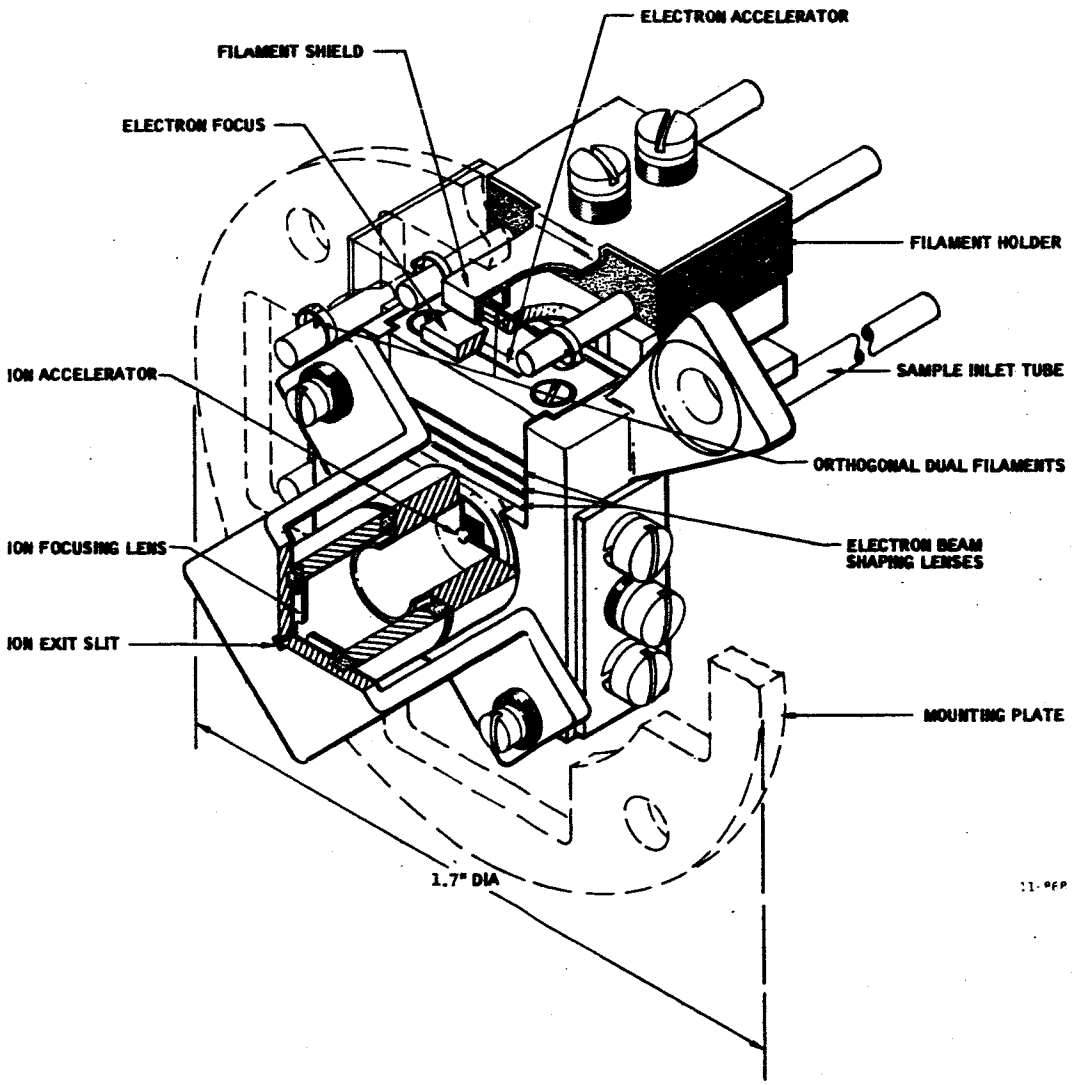

FIGURE 4-5
Dual Filament Ion Source

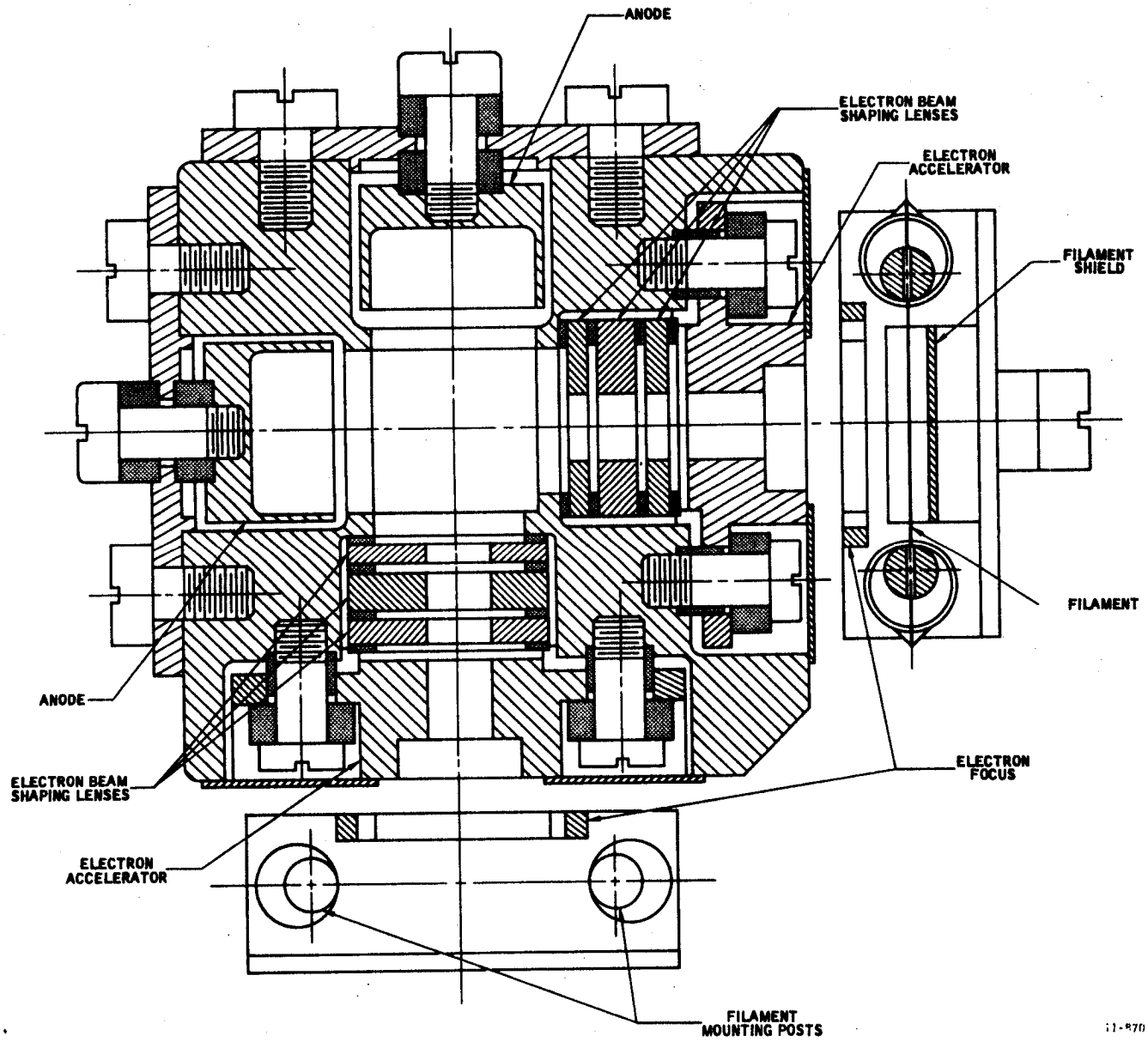

FIGURE 4-6
Dual Filament Non-Magnetic Ion Source

As mentioned previously, a non-magnetic ion source can only be used when the gradient in the ion source is low. Fortunately this is a desired feature for this instrument since the ion energy spread must be small. (A value of 3 V has been assumed in the analysis of the analyzer.) This is largely assured by having a low gradient in the ionizing region. There is a limit to how low the gradient can be, since at low levels ion space charge can affect the spacial voltage distribution, thereby charging the ion focusing and consequently the exit ion current density. This phenomena has been treated by W. M. Brubaker[10]. He defines a critical pressure given by:

$$P_c = \frac{3}{4dS} \left(V_r \, m/a \, V_e M \right)^{\frac{1}{2}} \qquad (1)$$

where

P_c = critical pressure (torr)

V_r = repeller to accelerator voltage (volts)

m = electron mass (Kg)

a = fraction of the repeller-accelerator distance at which the ionizing beam is located

d = repeller-accelerator distance (meters)

V_e = ionizing electron energy

M = ion mass (Kg)

S = number of ion pairs formed per electron per meter of electron path length at a pressure of 1 torr.

Letting V_r = 8 volts (for reasons to be established in Section 4.2.2), a = 0.5, d = 0.100 inch, V_e = 70 V, M = ion mass for m/e 44 (which is a worst case), and the sensitivity for N_2 with 70 V ionizing electrons, gives a critical pressure of 1×10^{-3} torr;

Then from Figure 4-7, which is reproduced from Brubaker's paper, the space charge depression can be determined. For an ionizing current of 50 μa, the ion space charge depression of the space potential is seen to be approximately 10% for the maximum ionizing region pressure of 2×10^{-4} torr. Ion focusing considerations show that effect due to this should be small. Therefore the assumed values can be used.

10 Brubaker, W. M., Influence of Space Charge on the Potential Distribution in Mass Spectrometer Ion Sources, J.A.P., Vol. 26, pg. 8, Aug. 1955.

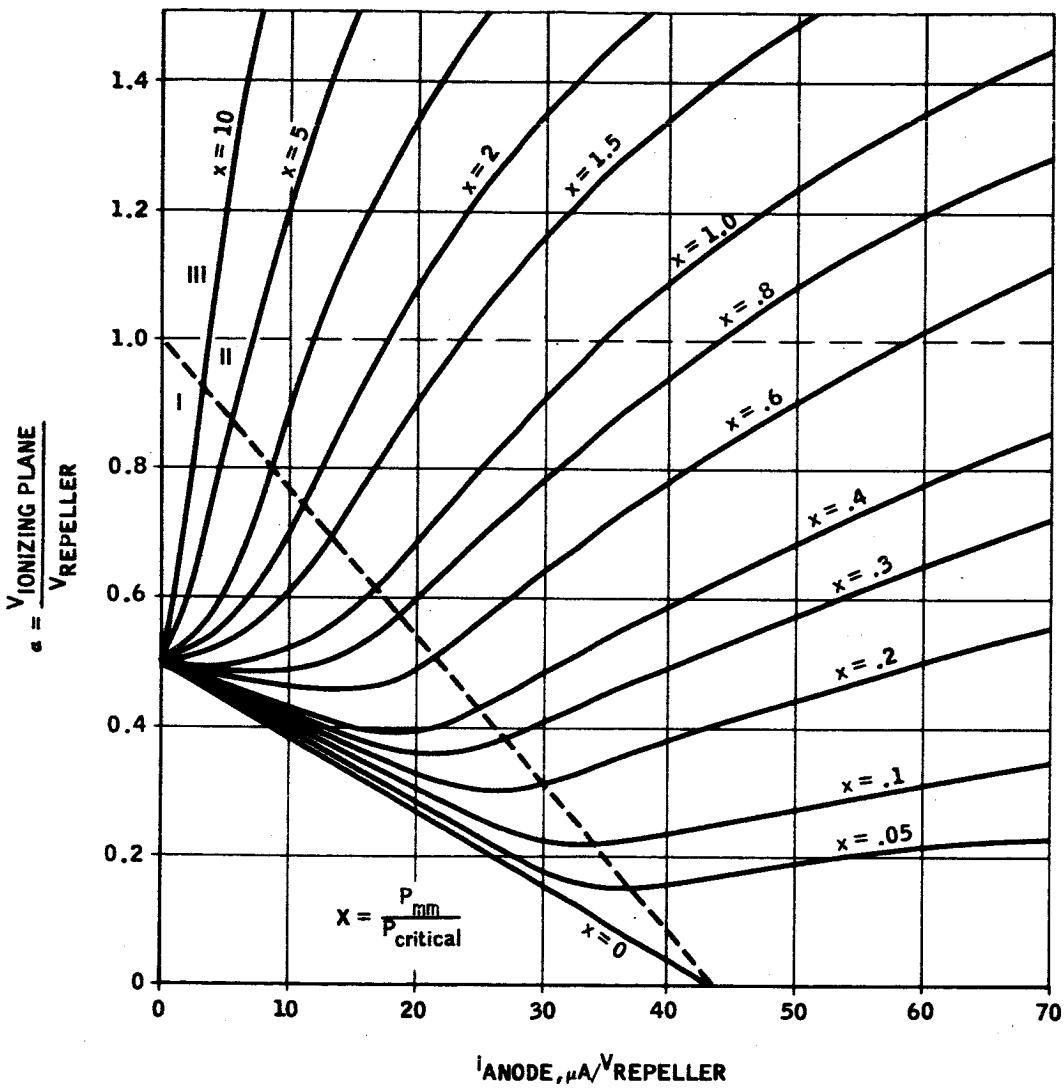

FIGURE 4-7
Potential of Ionizing Region as
a Function of i_V

If the potential across the ionizing region is 8 V and the thickness of the ionizing region is 0.100 inch, the gradient is 80 V/inch. If the electron beam is 0.010 inch thick where it enters the ionizing region and no spreading or bending takes place the energy spread across the beam would be 0.8 V. This is much less than the allowed value of 3 V. Next, then, beam spread and bending must be considered.

The electron beam spread can be approximately determined by use of a normalized space charge spread curve[7]. Several factors must be considered. While the desired electron beam energy is 70 V the beam must be accelerated to about 350 V in order to have an acceptable electron beam transmission efficiency through the low conductance aperture. Therefore the distance over which the electrons have the lower velocity is significantly reduced. In addition the electron beam shaping lenses (See Figure 4-7) will give the electron beam an initial convergence. Furthermore, where a 50 microamp electron beam has been considered previously it will be approximately 25 microamps due to a reduction in the electron accelerator slit width from 0.080 inch to 0.040 inch as dictated by differential pumping considerations. Applying these factors gives an expected beam spread of approximately a factor of two giving an electron beam energy spread of about 1.6 V.

Now the electron beam bending must be considered. This is done by assuming a uniform field to exist between the repeller and accelerator. If the central electron ray enters normal to this field it will experience a deflection given by

$$Z = \frac{1}{4} \frac{E}{V_o} r^2 \qquad (2)$$

where

Z = deflection
E = gradient
V_o = electron energy
r = distance at which the deflection is measured

When $r = 0.100$ inch, $E = 80$ V/inch and $V_o = 70$ V, Z is found to be less than 0.003 inch. This is definitely a worst case value. This corresponds to a voltage difference of .24 V, but only part of this variation occurs over the accelerator aperture. Then the total electron beam spread is less than 2 V. The calculations carried out have been sufficiently approximate to warrant the assumption of a 3 V energy spread as done in the analyzer optimization.

The third force which affects the electron beam is a focusing action which occurs as the electron beam enters and exits the ionizing region. This is caused by the action of the leakage field from the anode and the last electrode in the electron gun. This has been briefly investigated and the results indicate that the focusing actions can be used to advantage in reducing the electron beam thickness. The preliminary indications are that the electron beam shaping lenses, shown in Figure 4-6, can be eliminated. This is a highly desirable simplification.

It is important to consider the stability of the electron beam as a function of electrode voltages. This is difficult to do for the electron gun and shaping lenses until the design has been carefully worked out. Some feel for the problem can be gained by looking at the variation in the electron

7 O. Klemperer, Electron Optics, Cambridge Press, page 203

beam deflection as a function of the repeller-accelerator voltage difference. Substituting $E=V_r/d$ into Equation (2) and differentiating with respect to V_r gives:

$$\frac{dZ}{DV_r} = \frac{1}{4} \frac{V_r}{V_o} \frac{r^2}{d} \tag{3}$$

For the same values used above this gives a value of less than 0.002 in./V. V_r can easily be regulated to 1% giving a positional change of less than 0.0001 inch, which can be ignored.

The use of differential pumping has been mentioned quite frequently in the discussions thus far, and it is useful to see why it is important.

Differential pumping requires that the pressure in the ionizing region be high compared to the pressure in the analyzer. It is not necessary to maintain the entire source at this elevated pressure, and in fact, it is best to confine the high pressure to only the volume of the ionizing region.

One of the principal reasons for this is the reduction of sample distortion due to interaction with the filament. The interaction which is of most importance is that which converts O_2 to CO thereby reducing the m/e 32 peak and increasing the m/e 28 peak. The pumping processes involved can be represented as shown in Figure 4-8.

Considering the samples independently; for O_2:

$$Q_{O_2} = C_{in} p_o^{(O_2)} = \left(p_s^{(O_2)} - p_a^{(O_2)}\right) C_s = p_a^{(O_2)} (S_{O_2} + S_p)$$

This gives:

$$p_s^{(O_2)} = \frac{C_s + S_p + S_{O_2}}{S_p + S_{O_2}} \frac{C_{in}}{C_s} p_o^{(O_2)} \tag{2}$$

For CO:

$$Q_{CO} = 0 \,, \quad p_s^{(CO)} = p_a^{(CO)} \text{ and } p_a^{(CO)} = \frac{S_{CO}}{S_p} pa^{(O_2)} \tag{3}$$

Assuming that one O_2 molecule gives rise to two CO molecules then

$$S_{CO} = 2S_{O_2} \text{ and } p_s^{(CO)} = \frac{2S_{O_2}}{S_p} \frac{p_s^{(O_2)}}{D'} \tag{4}$$

where

$$D' = 1 + \frac{S_p + S_{O_2}}{C_s} \tag{5}$$

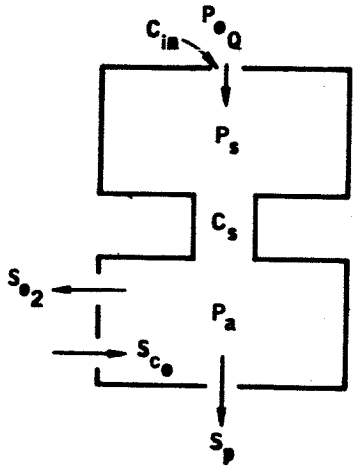

P_o = SAMPLE PRESSURE
P_s = IONIZING REGION PRESSURE
P_a = ANALYZER AND FILAMENT REGION PRESSURE
C_{in} = INLET LEAK CONDUCTANCE
C_s = ION SOURCE CONDUCTANCE
S_p = SPEED OF PUMP
So_2 = SPEED OF O_2 PUMPING DUE TO CO CONVERSION
S_{co} = SPEED OF CO PRODUCTION
Q = FLOW

FIGURE 4-8
Ion Source Pumping Diagram

Experimentally it was found on a small quadrupole mass spectrometer with a rhenium wire filament, with no differential pumping, and a pumping speed of 150 cc/sec, and for 50-50 N_2–O_2 sample that the m/e 28 peak was approximately twice the amplitude of the m/e 32 peak. If this entire effect is attributed to an interaction with the filament and the surrounding electrodes, then the following analysis is valid.

The experimental results are represented:

$$p_s^{(N_2)} + p_s^{(CO)} = 2\, p_s^{(O_2)} \tag{6}$$

No differential pumping appears as infinite ion source conductance, hence

Equation 6 becomes:

$$\frac{C_{in}\, p_o^{(N_2)}}{S_p} + 2\,\frac{S_{O_2}}{S_p}\;\frac{C_{in}\, p_o^{(O_2)}}{S_p + S_{O_2}} = 2\,\frac{C_{in}}{S_p + S_{O_2}}\; p_o^{(O_2)} \tag{7}$$

Solving Equation 7 gives $S_{O_2} = 1/3\ S_p = 50$ cc/sec.

Now for a differential pumping ratio of 100, i.e., $D = 1 + S_p/C_s = 100$ and assuming $C_s = 35$ cc/sec (which has been calculated for the dual filament ion source) then $S_p = 3.46$ liters/sec.

From Equation 2

$$p_s^{(O_2)} = 1.012\;\frac{C_{in}}{C_s}\; p_o^{(O_2)} \tag{8}$$

If there were no filament interaction then $p_s^{(O_2)} = \frac{C_{in}}{C_s}\; p_o^{(O_2)}$. There is therefore only about a 1% effect. If this effect remains relatively constant, then the error due to filament interaction can be reduced well below 1% by calibration. The value of differential pumping is then readily apparent. Further, if an ion pump were required on the system rather than the utilization of free space as a pump, differential pumping of the source is also helpful, since it will cause a minimization of preferential gas pumping from the source by the ion pump, thus insuring that the sample in the source would never build up a large partial pressure of a gas having a relatively low pumping speed.

Another factor in ion source design is its time response. The time response of an ion source is defined by

$$\tau = V_S/F_S$$

where

V_S = volume of the source

V_S = conductance out of the source

For the orthogonal non-magnetic ion source,

$$V_S < 3 \text{ cc.}$$

From the requirement for the differential pumping of the source it is shown that

$$F_S = 34.7 \text{ cc/sec}$$

Therefore, the source time constant is

$$\tau < 8.75 \times 10^{-2} \text{ sec,}$$

which is substantially less than the overall system response, and therefore acceptable.

Magnetic fringe fields from the analyzer magnet acting in the ionizing region of the source can cause deflection of the electron beam. This effect will be much more severe than any mass discrimination which might also arise. The effect of the analyzer magnet on this region, however, can be greatly reduced by placing magnetic shielding around the ion source housing. From magnetic field measurements of an existing larger magnet of the same general configuration, and by scaling down the gap to area ratio and the distances, it is estimated that the magnetic field in the ion focusing region should be approximately 10 gauss. By placing a .031 inches thick shell of Armco iron around the housing and using an expression for a spherical shell:

$$\alpha \cong \frac{1}{3} (3 + 2 Kt) *$$

* Author - Schweizer, Fred. Magnetic Shielding Factors of a System of Concentric Spherical Shells, J. of Applied Physics, Vol. 33, No. 3, March, 1962.

where

α = the shielding factor = flux density outside/flux density inside

K = the permeability of Armco iron, 1000 in a 10 gauss field

$t = 1 - (R_i/R_o)$

R_i = inner radium of the shell

R_j = outer radius of the shell

Using this relationship, then

$\alpha \cong 21$

and thus the magnetic field in the source due to the analyzer fringe field should reduce to approximately ½ gauss. This degree of magnetic fringe field is acceptable in so far as electron beam deflections are concerned.

In order to be sure that such a limitation does not exist in this case, it is necessary to consider the detailed design of a perfect imaging focal system. Even though a somewhat idealized configuration was assumed the calculation is quite lengthy and therefore it is found in Appendix B.

The results of this calculation indicate that the length of the ion focusing system is 0.645" which is acceptable. The constraints such as an ion energy of 225 volts, an ionizing region difference voltage of 8 volts across 0.1", a magnification of 1.75, and a theoretical exit angle of 0.40 were met. Another calculation (not given) indicated that the effect of the electron beam spread was tolerable leading to an increase in angle of less than 0.4° so that the total angle is less than the required 0.8°. A margin still remains for other aberrations. Experience with this type of focal system substantiates these numbers.

4.2.2 ION FOCUSING SYSTEM

There are two principal types of ion focusing systems used in ion sources. They are perfect imaging focusing, and thermal energy focusing. In a perfect imaging system the initial conditions imposed on the ions for their entry into the magnetic sector of the analyzer can be projected from the ion source exit aperature to the ionizing region by the use of Abbe's law. These conditions are discussed in Section 4.1.5.

A thermal energy focusing system generally focuses the ion beam to a crossover point at the exit slit of the source. Thus, the sensitivity of the ion source is dependent upon the ion source temperature, and can change as the source temperature changes. A change in the focal point of the source can then change the initial conditions of the ions into the analyzer. For systems

which require strict tolerances on their initial conditions, it has been necessary to limit the incurable aberrations in thermal focusing systems by geometrical means. Nevertheless, the sensitivity of the source must still be dependent on the ion source temperature. The considerations in Section 4.1.5 also showed the perfect imaging type of ion source to be unacceptable for other reasons. A perfect imaging focusing system utilizes a crossover of the beam to a given magnification before it exits from the source. A practical limitation on the use of perfect imaging systems has been the long focal lengths required in order to match the source conditions to those of the analyzer.

4.3 ATMOSPHERIC SAMPLING

The sampling of the atmosphere is an important factor in determining the ultimate performance of the sensor system. Sampling is accomplished by a continuous-flow inlet system which serves the function of transporting a small but representative quantity of the atmospheric gas to the mass spectrometer ion source which is at a pressure 10^{-6} times that of the cabin.

In some cases the appropriate sample is available at the instrument location. However, it is assumed in the following discussion that, due either to a remote instrument location or to the need for monitoring several locations or suit loops etc., a flexible "sniffer" line as long as two meters may be required. Multiple lines in parallel are also possible in order to obtain a more representative sample. The transport time of a long line is compared with transport by air circulation.

The key variables of the sampling system are the quantity of gas consumed, the time taken to produce a change in gas composition in the ion source of the mass spectrometer after a change in the original mixture, and the accuracy of the composition in the ion source. Size, weight, heating power (if required) and reliability are also factors in the design.

While the inlet and sampling system introduce time and accuracy factors, the performance and design are, except in the fastest response-time problems, separable from the basic analyzer design. This fortunate characteristic is due to the fact that the time constants of gas flow in the ion source and the flow of ions are generally short and not a function of the inlet system, the large pressure drop from the inlet system to the ion source precludes any upstream reflection of flow characteristics, and the inlet leak can, in principle at least, be set to any desired flow for ion chamber pressure.

The time constant of the sensor system is a result of the following three significant time factors which are additive and non-interacting.

a. The sample transport time Δt_g.

b. The ion source time constant $\tau_s = \frac{V_s}{S_s}$, where V_s is the ion source value and S_s, the pumping speed out of the ion source.

c. The time constant, τ_a, of the ion current amplifying system.

The sample delay time is often the dominant time factor and will be discussed in this section.

4.3.1 GENERAL INLET SYSTEM CHARACTERISTICS

It is important to first establish the nature of flow into the mass spectrometer necessary for accurate analysis. The three types of flow to be considered are molecular flow; viscous, non-critical flow, and viscous, critical

flow. Briefly stated, it is necessary that the flow into the spectrometer be molecular in nature in order to accurately analyze a variable pressure, variable mixture sample. This will be shown in Section 4.3.2.

The conventional design of a continuous sampling inlet system utilizes a viscous flow divider to reduce the atmospheric pressure, P_0, to an intermediate pressure P_1, where it is convenient to introduce the sample into the spectrometer by molecular flow. It is essential for accurate results that the viscous channel have the same flow characteristics up-stream and down-stream from the sampling point. Having common dependency upon such variables as temperature, T, viscosity, η , and pressure allows one to maintain P_1 and P_0 in a constant ratio and these points with identical compositions.

Until recently, the chief design conflict has been in placing the sampling point at low enough pressure in the viscous channel that practical molecular leaks could be made and yet at high enough pressure to assure viscous type flow down-stream. This conflict arises because the mean-free-path, λ, must be greater than D_L, the leak hole diameter for molecular flow and at the same time $\lambda << D_2$ (where D_2 is the diameter of the downstream channel) for viscous flow. This leads to surprisingly large channel diameters when conventional molecular leaks are used.

Several new developments by SDS Data Systems now allow the design of the inlet system to be considered in broader terms. Two types of molecular leaks for pressures approaching atmospheric have been successfully tested. In addition, the viscous flow theory has been extended to cover tapered flow channels where it is found that shorter sample time delays can be achieved for a given performance and line length. This has been coupled with the concept of using a critical orifice to terminate the downstream flow channel and avoid the large diameter lines otherwise indicated.

It is now possible to consider the logical development of an inlet system using any of the following techniques: The sample must be transported from an origin to the inlet leak and the driving force for this transport may be the pressure difference between the origin and the mass spectrometer vacuum system, between the origin and a second available vacuum system, between the origin and a separate circulating pump, or by uncontained flow with a circulating fan. Much of the choice among these methods will rest with availability of the elements required although sampling time and reliability will be found to be important factors. These will be discussed in the following text.

4.3.2 CHARACTERISTICS OF FLOW

Several useful types of flow are considered here from the point of view of direct flow into the mass spectrometer and as a general definition of the consideration to be made.

It is apparent that if molecular flow could be achieved directly from the atmosphere, the inlet flow problem would reduce to only a temperature measurement. The number of molecules passing through an aperture A cm^2 per unit time is

$$Q_i = \frac{n_i \bar{c}_i A_i}{4} \text{ molecules/seconds,} \quad (1)$$

where

n is the density in molecules/cc,

subscript i refers to inlet, and

$\bar{c} = \left(\frac{8kT}{\pi m}\right)^{\frac{1}{2}}$ is the mean molecular speed in cm/sec.

If this flow takes place directly into the ionizing region of the mass spectrometer and the flow out of the source is molecular, then

$$Q_s = \frac{n_s \bar{c}_s A_s}{4} = \frac{n_i \bar{c}_i A_i}{4} \text{ molecules/second} \quad (2)$$

or the source density for each species is

$$n_s = \frac{A_i}{A_s} \left(\frac{T_i}{T_s}\right)^{\frac{1}{2}} n_i \text{ molecules/cc} \quad (3)$$

Thus if the mass spectrometer is accurately calibrated as a function of molecular density (equivalent to partial pressure), the density of each species in the atmosphere is known by a knowledge of the temperature ratio T_i/T_s.

Viscous, non-critical flow may be achieved through a single narrow channel or through a multiplicity of channels such as in sintered materials. The single channel is sufficient to define the characteristics. For isothermal flow in a long constant-diameter capilliary channel, the boundary layer thickness grows rapidly and in approximately 8 diameters fills the opening at the entrance. When the intake region is a negligible part of the channel, the flow can be expressed as

$$Q_i = \left(\frac{1}{kT}\right) \frac{a_i^2 \left(P_1^2 - P_2^2\right)}{16 \eta \ell} A_i \text{ molecules/second,} \quad (4)$$

where:

Q_i = inlet flow (molecules/second)

$k = 1.38 \times 10^{-16}$ ergs/molecule/^oK

T = temperature (^oK)

a = radius of the capillary (cm)

P_1 = inlet pressure (dynes/cm^2)

P_2 = exit pressure (dynes/cm^2)

η = viscosity of mixture (poise)

ℓ = capillary length (cm)

A = capillary cross section (cm^2)

For direct flow into the spectrometer $P_1 >> P_2$ and P_2 is neglected. Converting to density, $P_1 = n_i kT_i$ and thus,

$$Q_i = \frac{a_i^2 \, n_i^2 \, A_i \, kT_i}{16 \, \eta \ell} \tag{5}$$

From (2) and (5), assuming equal flow into and out of the source,

$$n_s = \frac{a_i^2 \, kT_i}{4C_s \, \eta \ell} \left(\frac{A_i}{A_s}\right) n_i^2 \text{ molecules/second} \tag{6}$$

First it is observed that the density in the ionizing region increases as the square of the external density. Thus, a wider dynamic range of operation is required, for a given range of inlet densities. Secondly, the flow is a function of viscosity which is a complex empirical relationship depending upon the gases, temperature, and mixture. The chief difficulty here is that a pure gas calibration has little meaning when that gas is to be analyzed in a mixture. Due to these factors, it is virtually impossible to analyze a mixture except by post-synthesis.

Thus, it is clear that regardless of the techniques used to transport and reduce the inlet pressure (while preserving the accuracy of the composition) The flow into the mass spectrometer should be molecular in nature.

It is also easily shown that direct viscous flow into the system is undesirable as a means of transport over any great distance. From the continuity equation and since molecules in this case are neither destroyed or created,

$$Q = n_1 \, v_1 \, A_1 = n_2 \, v_2 \, A_2 \text{ molecules/second}, \tag{7}$$

where v is the transport velocity.

For typical system requirements we are in the range of 8 micron cc/second sample requirement or for air at room temperature approximately 2.7×10^{14} molecules/second.

If this sample is introduced directly into the source through a 2 meter long capillary tubing, the inside diameter of the tubing would be approximately

0.0032 centimeters and have an area of 8×10^{-6} cm^2. For an inlet molecular density of 1.4×10^{19} molecules/cc, the transport velocity at the inlet would be $2.7 \times 10^{14}/1.4 \times 10^{19} \times 8 \times 10^{-6}$ or 2.4 cm/second. Thus an inordinately long time would be involved in migrating along a 2 meter line.

On the other hand, the transport velocity in the molecular flow region (for instance at 2×10^{-4} torr) would be considerably greater. For instance, if a molecular leak could be used at the entrance of a two meter line having a cross-sectional inside area of 1 mm^2 the velocity would, under the above conditions, be $v = 2.7 \times 10^{14}/7 \times 10^{12} \times 10^{-2} = 3850$ cm/second. While this appears to be an attractive possibility, the increased surface area in close communication with the ionizing region and the reduced scrubbing effect of wall collisions at the low pressure is believed to preclude the use of this method for sampling condensibles such as water. Creation of this "memory" effect should be avoided if alternate methods are available.

The molecular flow and viscous flow Equations (1) and (4) can be obtained from the more general Knudsen flow equation[1] for round pipes. The conductance is given as

$$C = \left(\frac{\pi}{128} \frac{D^4 \bar{P}}{\eta L}\right) + \left(\frac{1}{6} \frac{2\pi kT}{m} \frac{D^3}{L}\right) \left(\frac{1 + \frac{m}{kT} \frac{K\bar{P}}{\eta}}{1 + 1.24 \frac{m}{kT} \frac{D\bar{P}}{\eta}}\right) \text{ c.g.s. units} \qquad (8)$$

where

D = Pipe diameter (cm), L = length (cm),

$\bar{P}$ = Average pressure = $(P_o + P_1)/2$ dynes/cm^2 and

where

$$Q = C\Delta P \text{ ergs/second} \qquad (9)$$

The first term represents pure viscous flow and the first bracket of the second term, pure molecular flow. The second bracket of the second term modifies the molecular flow equation (and is a function of viscosity) to represent the transition between the viscous and molecular regions.

We obtain a clear definition of the pressure region where pure molecular flow may be applied in the following manner. Knudsens equation is expressed as

$$C = \frac{1}{L}\left(aP + b \frac{1 + cP}{1 + fP}\right) . \qquad (10)$$

If L is considered to be an increment of length ΔL and since the flow Q is given by Equation (9), then

$$Q = \left(aP + b \frac{1 + cP}{1 + fP}\right) \frac{\Delta P}{\Delta L} \qquad (11)$$

---

[1] c.f., Any text on "Kinetic Theory of Gases" such as L.B. Loeb, McGraw-Hill, p. 295 ff (1934).

may be integrated[2] to provide

$$Q = \frac{1}{L}\left[\frac{a}{2}P^2 + \frac{bc}{f}P + \frac{b(f-c)}{f^2}\ln(1+fP)\right]_{P_2}^{P_1} , \qquad (12)$$

where P_1 is the entrance pressure P_2 the exit pressure and ln is the natural log. This equation covers viscous (non-turbulent) and molecular flow over wide ranges of pressure, channel length and diameter. This equation may be simplified, since $P_2 >> P_1$ in the cases to be considered, by letting the lower integration limit P_2 equal 0.

From the nature of the original equation, the coefficient (a) represents viscous conductance while the coefficient (b) represents conductance in the molecular flow region and (c) and (f) are coefficients effective in the transition region between viscous and molecular flow. Reforming (12),

$$QL = \frac{a}{2}P^2 + bP\left[\frac{c}{f}\left(1 - \frac{\ln(1+fP)}{fP}\right) + \frac{\ln(1+fP)}{fP}\right] \qquad (13)$$

or since the following are related numerically: $a = 0.029\ bf$ and $c/f = 0.807$; then

$$QL = 0.058\ bfP^2 + bP\left[0.807\left(1 - \frac{\ln(1+fP)}{fP}\right) + \frac{\ln(1+fP)}{fP}\right] \qquad (14)$$

Factoring bP and letting $fP = x$ and $bP = y$

$$QL = \left[0.058x + 0.807\left(1 - \frac{\ln(1+x)}{x}\right) + \frac{\ln(1+x)}{x}\right] y , \qquad (15)$$

where

$$x = fP = \left(\frac{m}{kT}\right)^{1/2}\frac{D}{\eta}P_1 \text{ (dimensionless)} , \qquad (16)$$

and

$$y = bP = \frac{1}{6}\left(\frac{2\pi kT}{m}\right)^{1/2} D^3 P_1 \text{ ergs/second in c.g.s. units.} \qquad (17)$$

As $x \to 0$, $\frac{\ln(1+x)}{x} \to 1$, and $QL = y$ which is equivalent to the molecular flow equation,

$$Q = \frac{\pi}{3}\left(\frac{kt}{2m}\right)^{1/2}\frac{D^3}{L}\Delta P \text{ ergs/second (c.g.s.)} . \qquad (18)$$

---

[2] c.f., Guthrie and Wakerling Vacuum Equipment and Technique, p. 191, McGraw Hill (1949) and Ochert and Steckelmacher, Brit J. App. Phys 2. 332 (1951)

Since, within the brackets of Equation (15) we have a function of viscosity and pressure which approaches the value 1 at low pressure, we may plot the deviation from molecular flow as a function of x = fP.

We let

$$\gamma' = \left[0.058\ x + 0.807\left(1 - \frac{\ln\ (1 + x)}{x}\right) + \frac{\ln\ (1 + x)}{x}\right] \qquad (19)$$

and plot γ vs x in Figure 4-9.

It is noted that up to $x \approx 1.6$ that the deviation from pure molecular flow is less than 1.5%. Thus for air at 20°C, the range

$$DP \leq 8.5 \text{ dynes/cm} \qquad (20)$$

may be considered to be molecular flow.

For direct molecular flow from the atmosphere the aperture or apertures must be quite small. As an example, for air at 100 torr the aperture length in microns is plotted against aperture diameter in microns with flow in micron-cc/second as a parameter in Figures 4-10 and 4-11. Multiple apertures may be used to achieve the desired total flow.

A summary of the conclusions to be reached at this point shows that of the four methods of transport; i.e.: 1) use of the mass spectrometer vacuum, 2) use of a second vacuum system, 3) use of a circulating pump, and 4) a circulating fan; the first may be eliminated on the basis of the previous discussion. The 2nd, 3rd and 4th remain sound methods of transport, however, the third is similar in analysis to the second and further depends upon additional equipment. Consequently, the second method will be considered further and compared to the fourth as a possible transport method.

4.3.3 OPTIMIZING THE VISCOUS FLOW CHANNEL

The general configuration of an inlet system utilizing a vacuum system to establish the driving force is shown in Figure 4-12. An atmospheric sample at a pressure, density, and temperature of P_o, n_o and T_o enters a viscous flow channel and drops to P_1 and n_1 at T_1 at the intermediate sampling point. A very small portion of the sample flows into the mass spectrometer through a molecular leak of conductance C_L while the bulk of the sample continues by viscous flow through the bypass line to a vacuum system at P_2, n_2 and T_2.

The advantages of this system are:

a. The transport velocity is relatively high due to the increased flow rate where >99% of the sample flows through the bypass line.

b. The ratio of flow and pressure to internal surface area is high which leads to rapid exchange with the wall and minimum time-delay due to absorption.

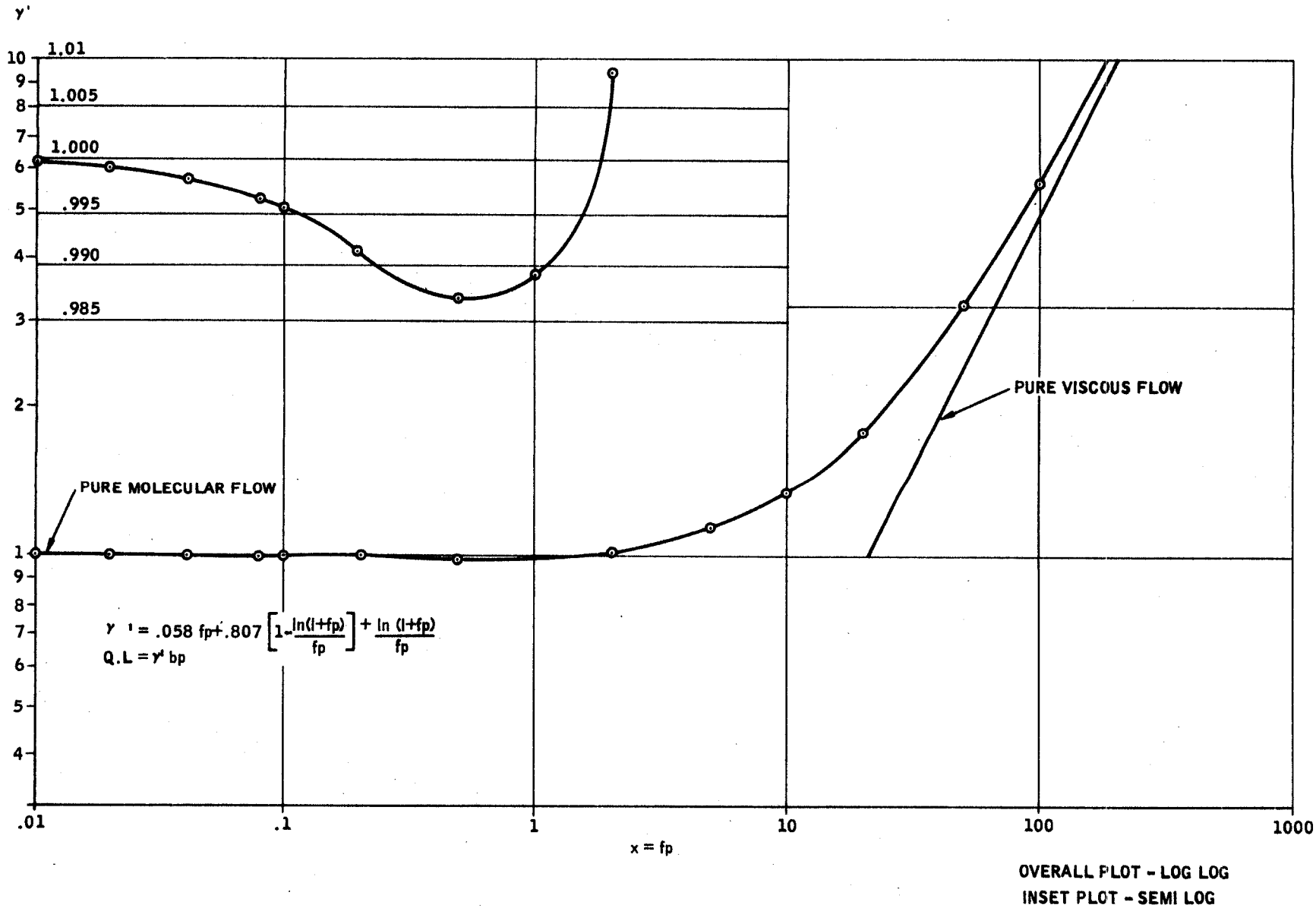

FIGURE 4-9
Plot of y vs x

$$Q\,L = 1.91\,D^4 + 9.170^3 + D^2 \ln 1 + 2.53D$$

FOR $P_a = 10^5 \mu$ Hg

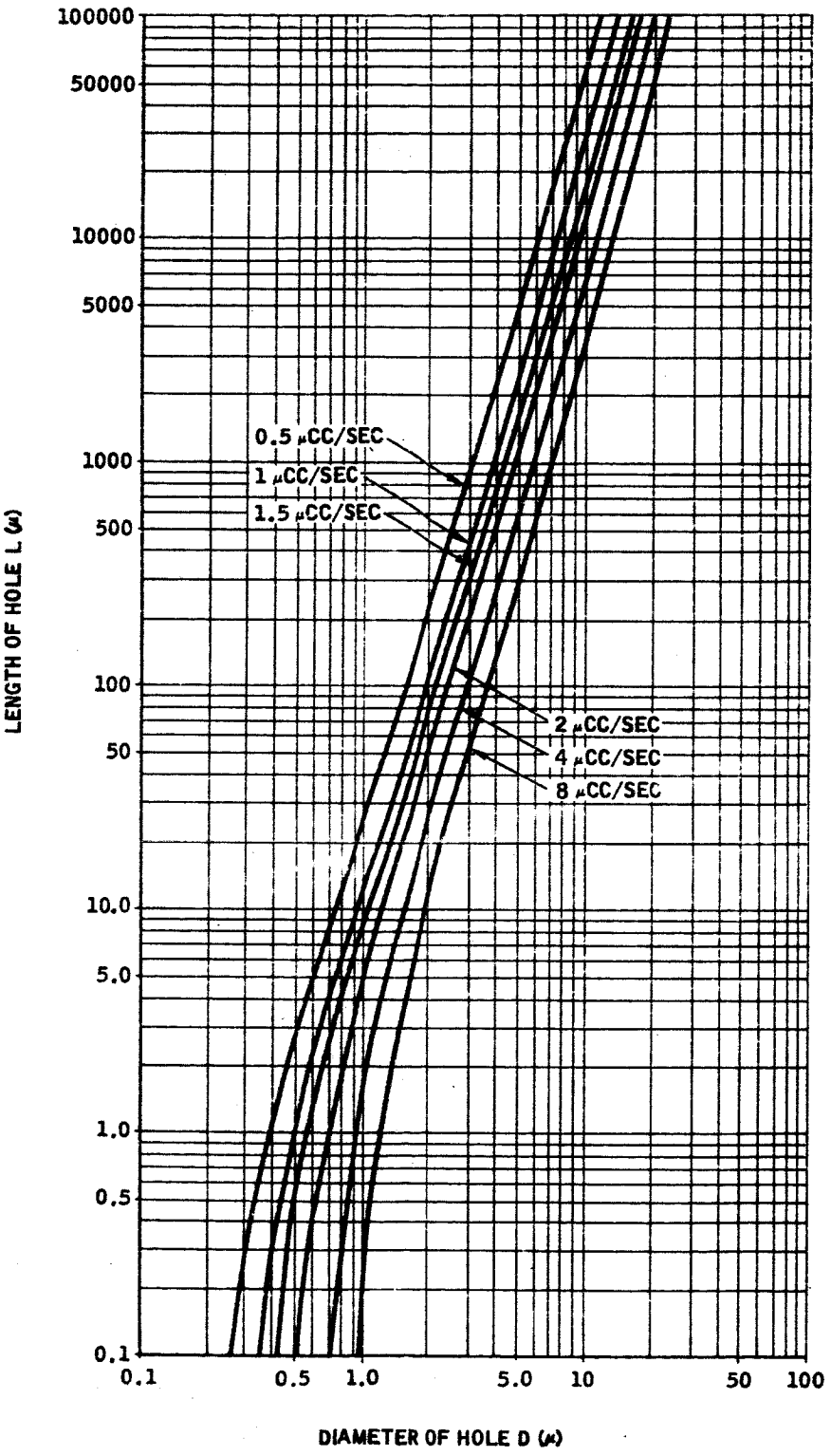

FIGURE 4-10
Aperture Length to Diameter Relationship

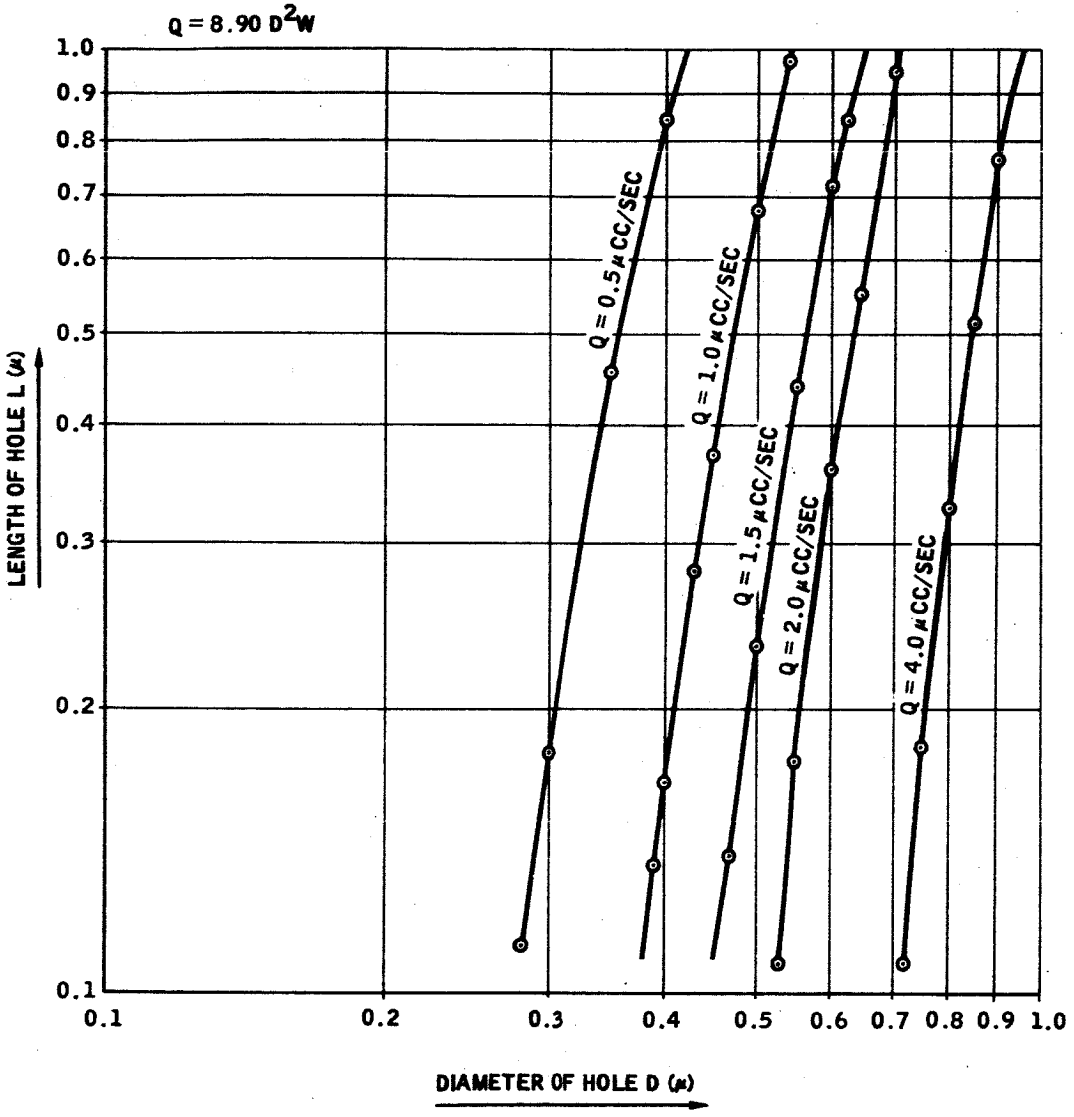

FIGURE 4-11
Aperture Length to Diameter Relationship - Expanded

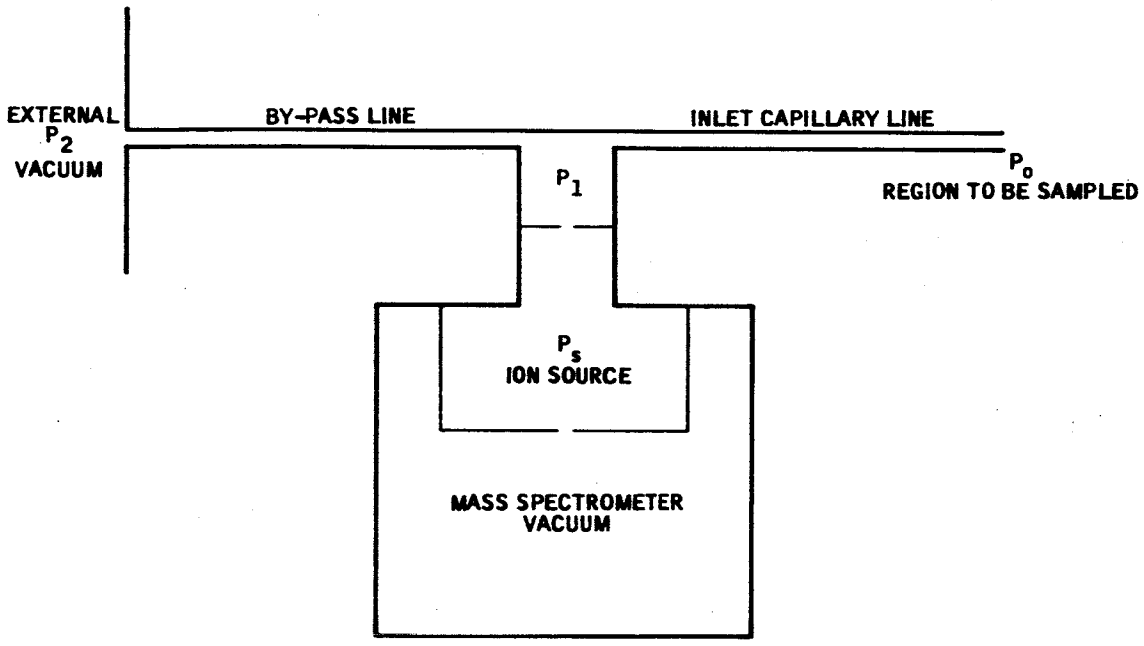

FIGURE 4-12
Inlet System Configuration

c. The intermediate pressure is accurate and proportional to the inlet pressure while maintaining accurate constant composition due to the bulk flow characteristics.

For purposes of illustration, we can assume that constant diameter lines radii a_1 and a_2 are used in the capillary line and bypass line respectively and

$$Q_1 = \frac{\pi a_1^4 \left(P_o^2 - P_1^2\right)}{kT_1\ 16\eta_1\ \ell_1} = \frac{\pi a_2^4 \left(P_1^2 - P_2^2\right)}{kT_2\ 16\eta_2\ \ell_2} = Q_2$$

or

$$P_o^2 - P_1^2 = \frac{\eta_1\ \ell_1\ T_1\ a_2^4}{\eta_2\ \ell_2\ T_2\ a_1^4} \left(P_1^2 - P_2^2\right)$$

Solving for $\frac{P_1}{P_o}$,

$$\frac{P_1}{P_o} = \frac{\left(1 + \frac{\eta_1\ \ell_1\ T_1\ a_2^4}{\eta_2\ \ell_2\ T_2\ a_1^4} \frac{P_2^2}{P_0^2}\right)^{1/2}}{\left(1 + \frac{\eta_1\ \ell_1\ T_1\ a_2^4}{\eta_2\ \ell_2\ T_2\ a_1^4}\right)^{1/2}} \tag{21}$$

In the usual case where

$$P_0 >> P_i > P_2 \quad , \tag{22}$$

Equation (21) simplifies to

$$\frac{P_1}{P_o} = \left(\frac{\eta_2\ \ell_2\ T_2\ a_1^4}{\eta_1\ \ell_1\ T_1\ a_2^4}\right)^{1/2} \tag{23}$$

It is apparent that if $T_2 \approx T_1$ and is a constant ratio then the ratio P_1/P_0 is dependent upon geometric factors only. It is one of the design goals of a good inlet system to have as slow a velocity and therefore as close to isothermal expansion as is consistent with the desired time delay.

Constraints on the viscous flow channel design are:

a. In order to remain viscous $\lambda << D$ where λ is the mean free path and D the channel diameter. We may establish a given degree of apprach

to pure viscous flow by the value of x chosen in Equation (19) and in Figure 4-9 (for instance, DP $\geq$ 1070 dynes/cm at x = 200).

b. The flow should remain laminar and the velocity not be allowed to approach the velocity of sound upstream of or near the intermediate sample region. Previous designs which did not consider this factor show appreciable deviation from constant composition in mass spectrometry analysis. This deviation is believed due to sample separation when the velocity reaches the velocity of sound at the exit of the (constant diameter) capillary and must dissipate the energy of a 30:1 pressure expansion in this region.

Prandtl[3] has shown that this energy will be dissipated by a series of expanding and contracting shock waves having a self-created boundary layer.

In order to meet these constraints, a tapered line was created by letting the line radius a = f(x) or f(p) where x is the position along the line. In addition to constant radius two tapered lines are considered:

a. Since the mean free path is given by $\lambda = k_3' p$, a, can be made a function of p (i.e., $a = k_3/p$) such that a/λ = constant as required to maintain a given degree of viscous flow.

b. The velocity can be held constant as follows; from conservation of matter $Q_n = n\ v\ A$ where n = (molecules/cc), v = velocity (cm/sec) and A = area (cm^2). If the velocity is held constant nA = k or for isothermal flow $a^2 = k_2/p$.

These solutions may be evaluated as follows:

The differential equation of Poiselle flow is

$$Q_n = \frac{-\pi a^4}{8\eta kT}\, p\, \frac{dp}{dx} \quad , \tag{24}$$

where

Q_n = flow in molecules/second

p = pressure in dynes/cm^2

and other symbols are as defined previously.

Case I: For reference, the constant diameter line integrates to

$$Q_n = \frac{\pi a^4 \left(P_o^{\,2} - P_1^{\,2}\right)}{kT\ 16\ \eta \ell} \tag{25}$$

---

[3] L. Prandtl, "The Physics of Solids and Fluid", Part II, Blackie & Sons, Ltd., Glasgow 1936, p. 356.

The pressure as a function of distance down the line is found by dividing the line into two parts of length x and (ℓ - x) and equating the flow. Thus, assuming isothermal flow,

$$\frac{\left(P_0^2 - P_x^2\right)}{x} = \frac{\left(P_x^2 - P_1^2\right)}{(\ell - x)}$$

or

$$P_x = P_0 \left[1 - \frac{x}{\ell}\left(1 - \frac{P_1^2}{P_0^2}\right)\right]^{1/2} \quad . \tag{26}$$

From an isothermal continuity equation

$$Q_p = pvA, \text{ and thus } v_x = \frac{Q_p}{p_x A} \quad . \tag{27}$$

Case II: For constant velocity let

$$a^2 = k_2/p \quad . \tag{28}$$

Thus, from Equation (24) and (28)

$$\int_{P_0}^{P_1} \frac{k_2^2 \, dp}{p} = \frac{-8\eta \; kT \; Q_n}{\pi} \int_o^{\ell} dx$$

and

$$Q_n = \frac{\pi}{kT} \frac{a_o^4 P_0^2}{\eta \ell} \ell n \; (P_0/P_x) \quad , \tag{29}$$

or from Equation (28) an alternate form is

$$Q_n = \frac{\pi a_o^4 P_o^2}{kT \; 8\eta \ell} \ell n \left(a_1^2 / a_o^2\right) \quad . \tag{30}$$

Intermediate pressures can be found by techniques similar to Case I.

$$P_x = P_o \left(\frac{P_1}{P_o}\right)^{x/\ell} \quad . \tag{31}$$

Case III: For viscous flow, let

$$a = k_3/p \tag{32}$$

From Equations (24) and (28)

$$\int_{P_o}^{P_1} \frac{k_3^4 \, dp}{p^3} = -\frac{8\eta \, kT \, Q_n}{\pi} \int_o^{\ell} dx$$

or

$$Q_n = \frac{\pi k_3^4}{16 \, kT \, \eta \ell} \frac{P_o^2 - P_1^2}{P_o^2 \quad P_1^2} \tag{33}$$

With Equation (32) this can be placed in an alternate form

$$Q_n = \frac{\pi a_1^2 \, a_2^2 \left(P_0^2 - P_1^2\right)}{16 \, kT \, \eta \ell} \tag{34}$$

This is similar to the constant diameter case except that $a_o^2 \, a_1^2$ is found in place of a^4.

By the techniques for Case I, the pressure at position x is given by

$$P_x = P_o \left[1 + \frac{x}{\ell}\left(\frac{P_o^2}{P_1^2} - 1\right)\right]^{-1/2} \tag{35}$$

As an example, Figure 4-13 is a graph of the pressure versus the position x/ℓ for a one meter capillary line in each of the three cases discussed. The quantity of flow and the initial and final values of pressure are held constant.

Figure 4-14 shows the variation of pressure, p, diameter, D, and ratio D/λ for three constant velocity lines having three terminal pressures.

After manipulation one may additionally obtain functions for the variation in inside radius, a_x, with distance along the line (normalized to $\chi = x/\ell$), velocity, the ratio of diameter, D, to mean-free-path, λ and the transport time Δt. These are shown in Table 4-4. With the continuity equation all of the necessary parameters of the line may be found.

In practice, it is found that the large ratio of pressure from ambient conditions to the vacuum system causes extreme variations of the parameters.

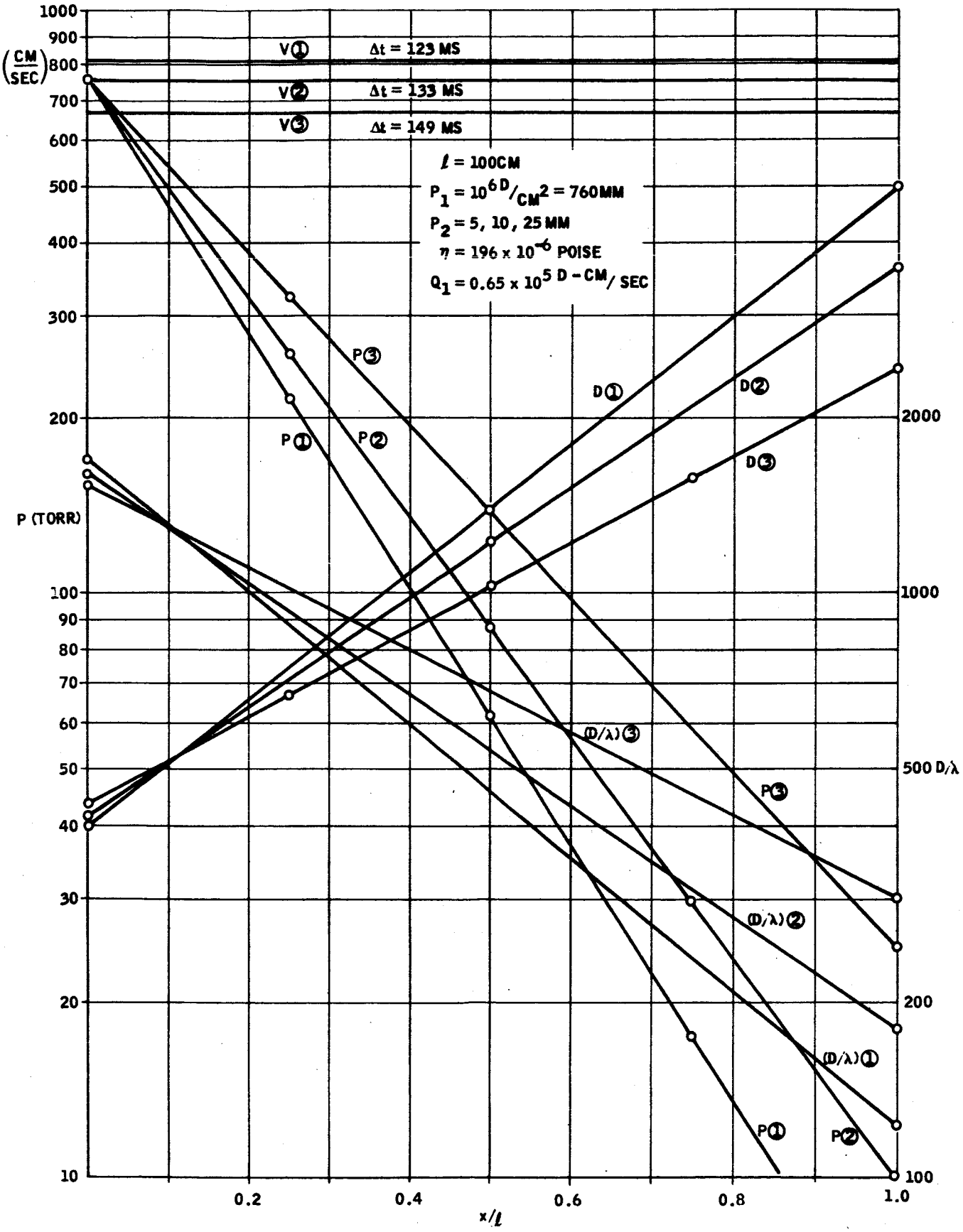

FIGURE 4-13
Constant Velocity Line Parameters

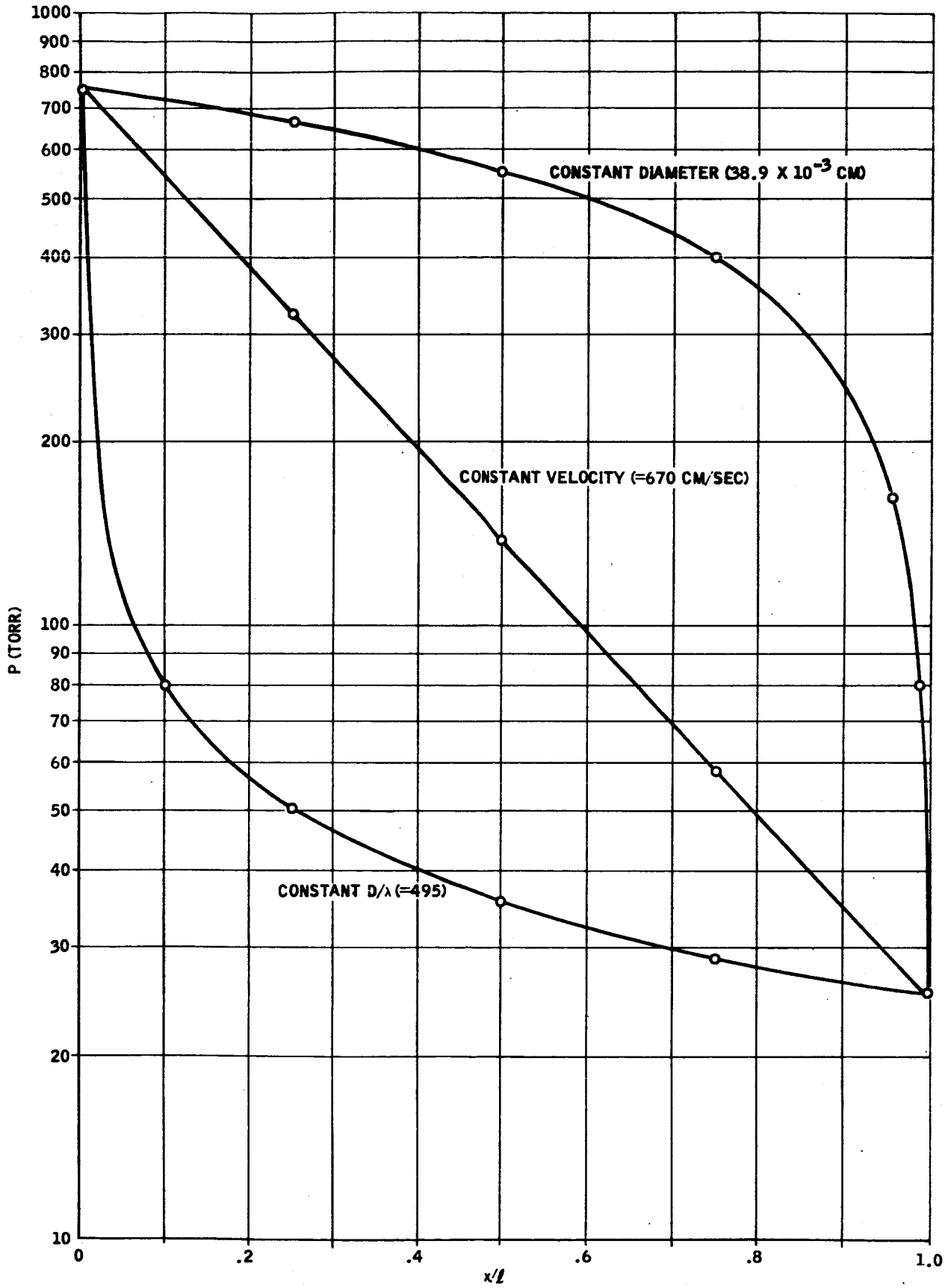

FIGURE 4-14
Comparison of Pressure Drop in Three Sample Line Types

FOR CONSTANT	$\frac{8\eta kT\, Q_n}{\pi}$	$\frac{P_x}{P_o} = f_1(x)$	$\frac{a_x}{a_o} = f_2(x)$	$\frac{(D/\lambda)_x}{(D/\lambda)_o} = f_3(x)$	$\frac{v_x}{v_o} = f_4(x)$	Δt
DIAMETER ($a = k_1$)	$\frac{a^4 P_o^2 \left(1 - y^2\right)}{2\ell}$	$\left[1 - x\left(1 - y^2\right)\right]^{\frac{1}{2}}$	1	$\left[1 - x\left(1 - y^2\right)\right]^{\frac{1}{2}}$	$\left[1 - x\left(1 - y^2\right)\right]^{-\frac{1}{2}}$	$\frac{2}{3v_o}\left(1 + \frac{y}{1+y}\right)$
Velocity ($a^2 = k_2/p$)	$\frac{a_o^4 P_o^2}{\ell} \ell n\left(\frac{1}{y}\right)$	y^x	$y^{-x/2}$	$y^{x/2}$	1	$\frac{\ell}{v_o}$
D/λ ($a = k_3/p$)	$\frac{a_o^2 a_1^2 P_o^2 \left(1 - y^2\right)}{2\ell}$	$\left[1 + x\left(\frac{1}{y^2} - 1\right)\right]^{\frac{1}{2}}$	$\left[1 + x\left(\frac{1}{y^2} - 1\right)\right]^{\frac{1}{2}}$	1	$\left[1 + x\left(\frac{1}{y^2} - 1\right)\right]^{-\frac{1}{2}}$	$\frac{2\ell}{3v_o y}\left(1 + \frac{y^2}{1+y}\right)$

Also $Q_n = n\ v\ A$ at any point in a given line

D = line diameter (cm)

k = Boltzman's constant = 1.38×10^{-16} ergs/molecule/°K

T = Absolute temperature (°K)

v = velocity (cm/sec)

Δt = total time of transport (sec)

x = x/ℓ

ℓ = line length (cm)

x = arbitrary position (cm)

a = line radius (cm)

y = $\frac{P_1}{P_o}$

Q_n = flow (molecules/sec)

P_o = inlet pressure (dynes/cm^2)

P_1 = outlet pressure (dynes/cm^2)

λ = mean-free-path (cm)

η = molecular density (molecules/cc)

TABLE 4-4

Viscous Flow Functions for Constant Diameter and Tapered Lines

Consequently, it is desirable to combine the properties of the three types of lines discussed to obtain an optimum system. Briefly the logic is as follows:

While it would be desirable to maintain a given, D/λ, throughout the system for for a constant degree of viscosity, this type has the greatest time delay as well as the most severe taper. On the other hand, the constant diameter line has the shortest time delay but runs into problems when the velocity approaches the speed of sound. The constant velocity line is a reasonable compromise until the ratio D/λ drops to values approaching 100 where the deviation from viscous flow may cause selective pumping of light gases.

Consequently, the following combination appears to optimize the system. A constant diameter line is used at the entrance to get the velocity to a desired value quickly; a constant velocity section is used for the bulk of transport and particularly through the intermediate sampling point; a constant D/λ section is used after the sampling point where transport speed is not important but chiefly to avoid flow separation that can reflect up-stream to the sampling point; and finally, the line can be terminated in a critical orifice. In extreme cases, the termination may affect the flow character at the sampling point by as much as 20%, although 1% is usually a design goal. The critical orifice is discussed below.

Figure 4-15 gives Δt using the combination of a constant diameter and constant velocity line. Figure 4-16 gives the dimensions of a stepped 2 meter line which approximates the shape of a combination line that has been tested. For air at 380 torr and 20°C, this line has a flow of 38 torr cc/second or 0.215 gms/hour. The low pressure end of the line is designed to operate at 5 torr and have $D/\lambda = 223$. The maximum transport time is approximately 0.4 second for two meters.

In the type of problem being considered here, the critical orifice is useful for the termination of the line since bulk flow takes place without separation of the sample components. It is limited in its application because the pressure drop across the orifice must be above the critical ratio and quantity of flow is proportional to pressure rather than P^2 as other portions of the line.

As a result of this characteristic, a small correction must be applied when used over wide ranges of inlet pressure and when the orifice constitutes a large part of the downstream impedance. In the cases considered here, the pressure range for accurate analysis is relatively small and consequently, the correction is not significant.

A brief but clear discussion of critical flow is found in Guthrie & Wakerling[4]. For our purposes, the pressure ratio is always greater than critical and the flow is then given by

$$Q_p = 20\ AP \text{ torr cc/second} \qquad (36)$$

where A is in cm^2.

[4] Guthrie & Wakerling ibid, pg. 16.

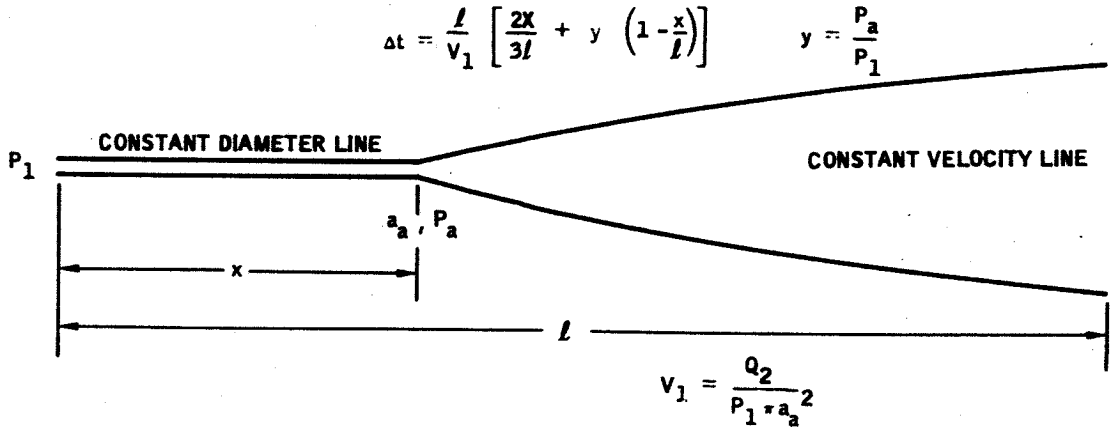

FIGURE 4-15
Combined Constant Diameter and Constant Velocity Line Relationships

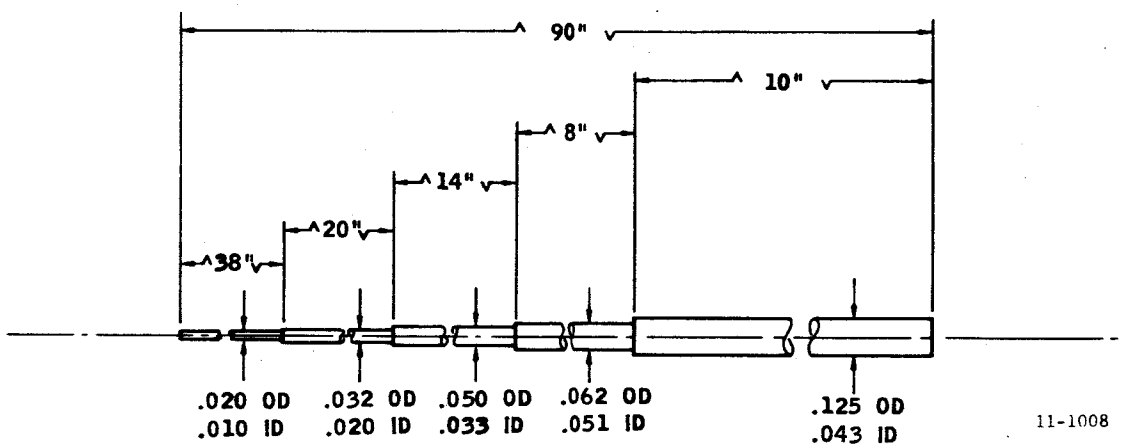

FIGURE 4-16
Sample Inlet Capillary Line

As an example, if Q_p = 38 torr cc/second and critical flow was required from a 5 torr termination pressure, an area of 0.38 cm^2 would suffice; providing the downstream pressure is less than 0.525 x 5 torr or 2.625 torr at this flow rate. With appropriate design, this presents no problem when using space vacuum.

4.3.4 CONCLUSIONS AND RECOMMENDATIONS

An examination of the two most desirable methods of transport, i.e., fan circulation at ambient pressure, or a viscous flow channel connecting to space vacuum through a valve, indicates the following:

a. The fan circulation method makes use of existing equipment and certainly involves lower weight than adding a flow line. It has the advantage that reactive or condensible molecules are surrounded in their transport by adjacent molecules of like kind and therefore no absorption or reactive effects take place. It has the disadvantage that the transport time from a disturbance may be one circumference time around the cabin or perhaps up to 30 seconds. It further requires the use of a molecular leak at ambient pressure which involves extremely small holes and for which limited experience has been obtained todate.

b. The viscous-flow capillary line has the advantages of a higher speed (the order of 0.4 second time delay) and a reduced pressure at the intermediate sampling point. While the flow is much higher than the direct (non-bypass) entry into the mass spectrometer, some adsorption takes place with water. The present experience on water vapor indicates that a time constant the order of 2 to 5 seconds is involved if the line is not heated. In respiratory analysis, the breath cycle (approximately 2 seconds) in H_2O may be observed with some rounding of a square wave change if the entrance to the line is heated to body temperature. While this is not believed to be a problem, study of the H_2O time constant is contemplated. In the most demanding case, it is expected that the first 6 inches of the line would have to be heated to 100°F. This can be accomplished possibly by placing the line in a heated location. The inlet line and valve also have the disadvantage of adding to the weight.

A special advantage of the capillary line is that it has a flexible sampling position. A routine check on the performance of each suit-loop can be made when each astronaut takes his turn in a suit. The extra-long line proposed also has the advantage of being capable of sampling most points in the cabin. Shorter and faster lines can be designed with no change in flow.

It is recommended that the capillary inlet line be used since it represents the most conservative effect upon weight, design of the inlet leak, and operational demand upon time constants and delays in the main control loop.

The use of a circulating fan for transports remains as an improvement potential in selected applications.

Two inlet leak assemblies that have received limited, but encouraging tests, are shown in Figures 4-17 and 4-18. The first figure shows the assembly of a multi-hole gold filter having the order of 1000, 0.19 micron holes, and a three hole leak having 0.26 micron holes. This leak is made[5] by thin film techniques involving coating around the uniform diameter latex molecule. One assembly has been tested to more than 500 torr with helium air mixtures and found to be linear (therefore, the flow is molecular in nature).

Figure 4-18 shows a ball-leak assembly that utilizes optical precision in the polishing of the seat. The ball is then roughened to a specified degree in order to provide multiple short-path molecular leaks. This leak has been tested and found linear up to atmospheric pressure.

In each of the leak assemblies, a filter is believed to be required. Additional study is anticipated in order to compare comercially-available filters such as "Millipore" and sintered metal types. Knowledge of the particle size distribution in typical sampling situations will contribute to the choice of filters.

It is concluded that a tapered capillary inlet line, tapered bypass line, critical orifice and valve combination can be designed to meet the requirements of the two-gas atmosphere sampling system. The ball leak in combination with a filter (to be designed after study) can be matched to the viscous flow system. No fundamental problems are foreseen.

---

[5] NASA Publication N66-11743*: L.G. Hall, M.R. Ruecker, and G.N. Wassels. "A Feasibility Study of the Mass Spectrometer Instrumentation for the Analysis of the Martian Atmosphere".

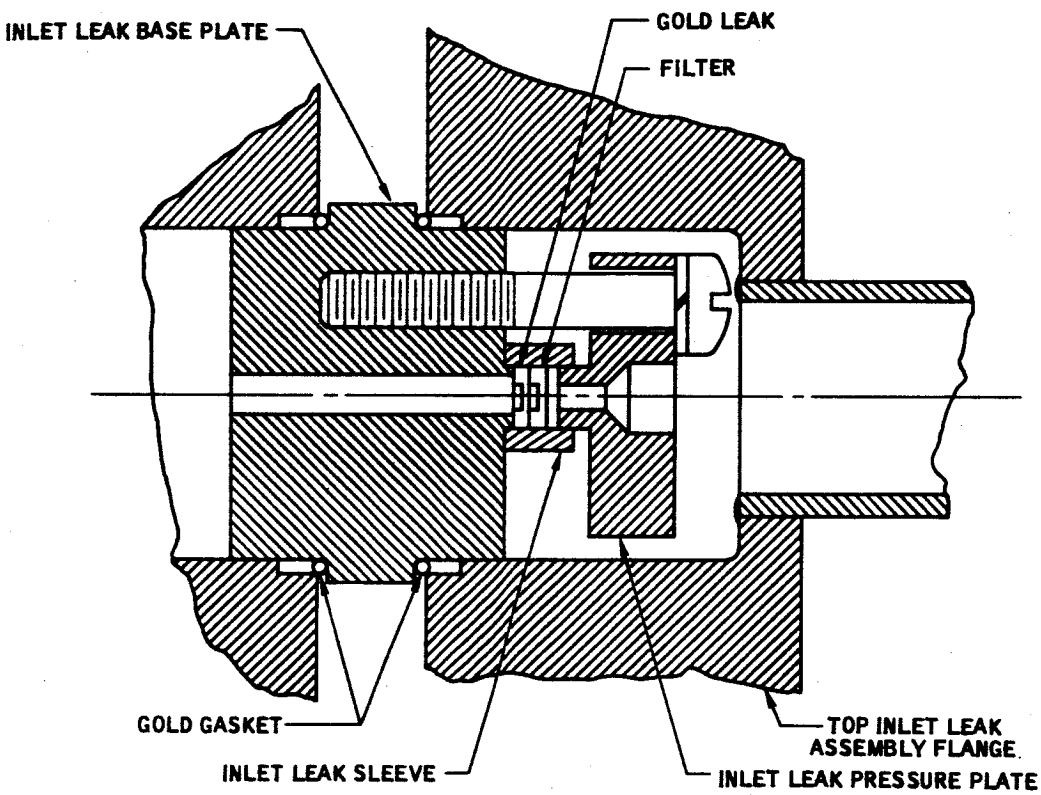

FIGURE 4-17
Gold Leak Assembly

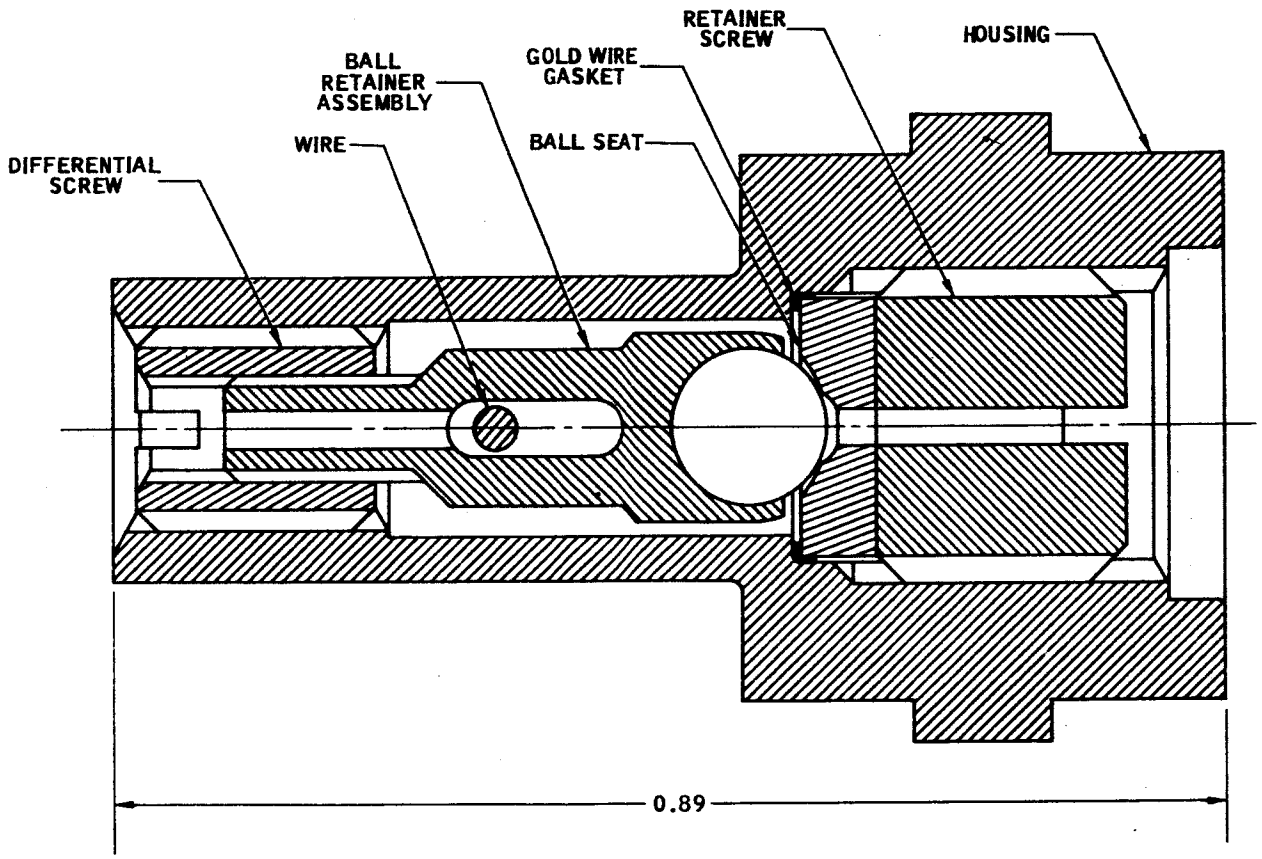

FIGURE 4-18
Ball Leak Assembly

4.4 PUMPING SYSTEM

The function of the pumping system is to maintain the necessary internal vacuum against the incoming sample flow. The required pumping speed is determined by the ion source conductance and the differential pumping which is desired. It has been shown that a differential pumping factor of one hundred should be sufficient to reduce the effects of filament interaction with the sample to an acceptable level. Therefore, this shall be used as a target value for the present design.

The ion source conductance is determined by applying the pumping speed curves in Figure 4-19, to the proposed dimensions of the electron apertures and the ion exit aperture. The results are tabulated in Table 4-5. The slit dimensions given in Table 4-5 are consistent with values that have been experimentally proven as acceptable in terms of the currents to be transmitted through them.

TABLE 4-5

APERTURE CONDUCTANCES

	$\bar{b}$	L	W	C	S
Ion Exit Aperture	.0121"	.050"	.0242"	6.11 cc/sec	
Electron Accelerator Aperture	.015"	.050"	.040"	14.30 cc/sec x 2 28.60 cc/sec	
Total				34.71 cc/sec	3471 cc/sec

($\bar{b}$ = average thickness, slots are tapered)

The necessary pumping speed is shown to be 3.47 liters/second. The question to be answered is how is the pumping speed to be achieved? Two primary possibilities exist. The first is the use of an ion pump and the second is the utilization of free space as a pump.

The demand factors associated with an ion pump of the required pumping speed would be somewhat prohibitive. Interpolating data available on commercial ion pumps indicates that a 4 liter/sec pump would weigh at least 6 pounds and require about 1 watt of power. A favorable trade between weight and power might be made which would reduce the weight to about 4 pounds and increase the power to 2 watts. This would be the limit of such a trade off since at this point the pump voltage required is approximately 6 to 7 kilovolts.

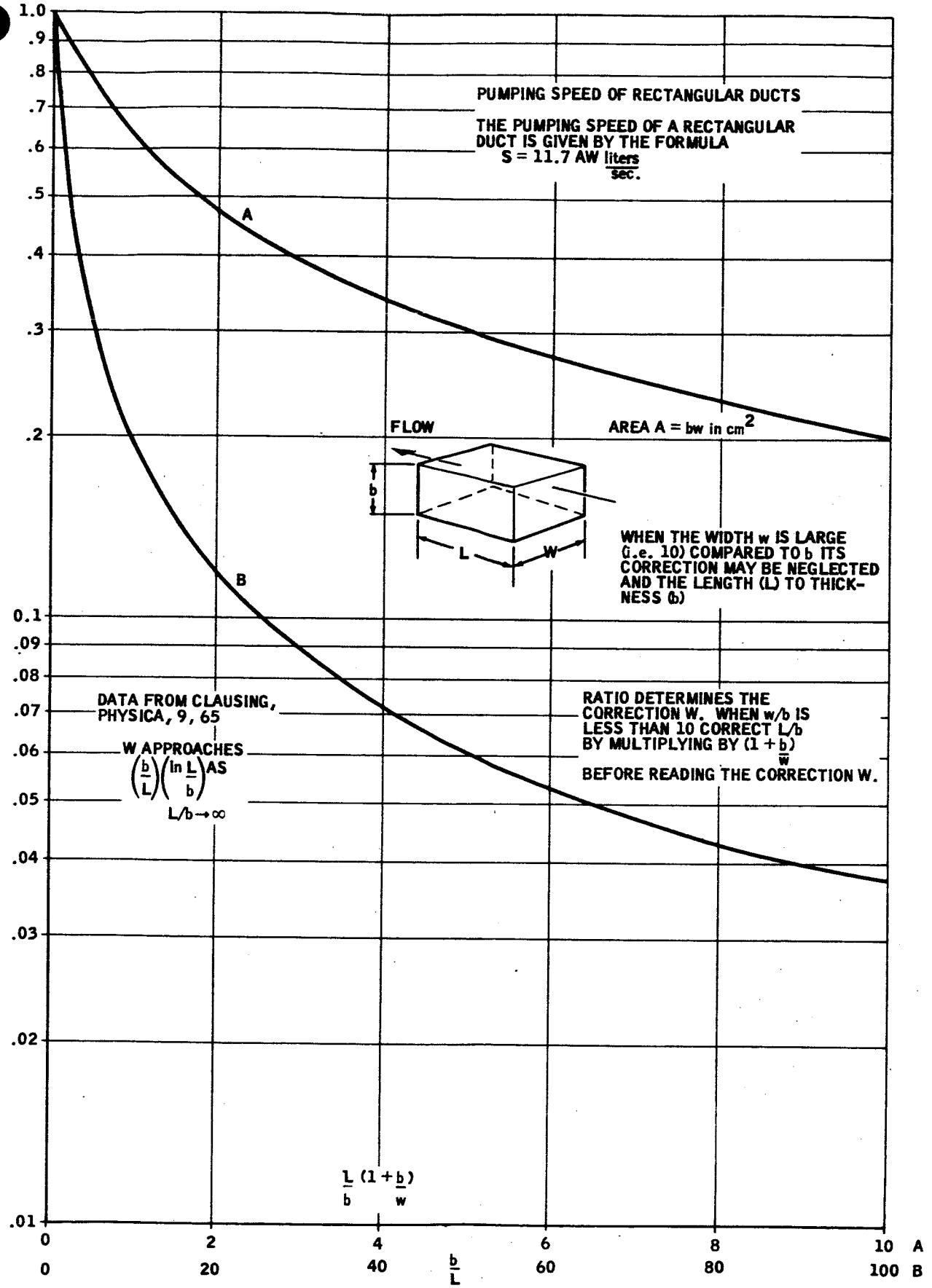

FIGURE 4-19
Pumping Speed of Rectangular Ducts

It can be concluded that the only possible way that an ion pump can be utilized is by reducing the pumping speed demands. This would mean a reduction in differential pumping which might be tolerated if the instabilities due to sample interaction with the filament can be reduced by the proper choice of filament wire material. However, another limitation exists from the fact that if the ionizing region pressure is to be maintained in order to hold the sensitivity up then the analyzer pressure would have to be raised. The present calculated analyzer pressure is 2×10^{-6} torr for D = 100. Experiments with the type of electron gun which is proposed show that stable operation cannot be counted upon above 5×10^{-6} torr especially with an 0_2 sample. Therefore if a maximum analyzer pressure of 4×10^{-6} torr is allowed and if the minimum detectible level on major components is increased from ±.2% to ±.6% thus allowing a decrease in ion source pressure from 2×10^{-4} torr to 6.6×10^{-5} torr, then a differential pumping ratio of 16.5 would be necessary resulting in a pumping speed of about 0.55 liters/second. A pump of this size would weigh approximately 1.25 pounds and require a power of half a watt. This might be an acceptable solution but it should be emphasized that experimental verification of the acceptability of the proposed pressure levels would first be required.

The use of outer space as a pump is much more amenable to the power and weight goals of this task. On the other hand the interfacing problems are somewhat greater than with an ion pump. Information on the spacecraft interfaces indicate that a bulkhead distance of approximately 18 inches is to be expected. The pump tube diameter required to obtain the specified pumping speed is based upon that length. In addition, a 1 inch valve is assumed to be in the line in order to seal the mass spectrometer from the atmosphere before the Apollo is in orbit. It is found that a 1 1/8 ID tube is required to obtain 3.94 liters/second which is slightly more than the required pumping speed. Insofar as the demand factors are concerned, the pump out tube and valve require no power. The weight of the pump out line is 0.47 pound, 0.031 wall tubing, and the valve weight was carefully estimated at 0.75 pound for a light weight bellows valve with an O-ring seal.

The valve should be placed very near to the surface of the spacecraft so that the pumpout tube itself can also be maintained in an evacuated state for maximum cleanliness. It is, of course, evident that the type of pumping precludes operation of the mass spectrometer before it reaches an altitude at which the residual pressure has reached the necessary low levels. This does not represent a severe limitation since the astronauts will be on their suit loops with a pressure controlled 0_2 atmosphere.

For pre-flight checkout two alternatives are possible. One is to connect a pump externally to the pumpout tube. If this presents too much of a problem then the auxiliary pump could be attached to the analyzer on the inside of the spacecraft. This would require the use of an additional valve. Special valve assemblies are available with removable bonnets so that when they are in the closed position only the valve seat and the valve remains in place. This part of the assembly weighs only 2.9 ounces for a 1" port.

It is necessary to check the pressure level of the outer space environment before this type of pumping can be assumed to be allowable. First it must be realized that no differential pumping action occurs with respect to this pressure component. Consequently, it exists merely as a superimposed partial pressure added to the pressure arising from the entering sample flow. The ambient pressure is about 1×10^{-6} torr at 150 km dropping to 1×10^{-7} torr at about 170 Km. But this pressure component inside the analyzer can be increased by as much as a factor of 5 due to the "ram effect". This is caused by the thermalization of the relatively energetic molecules which enter the pump tube when the angle of attack of the spacecraft is low. In view of this the operating altitude should be no less than 160 to 170 Km, unless degradation in performance is to be allowed.

In conclusion the use of outer space appears to be the best method for obtaining the necessary internal vacuum, however, the possibility of using an ion pump exists if certain trade offs can be realized.

4.5 DETECTOR SYSTEM

4.5.1 INTRODUCTION

The purpose of this analysis is to evaluate an approach to an ion detector system for a gas atmosphere sensor where the controlling design factors are power, weight, and reliability. The state-of-the-art in detector systems has advanced to high speed, maximum sensitivity, wide dynamic range systems as shown in Figure 4-20. In the illustrated system, high speed is attained by feedback compensation. Maximum sensitivity is accomplished using low noise electrometer tubes at the input and by using an AC or chopped system to eliminate amplifier drift effects. Relay range selection on the preamplifier and logarithmic compression of the output data accommodates the wide dynamic range. The complexity of such a system is counter to the requirements of minimum power and weight and maximum reliability. A much simpler detector as shown in Figure 4-21, with emphasis on these properties requires trade-off in sensitivity, response, and range.

4.5.2 SUMMARY

To satisfy the design parameters of minimum power and weight and maximum reliability, a DC, linear, non-ranging detector system with a solid-state input device is considered. The affects of such a system on sensitivity, response, minimum detectable signal, and dynamic range are examined. The parameters of minimum detectable signal and dynamic range are determined by the system requirements. It is found with a minimum detectable signal of 5×10^{-14} amperes that noise and drift must be less than 10 millivolts and that a non-ranging system implies a multiple collector system.

Detector amplifiers and their drift and noise characteristics are examined to find the controlling factors on sensitivity and response. With power supplies regulated to 0.1% and a system response of about 1 second, the proposed detector is feasible.

4.5.3 SIMPLIFIED DETECTOR

The need for an uncomplicated system, as shown in Figure 4-21, includes the following considerations;

a. Use of a solid-state insulated gate field effect transistor versus an electrometer tube for the input device,

b. Use of a direct coupled or DC system versus a chopped or AC system,

c. Use of a system with linear rather than logarithmic transfer characteristics,

d. Use of a non-ranging system versus a ranging system.

Such an approach to a simplified detector system requires tradefoff in the design parameters of sensitivity, response, minimum detectable signal, and dynamic range.

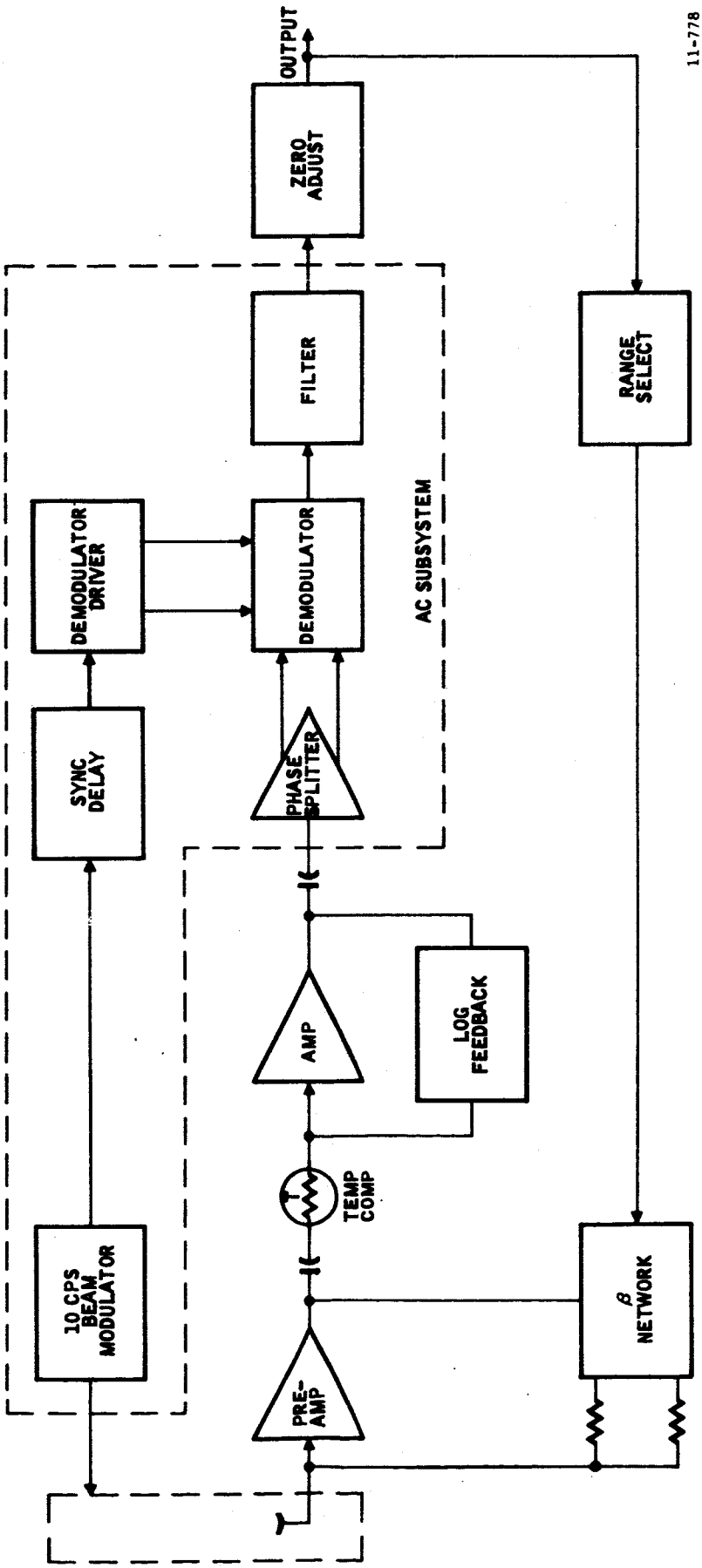

FIGURE 4-20
Block Diagram - Detector System

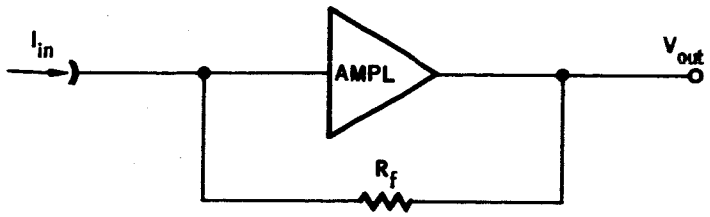

FIGURE 4-21
Simplified Detector

The parameters of minimum detectable signal and dynamic range are related to the system requirements. In this application for measuring CO_2 and H_2O, which fall in the range 0 to 20 torr, assume 20 torr fullscale and a minimum detectable pressure change Δp of 0.20 torr which is 1% of full scale. If the full scale voltage output is 5 volts and a 1.0% change is 50 millivolts, a minimum detectable input current of 5×10^{-14} amperes will fix the feedback resistor at 10^{12} ohms.

For the N_2 and O_2 measurements, assume a full scale of 200 torr and a minimum detectable pressure change Δp of 0.40 torr with 0.2% of full scale. A 0.2% change in the 5 V full scale reading is 10 millivolts and with a 5×10^{-14} ampere minimum detectable input current the feedback resistor is 1×10^{11} ohms.

The above results indicate that a non- ranging system requires two amplifiers with different feedback resistors to accommodate the desired measurements. This arrangement implies the use of a multiple collector system.

The analysis also indicates that the minimum detectable signal is 10 millivolts. A simplified operational system requires that the drift and noise must be less than the minimum detectable signal. This requirement dictates the sensitivity and response of the system. In order to determine if a DC, linear, non-ranging system can satisfy the requirements, it is necessary to examine such an approach. This examination follows in the form of defining the detector amplifier and analyzing its drift and noise.

4.5.4 DETECTOR AMPLIFIERS

The simplest form of electrometer amplifier is shown in Figure 4-22 where the current to be measured develops a voltage across a resistor and is amplified. The output voltage of this circuit is a function of the open loop amplifier gain making this configuration extremely sensitive to drift and noise.

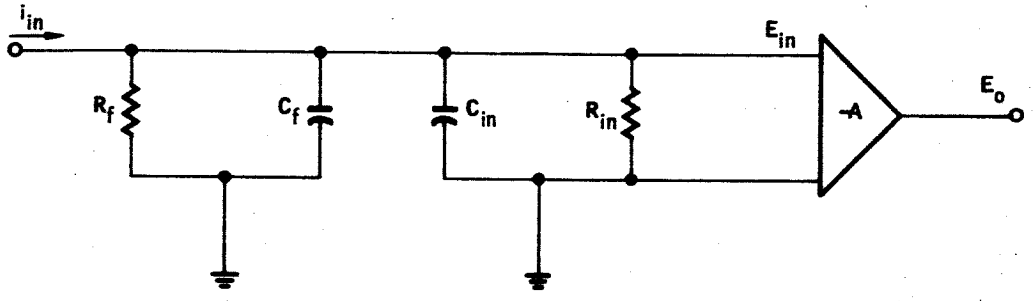

INPUT RESISTANCE $R = \frac{R_f R_{in}}{R_f + R_{in}} \simeq R_f$ WHEN $R_{in} \gg R_f$

INPUT CAPACITANCE $C = C_{in} + C_f$

INPUT TIME CONSTANT $\tau = RC = R_f (C_{in} + C_f)$

INPUT VOLTAGE $E_{in} = i_{in} R$

OUTPUT VOLTAGE $E_o = -A E_{in}$

FIGURE 4-22
Electrometer Amplifier Without Feedback

The usual method for obtaining amplifier stability is by employing negative feedback. This technique results in the circuit as shown in Figure 4-23. A comparison of the equations for the two configurations yields some subtle trade-offs. Without feedback, fast response can be obtained by reducing R and increasing the gain with a resulting sacrifice in stability. Simple feedback affords gain stability but requires larger feedback resistors. The response does not suffer proportionately, however, because the input resistance is reduced by a factor of the gain. The response time is not completely reduced by the gain because the feedback portion of the input capacitance is increased by the Miller effect.

The effects of the Miller capacitance can be neutralized with the use of compensation techniques in the feedback as shown in Figure 4-27. If it is accepted that the circuit is compensated when $R_1C_1 = R_f C_f$ and if R_f is large and C_f small, the equations of Figure 4-24 are easily seen to be valid. The net result including compensated feedback is seen to be stricly an improvement in DC stability which is of considerable value for the electrometer applications being considered.

4.5.5 DRIFT CONSIDERATIONS

A reasonably stable system requires the use of an operational amplifier with feedback as was shown in Figure 4-23.

This basic electrometer circuit can be analyzed for its stability by expanding the circuit as shown in Figure 4-25, and inserting a noise drift component e_n, in the system. If it is assumed that the input signal is zero, the circuit equations become,

$$e_1 = A_i \beta e_{out} \tag{1}$$

and

$$e_{out} = A_o (e_1 + e_n) \tag{2}$$

such that

$$e_{out} = \frac{A_o e_n}{1-A_o \beta} \tag{3}$$

Equation (3) holds for power supply drift, temperature drift and noise. Noise can be considered to be a form of drift with a frequency consideration. Power supply and temperature drift are normally long term and for this consideration is unity. With $A_o A_i >> -1$, Equation (3) reduces to

$$e_{out} = \frac{e_n}{A_i} \tag{4}$$

for power supply and temperature drift. This equation states that the output drift is equal to the injected drift component divided by the gain to the input, A_i.

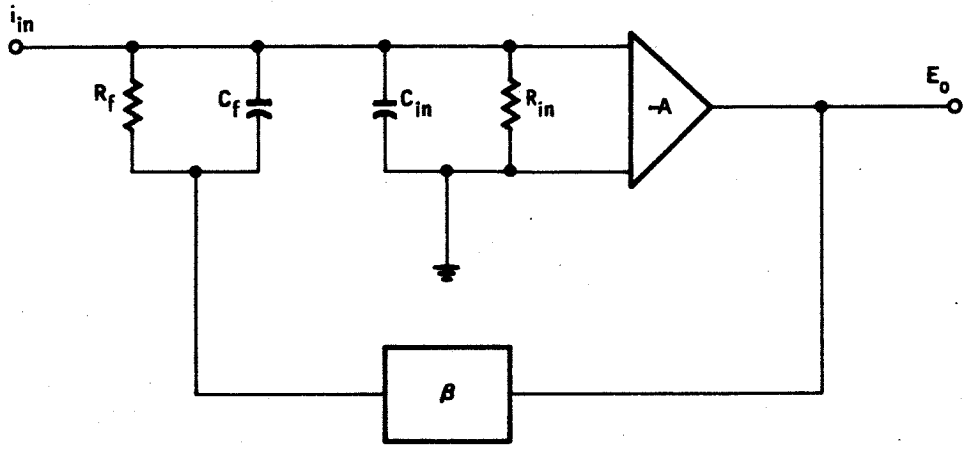

INPUT RESISTANCE $R = \frac{R_{in} R_f}{R_f + R_{in}(1+A\beta)} \approx \frac{R_f}{1 + A\beta}$ WHEN $R_{in} \gg R_f$

INPUT CAPACITANCE $C = C_{in} + (1+A\beta)\, C_f$

INPUT TIME CONSTANT $\tau = RC = \frac{R_f C_{in}}{1+A\beta} + R_f C_f$

OUTPUT VOLTAGE $E_o = \frac{-i_{in} R_f}{\beta}$ WHERE $A\beta \gg 1$ AND $\beta = 1$ FOR 100% FEEDBACK

FIGURE 4-23
Electrometer Amplifier With Compensated Feedback

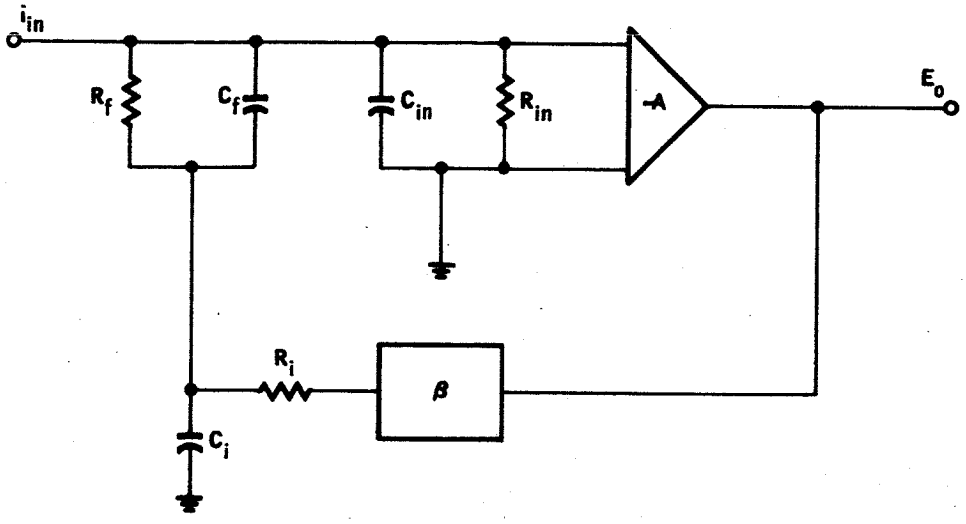

FOR COMPENSATION $R_1C_1 = R_fC_f$

THUS $R_1 \ll R_f$

AND $C_1 \gg C_f$

INPUT RESISTANCE $R = \dfrac{R_{in}R_f}{R_f+R_{in}(1+A\beta)} \simeq \dfrac{R_f}{1+A\beta}$ WHEN $R_{in} \gg R_f$

INPUT CAPACITANCE $C = C_{in}\dfrac{C_fC_1}{C_1+C_f} \simeq C_{in}+C_f$

INPUT TIME CONSTANT $\tau = RC = \dfrac{R_f(C_{in}+C_f)}{1+A\beta}$

OUTPUT VOLTAGE $E_o = -i_{in}\dfrac{(R_f+R_1}{\beta} \simeq \dfrac{-i_{in}R_f}{\beta}$

FIGURE 4-24
Electrometer Amplifier With Compensated Feedback

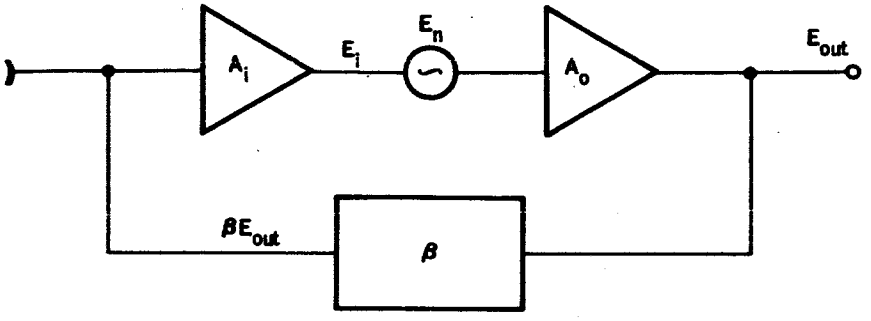

FIGURE 4-25
Detector Amplifier With Injected Drift Signal

For multistage amplifiers, the total long term output drift becomes the sum of the individual stage drifts so that,

$$e_{out} = \sum_{K=1}^{X} \frac{e_{n_K}}{A_{i_K}} \tag{5}$$

$$= \frac{e_{n_1}}{A_{i_1}} + \frac{e_{n_2}}{A_{i_2}} + \frac{e_{n_3}}{A_{i_3}} + \ldots + \frac{e_{n_x}}{A_{i_x}} \tag{6}$$

where x equals the number of stages and

$$A_{i_K} = \prod_{K=1}^{K} A_K \tag{7}$$

$$= A_1 \cdot A_2 \cdot A_3 \ldots A_K \tag{8}$$

From (6) and (7) it is implied that the first stages contribute the greater portion of the drift since A_i increases as a product of the succeeding stage gains as k becomes larger. The implication is also that the forward stages should have maximum gain to minimize the drift.

Since the front end stages contribute essentially all the drift, temperature drift can be minimized by compensation techniques in the forward stages. The usual method of bridge compensation by differential amplifier techniques will not be considered because of the additive effect on input noise. Thus, limited to single ended amplifiers, temperature compensation must be applied

by using input devices with zero TC operating points. The degree of temperature stability for these devices is a function of the time and effort spent in selection and trimming, however, the required results can be obtained.

Power supply drift in single ended amplifiers cannot be compensated and must therefore be minimized. Three cases of interest, collector supply, bias supply, and follower input considerations, affect the power supply drift as given by Equation (6). If the assumption is made that the power supply drift appears equally on all stages and only the first two terms are important, Equation (6) for the collector supply case becomes

$$e_{out} = e_{n_1}\left(\frac{1}{A_1} - \frac{1}{A_1 \cdot A_2}\right) \tag{9}$$

where each stage is an inverting stage. For the bias supply case where the drift can precede the first stage gain Equation (6) becomes

$$e_{out} = e_{n_2}\left(\frac{1}{k_o} - \frac{1}{A_1 k_1}\right) \tag{10}$$

where the k_n term represents the division of the bias supply to establish the various operating points in a direct coupled amplifier. The low levels involved in the forward amplifier stages cause these bias points to be quite low which causes the drift to be divided significantly. For the follower input case where the first stage is unity non-inverting gain and supplied by the bias supply, Equation (10) becomes,

$$e_{out} = e_{n_2}\left(1 + \frac{1}{K_1} - \frac{1}{A_2 K_2}\right) \tag{11}$$

The total drift for a multistage amplifier can be found to be the sum of Equations (9) and (10) for an amplifier with a gain stage input and the sum of (9) and (11) for a follower input. In these equations, it must be remembered that the drift components, e_{n_1} and e_{n_2} are usually independent between the collector supply and the bias supply. Examination of Equation (11) reveals that a follower input should be avoided which is in agreement with the fact that the first stage should have maximum gain.

If a follower input is not considered, the worse case total drift from (9) and (10) will be

$$e_{out} = e_{n_1}\left(\frac{1}{A_1} - \frac{1}{A_1 \cdot A_2}\right) + e_{n_2}\left(\frac{1}{k_o} - \frac{1}{A_1 K_1}\right) \tag{12}$$

If it is assumed that both the collector supply and the bias supply are 20 V and regulated to 1.0%, then e_{n_1} and e_{n_2}=0.2 V. If all stages have a gain of 10 and k_o = 10 and k_1 = 5, then from (12)

$$e_{out} < 34 \text{ millivolts} \tag{13}$$

If it is assumed that the system is to have less than ten millivolts total drift and noise, it appears from (13), the power supplies must be regulated to 0.1% or better. This does not appear to present any insurmountable problems.

4.5.6 NOISE CONSIDERATIONS

The critical noise souces in electrometer amplifiers are located at the amplifier input. There are three input noise sources which require consideration:

a. Noise due to input device leakage currents,

b. Noise due to current flow through the feedback resistor,

c. Noise internal to the input stage.

The input devices considered for electrometer applications are the electrometer tube and the insulated gate field effect. In the vacuum tube, input leakage appears in the form of grid current which is a function of the number of electrons which collide with the grid structure. Electrometer tubes exhibit typically 10^{-14} amperes of grid leakage. Insulated gate FET's have input leakage or gate leakage which is a function of mobile charges in the insulating gate dielectric and external header leakage. Experience in the use of this device has shown consistent leakage levels which are unmeasureable as compared to electrometer tubes.

The second noise source of interest is the resistor noise or Johnson noise. This noise comes from the feedback resistor and is given by

$$i_j = \left(\frac{4k\ T\Delta f}{R} \right)^{\frac{1}{2}} \tag{14}$$

In sensitive electrometers, the feedback resistor R is on the order of 10^{12} ohms. This resistance and its own stray capacitance allows a bandwidth Δf of less than 1 Hz. Using these values for R and Δf in Equation (1) results in Johnson noise of less than 10^{-15} amperes.

It is thus seen that the leakage noise current and Johnson noise current at the input can be kept less than 10^{-14} amperes. Since minimum signal is greater than 10^{-14} amperes, these two noise sources are negligible. In addition, signals directly at the input deteriorate with frequence due to the input capacity.

The noise internal to the input device is found to be of a different nature. This noise has been well defined for vacuum tubes but not for insulated gate FET's. The vacuum tube has been found to exhibit better characteristics than the FET in this respect. A comparative test resulted in roughly 20 microvolts of noise for the electrometer tube versus 120 microvolts for the FET.

Regardless of which device is used, internal noise appears as a drift signal as shown in Figure 4-25. Since this noise signal appears in the input stage prior to any gain, Equation (3) of the previous section is modified and appears as

$$e_{out} = \frac{-A_o\ e_n}{1 + A_o\ \beta(\omega)} \tag{15}$$

where it can be shown that β is a function of frequency. Two cases can be considered when examining what happens to internal noise with frequency, one case with uncompensated feedback and the other with compensated feedback.

With uncompensated feedback, the circuit takes the form as shown in Figure 4-26.

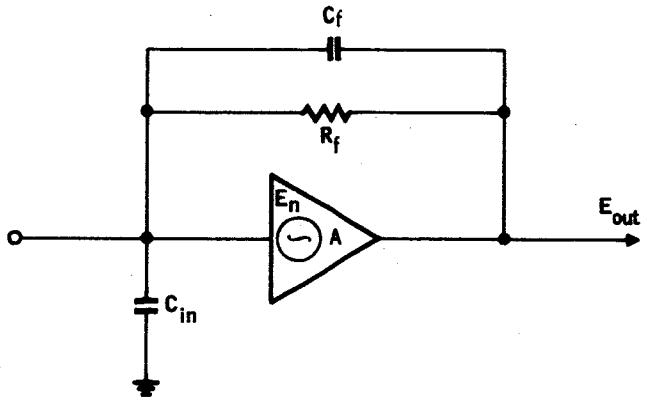

FIGURE 4-26
Circuit for Noise Consideration With Uncompensated Feedback

The term $\beta(\omega)$ of Equation (15) for this circuit can be found to be

$$\beta(\omega) = \frac{j\omega C_f R_f + 1}{j\omega C_f R_f + j\omega C_{in} R_f + 1} \tag{16}$$

If typical values are taken for C_{in} C_f, and R_f, the noise gain of such a system can be found over frequency as shown in Figure 4-27.

With compensated feedback, C_f can be neglected and the circuit appears as shown in Figure 4-28.

The term (ω) of Equation (15) becomes

$$(\omega) = \frac{1}{j\omega C_{in} R_f + 1} \tag{17}$$

With the previous values for C_{in} and R_f the noise gain of this system is found to be as shown in Figure 4-29.

A comparison between Figures 4-27 and 4-29 shows that the compensated system has about 15 DB more noise gain at 1 Hz than the uncompensated system. It appears therefore that a slow system is less noisy than a fast one. It must be remembered that the uncompensated system is band limited by the time constant of the feedback resistor and its stray capacity.

If it is considered that the input device has 120 microvolts of noise and the bandwidth is 1 Hz the uncompensated system will result in 1.2 millivolts of noise. The compensated system will exhibit about 6.6 millivolts of noise.

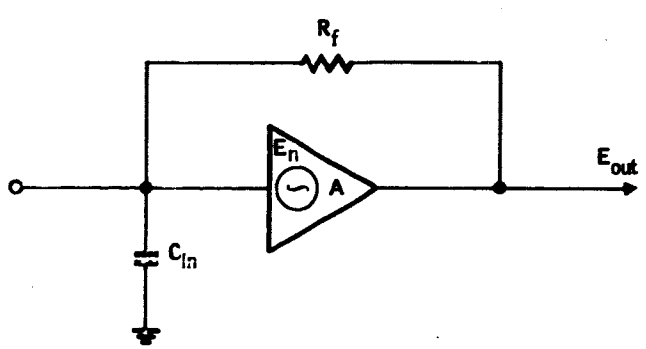

FIGURE 4-28
Circuit For Noise Considerations With Compensated Feedback

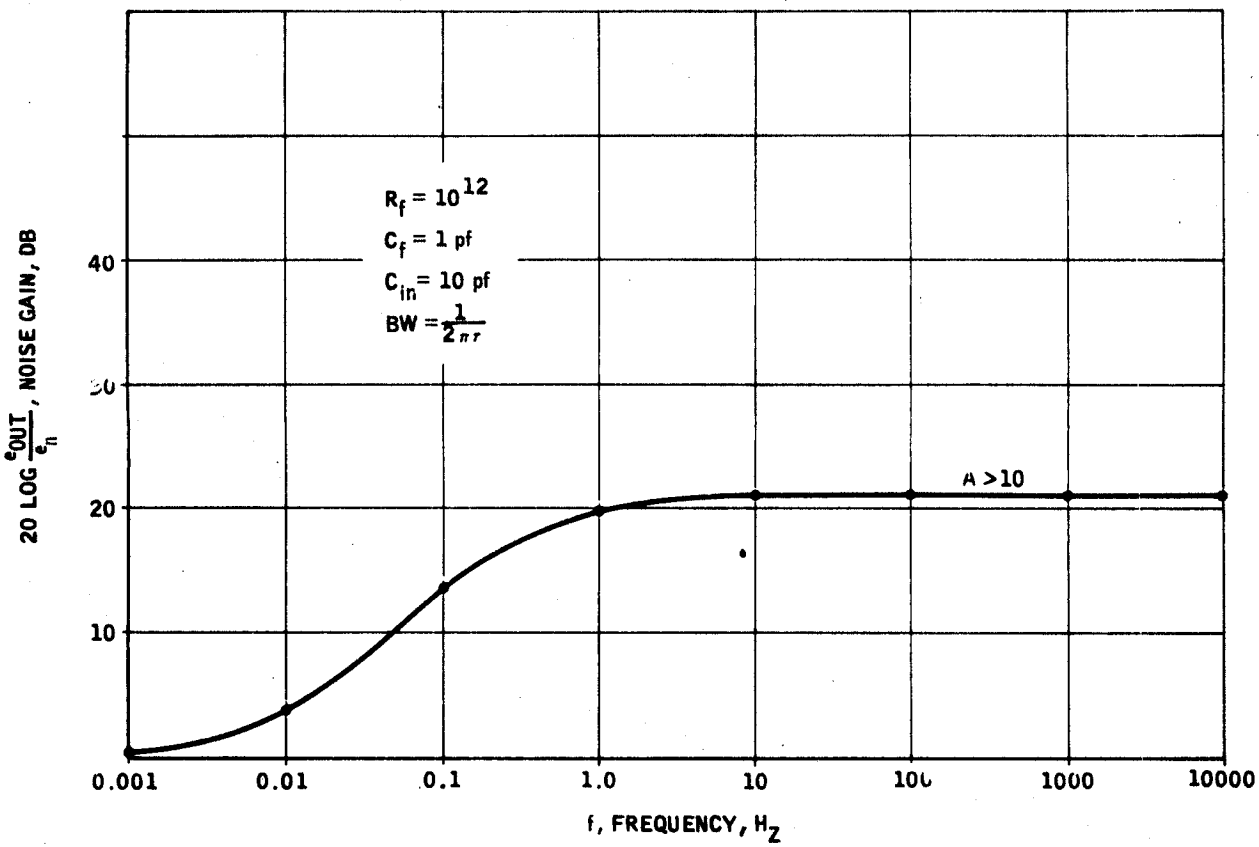

FIGURE 4-27
Noise Gain Versus Frequency for an Uncompensated System

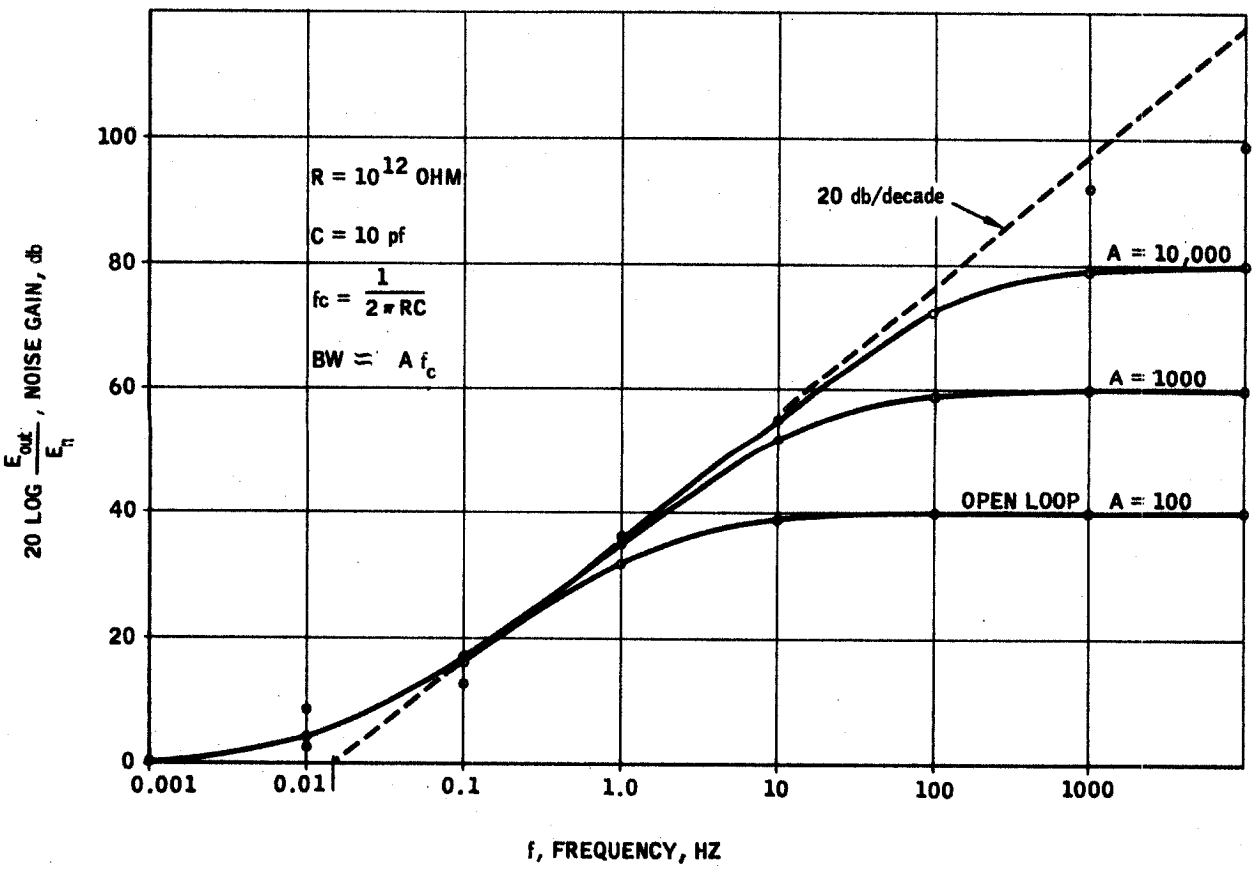

FIGURE 4-29
Noise Gain Versus Frequency For a Compensated System

Test data is available on a DC system using a solid-stage input device. The information shown in Figure 4-30 was taken from a system with a 5×10^{12} ohm feedback resistor and a response of 650 milliseconds. The upper trace shows to what extent a 10^{-14} ampere input signal can be resolved. The lower trace shows that the minimum detectable signal is above 3×10^{-15} ampere. The measurable noise is approximately 35 millivolts. A slower system with a smaller feedback resistor will realize lower noise.

Figures 4-31 and 4-32 show comparison data for an electrometer tube input versus an insulated gate field effect transistor. The electrometer tube shows an offset of 10^{-14} ampere due to grid leakage. The solid-state device shows no measurable offset indicating very low gate leakage. The relative noise of the two devices can also be compared and it is seen that the tube has lower noise.

4.5.7 CONCLUSIONS

The primary design requirements of minimum power and weight and maximum reliability gives a definite direction to the design approach. This is one of using uncomplicated minimal circuits. The simplified approach to the detector system is one of using a basic feedback amplifier to achieve the desired stability. Some sensitivity is sacrificed by using a solid-state input device but at a saving in power, weight, and reliability. To reach the desired sensitivity, the system bandwidth is narrowed and uncompensated feedback is used to minimize noise. With the use of a solid-state input device, it is calculated that the drift plus noise can be kept to less than the minimum output signal of 10 millivolts. Such an approach limits the system response which in this case is determined to be about one second. The detector system response suffers the largest tradeoff to accommodate the DC solid-state approach. The response of an uncompensated system is given by

$$\tau = \frac{R_f C_{in}}{1 + A} + R_f C_f$$

where it is seen to be a function of the feedback resistor R_f, and its stray capacitance C_f, if the gain A is sufficiently high to negate the first term of the expression. With practical values for R_f and C_{in}, it is determined that the gain should be at least 1000.

A typical detector capable of meeting the requirements is shown in Figure 4-33. This circuit utilizes three gain stages and an emitter follower output stage. Each gain stage is by itself gain stabilized because of its series feedback configuration. The input device is a solid-state, insulated gate field effect transistor and the second stage is a temperature compensated, junction field effect transistor. The power requirement of this circuit is determined to be less than 100 millivolts.

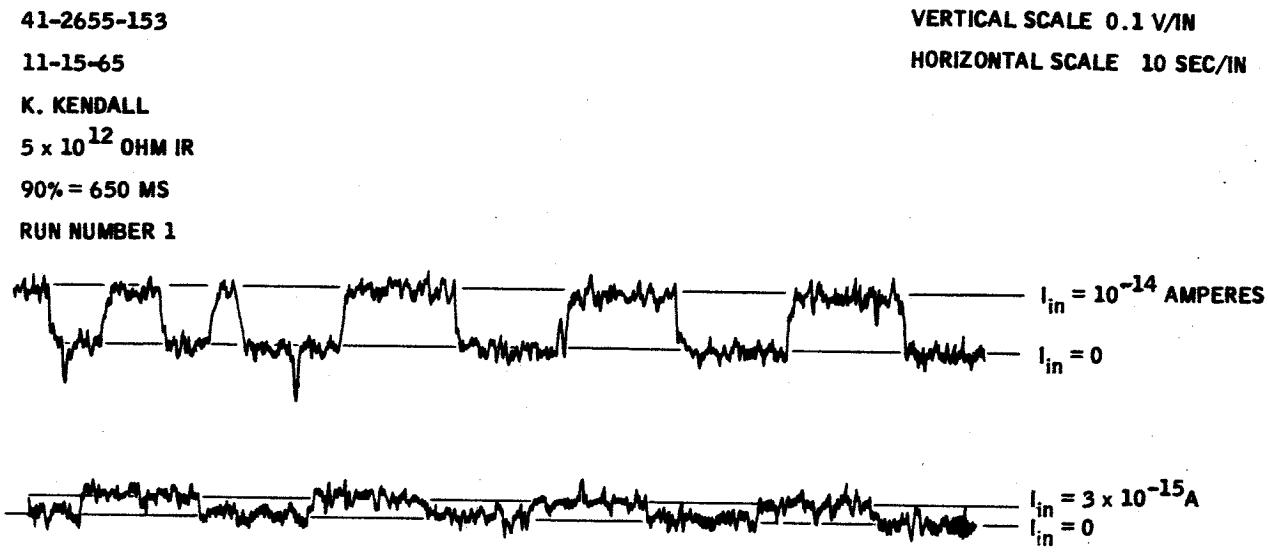

FIGURE 4-30
Signal Resolution of a DC Amplifier

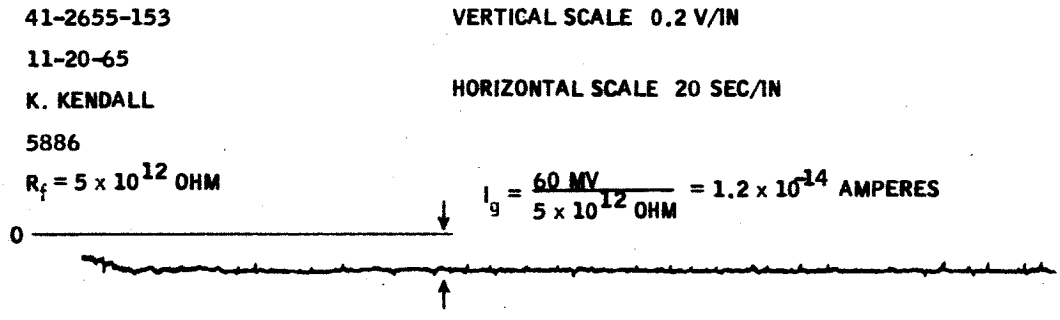

FIGURE 4-31
DC Preamplifier Using an Electrometer Tube

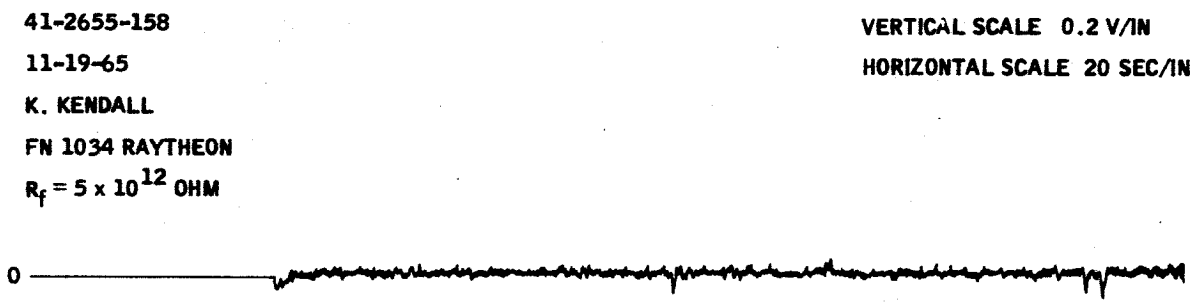

FIGURE 4-32
DC Amplifier Using an Insulated Gate Field Effect Device

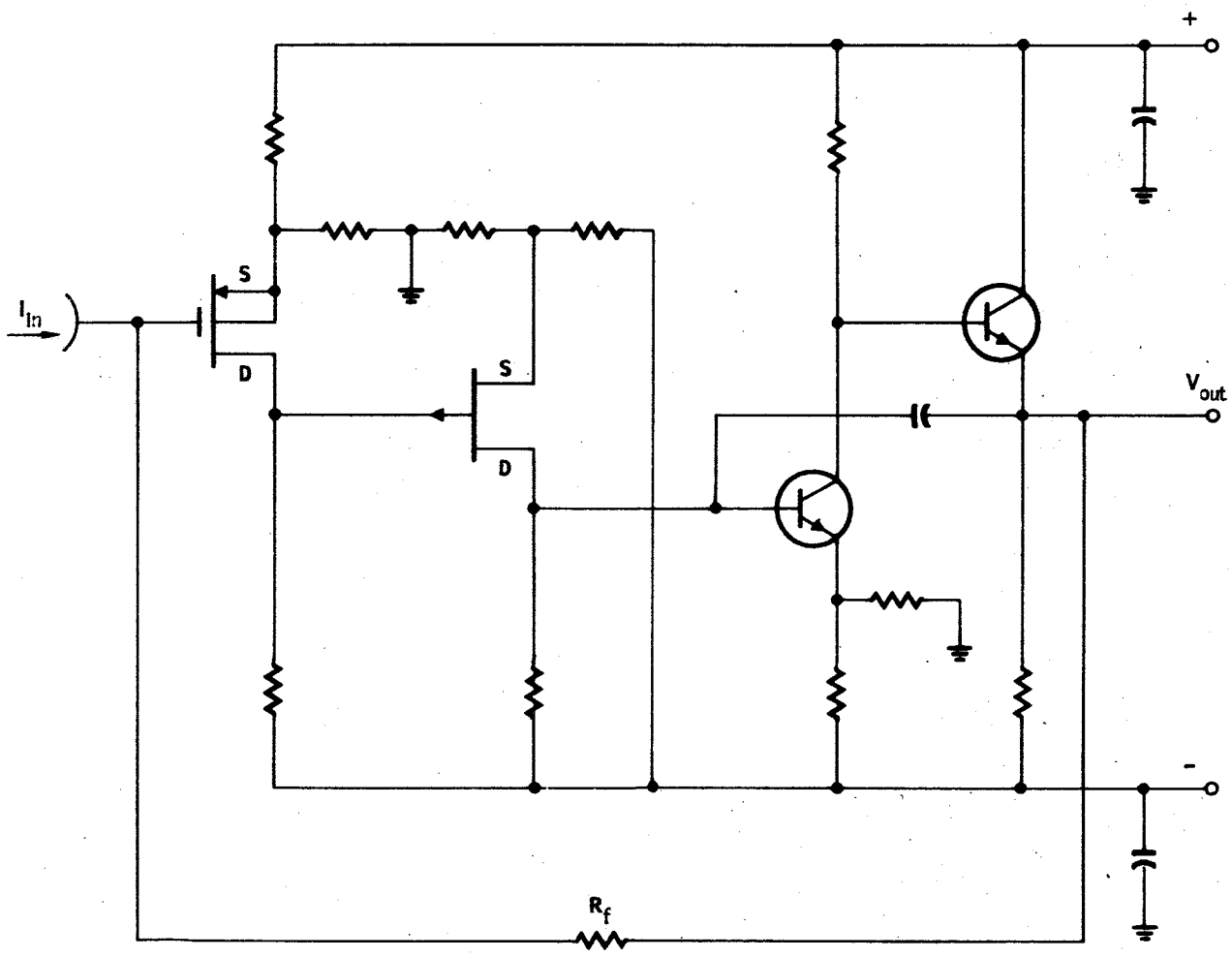

FIGURE 4-33
Solid-State Detector Circuit

The size and weight of this detector is not so much determined by the components as by the shielding necessary for the feedback resistor and the input device gate circuit. It is estimated that the component weight should be less than 25 grams, and the shielding and packaging should be on the order of 80 grams.

The complete system will consist of four separate detectors, one for each ion collector. There will be two different detectors with the difference being the value of the feedback resistor. The packages with identical feedback resistors will be modular and interchangeable.

4.6 SENSOR SYSTEM SUPPORT ELECTRONICS

4.6.1 GENERAL CONSIDERATIONS

The sensor system support electronics group is made up of the power supplies shown in Figure 4-34. The filament supply, ion source supply, and detector supply are required for operation of the analyzer; while the input regulator may be needed if the spacecraft power is not sufficiently regulated and noise free. This portion of the report describes the optimum conceptual design of the four supplies to best meet the needs of the proposed sensor system.

The design decisions made during the study were based on four factors:

a. The requirements of the sensor system as outlined in other sections of this report.

b. An analysis of previous systems built by SDS Data Systems for similar uses.

c. A literature search which disclosed new methods at doing established tasks in an improved manner.

d. A determination of the best trade-off between reliability, efficiency, size and weight.

The reasons for each decision are discussed separately for each supply.

The following discussion is logically broken into two areas: power converter and regulators. Power supplies cover a broad spectrum of the electronic circuit design field. Both analog and digital techniques may be used and a variety of electronic components are available to perform specific power supply functions. Power supply systems may be placed in three categories:

a. ac to dc systems

b. dc to ac systems - usually called inverters

c. dc to dc systems - usually called converters

In this report, only the latter two systems need to be considered since the spacecraft power is dc.

The dc to ac conversion is typically done by using a solid-state switching circuit to chop the dc input into pulses. The pulses are then applied to the primary of a transformer and the ac signal appears at the secondary. Conversion of dc to ac may be used to alter the voltage level available or to provide dc isolation between portions of the system. The support electronics uses inverters for both reasons.

Dc to dc conversion is actually done by an inverter (dc to ac) with the resulting ac output being returned to the dc state by rectification. This can

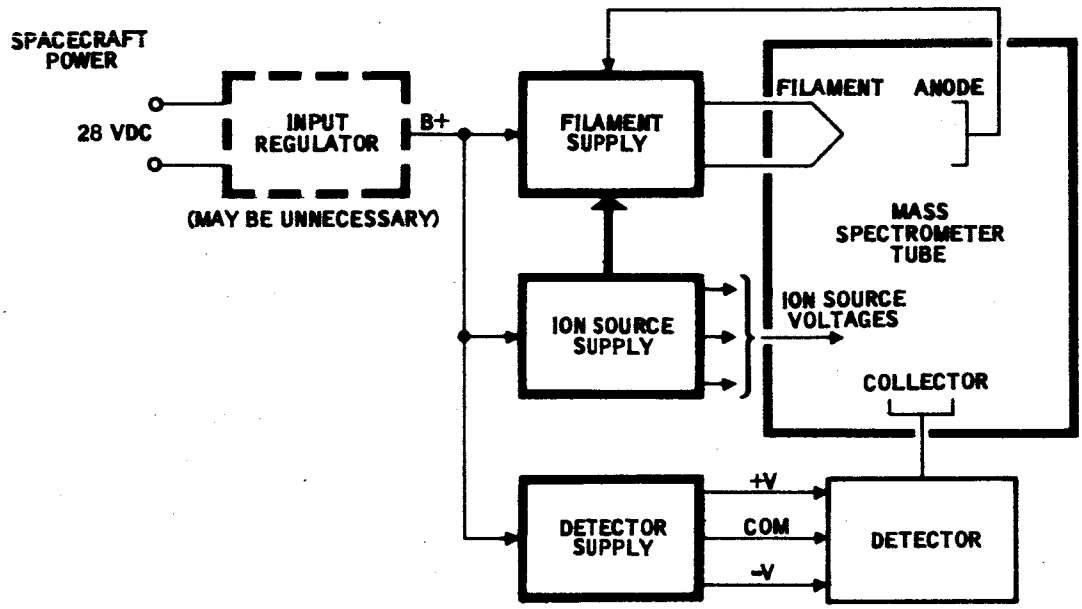

FIGURE 4-34
Sensor System Support Electronics

implement dc isolation but more usually it is done to make another voltage level available. The converter is used in the support electronics, too.

Electronic systems depend on their power supplies to provide a stable source of voltage. A centralized source of power, such as a battery or fuel cell, is normally not stabilized to the required degree. For this reason, most electronics systems must use one or more regulators between the power source and the electronics. Voltage regulators are placed in three broad categories:

a. Shunt regulators

b. Series regulators

c. Switching regulators

Each type has certain advantages and disadvantages which must be weighed in order to determine the best regulator for a particular application.

The shunt regulator can be the least complicated type of regulator, in its simplest form, requiring only a breakdown diode in parallel with the load and a resistor in series with the diode-load combination. However, it is also the least efficient. It is mainly useful in applications where the input variations and load variations are very small. This type of regulator will not be considered further in this analysis.

The series voltage regulator places the regulating element in series with the load. The usual series element uses transistors and regulation occurs as the result of varying the voltage drop across the element. This regulator is somewhat more complex than the shunt type but it is also much more efficient. The major source of loss is the series transistor. The series regulator can offer extremely good regulation, low ripple, and fast response.

The switching regulator also utilizes a series regulating element which may be a transistor, silicon controlled rectifier, or similar device. The series element is switched between its on and off state, thus chopping the dc input into a series of dc pulses. These pulses are then utilized in the ac system by applying them to a transformer or are integrated by an L-C filter and returned to the dc state. Regulation is achieved by varying the pulse width and/or frequency of the pulses. This regulator is very efficient since maximum current flows through the series element when the voltage drop across it is minimum. A major portion of the losses can occur during the switching interval which should be minimized. A major disadvantage is the complexity of the circuitry necessary to maintain proportional control between the output voltage and switching element.

A summary of the advantages and disadvantages of a series regulator and switching regulator indicates that in most applications the switching regulator provides optimum performance. This is particularly true at currents above approximately thirty milliamperes.

Series Regulator

Advantages	Disadvantages
a. Fewer Components	a. Less efficient
b. Faster Response	b. Losses dependent on input voltage.
c. Lower ripple	

Switching Regulator

Advantages	Disadvantages
a. More efficient	a. Slower response
b. Lower power transistors may be used.	b. More components
c. Losses are not so dependent on input voltage.	c. Higher ripple
d. Less heat is produced	

A special type of switching regulator utilizes pulse duration modulation (PDM). In this circuit, the input is an ac square wave while the output is a series of ac pulses. The regulator controls the width of the pulses and thus the total power content of the output. This PDM regulator is extremely efficient in an ac system because it avoids rectifying the input and then chopping it again at the output.

The schematic diagrams presented in the support electronics section are representative of the type of circuit proposed. No detailed design effort was made and it is probable that the actual circuits will be less complex and more efficient than those shown. Each supply was chosen to fit the needs of the subsystem it was powering with regard to the critical characteristics of that subsystem - such as regulation, ripple, and time response. When all the subsystem supplies had been determined, the overall system was scrutinized for incompatibilities and necessary corrections were made. The result is an optimum support electronics group for the proposed sensor system.

4.6.2 FILAMENT SUPPLY

The function of the filament supply is to provide power to the source of electrons in the analyzer. The electron source is a low voltage, high current ac filament. It is also necessary for the filament supply to be part of a control loop which holds the anode current constant. The actual control is

done by varying the amount of power supplied to the filament which in turn determines the number of electrons emitted. The specifications for this supply are given below:

Output:

Voltage Range -	0.5 - 2.0 V peak-to-peak
Current Range -	0.0 - 2.5 amperes
Anode Current Range -	50 - 200 microamperes
Anode Current Regulation -	±0.5%

Input:

Voltage Range -	28 ±0.5 Vdc
Ripple and Noise -	not available
Maximum Input Transient -	not available
Rise Time at turn-on -	not available

Environmental:

Temperature -	0 - 35°C

The fundamental circuit is shown in a modified block diagram form in Figure 4-35. The dc input signal is chopped by a multivibrator and the resulting signal is impressed across the primary of the isolation transformer. The ac signal developed by the secondary of the transformer may or may not be rectified depending on the type of regulator employed. The power applied to the primary of the filament transformer is varied by the regulator which is controlled by a feedback signal developed from the anode current. The ac signal appearing at the secondary of the filament transformer drives the filament causing electrons to be emitted. The amount of power applied determines the number of electrons being generated, while the thermal time constant acts as an integrator and maintains constant emission. The majority of the electron emission is collected at the anode. The regulator, filament, anode, and control signal section make up a closed loop control system and maintain anode current at a constant level. The entire loop is floating above ground at the anode supply potential. This necessitates a careful design to avoid leakage to ground and eliminate voltage stresses on the components.

The recommended inverter is shown in Figure 4-36. It is a simple yet reliable circuit using the practical minimum number of components, while still providing self-starting and good operating characteristics. The transformer is wound on a toroidal core made of soft magnetic material possessing a square hysteresis loop. The square loop minimizes inductive kickback stress on the components since in its saturated state it exhibits very little inductance. A two transformer circuit, in which oscillation is maintained by a square loop core and the output is taken from a linear core, was considered because of its high efficiency. However, at the power level required in this application, the increase in size, weight, and complexity was considered to negate such an advantage.

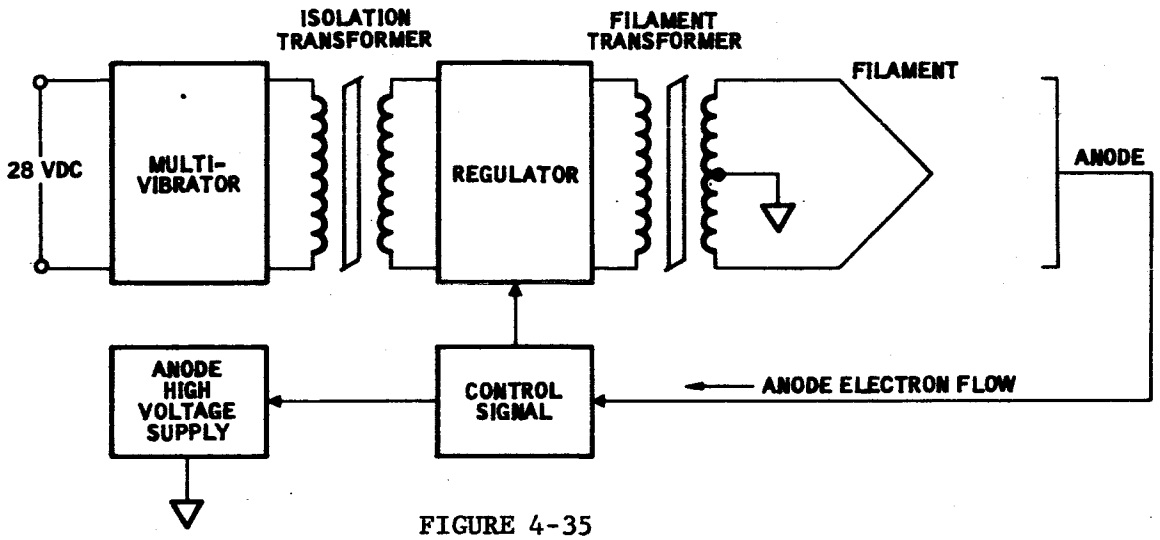

FIGURE 4-35
Filament Supply Circuit

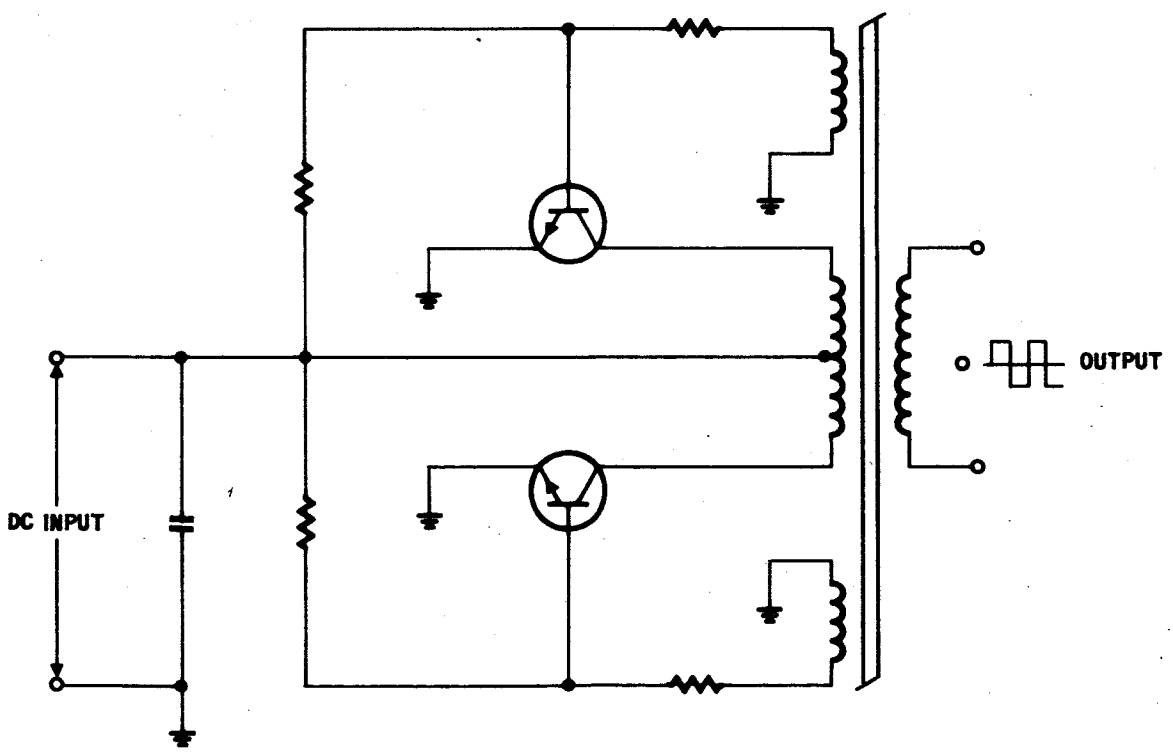

FIGURE 4-36
DC to AC Inverter

The transistors used must be able to withstand twice the supply voltage and should have a frequency cut-off characteristic ten times greater than the switching frequency to decrease switching losses. By using transistors with high current gain and by using separate feedback windings for impedance matching, efficiency is improved. The overall efficiency of this inverter should exceed seventy-five percent in this application.

The function of the regulator and control signal section is to maintain the anode current at a constant amplitude. An examination of the total system indicated that the most logical approach was to modulate the pulse duration of the ac output produced by the isolation transformer; in this way conversion to dc with its inherent losses can be avoided. A modified block diagram of such a system is illustrated in Figure 4-37.

The amplifier stage shown may or may not be necessary depending on the anode current amplitude and the allowable impedance in series with the anode supply. The Schmitt trigger circuit can be designed with a combination of positive and negative feedback to reduce hysteresis effects. The output of the Schmitt trigger consists of a series of pulses proportional to the amount of anode current flowing. The output pulses are used to turn the series transistor switches in the regulator off and on modulating the ac signal, driving the primary of the filament transformer. The three advantages of this approach are that the circuit uses less components than other types; the series transistors as well as the Schmitt trigger transistors operate in a switching mode; and there is no ac to dc conversion necessary in the high current portion of the regulator. The only apparent drawback to the described arrangement is the inability to filter switching transients which might be coupled back to the power source.

The number of active components required is estimated to be 6 transistors, 5 diodes, 1 breakdown diode. Power consumption should not exceed 100 milliwatts.

A regulator of this form has not been used previously in this type of system, so an alternate system with a more conventional approach was analyzed. See Figure 4-38. The rectified output of the isolation transformer is applied to a standard switching regulator. The output of the switching regulator drives the primary of the filament transformer with a pulsed dc signal and the amount of power in the secondary is adjusted by changing the duty cycle and repetition rate of the regulator output. The regulator is controlled by the output of a voltage-controlled oscillator whose signal is proportional to the voltage developed across a series impedance path in the anode circuit. In Figure 4-39, a typical voltage-controlled oscillator and switching regulator system is shown adapted to the present application. The circuit contains a differential amplifier, a voltage-controlled multivibrator, two driver stages, and a series switch.

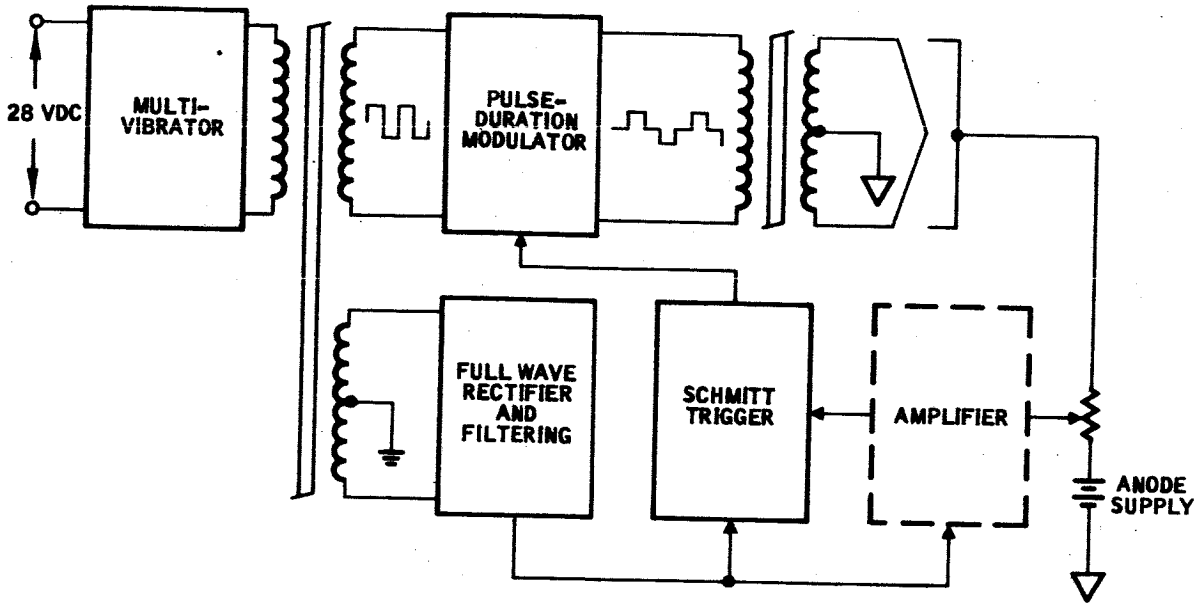

FIGURE 4-37
Emission Regulator

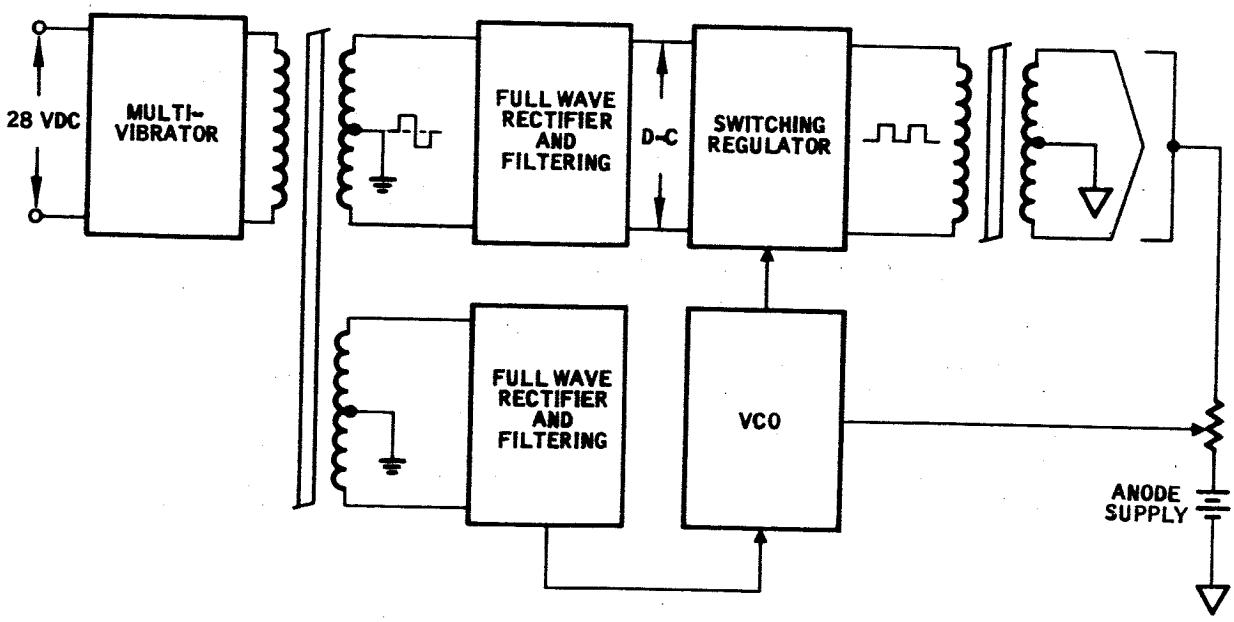

FIGURE 4-38
Regulator Analysis

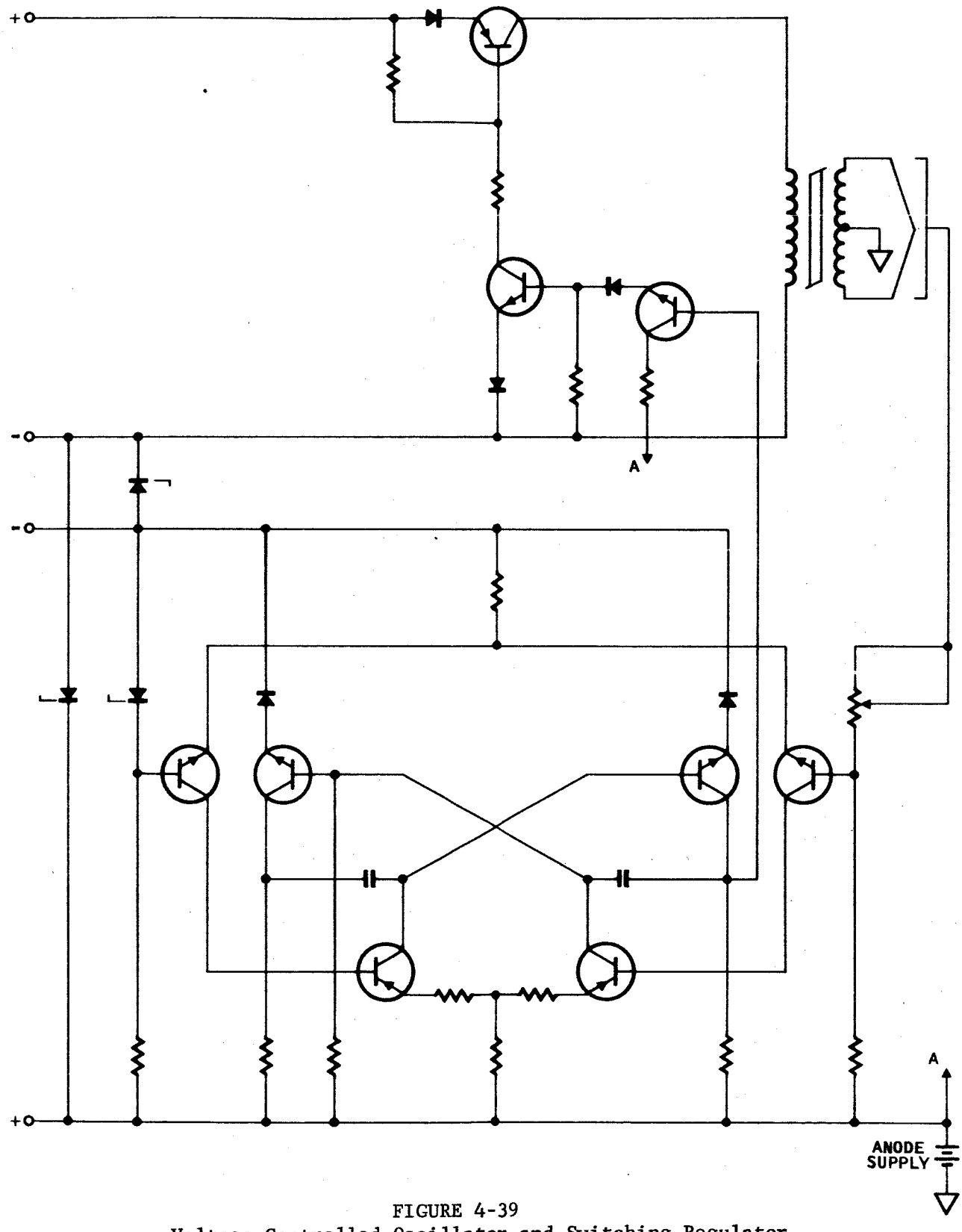

FIGURE 4-39
Voltage Controlled Oscillator and Switching Regulator

The total number of active components for the switching regulator system is estimated to be 9 transistors, 9 diodes, and 3 breakdown diodes. Filter components will be necessary also. The efficiency of the regulator should approximate 70%.

The conclusion must be drawn that the pulse duration modulation regulator with nearly fifty percent fewer active components than the switching regulator should be examined first in the design stages. If design difficulties are experienced, the switching regulator with its higher degree of development may be substituted without a significant increase in effort.

4.6.3 ION SOURCE SUPPLY

The ion source supply provides the various electrodes within the analyzer with their required potentials. The electrodes accelerate and focus both the electron beam emitted by the filament and the ion beam formed in the ion source. For the total system to be accurate, the potentials must be very stable and have a low ripple content. The specifications for this circuit are given below:

Output:

Voltage Range:

Low Supply -	100 - 200 volts
High Supply -	200 - 300 volts

Current Range:

Low Supply -	0 - 100 microamperes
High Supply -	0 - 500 microamperes

Regulation:

Low Supply -	0.5%
High Supply -	0.5%

Ripple and Noise:

Low Supply -	0.1%
High Supply -	0.1%

Input:

Voltage Range -	28 ±0.5 V
Ripple and Noise -	not available
Maximum Input Transient -	not available
Rise time at turn-on -	not available

Environmental:

Temperature -	0 - 35°C

The ion source supply actually consists of two individually regulated supplies stacked one on the other. See Figure 4-40. The lower supply establishes the reference voltage for the filament and the operating potential for the filament shield; the upper supply provides the operating voltages for the anode, the electron accelerator, the repeller, the ion accelerator, the electron focus, and ion focus electrodes. These electrodes must have a very stable potential and the ripple content must be extremely small so that there will be minimal deviations of the electron and ion beams.

The problem of close regulation is complicated by the fact that several of the electrodes may draw current under certain conditions. In addition, some potentials must be adjustable. To maintain low output power, a high resistance voltage divider is necessary. However, the resultant high output impedance causes the regulation to be degraded for voltage taps within the divider string.

The two supplies are very similar in function and design and the following general discussion will hold true for both of them. Differences will be noted as they appear.

The regulator will control currents of ten milliamperes or less. Under this condition, fixed losses, such as those introduced by the transformer core, are a significant part of the total losses, and the increases in efficiency of a switching regulator does not justify its added circuit complexity. For this reason, a series regulator similar to the one illustrated in Figure 4-41 is recommended.

At the current and voltage levels encountered, the circuit offers excellent regulation with changes in line, load, or temperature. The design is simple and extremely stable. The use of low current temperature-compensated reference diodes in conjunction with a differential pair offers the opportunity to maintain a very small overall temperature coefficient.

The circuit uses five transistors, two diodes, and two temperature-compensated breakdown diodes. Circuit efficiency should be greater than 50%, which is adequate, since the whole system consumes very little power, approximately 150 milliwatts, depending on the actual potentials necessary.

Figure 4-42 represents the dc to dc converter. The multivibrator is identical to the one used in the filament supply. Its advantages are simplicity and efficient operation. The transformer is a toroidal type with a square hysteresis loop. Conversion to dc is done with a full wave bridge to take advantage of the low ripple characteristics that the bridge offers. The converter needs an estimated 150 milliwatts for its operation.

The electrodes in the mass spectrometer need a variety of potentials. Several factors influence the manner in which these potentials are obtained. To insure accuracy, the voltage must be stable to insure low dissipation, the resistance must be high; and certain potentials must be adjustable so that system operation may be maximized.

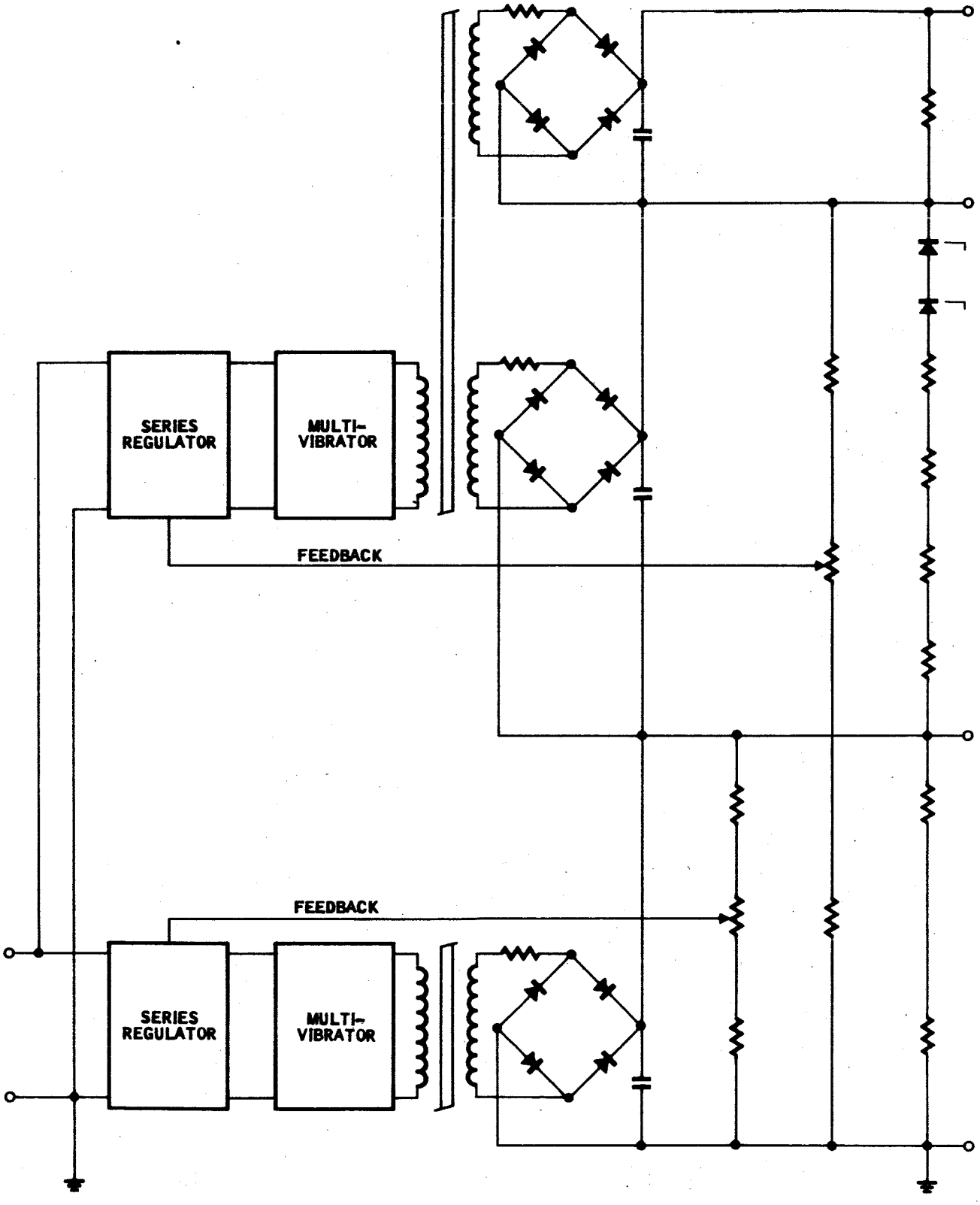

FIGURE 4-40
Ion Source Voltage Supply

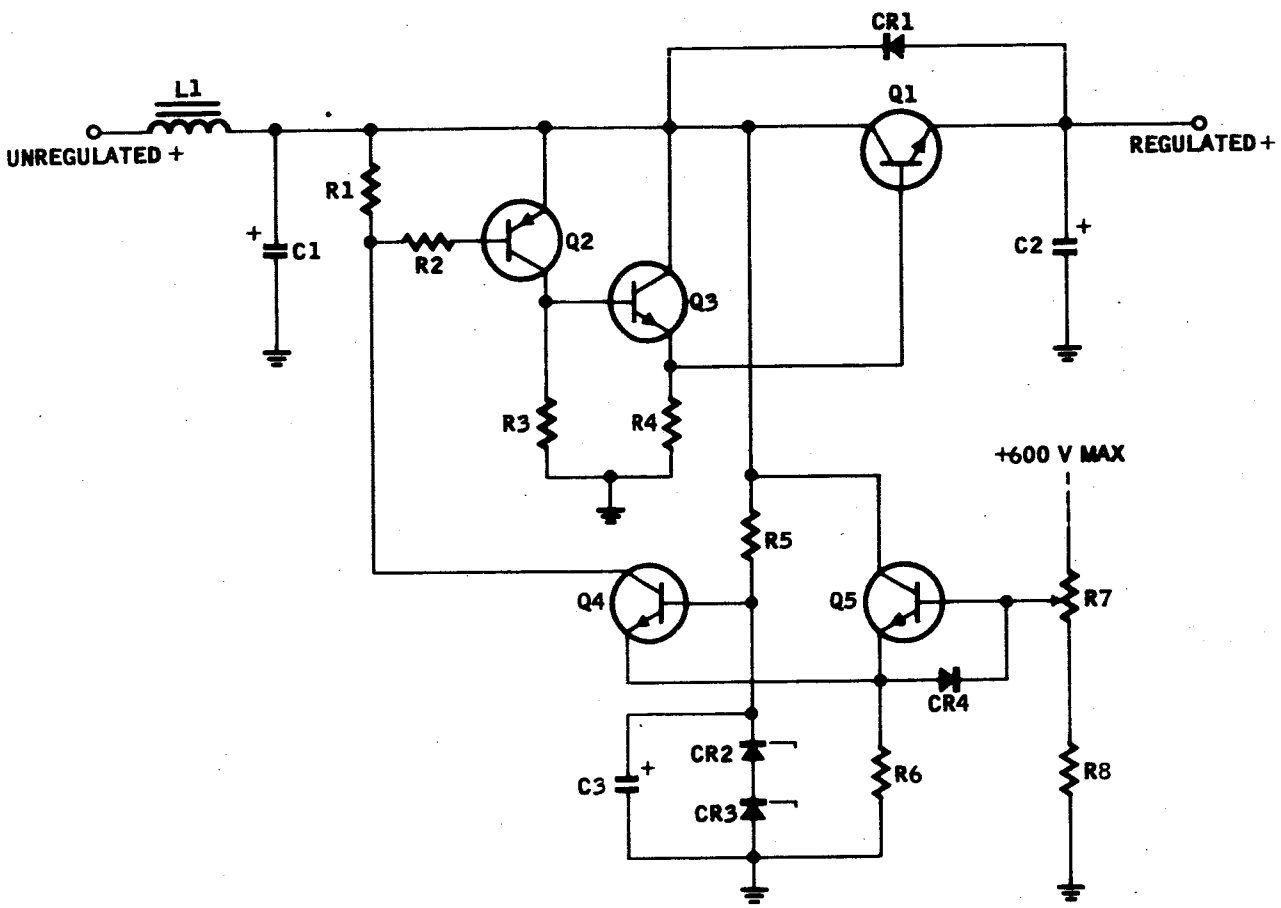

FIGURE 4-41
Voltage Regulator

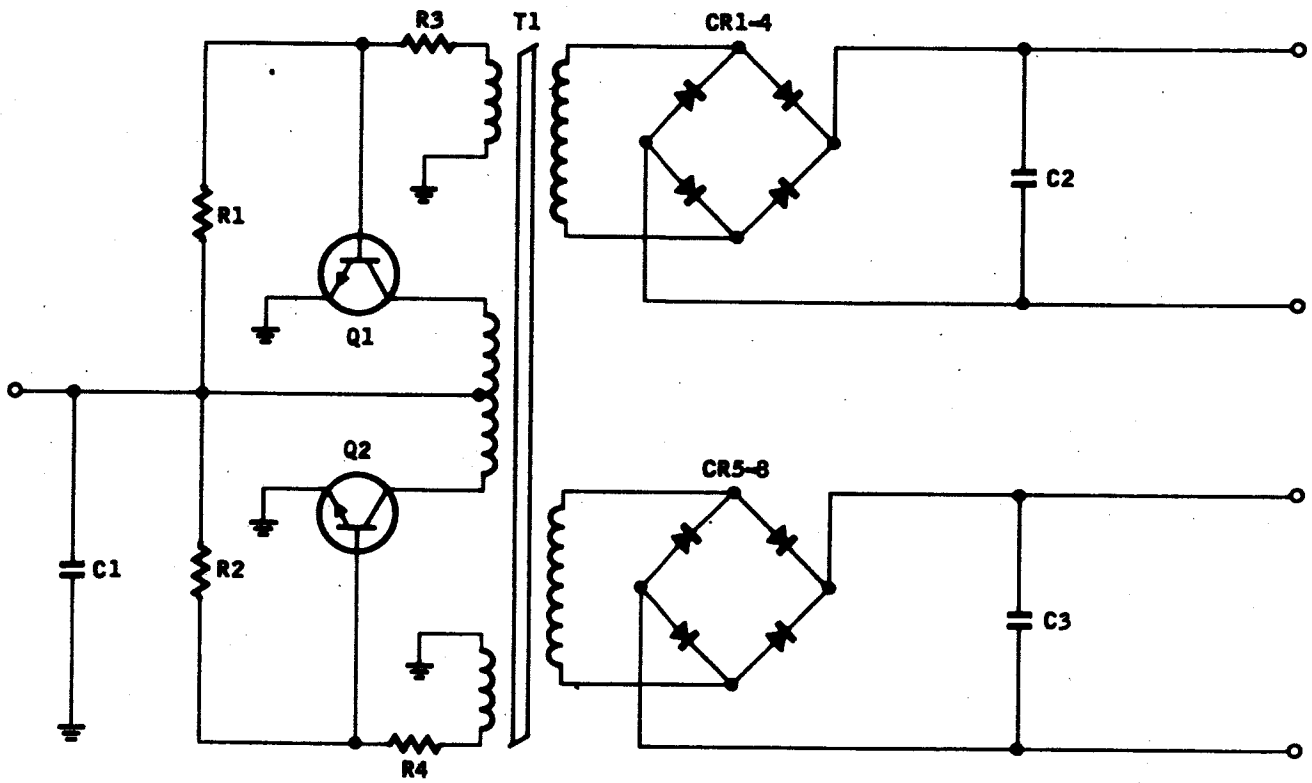

FIGURE 4-42
DC to DC Converter

A design complication is that some of the electrodes may have current flowing through them. The anode receives the majority of electrons emitted by the filament and between fifty and two hundred microamperes may be expected to flow. The electron accelerator, which operates at or near the anode potential, may also collect electrons and currents between zero and one hundred microamperes may flow. Fortunately, the anode and electron accelerator voltages may have minor variations without adversely affecting operation. With this in mind, the circuit of Figure 4-43 was designed. The anode and electron accelerator are driven from an unregulated, low impedance source so that the voltage variations produced by current changes are not significant.

The potential appearing between the repeller and ion accelerator is the most important in the entire system. Small variations can cause the electron beam to be improperly deflected and impinge on the ion accelerator electrode. The electrons striking the ion accelerator cause a secondary emission of electrons which are attracted to the higher potential of the repeller, causing current to flow. If these two electrodes were connected to a high impedance divider, the current flowing through them would further change the interelectrode potential and cause a concomitant change in beam deflection. The result would be an ever worsening condition ending with the system being inoperative. To avoid such an occurrence, the repeller is connected to a low impedance, well regulated point and the ion accelerator voltage is clamped to the same point by a series string of temperature-compensated zener diodes in series with a small resistance. The resistance is necessary to provide an adjustment range. If the electrodes are set properly so that very little current flows in them, the major change in voltage will occur with temperature. Using presently available 500 microamperes diodes having a temperature coefficient of five parts per million per degree centigrade, a maximum change of five millivolts can be expected. A variation of this magnitude should not cause any problems.

The ion focus and electron focus electrodes do not carry any current under normal conditions so that the simple resistive string shown in Figure 4-43 is adequate.

The entire system is referenced to the center tap of the filament. For this reason, the filament reference potential must be closely regulated. The present design uses a separate supply with its own regulator to maintain the necessary regulation.

The filament shield does not carry current so that it is possible to use a high resistance voltage divider without having any deleterious effects on the system.

Using typical values, the power output of the combined ion source supplies total 110 milliwatts. Core losses in the two transformers plus the fixed losses in the regulators cause the efficiency figures to be very low and essentially nonrepresentative of the system. The entire ion source supply can operate with less than 750 milliwatts of input power.

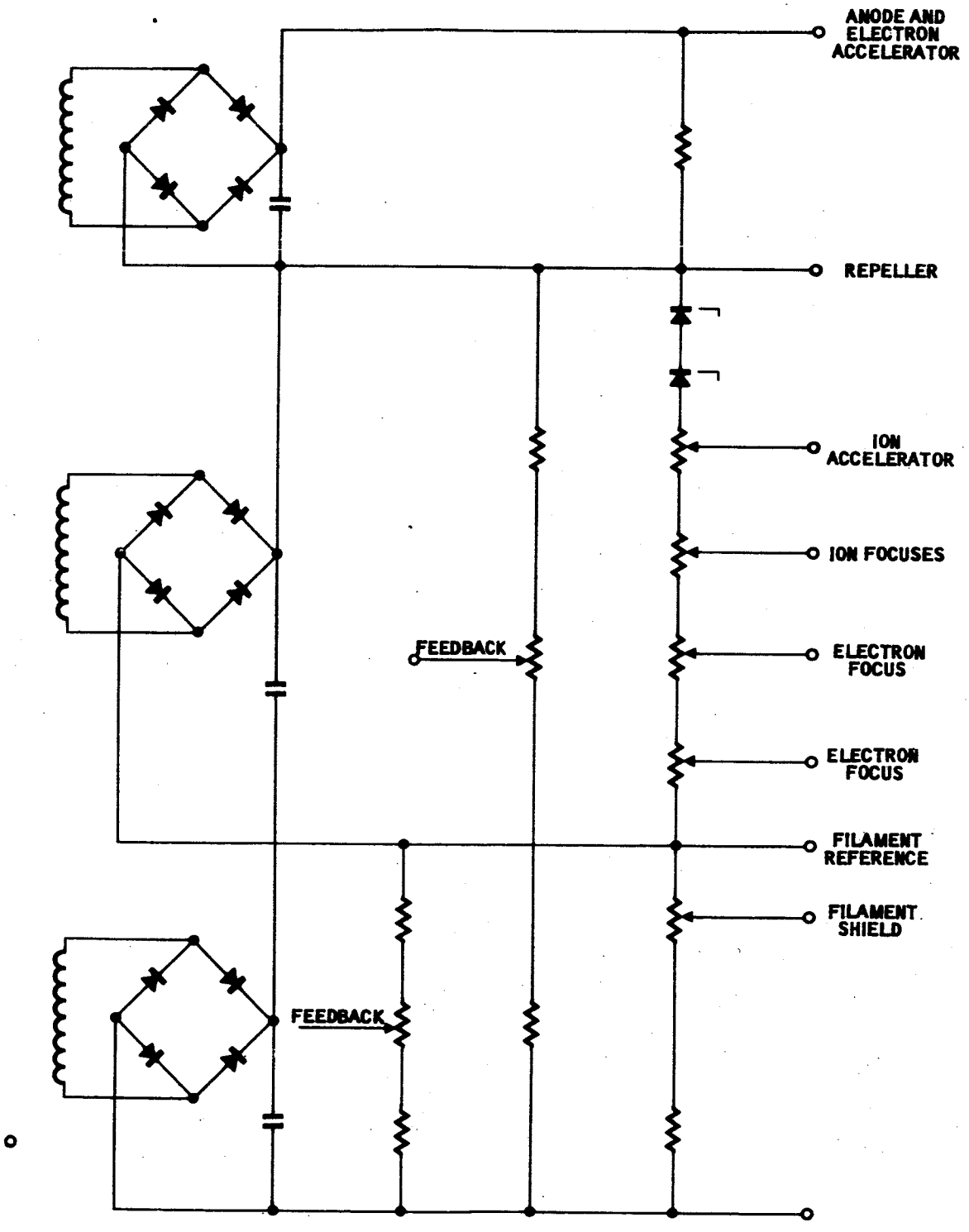

FIGURE 4-43
Voltage Divider

4.6.4 DETECTOR SUPPLY

The detector supply, Figure 4-44 is required to furnish well regulated low ripple power to the detector electronics. Two voltages are necessary; +15 V and -25 V. Four separate detector packages will be used, but the total power consumed will be very small. The specifications for this supply are given below:

Output:

Voltage Range:	
Positive Supply -	+15V ±10%
Negative Supply -	-25V ±10%
Current Range:	
Positive Supply -	5 milliamperes maximum
Negative Supply -	10 milliamperes maximum
Ripple -	0.5% maximum
Regulation -	0.1% maximum

Input:

Voltage -	28 ±0.5 V_{dc}
Ripple and Noise -	not available
Maximum Input Transient -	not available
Rise Time at Turn-on -	not available

Environmental:

Temperature	0 to 35°C

The entire supply consists of a dc to dc converter followed by two series regulators. At the extremely low currents provided to the detector, the switching regulator does not offer any significant power saving advantages. To assure an accurate output, the supplies must be well regulated and contribute very little ripple. These requirements are fulfilled by the series regulator quite economically in this application.

The dc to dc converter schematic is illustrated in Figure 4-45. The multivibrator is the standard common emitter type described previously. The transformer utilizes a toroidal core with a square hysteresis loop and consists of a primary winding, two feedback windings, and two secondary windings. Each output winding is bridge rectified to ensure an initial minimum value of ripple. The bridge feeds a capacitive filter which further reduces ripple and noise. Approximately 175 milliwatts are needed to power this circuit.

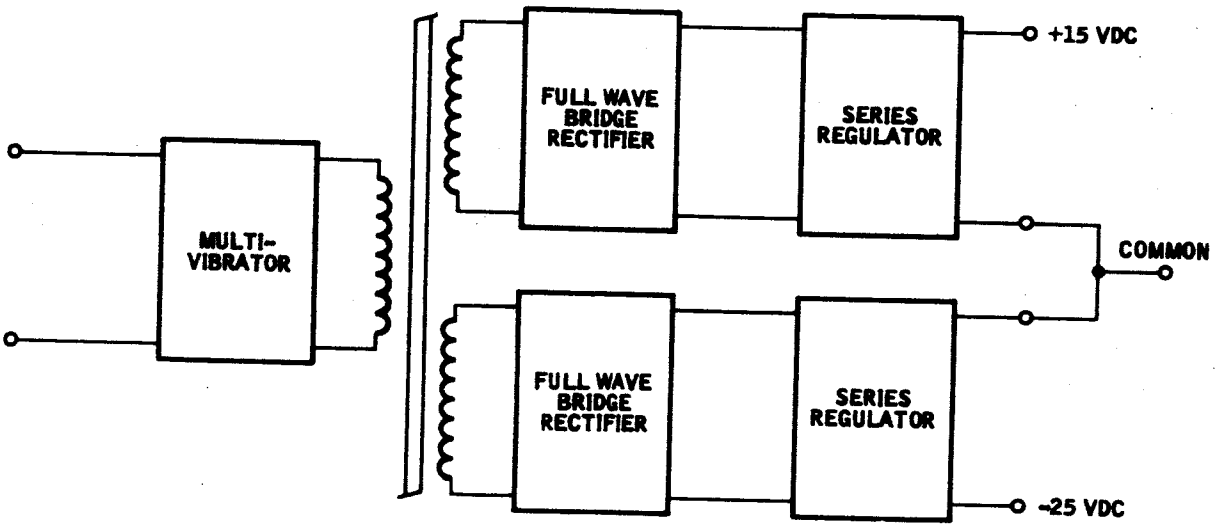

FIGURE 4-44
Detector Supply

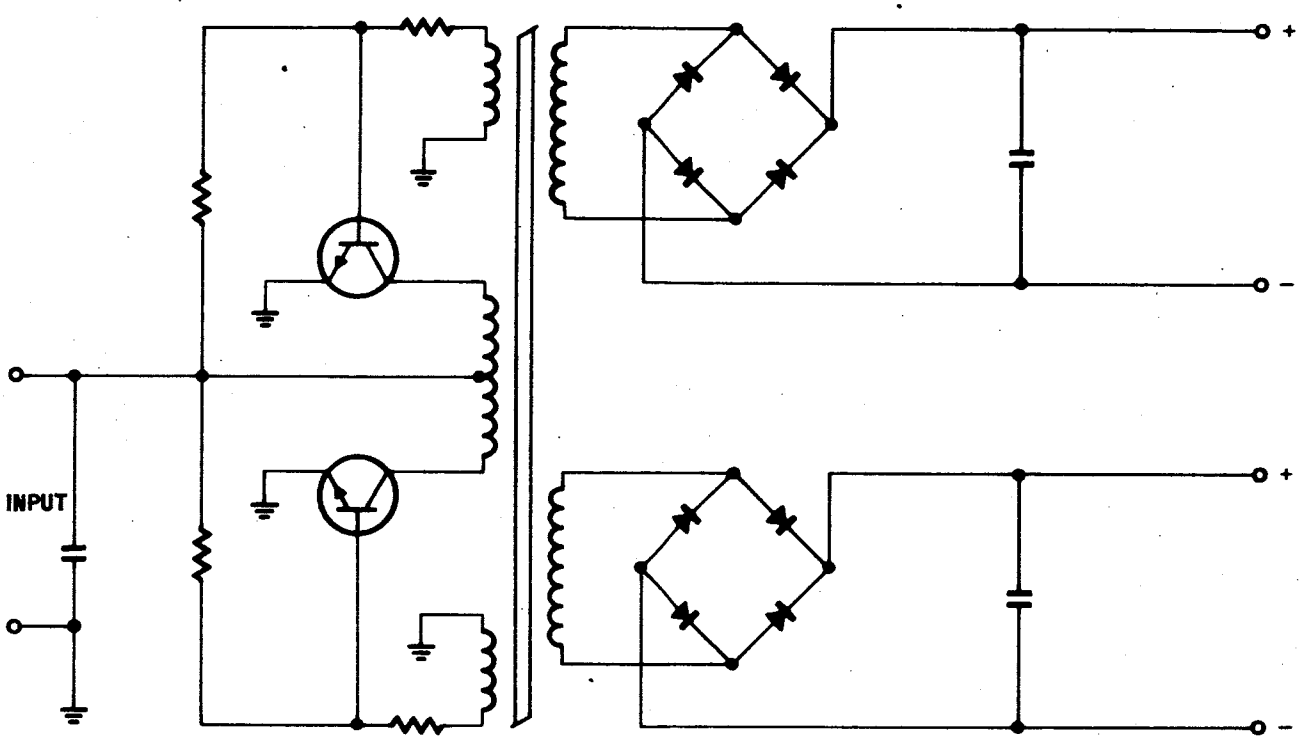

FIGURE 4-45
DC to DC Converter

A representative series regulator is shown in Figure 4-46. The circuit features two stages of amplification and low output impedance. Adequate temperature stability is realizable without selecting components. At the voltage and current levels present in this circuit, very high gain silicon transistors may be used, enhancing the stability and reliability of the supply. Power consumption is low, an estimated 100 milliwatts for each regulator.

The circuits shown meet the needs of the detector electronics well. The cost in components and power is low. There are 22 semiconductors; 8 transistors, 12 diodes, and 2 reference diodes. The nominal power consumption of the supply is estimated to be less than 700 milliwatts.

4.6.5 INPUT REGULATOR

The input regulator may be necessary if the origin of input power is the primary source of power for the other spacecraft systems. If this is the case, it is very probable that the input power will be subject to a great deal of noise, large transient variations in voltage and current, and will be a source of ground loops due to interface connections. The input regulator will act as a buffer stage, providing dc isolation as well as presenting a filtered, regulated voltage to the remainder of the support electronics. The specifications for this circuit are given below:

Output:

Voltage -	28.0V ±1%
Current -	150 milliamperes maximum
Ripple and Noise -	500 millivolts peak-to-peak maximum
Regulation -	1% line, load, and temperature
Output Impedance -	0.5 ohms maximum

Input:

Voltage -	28 ±3V
Ripple and Noise -	not available
Maximum Input Transient -	not available
Rise Time at turn-on -	not available

Environmental:

Temperature	0 to 35°C

A modified block diagram is given in Figure 4-47. The input filter is an important part of the system since it serves the dual purpose of reducing the noise present on the input voltage and reducing the magnitude of the switching transient being fed back to the power source from the multivibrator. The multivibrator and transformer perform the function of isolating the entire electronics package to held prevent ground loops. The rectifier circuit provides a dc source for the regulator. To obtain high efficiency at the power levels involved in the input regulator, the decision must be to use a switching

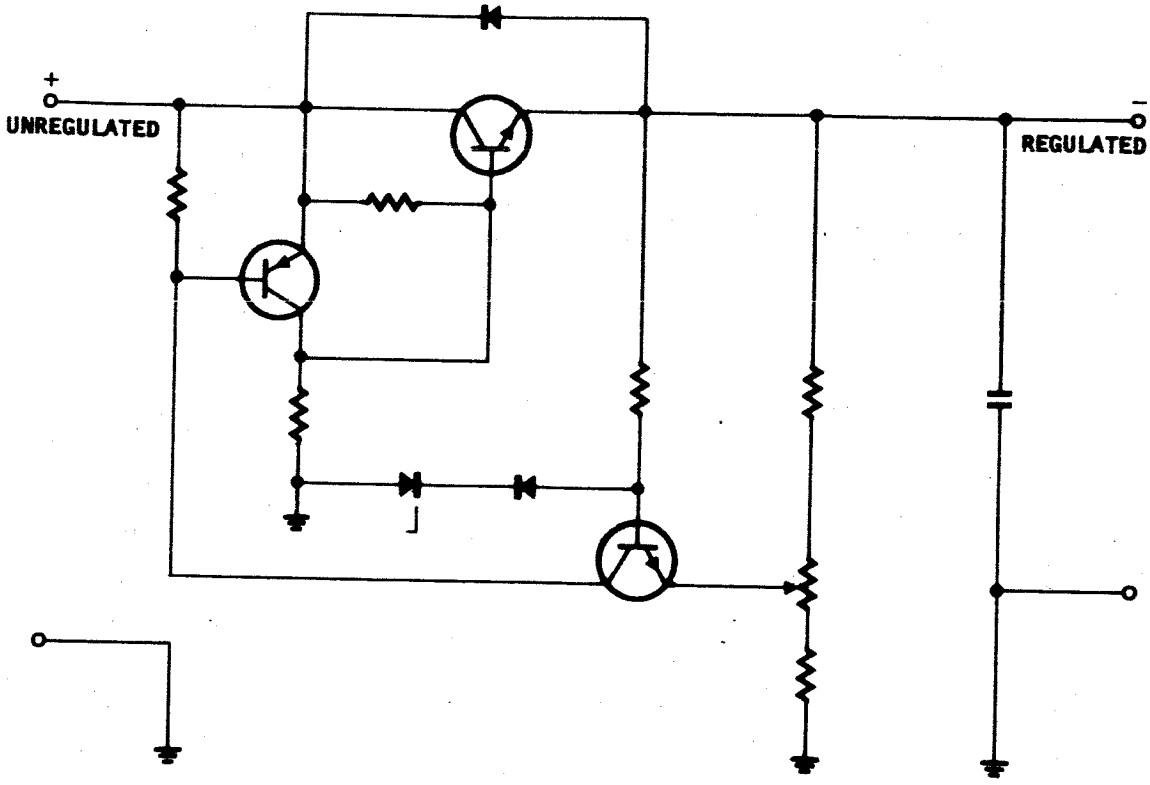

FIGURE 4-46
Series Regulator

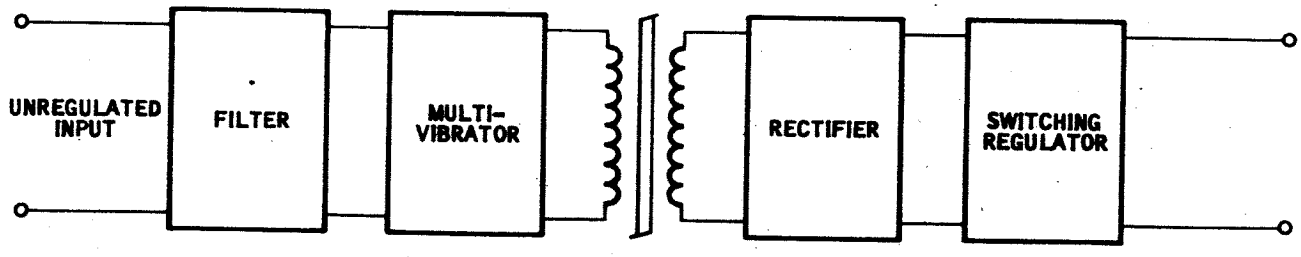

FIGURE 4-47
Input Regulator

regulator. This is particularly true because this is essentially a pre-regulator and does not need fast response or extremely close regulation.

The input filter must be carefully considered because of the important function it fulfills. It must not only block ripple and noise flowing in both directions but it must suppress line transients that could damage the multivibrator components. The circuit resulted from the conceptual analysis of these tasks is illustrated in Figure 4-48. It consists of an L-C pi filter employing a bi-filar wound inductor on a toroidal core. The bi-filar approach is outstanding in its noise cancelling capacity. The transient suppression diode may not be necessary, depending on the characteristics of the input power source.

The multivibrator is the efficient and reliable common emitter type shown in Figure 4-49. It drives a square hysteresis loop toroidal core transformer. Efficiency of this portion should be greater than seventy percent.

Figure 4-50 shows the schematic of the rectifier. A full wave bridge is used followed by a L-C pi filter. The filter provides a reservoir of energy so that the current to the switching regulator does not flow in pulses and improves the efficiency of the system.

The switching regulator illustrated in block diagram form in Figure 4-51 was chosen for this application. It is very efficient at the power level under consideration and achieves good regulation without a great deal of circuit complexity.

The circuit shown uses a method of regulation which could be called ripple detection regulation. The ripple present at the center of the split inductors L_1 and L_2 appears across the voltage divider string, where it is sensed by the amplifier. After amplification, the ripple signal is used to activate a Schmitt trigger circuit which produces pulses. Frequency and pulse width of the pulses are dependent on the frequency and amplitude of the ripple signal respectively. The output of the Schmitt trigger is amplified by a driver stage and applied to the series switching transistor. The pulse output is integrated by L_1, L_2, and C_1 to provide the direct current required. D_1 is a "free-wheeling" diode that provides a path for current to charge C_1 even when the switching transistor is in its nonconducting state. A representative schematic is presented in Figure 4-52. The semiconductor complement is seven transistors, seven diodes, and one breakdown diode. This system is extremely efficient and should operate above 80% if used.

4.6.6 ION PUMP SUPPLY

It is possible that the analyzer cannot use space to pump out the ions. If such is the case, it will be necessary to provide an electronic ion pump. It is a very high voltage power supply without regulation. The approximate specifications are given below:

Output:

Voltage Range -	4500 V_{dc}
Current Range -	100 microamperes maximum
Ripple -	10% maximum

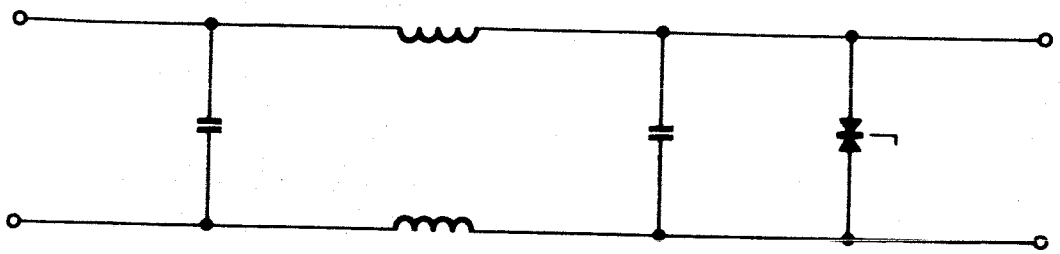

FIGURE 4-48
Input Filter

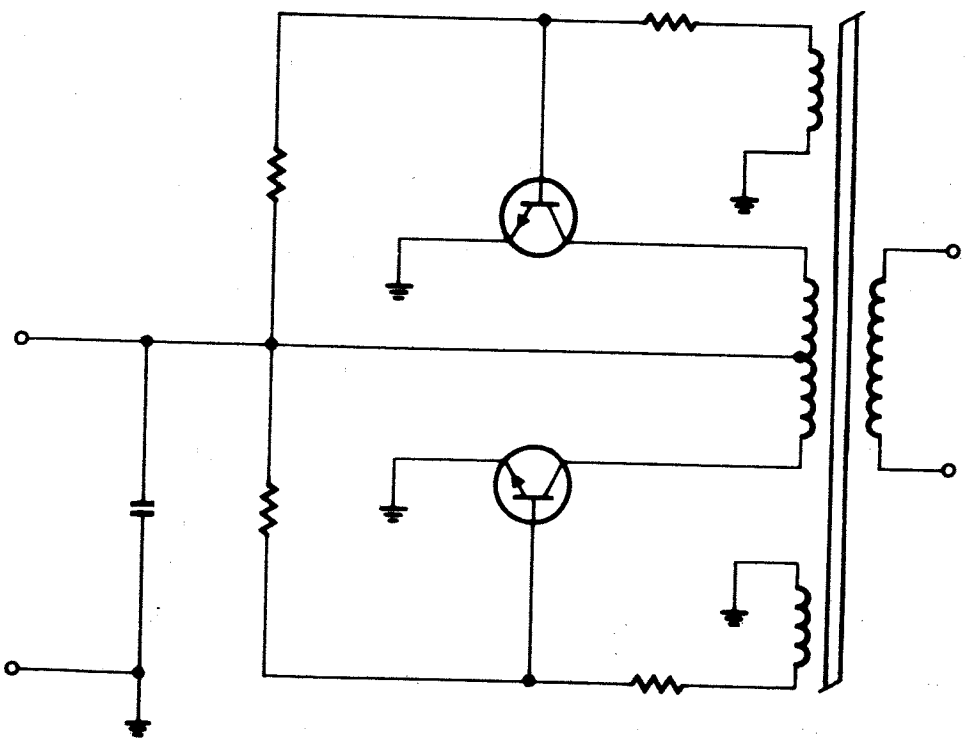

FIGURE 4-49
Multivibrator and Transformer

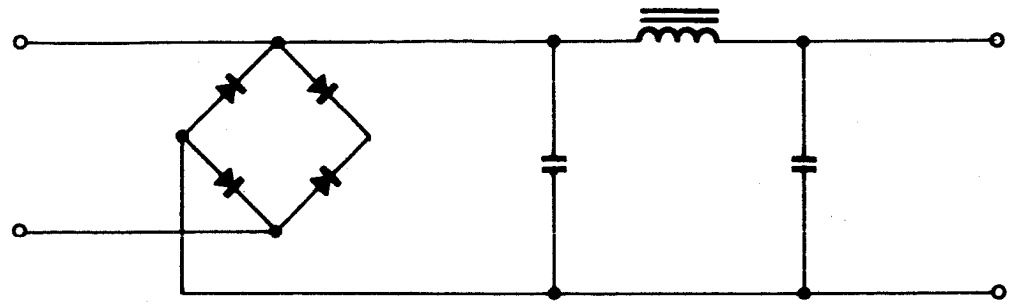

FIGURE 4-50
Multivibrator

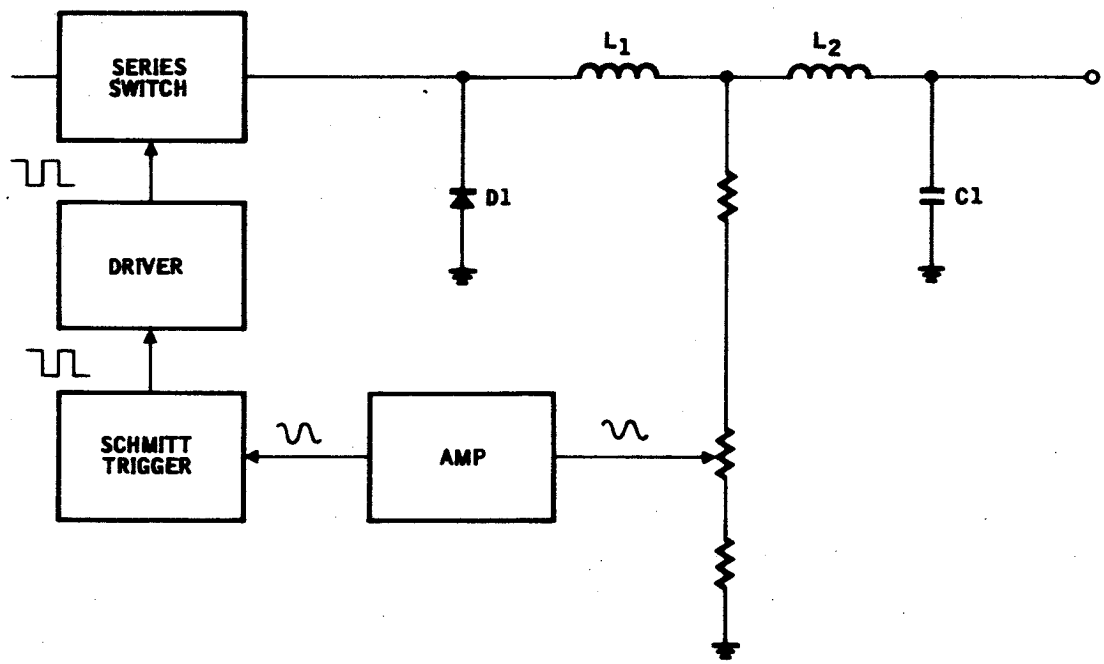

FIGURE 5-51
Diagram Regulator Block

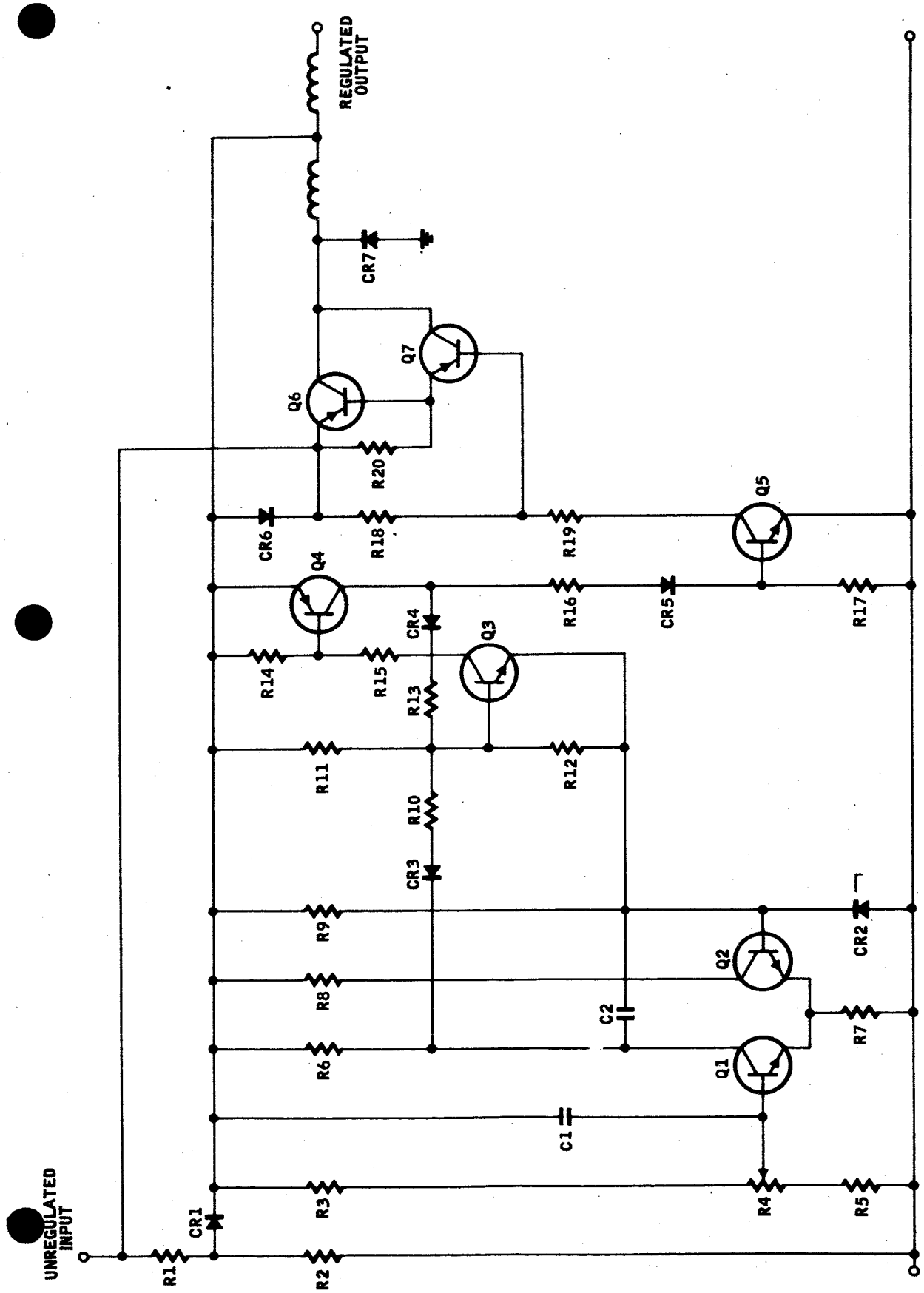

FIGURE 4-52
Regulator Schematic

Input:

Voltage Range -	28 ±0.5 V_{dc}
Ripple and Noise -	not available
Maximum Input Transient -	not available
Risetime at turn-on -	not available

The ion pump supply will consist of a dc to dc converter followed by a multiply by six circuit. The complete circuit is shown in Figure 4-53. This type of circuit provides adequate characteristics at optimum efficiency.

The inverter is the typical one described previously except it has an input filter to reduce the ripple fed back to the input power. The multiply by six circuit is used to avoid the necessity of a large transformer with a great number of turns. Since regulation of the supply is not an important consideration, the diode-capacitor network performs admirably. The circuit will add approximately 16 cubic inches to the electronics package, mainly due to the choke and transformer. Weight should be approximately 6 ounces. The input power necessary at full load should not exceed 800 milliwatts.

4.6.7 CONCLUSIONS

The conceptual design of the support electronics represents the most desirable approach within the boundaries set up by the analyzer system and the spacecraft environment. In each case, the effort directed toward keeping the design simple without sacrificing performance was worthwhile. The task was simplified by the analyzer design which negated the need for a radio frequency oscillator, a mass scanning system, or a digital control section.

Since the mission was man-rated, reliability of the system was assumed to be of prime importance. Component counts were held to a minimum and non-qualified devices were eliminated from consideration. The SDS Data System design practice of incorporating a worst-case analysis in the design phase results in the desirable properties of the system being optimized and assures that the reliability goal has been achieved.

The only sources of electromagnetic interference within the support electronics package are the converters and switching regulators. For the relatively low power operation of these circuits, L-C filters and a minor amount of shielding has proven to be adequate. Interference within the package should not be a problem and electromagnetic radiation to other spacecraft equipment should be easily prevented.

Interwiring depends to a great extent on the physical configuration used. The detector packages must plug directly into the analyzer header but the power supplies may be somewhat remote without harming system operation. The final package should be designed to minimize all wiring runs.

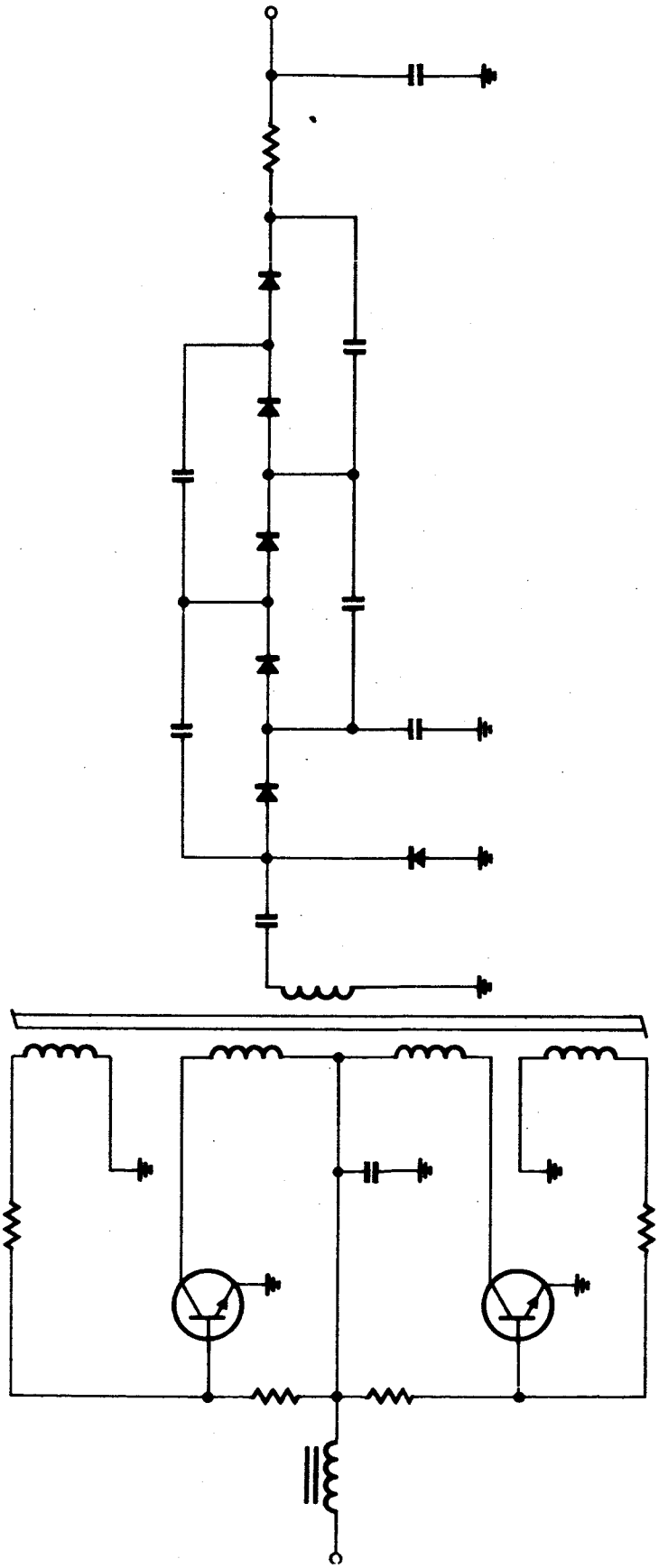

FIGURE 4-53
Ion Pump Supply

4.6.8 POWER CONSUMPTION

Power consumption was minimized during the conceptual design by using the most efficient circuit possible for each task. For a system using a heated filament as one of its main elements, very little power is consumed. The system power is strongly dependent upon the type of filament used. The filament upon which these numbers are based is believed to be realistic in view of the investigations of Section 4.7. At the same time there is a distinct possibility that even lower filament powers can be achieved after the results of the proposal filament study are known.

Table 4-6 illustrates the estimated power consumption of the various circuits.[1]

TABLE 4-6

Filament Supply	
Filament Power*	1.50 watts
Filament Transformer - 80% efficient	.375
Switching Regulator - 75% efficient	.675
Regulator and Control Signal Section	.100
Dc to dc Converter - 75% efficient	.870
Total	3.520 watts
Ion Source Supply	
Low Supply	
Output	0.025 watts
Dc to dc Converter	0.150
Series Regulator	0.150
High Supply	
Output	0.085
Dc to dc Converter	0.150
Series Regulator	0.150
Total	0.710 watts

[1] Typical power calculations are given in Appendix L and M.

* Assumes a 0.003 inch diameter rhenium-tungsten alloy wire filament with no coatings.

TABLE 4-6 (CONT'D)

Detector Supply		
+15 Volt Supply		
Output		0.075 watts
Series Regulator		0.100
	Subtotal	0.175 watts
-25 Volt Supply		
Output		0.250
Series Regulator		0.100
	Subtotal	0.350 watts
	Total	0.525
Dc to dc Converter - 75% efficient		0.175
	Total	0.700 watts
Complete system power consumption without the input regulator		4.930 watts
Input Regulator (if required)		
Support electronics		4.93 watts
Switching Regulator 80% efficient		1.22
Dc to dc Converter 75% efficient		2.15
Total system power including Input Regulator (if required)		8.30 watts

4.6.9 SIZE AND WEIGHT

With any spacecraft system, size and weight is a prime consideration. This was kept in mind throughout the conceptual design of the support electronics. An appraisal of this type is difficult without having actual designs completed, but by studying designs of similar systems built by SDS Data Systems the following estimates were made.

The areas of the various boards were determined by laying out each one utilizing the sizes of transformers, chokes, and other components used on boards of a similar nature in other mass spectrometer systems. The dimensions are not necessarily the actual ones that would be used.

a.	Filament Supply -	6" X 6" X 0.75"	= 27 cu. in.
b.	Ion Source Supply -	6" X 6" X 0.75"	= 27 cu. in.
c.	Detector Supply -	3" X 3" X 1.0"	= 9 cu. in.
d.	Detector Electronics-	4 at 3" X 3" X 0.5"	= 18 cu. in.
e.	Mother Board (optional) -	4" X 6" X 0.5"	= 12 cu. in.
		TOTAL	= 93 cu. in.

The weight estimates were extremely difficult because the transformers and chokes are a major portion of the total and the weight of these components depends on many variables. The following figures comprise the best estimate possible without extensive design work.

a. Filament Supply:

Choke -		0.5 oz
Isolation Transformer		2.5 oz
Filament Transformer		1.5 oz
P. C. Board -		1.0 oz
Other Components -		2.0 oz
	TOTAL	7.5 oz

b. Ion Source Supply:

Chokes (2) -		1.0 oz
Transformers (2)		4.0 oz
P. C. Board -		1.0 oz
Other Components -		3.0 oz
	TOTAL	9.0 oz

c. Detector Supply:

Chokes (2) -		1.0 oz
Transformer -		2.0 oz
P. C. Board -		1.0 oz
Other Components -		2.0 oz
	TOTAL	6.0 oz

d. Detector Electronics:

Components (4) -		4.0 oz
Shielding (4) -		4.0 oz
Board (4) -		1.5 oz
	TOTAL	9.5 oz

e. Mother Board and Interwiring

Board -		1.0 oz
Wiring -		3.0 oz
Hardware -		4.0 oz
	TOTAL	8.0 oz

Total of all electronic modules 2 lbs 8 oz.

4.7 EMITTER STUDY

4.7.1 INTRODUCTION

The bulk of the literature and experimentation with thermionic emitters has been devoted to the application of these electron sources to the vacuum tube industry. The work done in the field of Mass Spectrometry has been limited in extent for three basic reasons:

a. Efficiency of operation was not of concern as sufficient power was available;

b. Most of the undesirable effects attributed to emitters affecting the operation of a mass spectrometer could be eliminated by the selection of metallic emitters;

c. The life of the emitter was a secondary consideration with laboratory instruments.

With the advent of extensive investigation of the earth's atmosphere using rocket probes and earth orbiting, instrument bearing vehicles, the mass spectrometer found a new role. With this came the more exacting requirements for the performance characteristics of the thermionic emitter.

It is the purpose of this study to review as much of the literature on thermionic emitters as is possible in the light of these new requirements, to search for the most applicable materials for this application, and to suggest areas wherein study programs could provide a significant expansion in the knowledge of the more promising materials.

The scope of this study was confined at the outset to the acquisition of quantitative performance data on the various filament materials and thermionic emitter techniques. The literature was searched for the latest reports in this area as well as for new techniques in this field. There were several surveys reviewed as well as particularly slanted articles. These revolved around the solutions to particular problems encountered in mass spectrometric analysis such as analysis of coal hydrogenation products. These were not too beneficial and data from which direct comparisons could be made were difficult to find. There seem to be many users with little cross fertilization of information available in their reporting. The primary interest is centered around the rather obvious characteristics of emitters and of the expected life, the chemical reactivity, outgassing characteristics, emitter efficiency, evaporation rate, and mechanical characteristics such as strength, shock resistance, and secondarily sagging characteristics. These, of course, were coupled with the availability of the material which has at times been a problem.

The effort began with a survey of potentially applicable techniques. Included within the survey were the oxide coated cathode, matrix or diffusion cathodes, refractory coated cathodes, thoriated cathodes, thin film emitters, metal cathodes. The results of this survey follow in the above order.

4.7.2 OXIDE COATED EMITTERS

The oxides of the alkaline earths have been used in the manufacture of cathodes for probably 40 years. This has been due primarily to their efficiency or high electron emission at relatively low temperatures. Their application to mass spectrometry however is limited because of their susceptibility to poisoning. Poisoning occurs, for example, by a donor destruction process wherein oxygen fills a vacancy or by becoming bound to an excess alkaline earth atom. There is another problem, one of decreasing emission, attributable to overall donor decreases and caused by ion bombardment, excessive heating, evaporation, etc. Of course, they are not extremely strong, mechanically, and are subject to flaking and other mechanical damage.

This type of emitter was discounted as having any realistic application to the present requirements although the low power requirement which is shown in Figure 4-54 is very desirable.[1]

4.7.3 MATRIX CATHODES

Matrix cathodes were developed along lines to obviate some of the difficulties of the oxide coated cathodes. They are formed of a metal matrix with the active material dispersed throughout. These emitters which are much less sensitive to mechanical shock are also subject to poisoning. For example, air mixtures at pressures greater than 5×10^{-6} mm Hg are sufficient to poison the matrix emitter operating at approximately 1100°C. There is a greater capacity for recovering from these effects due to donor migration to the surface, but ion bombardment is still a problem.

It seems necessary to explain at this point, that emitters of all sorts were investigated without prejudice or consideration for the possible complexity or difficulty of imaging the electron source. This was done deliberately in order not to miss an opportunity or to evolve a workable combination of approaches. It was interesting to note, in this regard, that Rhenium was employed in matrix diodes for, in addition to other reasons, its improved strength properties and has been used since in other alloying for much the same reason.

4.7.4 REFRACTORY COATED CATHODES

The refractory coated cathodes were developed as rather a compromise between improving the mechanical characteristics of oxide coated emitters and the complexity of fabrication of the matrix emitters. (Emitters and cathodes are used interchangeably in these discussions.)

These cathodes have in general higher work functions and are normally operated at higher temperatures. The activation of the coatings usually takes place at temperatures sufficiently high to preclude the use of sleeves and indirect heating. The methods of application of the various materials have included painting, spraying, and cataphoresis. The materials employed have been

---

1. Thermionic Electron Sources - NRL

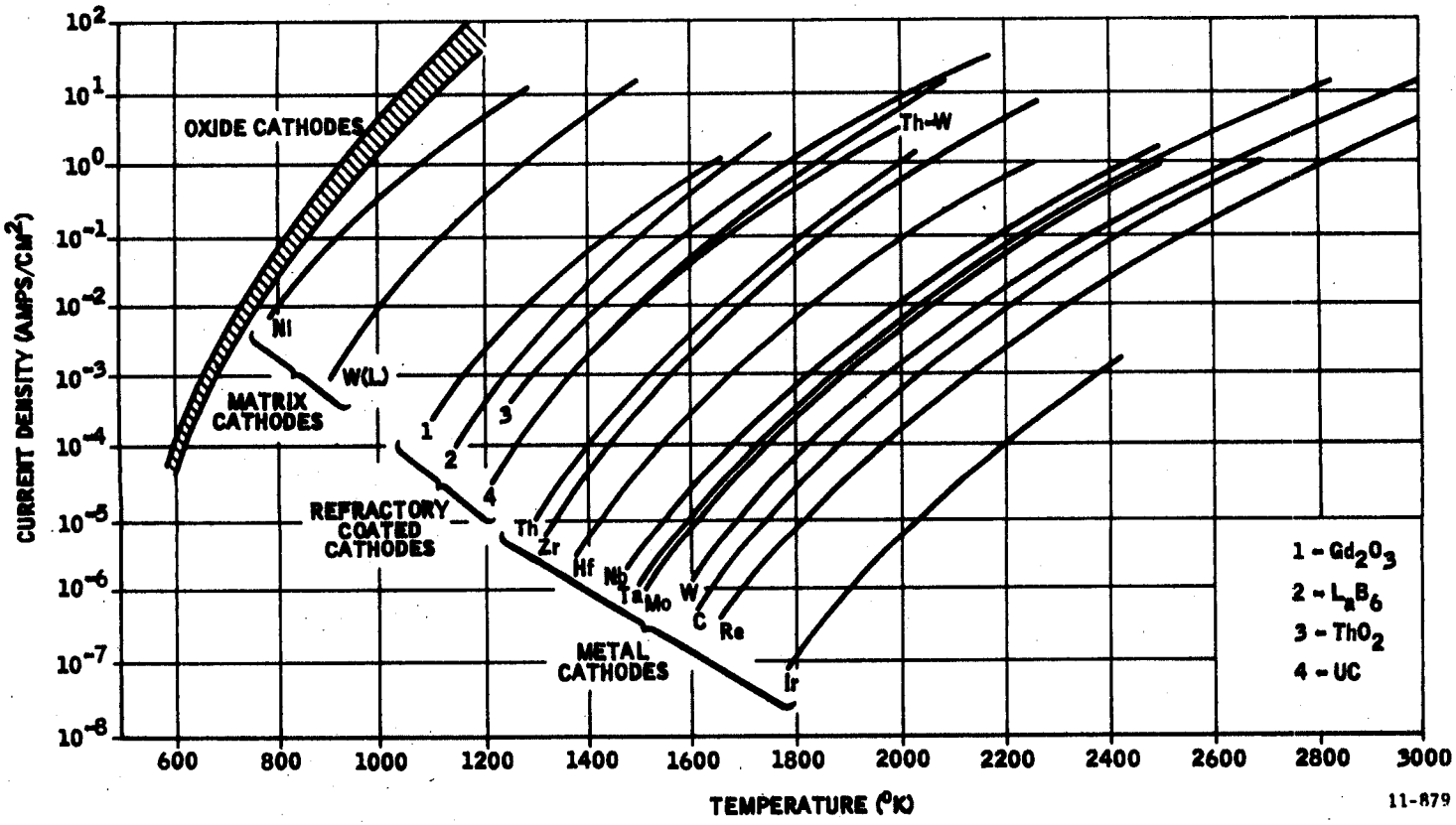

FIGURE 4-54
Emission Characteristics of Various Thermionic Cathodes

thoria, hexaborides, rare earth oxides, carbides, borides, and nitrides. The base materials have included W, Ta, Mo, and Ni.

The work on the rare earth oxides, the carbides, borides, and nitrides has been limited and only certain of the rare earth oxides (eg: yttrium oxide) and carbides (uranium) have received much mention. As a general group, these emitters are more stable but suffer, because of the higher operating temperatures from evaporation and base metal failure. SDS Data Systems has experimented with lanthanum boride coated Rhenium filaments but not with confirmed success. The immediate advantage was an approximate 50% reduction in power over the uncoated Rhenium emitter. For a 100 microampere emission current, the uncoated Rhenium emitter required 450 milliamperes of filament current while the identical uncoated filament required 800 milliamperes. This improvement in efficiency was not obtained without difficulty. The ion source exhibited considerable instability and eventually a change was experienced in some of the currents throughout the various ion source elements. This was attributed to the change in the emission profile or distribution of emission along the filament. There appeared to be physical evidence of migration of the lanthanum boride coating along the wire. Microscopic examination of aged filaments showed a globulation of material at irregular intervals along the wire. There was also a change in color of the wire, symetrically, from the center of the filament outward to the mounting posts. This, to some extent, supported the conjecture that the emission profile changed on a long term basis as well as short term changes from coating migration.

When the stable ion source operation was restored by replacement of the coated filament with an uncoated filament of the same diameter, the first substantiation of the nature of the problem was obtained. Efforts have since been focused on obtaining comparable emission efficiency without the sacrifice attendant with the use of refractory coatings.

4.7.5 THORIATED CATHODES

Referring to Figure 4-54 shows that the magnitude of the change in emission efficiency of tungsten is accomplished by the simple expedient of adding approximately 2% Thoria. Because of this, thoriated tungsten cathodes are perhaps the most widely used emitters in commercial tubes today. These emitters can be operated at temperatures higher than the melting temperature of the active material without excessive evaporation. However, it has become somewhat standard procedure to carburize the thoriated tungsten emitter in order to further reduce, by a factor of 10, the evaporation rate of thorium, and reduce the sensitivity of poisoning by oxygen. This process essentially forms a layer of tungsten carbide at the surface and must be carefully done as excessive carburizing will cause embrittlement of the filament wire. The life of the filament, however, increases exponentially as the percent of carburizing increases.[2]

---

2. Materials and Techniques for Electron Tubes - Kohl

The technique of thoriating metallic emitters in order to improve emission efficiency has been employed with Rhenium and Iridium. Various percentages of Thoria have been tried with Rhenium and approximately 3% Thoria was found to give the best results.(1) Thoriated Rhenium filaments were found to operate or activate at about 400°K below Thoriated tungsten emitters. It was also found, however, that the evaporation rate was higher, necessitating the lower operating temperature. The emission level was found to be higher for the thoriated Re than for thoriated W.

There are two important potential disadvantages in the use of tungsten emitters. One is the so called water cycle wherein tungsten at elevated temperatures is destroyed in the presence of traces of water vapor by the formation of $WO_3 + W_2O_5$. The second is the evolution by carburized thoriated tungsten filaments of CO and CO_2. The equilibrium reaction is $ThO_2 + 2W_2C \quad 4W + 2CO + Th$.(2) Quantitative data were not located regarding the severity of this reaction. One can infer that it is apparently insignificant to the extent of venting electronic vacuum tubes within the life expectancy of the filament itself.

Both of these effects are apparently minimized in the case of thoriated Re.

Rhenium does not form a carbide and this results in two valuable characteristics. One, it does not embrittle in the presence of hydrocarbons and two, it does not contribute to the formation of oxides of carbon. It has been reported(3) that by the replacement of a tungsten filament by Rhenium, a reduction of a factor of 5 in the CO_2 background in a mass spectrometer was experienced. This was observed in the presence of a 100 micron oxygen sample.

The concern over gas evolution, however, is diminished by differential pumping of the ion source. Since the proposed design incorporates a differential pumping rate of approximately 100, a very pronounced gas evolution by the filament would be required before its effect would be noticed in the sample gas.

4.7.6 THIN FILM EMITTERS

Thin film emitters are comprised of a thin film, usually monatomic, of some absorbent on a metal substrate. Actually, the thoriated tungsten emitter falls in this category but as rather a special case. There is such a limited life of adsorbed film, except in the case where there is continual replacement from the metal substrate, that thin film emitters offer little potential for serious consideration.

4.7.7 TUNNEL EMITTERS

Tunnel emitters are formed by a sandwich technique where a thin film is deposited over an insulating oxide of the base metal. This has been typically a gold film over aluminum oxide. The proximity of the two conductors

---

3. Use of Rhenium Filaments and Low Ionizing Voltages for Analyzing Liquid Products from Coal Hydrogenation by Mass Spectrometry - A. G. Sharkey et al

enables the application of a potential gradient sufficient to extract electrons from the base metal. A small percentage of these pass through the gold film with resultant emission current. This technique is basically experimental and thus far has exhibited insufficient emission stability to be seriously considered as an emitter.

4.7.8 METAL CATHODES

Pure metal cathodes have the immediate disadvantage of having much lower emission levels at comparable temperatures than the emitters thus far discussed.

This disadvantage is to some extent overshadowed by some of their desirable features. They are more rugged and significantly more resistant to damage from mechanical shock. They are more resistant to damage from ion bombardment and relatively immune to gas poisoning. Their low vapor pressure extends their life expectancy and allows for their use in ultra clean systems such as mass spectrometers. Their high temperature of operation effectively maintains a thoroughly outgassed emitter which results in a surface from which highly repeatable emission levels can be achieved.

The metals which are most commonly considered as having these properties are W, Re, Mo, Ir and Ta. The real, practical usefulness of these materials is determined by their ability to provide sufficient emission at temperatures which do not result in prohibitive evaporation of the metal. The metals shown in Figure 4-54 have emission capabilities of at least 0.1 ampere per cm^2 at temperatures below a vapor pressure of 10^{-5} mm Hg.

The one exception is iridium which is not damaged by exposure to air while operating at high temperatures. It is appropriate to discuss these emitters independently. At the same time their important alloys can be reviewed.

Tungsten is a copious emitter of electrons at temperatures from 2000 to 3000°C which accounts for its widespread use. The preferred position which tungsten holds is also due to its high mechanical strength even at elevated temperatures. There are some problems, however, associated with the tungsten wire emitter. There is a problem of grain growth, the associated embrittlement and offsetting which becomes particularly critical around 2600°C. This condition is remarkably attenuated, as discussed earlier by the addition of small amounts of thoria. It really becomes necessary in the case of tungsten, to discuss the alloyed material, as its characteristics are so markedly improved by the alloying process.

One of the more important alloys of tungsten is the thoriated tungsten rhenium alloy. Various compositions have been experimented with, resulting in the identification of the 25% rhenium alloy as having superior characteristics.(4) Rhenium was added originally to improve the ruggedness of filament material. The results showed this additive to be very beneficial. The addition of Re raised the shock level required to fracture the tungsten

---

4. Thoriated Rhenium - Tungsten Alloys for Electron Tube Applications - Fred A. Foyle

filament from 350 G's to above 650 G's. The vibration load survival, over the frequency range of 50 to 2 kilocycles, was increased from 15 G's to greater than 20 G's.[5] Also associated with the addition of Re were reduction in gas sensitivity and improved welding characteristics.

This was achieved at some sacrifice in emission however. For comparable emission levels, the filament voltage increased approximately 17%.

Tungsten has also been alloyed with molybdenum in order to obtain a higher electrical resistivity. The results have not been too favorable, however, as the combination is subject to erratic burnouts.

Molybdenum ranks among the materials considered for emitters primarily because of its strength characteristics at elevated temperatures and perhaps because it is considerably cheaper than tungsten. Its major disadvantage, probably accounting for the absence of significant use as an emitter, is the prohibitive evaporation rate at emission levels equivalent to that of tungsten.

Tantalum also has a high melting temperature but cannot be seriously considered for use in mass spectrometry due to its gettering action even at low temperatures. Absorption of oxygen and nitrogen becomes significant at 700°C and above.

Rhenium is second only to tungsten in melting point and has a vapor pressure similar to tantalum or an order of magnitude lower than tungsten. It is resistant to the water cycle which rapidly destroys tungsten, does not form carbides, and is thus not embrittled in the presence of hydrocarbon vapors.

Rhenium filaments have been used at SDS Data Systems for over 5 years. Wire diameters of 7, 5, and 3 mils have been used for emitters in various ion source configurations. The major difficulty has been in the apparent quality of the wire and may be a reflection of the unusual work hardening characteristics of rhenium. Our experience has been that the 3 mil diameter wire is the most erratic in this regard.

Since power conservation is of prime concern in flight type mass spectrometers, we have been particularly interested in the smaller diameter wire and have been investigating some of the more promising alloys. Currently undergoing life testing is a 3 mil tungsten - rhenium alloy filament. The composition is 25% Re and 75% tungsten. There has been accumulated in excess of 1000 turn on cycles and a total operating time in excess of 1000 hours without any degradation in performance or emission efficiency. Other life testing has been reported wherein this type of filament has exceeded 5000 hours of testing and still going.[4] This effort needs to be expanded as there appears reason to believe a successful 3 mil filament can be obtained.

Iridium and particularly thoriated iridium is beginning to be found more and more in commercially available mass spectrometers and ionization gages. Quantitative data upon which an evaluation of this emitter material could be made

---

5. Thoriated Rhenium - Tungsten as a Thermionic Emitter - James A. Jolly.

were not available for this investigation. It is available in the diameter of interest for our application and performance data are definitely required.

4.7.9 RECOMMENDATIONS

The recommendations resulting from this study have become obvious during the performance of the work and have been pointed out to some degree in this text. The desired emitter should be stable, mechanically rugged, strong, require minimum power for the desired emission levels, have good life expectancy and negligible gas interaction and evolution in order that differential pumping of the ion source can be minimized or obviated. Certainly, the material to be selected to meet all of these requirements is not obvious as the preceding discussions have made clear.

It is therefore necessary that a quantitative study be performed of the most promising approaches under the actual conditions of the intended use. Our tentative recommendation would be to perform such a quantitative study on the thoriated tungsten rhenium alloy, thoriated rhenium, iridium and thoriated iridium alloys. The emission efficiency of thoriated tungsten rhenium wire puts it in a preferential position but the degree of the problem of gas evolution and sensitivity to water vapor must be ascertained. Thoriated rhenium appears to have more promise than rhenium due to the increase in emission efficiency and the unproved work hardening characteristics. There may, however, be a problem in procuring this wire in the desired diameters. Iridium and thoriated iridium requires an investigation of performance in our application. The reported resistance of this material to high pressure burn out merits investigation and may therefore be a rather large step in improvement of filament reliability.

For the purpose of estimating the expected instrument performance, a .003" diameter tungsten-rhenium alloy filament will be assumed. This choice is based upon the current experimental investigations which indicate that the necessary filament life can be obtained with this configuration. It is expected that the results of the suggested study program will lead to an improved emitter with lower power and the life characteristics.

4.8 MECHANICAL DESIGN AND PACKAGING

This section covers the mechanical design of the analyzer and the packaging of the entire system. In both areas, the approach was to develop a design which would give the necessary strength and rigidity required to meet vibrational loading, without over-designing to the point of excessive weight. The analysis given here is necessarily crude in view of the complexity of the analyzer and package structures but the safety margins are in all cases substantial enough to allow for any errors arising from the approximations.

The analyzer size and configuration is governed largely by the parameters $\emptyset$, r_o, n_i, n_o and z. The analyzer configuration based upon the parameter values of Section 4.1.5 is shown in Figure 4-55. The analyzer housing consists of two principal parts, the ion source housing and the analyzer envelope. These sections consist essentially of 0.032 inch wall shells. Since the object slit, collector buckets, and analyzer magnet must be accurately positioned with respect to each other it is essential that a stable structural member link these three areas. This function is provided by the combined action of the ion source mounting surface, strongback, and collector flange mounting surface. These elements have thicker cross sections for greater rigidity and are all linked together to form the integral structural member which supports all other analyzer elements. The ion source and collector flanges are mounted on their respective mounting surface. The magnet is mounted to the strongback by a rigid clamping arrangement utilizing aluminum stand-offs.

The analyzer envelope cross-section is 0.135 inch in the region where the magnet must slip over it. It then flares out to 0.250 inch at the collector flange in order to allow for ion beam spread as enhanced by z-axis defocusing. The ion collectors are mounted to the collector flange in a manner which allows motion along the flange and along the ion beam. During test, the collector flange will be sealed to the analyzer housing using an O-ring seal (Viton-A or equivalent). The necessary clamping action is obtained by the use of removable flanges. When the bucket locations have been determined, and the instrument is readied for flight, the collector flange is welded on by the use of a weld lip. The flange would be doweled to the envelope to maintain alignment. The weld lip can be ground off and rewelded at least twice in case it is necessary to remove the flange. (This type of welding has been used in the past with good success.)

The location of the pump out tube was chosen so that the maximum effective pumping speed exists at the filament. There is a substantial restriction between the envelope volume and the ion source housing and therefore the pump out tube must be connected directly to the ion source housing.

The fabrication of the analyzer is best accomplished by machining the majority of the housing out of a single piece of 304L stainless steel. Welding operations should be limited to a cover to fully enclose the envelope area.

The configuration of the analyzer has some definite implications in the design of the overall package. These considerations follow. In order to minimize the effects of vibrational stresses on the analyzer, the primary vibrational axis (the axis of the launch vehicle) should lie in the plane parallel to the magnet pole faces. The pump out tube must protrude from the rear of the package in order to have a minimum length through the bulkhead. Further,

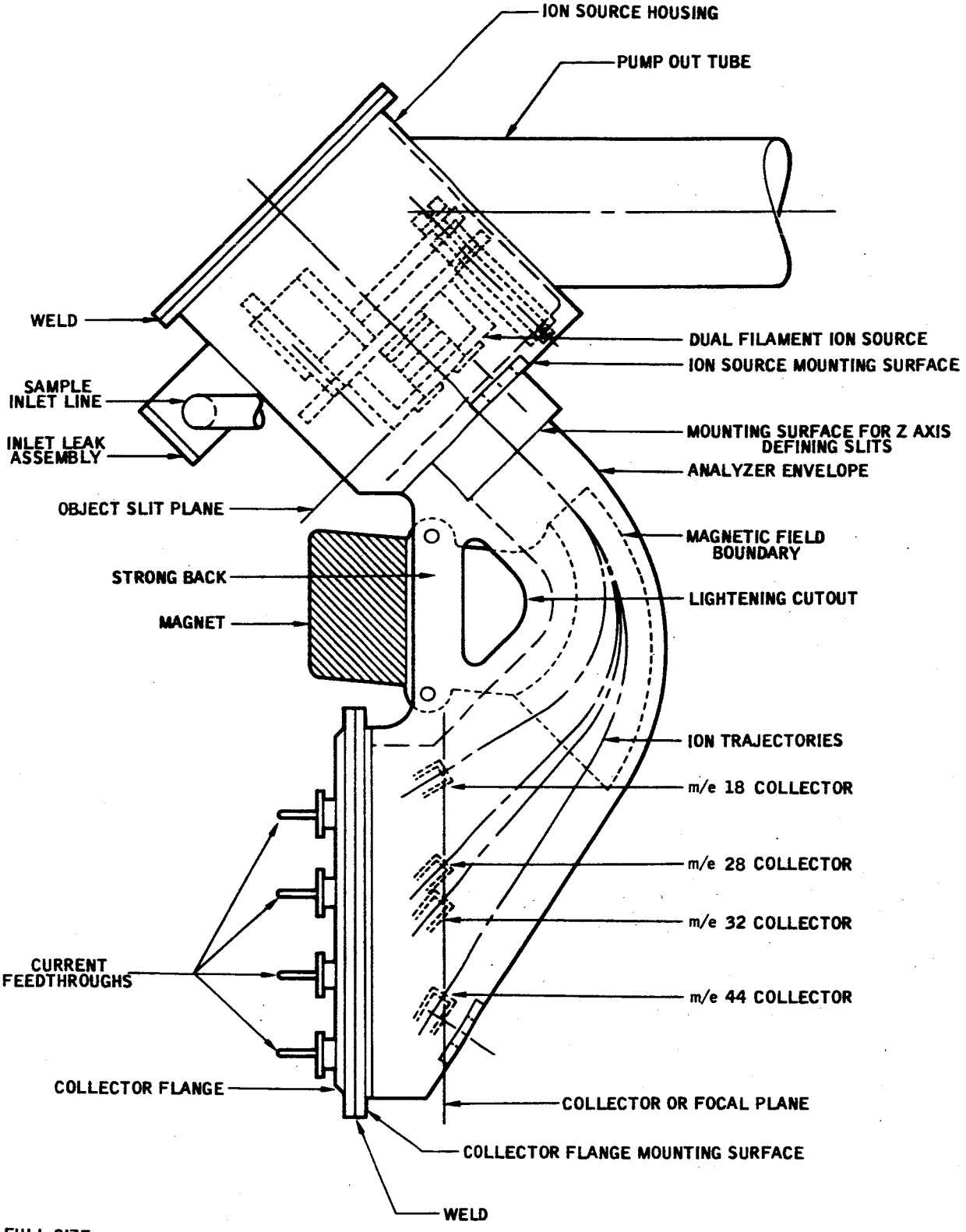

FULL SIZE

FIGURE 4-55
Analyzer Envelope

since the detector modules are to be interchangeable, a convenient access to them was required at the front of the package. A last consideration involved the possible necessity for access to the end of the ion source housing for pumping purposes. While this feature has not been incorporated at this time, it was felt that the package configuration should allow for its adoption at a later date should it be found necessary. All of these factors lead to the configuration shown in Figure 4-56. A compromise between efficient space utilization, simplified module designs, and an optimum package height to cross section lead to the location of the other system components as shown.

The primary supporting element of the package is the case itself. For maximum strength and lightness a dip brazed aluminum construction would be used.

The case would be fabricated from 0.032 inch 6061 aluminum sheet stock, the machined parts attached and fitted prior to the dip brazing. Some of the salient features of this type of construction are freedom from warping, the strength of the joints, lack of fillets, and the high strength of the heat treated case. Vendors have shown their ability to meet the following specifications and standards for dip brazing and inspection:

MIL-823362 and MAS 2673 for dip brazing

MIL-H-6088 - Condition for heat treating

MIL-I-6865 - For radiographic inspection

ASTM-8-260-Alcoa Number 718 brazing alloy

When a non-toxic environment is required, the following material composition is listed below for reference.

Alcoa 718 Brazing Alloy	
Silicon	11.0 to 13.0 %
Copper	0.30
Chromium	0.80
Zinc	0.20
Magnesium	0.10
Mangonese	0.15
Aluminum	86.45%
	100.00%

Composition of Aluminum 606	
Silicon	0.6 %
Magnesium	1.0
Cromium	0.25
Copper	0.27
Aluminum	97.88
	100.00%

It is expected that this package will have to meet the severe qualification testing of the Apollo Program. This includes several tests which demand that the package be sealed. Therefore, all covers have captive O-ring gaskets. A minimum number of screws are provided to insure the seal. The case material

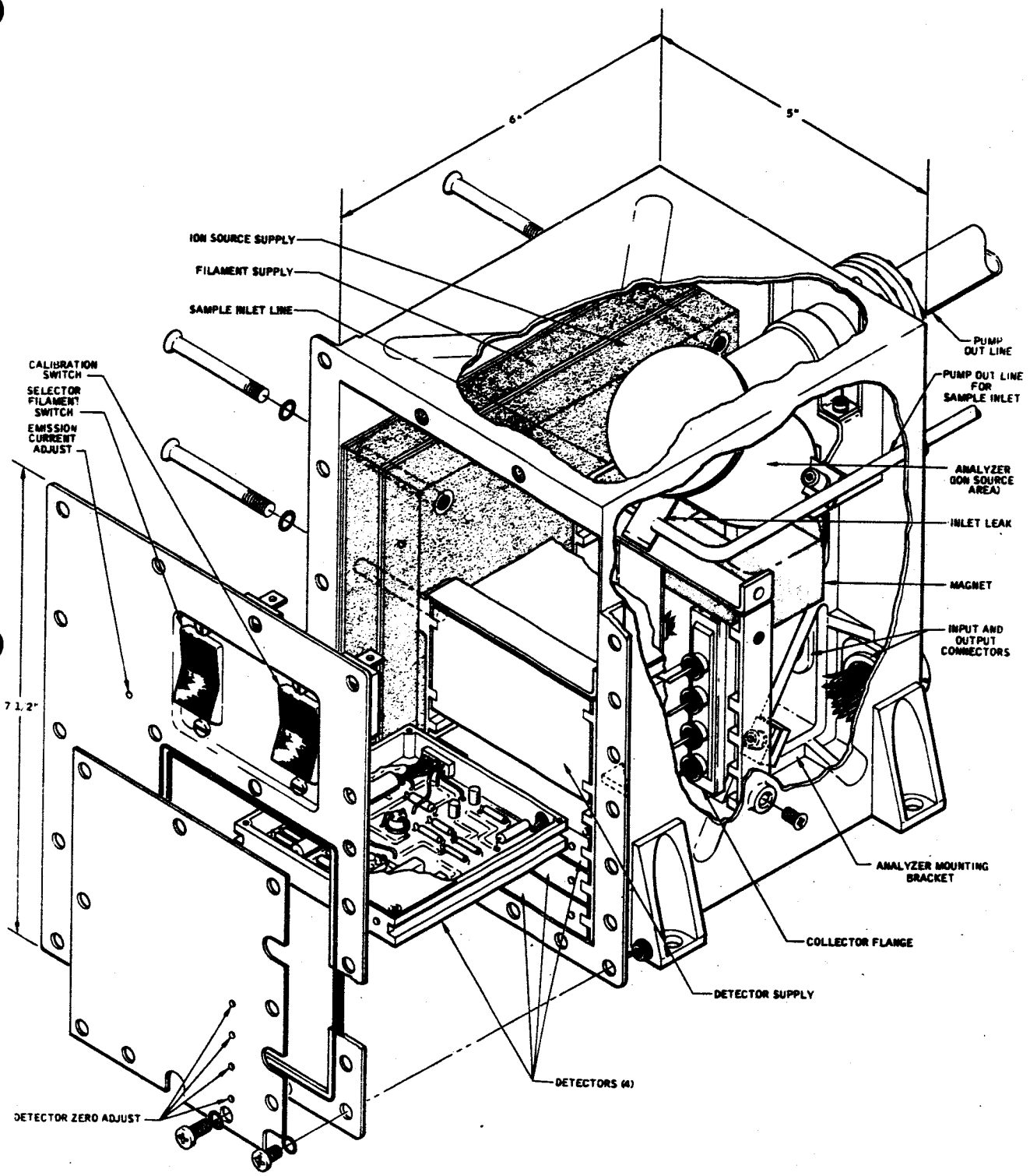

FIGURE 4-56
Conceptual Sensor System Configuration

must be 0.093 inch thick where the gasket seals are made to supply the necessary rigidity for the uniform compression of the gasket. An R.F.I. gasket can be employed when and if R.F.I. specifications must be met.

The three modular units (ion source supplies, detector system, and analyzer) are supported in somewhat different manners. The analyzer is supported by a contour brace structure which is brazed to the top, back, and bottom of the case. The detector electronics are mounted in slide-in modules for easy removal. The ion source electronics are mounted on two printed circuit boards which are secured to the left hand wall on seven standoffs. Four of these standoffs anchor into the detector support brackets. This ties the opposite walls of the package together to eliminate the possibility of buckling.

There is space available in this package for the addition of monitoring or control functions if it is desired to locate them with the instrument. Provisions are shown for areas for adjustments such as zero levels sets on the amplifiers and the electron emission.

A preliminary stress analysis of the package is given in Appendix C.

5. REFERENCE TWO GAS ATMOSPHERE SENSOR SYSTEM

The detailed analysis presented in Section 4 has lead to the conceptual design of a two gas atmosphere sensor system. This conceptual design is the reference system which is discussed in the Statement of Work. The definition of this system is the principal end product of this study program. In order to insure that it has been adequately defined, the following discussion is given. It includes a summary description; discussions of operational characteristics, power, weight and size requirements; environmental compatability, reliability, maintainability, and calibration; and the state of development of the proposed instrumentation, its improvement potential, and adaptability.

It is to be emphasized that the system described here represents only a conceptual design. While a great deal of thought has gone into this conceptual phase, it is inevitable that changes will occur during the design phase. It is also likely that refinements of various types may be added at a later date in order to make the sensor compatible with a specific spacecraft environment. Some of these possibilities are discussed later in this section.

5.1 DESCRIPTION

The reference two gas atmosphere sensor system utilizes a small single focusing magnetic sector type mass spectrometer. This analyzer utilizes a non-magnetic, dual electron gun, high differential pumping ion source with a parallel plate ionizing region and a perfect imaging type of ion focusing. This ion source uses two 0.003 inch diameter tungsten-rhenium wire filaments for electron emission. Other filament materials may be selected after an experimental investigation of the properties of several emitters. The ion source is mounted in a thin-walled housing which is an integral part of the analyzer envelope and collector flange assembly. The mass resolution is accomplished by the action of the magnetic field (from an Alnico V permanent magnet) as the ions pass through the envelope section of the analyzers. The four gases of interest will be separated and collected in separate ion collectors which are mounted on the collector flange. These gases are H_2O, N_2, O_2, and CO_2 which correspond to ion mass to charge ratios of m/e 18, m/e 28, m/e 32 and m/e 44. The important parameters of the analyzer section are given in Table 4-3.

The cabin atmosphere will be admitted to the ion source through a viscous pressure divider inlet system. This consists of a single two meter capillary line, a pump out line with a platinum aperture molecular leak at their conjuncture. This system can sample at various points in the cabin or be attached to a suit loop or calibration source.

The internal vacuum necessary for operation of the analyzer will be maintained by pumping to outer space through a pump out tube.

During preflight and launch periods, the analyzer will be maintained in a sealed off condition by the action of a light-weight bellows valve in the pump out line.

Each of the collected ion currents will be amplified to the required output level by an all solid-state electrometer amplifier. Each amplifier is set for the sensitivity commensurate with the expected sample range of that atmospheric component.

The support electronics consists of only three modules; the filament supply and emission regulator, the ion source electrode bias supplies, and the detector power supply.

The filament supply and emission regulator circuit is a closed loop control system which detects the ionizing electron current collected at the anode and regulates the current supplied to the filament as required to keep the emission current constant. Two alternate circuits will be investigated for this task. The first employs a switching voltage regulator which is driven by a voltage controlled oscillator which is driven by the anode current signal. The second technique utilizes a pulse duration modulator which allows the filament current to be maintained as an ac signal at all points in the circuit. In either of these systems an inverter is required to float the system and the filament is operated in an ac mode.

The electrode bias supplies consist of two stacked high voltage supplies which drive a high impedance voltage divider. Sample voltages from the divider string are fed back to the primary where the regulation is accomplished by use of series regulators on the inverter B+ voltages. The voltages required for the ion source electrodes are tapped off the divider string in the potentiometers and transmitted to them through multi-pin headers in the ion source housing. Low temperature coefficient zener diodes are also used at one point in the divider string to provide additional regulation of a sensitive voltage.

The detector power supply consists of a single dc to dc converter delivering +15 V and -25 V each of which is regulated by series regulators.

The system components described above are mounted in an O-ring sealed case. The case is fabricated of aluminum by the use of a dip brazing process. Two removable panels allow access to the modules.

5.2 CONFIGURATION

The configuration of the reference sensor system is described in three accompanying figures. A conceptual design of the dual filament ion source is shown in Figure 4-8. The important elements of the ion source are called out in the figure. A cross-section view of the conceptual design of the ionizing region is shown in Figure 4-9. The complete analyzer assembly is shown in Figure 4-54. Here the relative location of the ion source, magnetic and ion collectors are indicated as well as the other important features.

The complete sensor system is depicted in Figure 4-55. The salient features of the packaging and the location of the subsystem components are clearly shown, in addition to the expected overall dimensions.

5.3 PERFORMANCE

The expected performance parameters for the reference system are given in Table 5-1.

TABLE 5-1

Expected Performance Parameters

System Parameters

Gases to be Monitored	System	H_2O	N_2	O_2	CO_2
Resolution (m/m)		1/17.5	better than 1/7.5	better than 1/7.5	better than 1/9.5
Minimum Detectable Pressure Change		0.2 torr	0.4 torr	0.4 torr	0.2 torr
Sample Pressure Level for Maximum Channel Output (5 V)		20 torr	200 torr	200 torr	20 torr
Sensor Linearity within 2% up to a Total Pressure of	400 torr				
Output Voltage Range (Linear)		0 to -5 V	0 to -5 V	0 to -5 V	0 to -5 V
Detector Time Response (One Time Constant)		1 sec	0.2 sec	0.2 sec	1 sec
Capillary Inlet Line Time Delay		10 sec	0.4 sec	0.4 sec	0.4 sec
Maximum Total Pressure above which Instability may occur	800 torr				

5.4 INTERFACE REQUIREMENTS

The following is a list of interface requirements for the reference sensor system.

5.4.1 INPUT POWER

The input power is assumed to be 28 ± 1/2 V_{dc} and power ground. A less regulated voltage source will require the use of an input voltage regulator as described in Section 4.6.5. If input isolation is required, an isolating dc to dc converter can be supplied as discussed. It is recognized that power supply voltages generally are not clean but have ac components. When specifications covering this area become available, specific recommendations can be made.

5.4.2 INPUT COMMANDS

The sensor system is turned on and off by a remote command which supplies or cuts off the 28 volt power. In other words, there are no provisions for an on-off command to be received directly by the sensor. A manual toggle switch will be provided to place the instrument in a zero check mode. A toggle switch will also be provided for switching between one filament and another. Both switches will be mounted in the front cover.

5.4.3 SAMPLE INLET

A single flexible two meter capillary line will accept the sample gas. Provisions for heating the line will not be included at this time.

5.4.4 OUTPUTS

There will be four system outputs; one corresponding to each of the sampled gases. All outputs are 0 to -5 V with an output impedance of 500 ohms in the operating frequency range.

5.4.5 ELECTRICAL CONNECTIONS

The input power will be supplied through a connector located at the base of the rear panel. The output signals will be delivered through a standard MS series connector which is also mounted at the base of the rear panel. These connectors are different so that a misconnection cannot occur.

5.4.6 VACUUM CONNECTIONS

The analyzer pump out tube shall be approximately one inch in diameter and shall project through the rear of the package. It will connect to the pump out line with flanges and an O-ring seal. (For laboratory test, a vacuum system can be mounted at this point.) A second pump out line of smaller diameter (1/4 inch) will also project through the rear of the package. Connection to this line will be made with a Swagelok type fitting.

5.4.7 ACCESS

Access to the sensor system components will be provided by a dual front cover. The primary cover covers the entire front surface of the package and allows access to all of the modules. A secondary and smaller cover is provided for rapid access to the detector slices for interchanging purposes. Both covers will be hermetically sealed. These gaskets will not be of the RFI shielding

type. Access will also be provided for adjustments which must be made in flight. These parts will be in the front cover and will also be hermetically sealed.

5.4.8 ADJUSTMENTS

External adjustments in the form of potentiometers will be provided for the following purposes:

a. H_2O detector zero adjust

b. N_2 detector zero adjust

c. O_2 detector zero adjust

d. CO_2 detector zero adjust

e. Ionizing current

Other adjustments will be required for power supply voltage levels and ion source electrode voltages but these are not considered to be normal in-flight adjustments and therefore will only be accessible by removing the front cover.

5.4.9 MOUNTING

The sensor system package is provided with clearance holes for four screws which will mount the package to a flat horizontal surface. The required surface area will be about 30 square inches.

5.5 DEMAND FACTORS

The power, weight, and size estimates for the reference have been accurately estimated based on available information. The basis for the power estimate is given in Section 4.6. The weight and volume estimate were made with the aid of the analyzer and system package drawings. Volumes of all metal members were computed and multiplied by the density of the material in question.

5.5.1 EXPECTED SYSTEM POWER

The expected system power is 4.88 watts. Of this number 3.47 watts is consumed by the filament and filament supply system. The filament assumed for this estimate was 0.003 inch diameter tungston-Rhenium wire. This is believed to be a fairly conservative choice based upon the results of the emitter study (see Section 4.7). Since we do not have conclusive experimental verification that lower power filaments will have the required life in this application, this emitter has been selected.

5.5.2 EXPECTED SYSTEM WEIGHT

The expected system weight is 6.68 pounds. The weight breakdown is given in Table 5-2. The supporting equipment for the sensor system weighs an additional 2.07 pounds. The maximum expected pump out tube length of 18 inches has been used. If this length were reduced the weight of the line and valve would be reduced correspondingly.

TABLE 5-2

Reference System Weight Distribution

Reference System	Pounds
Analyzer Tube (Includes pump out tube to flange)	1.1
Analyzer Magnet	0.9
System Package (Includes internal structure)	1.3
Electronics Modules*	2.5
Potting	0.25
Input and Output Connectors	0.5
Capillary Inlet Line (2 meters long)	0.1
Control Switches	0.05
Mating Flanges and Swagelok Fitting for Pump Tubes	0.15
Mounting Hardware	0.18
Total Pounds	6.68

Supporting Equipment	Pounds
1-1/8 inches I.D. x 18 inches long x 0.031 inch wall pump out tube	0.47
1 inch bellows valve for pump out line	0.75
Valve and pump out line for sample system	0.2
Extension shaft (18 inches) and handle for large valve	0.2
Extension shaft (18 inches) and handle for small valve	0.05
Calibration Bottle (Flight Weight)	0.4
Total Pounds	2.07

*See Section 4.6.7 for a weight breakdown

5.5.3 EXPECTED SIZE

The reference sensor system is essentially a rectangular box with the following dimensions: Height - 7-1/2 inches; width - 5 inches; depth - 6 inches. In addition to these basic dimensions, the mounting feet and frontcover flange increase the width to an overall dimension of 6-1/16 inches. There is not complete utilization of the package volume in the present layout. A modified design could reduce the volume.

5.6 RELIABILITY

As discussed in Section 2, the design of a high reliability instrument has to be considered as a primary goal for this task. Several techniques have been applied to insure a design of maximum reliability. First, basic design simplicity has been a primary goal. The choice of the magnetic sector analyzer over the quadrupole analyzer leads to a great reduction in the amount of support electronics which the analyzer required. Second, an effort was made to minimize the number of components in series with the output. This was implemented by going to multiple output channels as opposed to single collector and detector. This reduced the complexity of the electrode bias supply (non-scanning) and eliminated the need for a logic circuit or multiple ranges on the detectors. Third, safety margins were applied throughout the design analysis which allow degradation in performance, without a serious effect upon the essential content of the output information. Fourth, a reliability analysis was carried out on a set of electronics circuits which are similar to the proposed designs. This analysis indicated that the reliability of the electronics package would be compatible with mission requirements. The details of this analysis are given in Appendix E. As part of this work, a preferred parts list was generated as a guideline for the future design effort. Fifth, redundancy was applied in two areas where the penalty in terms of added demands was low. These areas were the dual filaments in the ion source and the interchangeability of ion detectors. In the first instance redundancy was employed due to a genuine concern over the ability of the component to meet the mission life time requirements.

In the second case, it was applied primarily because of the opportunity to make maximum use of available modules.

In addition to applying the above-mentioned considerations during the conceptual design phase, other similar methods would be applied in the design and fabrication phases. These would include worst case electroncis design; careful design of the analyzer and overall package with design reviews to insure that all factors have been adequately investigated; and selection of qualified components in conjunction with component derating.

These combined factors placed in an integrated program from concepted design through manufacture will lead to a highly reliable instrument.

5.7 ENVIRONMENTAL COMPATIBILITY

The proposed reference system is designed to meet the performance parameters given in Section 5.3 under the following environmental conditions.

5.7.1 OPERATING TEMPERATURE RANGE

40°F to 90°F

5.7.2 VIBRATION

The sensor system will function normally after passing through an Apollo launch vibration profile. Operation is not intended during launch or re-entry of the spacecraft.

5.7.3 EXTERNAL PRESSURE

The instrument can only be operated at altitudes where the ambient pressure is less than 1×10^{-6} torr. Above this pressure stability may not be maintained.

5.7.4 LEAKAGE RATE

The rate of gas loss due to the sample inlet system is less than 0.001 pounds/hour or 1/30 of the total cabin leakage, rate.

5.7.5 ZERO GRAVITY OPERATION

There is no problem in operating the sensor system in a zero environment, since its operation is in no way affected by gravitational fields.

5.7.6 EXPOSURE TO HARD VACUUM

Exposure to hard vacuum will not affect any of the sensor system components. It is a potential problem only due to the possibility of a pressure differential across the O-ring sealed case. If this is shown to be a problem, a two-way pressure relief valve can be incorporated.

5.7.7 SHELF LIFE

The shelf life of the sensor system is limited only by degradation of electronic components. The analyzer tube should preferably be pumped in order to keep it clean, but it can be kept in a "pinched off" condition for long periods of time with no harmful effects.

5.8 ACCURACY

The accuracy of the two gas atmosphere sensor system is controlled by several factors. A brief summary of sources of errors is given below:

a. Inlet line memory effects (small except in the case of water).

b. Ion source temperature dependences (ionization sensitivity and ion focusing).

c. Feedback resistor temperature coefficient (compensatable).

d. Changes in the sample distortion due to filament interaction. (Relatively long term and therefore minimized by calibration; also reduced by differential pumping and the constant nature of the sample.)

e. Detector zero drift (very small and capable of adjustment).

f. Variations ionizing current (controlled by the emission regulator).

g. Variations in the ion source sensitivity due to voltage variations (controlled by power supply voltage regulation).

Examining these sources of error leads to the following conclusions:

a. Variations due to ambient temperature changes will not be of major significance, due to the relatively small temperature range and partial compensation of different effects.

b. Variations due to voltage instability can be minimized to the necessary levels by power supply design.

c. The error due to emission level variation is probably the most significant contributor with a value of about ±0.5%.

d. The overall accuracy should be close to 1% in the normal cabin temperature range (70° ± 5°F).

5.9 MAINTAINABILITY AND CALIBRATION

The reference sensor system is designed such that only the following minimal maintenance functions will be necessary in flight:

a. Checking the zero by throwing the zero check switch and resetting the detector zero levels with a screwdriver potentiometer adjustment. This should be necessary once every few days.

b. Calibration of the instrument by attachment of the calibration sample source to the capillary input and adjusting the emission current set. This should be required once every one or two days and will take approximately one minute.

c. Switching the filament if one of them burns out. This is accomplished by rocker switch mounted on the front cover.

d. Switching the detectors if one becomes inoperative. The O_2 and CO_2 channels are assumed to be of greater importance than the N_2 and H_2O channels. Therefore, if the detector in one of the former channels should fail the latter detector of corresponding sensitivity could replace it. This is done by removing the small front cover and switching two of the slide-in modules.

e. When the sensor system is first required to operate, the valves sealing the main and sample pumpout lines must be opened. This is done by turning the extension handles which protrude through the bulkhead.

Several calibration sources were considered. It was decided that the most practical one would be a thin-walled high-pressure gas bottle with a pressure regulator which would deliver a known sample pressure when attached to the capillary line. The proposed sample is an oxygen, nitrogen, carbon dioxide mixture.

5.10 STATE OF DEVELOPMENT

The analyses carried out in Section 4 have shown that the design of a mass spectrometer sensor system is an involved process requiring the combination of disciplines from many areas. Experience has shown that a thorough analysis of the instrument during the design phase reduces the problems encountered in the experimental work.

In addition to a firm theoretical understanding, a successful instrument should employ design concepts which have been experimentally proven. This procedure has been followed during this conceptual design. The following is a recap of the important areas in which existing technology is being applied.

a. Ion Source - Most of the features of the proposed ion source have been experimentally proven in other SDS Data Systems designs. These include the non-magnetic ion source concept, the low ion source conductance, the electron gun design, ion focusing methods, expected sensitivity and emission levels, filament configuration and mounting, and fabrication techniques. The only untested feature of the ion source is the orthogonal electron guns and it is unlikely that any difficult problems will be encountered in this area. Details of the ion and electron focusing must be worked out but the techniques are well understood.

b. Analyzer - The 90° sector single focusing magnetic analyzer has a long history of proven performance. SDS Data Systems has built double focusing mass spectrometers (90° magnetic sector) which have been flown on Explorer 17 and Geoprobe. These instruments were somewhat more complex than the proposed design due to the addition of an electric sector for energy focusing. The development of this and other instruments has given SDS Data Systems the necessary experience in general fabrication techniques, collector buck mounting, characteristics of permanent magnets, analyzer testing, materials selection, vacuum welding, and other facets of analyzer design, fabrication, and testing. The analyzer design concept does not deviate from proven practices in these areas.

c. Sample Inlet - The capillary inlet line and the ball leak to be used as the molecular flow orifice have both been fabricated and tested on previous NASA contracts. The only deviation is that the diameter profile of the capillary line and the pump out line will have to be modified.

d. Detector System - The solid-state electronics to be employed as the ion concept detectors are similar in design to existing circuits. The most critical area in the detector design is at the input where high impedance and low noise limitations must be met. The input device to be employed has been shown to meet these requirements through extensive testing.

e. Support Electronics - The types of power supplies which are required in the support electronics represent state-of-the-art designs. The biggest innovation in their development is the application of worst case design to insure that the circuits will operate reliably under the expected environmental conditions and component degradation. The optimization of circuit efficiency also requires some effort, but similar requirements have been found in the past. A new type of emission regulator will be investigated, however, this is backed up by a slightly modified version of a proven design.

The other aspects of the instrument design are also considered to be within the state-of-the-art. The principal effort required is in the area of design optimization which is concerned for the most part with the diligent application of existing technology.

As has been shown in the preceding discussion, in most instances, the proposed instrumentation is based upon modifications of existing designs. These modifications do, however, imply changes in performance of the various subsystems. Therefore, experimental data for them does not exist, and consequently cannot be presented here. Data from existing mass spectrometer systems could have been given, however, in most cases it would not have any great significance relative to the proposed design.

5.11 IMPROVEMENT POTENTIAL

The reference system represents a realistic approach to the solution of the two gas sensor system. As discussed in the preceding section, it is largely based upon accepted state-of-the-art components. As a consequence, the design is a fairly conservative one, which is in agreement with the philosophy presented in Section 2. There are several areas where additional study and application of more advanced techniques would lead to improvements in the instrumentation. At the same time, changes in the performance or environmental constraints could be reflected in reduced system demands. These possibilities are briefly considered below.

The analyzer optimization which was carried out in Section 4.1.2 was based on an assumption of constant resolution which lead to resolution margins on the m/e 28, m/e 32, and m/e 44 mass peaks. If these margins are reduced, certain parameter changes are implied in the analyzer design which could lead to a weight reduction in the magnet.

The discussions in Sections 3.2 and 6 indicated that the detectable limit requirement which has been imposed is possibly more stringent than is actually necessary to perform the controlling function. An increase in the detectable limit would lead to less restrictions upon the analyzer and consequently improvements could be effected in several areas such as analyzer weight or pumping requirements.

The preliminary emitter study given in Section 4.7 revealed that several possibilities exist for the application of improved filament materials. This could lead to lower filament power and reduced pumping requirements. Since the filament power accounts for a major portion of the total system power, the improvement potential is obvious. It is estimated, for instance, that if a 0.003 inch diameter thorium alloy filament could be employed that the filament power could be reduced to about 0.5 watts. When multiplied by the efficiency factors of the filament supply, and emission regulator the total power saving is over two watts. This would reduce the total system power to less than three watts. An experimental program as outlined in Section 4.7 is strongly recommended to explore this avenue for improvements.

The sample inlet system recommended is based upon the assumption that monitoring the suit loop is a desirable feature of this instrument. Should this prove to be of little necessity, it might then be possible to go to a direct molecular inlet leak which would eliminate the capillary line, and associated pump out line and valve.

There is also potential for improvement in the pumping system. The dimensions and weights given for the pump out line and valve assumed an 18-inch line to be required. More specific information regarding instrument location might indicate that a reduced line length could be allowed. This would allow a reduction in the tube diameter and valve orifice with a corresponding saving in weight.

The possibility of going to an ion pump in place of the pump out tube was described in Section 4.4. This was predicated on a reduction in the pumping speed requirements by allowing a decreased value of differential pumping.

This depends, in turn, upon other factors as pointed out in Section 4.4. This alternative may be made more attractive by improving the ion pump magnet design. The weights given were for standard magnets which do not employ high energy product material.

The area of packaging offers several possibilities for weight reduction. The electronics packaging was assumed to be based upon standard printed circuit board construction. Generally, this type of construction does not allow a very high component packing density. By going to other packaging methods, size and weight reductions can be realized. Several stages of compression could be considered. These range from reduced component spacing and bend radii on component leads (thus deviating from NASA NPC 200-4), Japanese cord wood, and welded wire module, to the use of hybrid integrated circuits. These last two techniques should not be attempted until after the design and performance of the entire instrument is well proven.

Insofar as the overall package is concerned, weight and size reductions can be effected by more efficient space utilization to obtain a more compact package and use of more exotic materials in the case and structural supports.

In conclusion, it can be stated that many areas for improvement in this instrument exist which could substantially reduce its power, weight, and size demands while maintaining the required performance.

6. CONTROL SYSTEM CONSIDERATIONS

To adequately define the role a mass spectrometer will play in an atmosphere control system, it is necessary to consider the constraints such a system would place on a mass spectrometer sensor. In order to facilitate this discussion, a typical two gas atmosphere control system derived from the current state of atmosphere control technology has been proposed. This will allow operational interfaces to be considered more completely.

Figures 6-1 and 6-2 depict a typical two gas atmosphere sensor system under consideration. The following requirements are necessary to facilitate the design:

Total pressure for calibration should be available from a separate mechanical total pressure measuring device. The knowledge of cabin response time constants and the response time constants of necessary subsystems is assumed to be known. All electronics are assumed to be within state-of-the-art capabilities.

It was assumed that devices for removal of CO_2 and H_2O from the cabin atmosphere are capable of operating in varying modes, i.e., the rate of removal of the contaminant can be controlled to the extent that the subsystem will possess the capability to remove the contaminant at both a normal rate continuously and a high rate intermittently.

The proposed system (Figure 6-1) is shown in a functional block diagram of the mass spectrometer two gas atmosphere sensor system. Before describing the system in detail, a functional description is in order.

In the typical AES mission, a 50-50 mixture of O_2 and N_2 at a total pressure of 362 ±11 torr is anticipated. Human metabolism will cause an imbalance in the atmosphere by removing 2 pounds of O_2 per man day and adding new CO_2 at 2.25 pounds per man day and H_2O vapor at 2.20 pounds/man day. In order to obtain maximum crew comfort, it is necessary that, among other considerations, the humidity in the cabin be maintained within predefined levels (35 to 75% relative humidity, corresponding to 5 to 16.5 torr). The CO_2 level should be maintained below 7.6 torr with brief excursions to 15 torr allowable.

The following functional controls, then, should be provided: Periodic addition of O_2 to replace that used in metabolic processes; occasional addition of N_2 to replace leakage loss; intermittent operation of H_2O removal to maintain humidity in stated range; periodic operation of CO_2 removal unit to eliminate all metabolically produced CO_2 from cabin, not allowing the level to

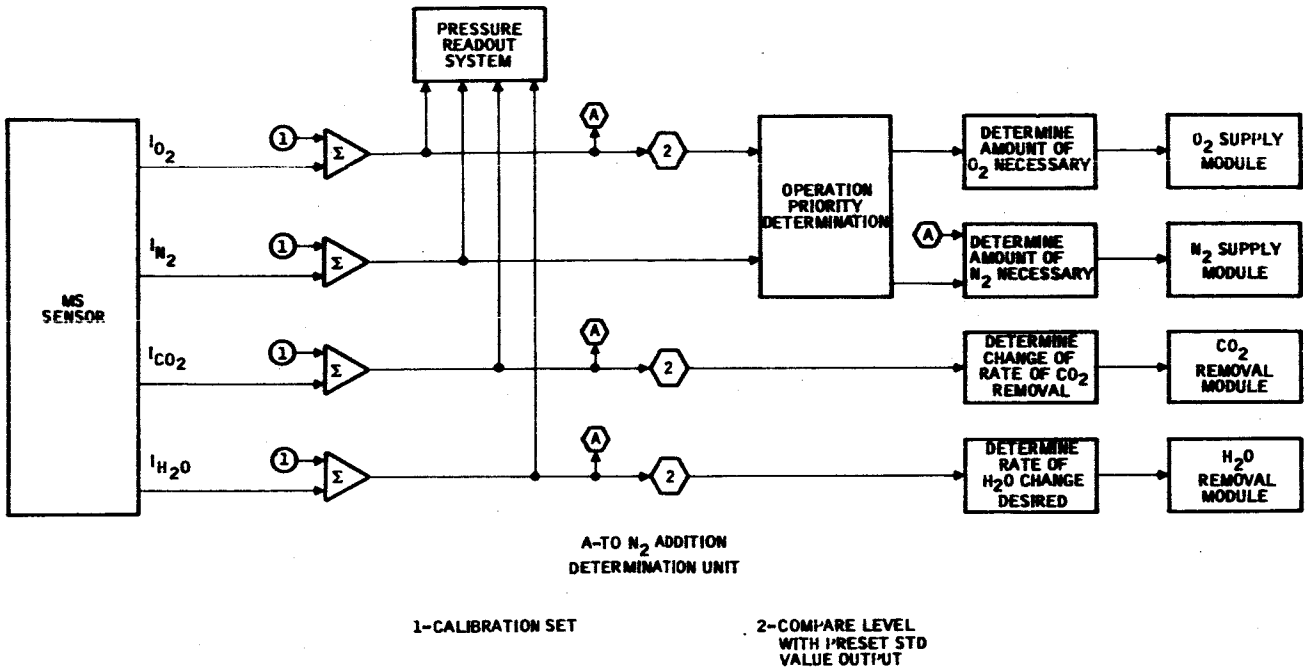

FIGURE 6-1
Basic Two-Gas Atmosphere Control System

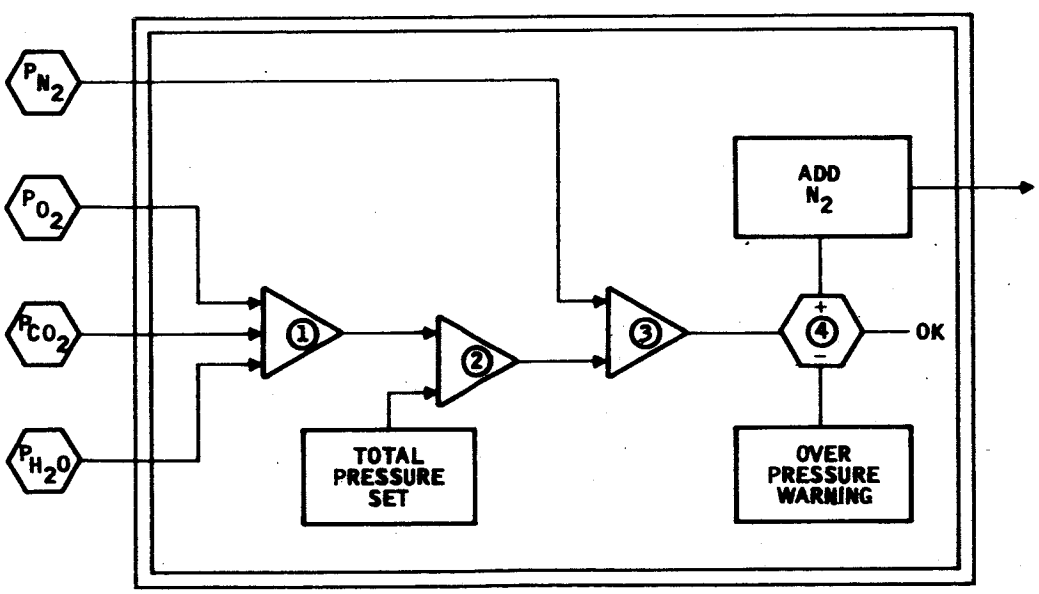

1 - SUM ALL PARTIAL PRESSURES EXCEPT N_2
2 - DIFFERENCE BETWEEN REQUIRED TOTAL AND 1
3 - DIFFERENCE BETWEEN AMOUNT OF DILUENT REQUIRED (2) AND AMOUNT OF DILUENT PRESENT
4 - INTERROGATION - IF DILUENT LEVEL GREATER OR LESS THAN REQUIRED LIMITS, APPROPRIATE ACTION TAKEN

FIGURE 6-2
N_2 Addition Circuitry

rise above 7.6 torr (nominally). Trace contaminant removal, heating and cooling, and air circulation are also integral parts of the environmental control system but are not considered within the scope of this report.

The control system should derive outputs from the sensor, preferably parallel, indicating the four partial pressures of interest. Periodic calibration against a known sample gas will insure that the required accuracy was being maintained.

Continuous output from the sensor would allow monitoring of the pressures at all times while delay circuitry would permit control functions only in accord with predetermined logical coordination (dependent on requirements described above).

Continuous monitoring of the four components is recommended in order to increase the system time response and supplement warning system operation. Continuous measurement would allow rapid partial pressure rate of change measurements to be made in addition to the partial pressure measurements themselves. This feature would allow detection of cabin leaks, leaks into the cabin, or contaminant buildups.

The individual partial pressure outputs, when compared with a preset, adjustable standard value, will give an error signal. If predetermined limits are exceeded, signals can be forwarded to the appropriate subsystem control network whereupon the control function can be carried out under the jurisdiction of a predetermined priority of operation requirement.

System operational guidelines are, at present, dependent on some quantitative unknowns. Qualitative estimates allow preliminary requirements of the atmosphere control system to be described herein.

Oxygen should be added when the partial pressure falls below the required level by a predetermined amount. The desired ambient level is approximately 3 pounds or less of O_2 in the Apollo cabin (138 cubic feet at 180 torr). For three men, the rate of use is approximately 0.014 pounds/man-minute (with 0.015 lb/torr in the cabin). The O_2 partial pressure must be held within ±5.5 torr. The O_2 pressure, however, will drop by 5.5 torr within two minutes. This would then require knowledge of the O_2 partial pressure well within the two minutes. Therefore it is required that the cabin air circulation system coupled with pure gaseous diffusion and favorable sensor location will permit the sensor to detect total cabin O_2 partial pressure changes of at least ±0.5 torr within 0.5 minutes. A mass spectrometer response time on the order of one second is achievable. Control system response times of this order also seem possible. The controlling variable then is the cabin time response to partial pressure changes; i.e., how soon will a change in gaseous composition at constant pressure be distributed uniformly throughout the cabin? A desirable time would be 15 seconds or less. This time, however, is unknown.

CO_2 is produced by human metabolism at a rate slightly greater than that at which O_2 is used (2.25 lb/man-day), the excess CO_2 being derived from water. Since CO_2 is a potentially toxic contaminant, continuous removal should probably be utilized to keep the CO_2 concentration to a minimum. The removal rate should be at only a fraction of the capacity of the removal unit to allow reserve capacity for emergency situations where higher removal rates would be desirable (such as the case where a fire might generate CO_2 or operation after a brief shutdown of the CO_2 removal equipment). Action from the sensor system would only be necessary in cases where excursions in CO_2 partial pressure exceeded 7.6 torr or where the rate of increase in CO_2 pressure would predict exceeding that limit.

Water vapor is the other major contaminant produced by human metabolism. The typical generation rate is 2.2 pounds/man-day. Since it is desirable to maintain the relative humidity between 35 and 70 percent (corresponding to 5 to 16.5 torr), it would be necessary to have two control points for dehumidiffication. The first control point should be set at the high limit to increase water vapor removal rates when the water vapor partial pressure (P_{H_2O}) is greater than, say 13 torr. To prevent dehydration and increase crew comfort, a nominal relative humidity should be maintained. Therefore, the rate of removal of water vapor should be decreased as the lower limit of P_{H_2O} is reached. To adequately perform this function, it is desirable to not only monitor the partial pressure, but to monitor the rate of change of P_{H_2O} to predict probable operational modes of the system. High rates of change could initiate changes in system operational status prior to zero set levels being exceeded. The prime removal rate should be in equilibrium with the rate of generation to facilitate control of a stable total pressure.

Nitrogen is proposed as a diluent gas in the cabin to maintain the required 362 torr total pressure. The requirement for the diluent is twofold. First, the physiologic effect of long-term exposure to a pure, higher than normal pressure O_2 environment is not fully known, as some physiological effects have been noted after long exposure. Secondly, fire hazards are greater in a pure O_2 environment. The total pressure need be maintained to ±11 torr, but because of contribution from CO_2 and H_2O vapor, it is quite easy to have an over pressure situation (2 torr total of CO_2 and H_2O out for every 1 torr of O_2 in). Hence, with efficient operation of H_2O and CO_2 removal and O_2 supply, equilibrium should be maintained to within approximately ±5 torr. It is more probable that an overpressure condition could exist if N_2 leakage was not negligible. In order to prevent this, equilibrium pressures of O_2, CO_2, H_2O, could be measured and the N_2 pressure standard then adjusted to make up the difference. Circuit logic could be provided to prevent adding N_2 in an amount that would cause an overpressure situation to be reached. This logic system has been shown in block diagram in Figure 6-2.

Buildup of toxic and nontoxic contaminants in the cabin is easily deductible by subtracting the partial pressures of the four gases measured from the total measured pressure. This would serve as an additional check on contaminant

monitoring equipment and allow tighter control of nitrogen added to the cabin (this will become a significant quantity when and if the concentration of unknowns becomes 0.1% or greater).

The purpose of the visual display and warning system is to provide crew and ground observers with an accurate indication of the status of the cabin atmosphere and the atmosphere control system.

Provision should be made to display or make readily available two types of indications. The first is of the general information type, i.e., partial pressures, O_2 and N_2 consumption rates, etc. The second type of indication is that required to adequately describe system malfunctions that might occur or, preferably, a prediction of a malfunction. Needless to say, it is in this respect that the display system takes on its most important role, for crew safety and mission success or failure is dependent on atmosphere control system performance. General information warnings include partial pressures and total pressures.

Warning indications include those warnings that indicate system status and system or atmosphere malfunctions. These warnings include:

Atmosphere Status Indication

O_2, N_2 supply levels

O_2, N_2 rates of use (from rate of change of P_{O_2} and P_{N_2})

CO_2, H_2O rates of removal (from rate of change of P_{CO_2} and P_{H_2O})

System Status

Monitors of critical voltages and currents in the mass spectrometer electronics, control electronics or control subsystems.

Atmosphere Warning

High rates of change of partial pressures indicating malfunction of the particular subsystem.

High rate of change of total pressure indicating possible cabin leak malfunctions in control circuitry.

System Warnings

Derived from above plus indications of control system failures that cause the above indications or electronics and/or analyzer failures that prevent the control system from functioning in a normal manner in the automatic or manual mode.

This module will derive inputs from the atmosphere control system. It should contain all equipment necessary to provide the above indications to both the crew ground monitoring stations. Further considerations are not necessary at this time. The conclusion that can be drawn is that the mass spectrometer will provide partial pressure indications at a high enough rate (fast time response) and at a high enough accuracy to provide all the information that is needed to adequately display the status of the cabin atmosphere.

Priority levels for various operational modes can be established and instituted in the warning system as operating conditions permit. (Warnings used in automatic mode may be meaningless when operation is in manual mode.)

During periods of transition in the cabin atmosphere, it would be advisable to utilize manual setting of the cabin atmosphere before putting the system in the automatic control mode. This would occur primarily when recovering from cabin venting to bring the atmosphere up to the desired level in a short time. The partial pressures could be monitored on the visual display. This mode would also find use in emergency situations where control system malfunctions, excluding the mass spectrometer, occur. Manual operation procedures could be set to allow little interruption of the planned mission while system repairs or replacements are made.

Mass spectrometer failures would leave the cabin with no control ability. In this case, atmosphere control would be dependent on predetermined human metabolic rates to control O_2 input and CO_2 and H_2O removal. In this mode, the use of an auxiliary mechanical pressure gage would be used to monitor cabin pressure. Use of a pure O_2 atmosphere during this period would simplify the procedure even more.

Once the cabin atmosphere has been established, by either manual means or by pre-programmed automatic fill procedures, the atmosphere control system would be put into operation and serve as the feedback control system maintaining proper cabin constituents partial pressure levels. During this phase of operation, no crew intervention should be required.

7. CONCLUSIONS

A study of a two gas atmosphere sensor system has been conducted using a mass spectrometer as the sensing device. Two types of analyzers were compared: the single focusing magnetic sector and the quadrupole mass filter. The single focusing magnetic sector type was found to be superior with respect to power, weight, complexity, and compatability with system performance goals A detailed analysis of the magnetic sector analyzer lead to an optimized design. The other mass spectrometer subsystem elements were also analyzed and their necessary characteristics found. The results lead to the definition of a reference sensor system which should meet the performance goals while having acceptable weight, power, and size requirements. No fundamental problems were found to prohibit the attainment of the objectives set forth in the statement of work.

APPENDIX A

This appendix covers the preliminary design of a 90° sector analyzer magnet. The design requirements were the result of computer aided optimization of a single focusing magnetic mass spectrometer. Given constraints that defined the pole face size, gap width, and magnetic field strength, a preliminary design was produced.

The following symbols are used for the magnet design

A_g = Area of air gap

L_g = Length of air gap

L_m = Mean magnet length parallel to flux path

A_m = Area of magnet cross section (generally the minimum cross section area perpendicular to flux path)

D = Major diameter

d = Minor diameter

f = Reluctance factor, depends on mmf drops in magnetic circuit— for small gaps and few joints a value between 1.1 and 1.3 is appropriate.

F = Leakage factor — a geometry dependent factor generally ranging upwards from 1.5.

B_d = Flux density in the magnet

B_g = Flux density in the gap

H_d = The H coordinate on the magnetization curve corresponding to B_d.

Based on the radii of curvature of the ions of interest, a magnet pole size was found. The pole face is bounded by the sides of a 90° angle and two circular arcs. The dimensions were chosen to allow at least one gap width from the edge of the maximum or minimum ion trajectories to the edge of the magnet. This pole face with ion trajectories is shown in Figure A-1.

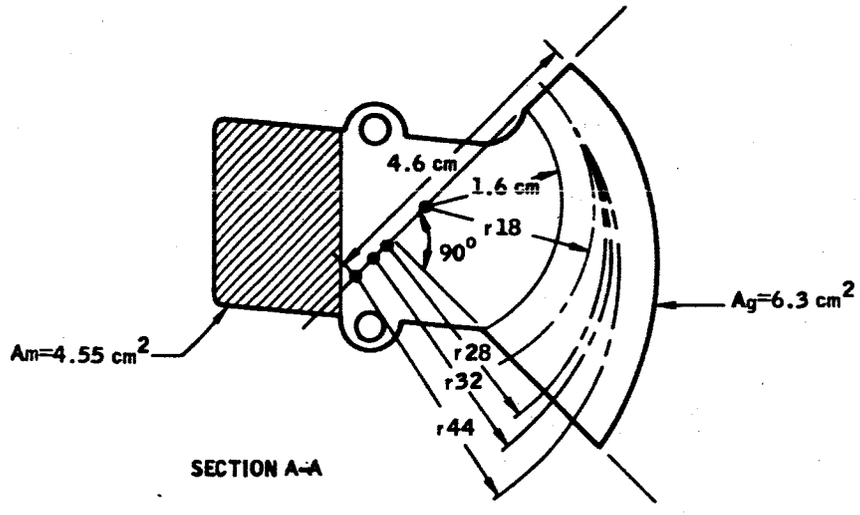

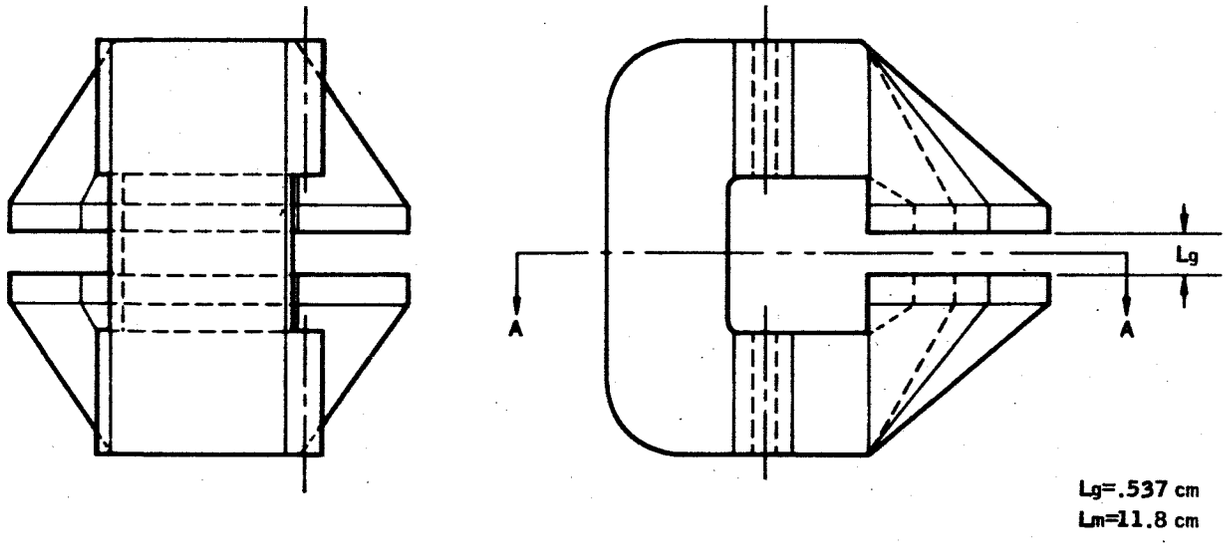

FIGURE A-1
Analyzer Magnet Design

Guidelines can be calculated from the given pole area, gap width, and the field required in the gap of the magnet design. It is necessary to note that magnet design is as much an art as it is a science, and for that reason caution should be taken to not depend entirely upon the results of calculations. Design models to check applicable equations should be utilized before pursuing final designs.

An existing magnet, as shown in Figure A-2, similar to that needed for this application was used to check the design equations.

Equation 24* gives a leakage factor F by

$$F = 1 + \frac{L_g}{A_g}\left[C\left(\frac{1.6(D + G) - Lg}{D + d + 3\,L_g}\right)\right]$$

This equation assumes that C (circumference of the yoke), D, and d all represent circular areas. Substituting parameters from Figure A-2 gives

$$F = 3.28$$

Next it is necessary to find the shear line slope. This is done by taking the magnet length, gap width, magnet area, and gap area to give a $B_d/H_d = 18$. The intersection of this line and the B-H curve for Alnico V yields a B_d of about 10,200 gauss for this configuration (See Figure A-3). Applying this to the above results, the field necessary to produce 3800 gauss in the magnet gap is determined. Using Equation 5 from the magnet design manual*,

$$B_d = \frac{B_g A_g}{A_m} F = 2.065\, B_g = 8300 \text{ gauss}$$

Thus, for this magnet, an observed field of 3800 gauss should be produced with a field in the magnet of 8300 gauss while theoretical calculations predict that just over 10,000 gauss are available to produce that field. Hence, rough agreement between theoretical and actual considerations is achieved with the above equations.

It is now appropriate to use these equations to derive a magnet for the mass spectrometer in question. The fact that the single focusing magnet will essentially be a scaled down version of the double focusing magnet indicates some confidence in the method.

* All formulae used in this Appendix from the Thomas and Skinner Company's Bulletin M303, Permanent Magnet Design.

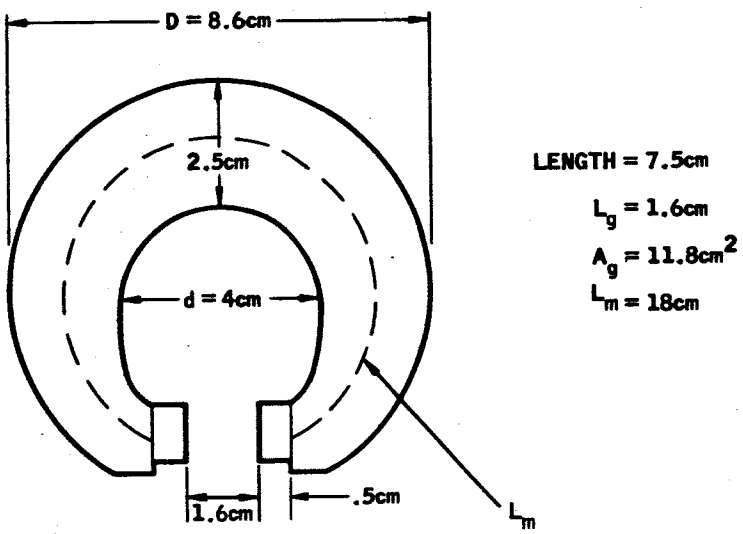

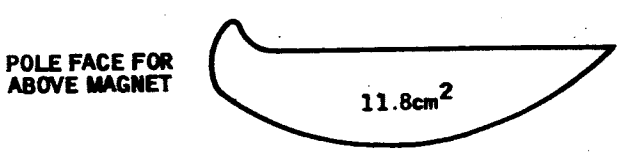

FIGURE A-2
90° Double Focusing Mass Spectrometer Magnet

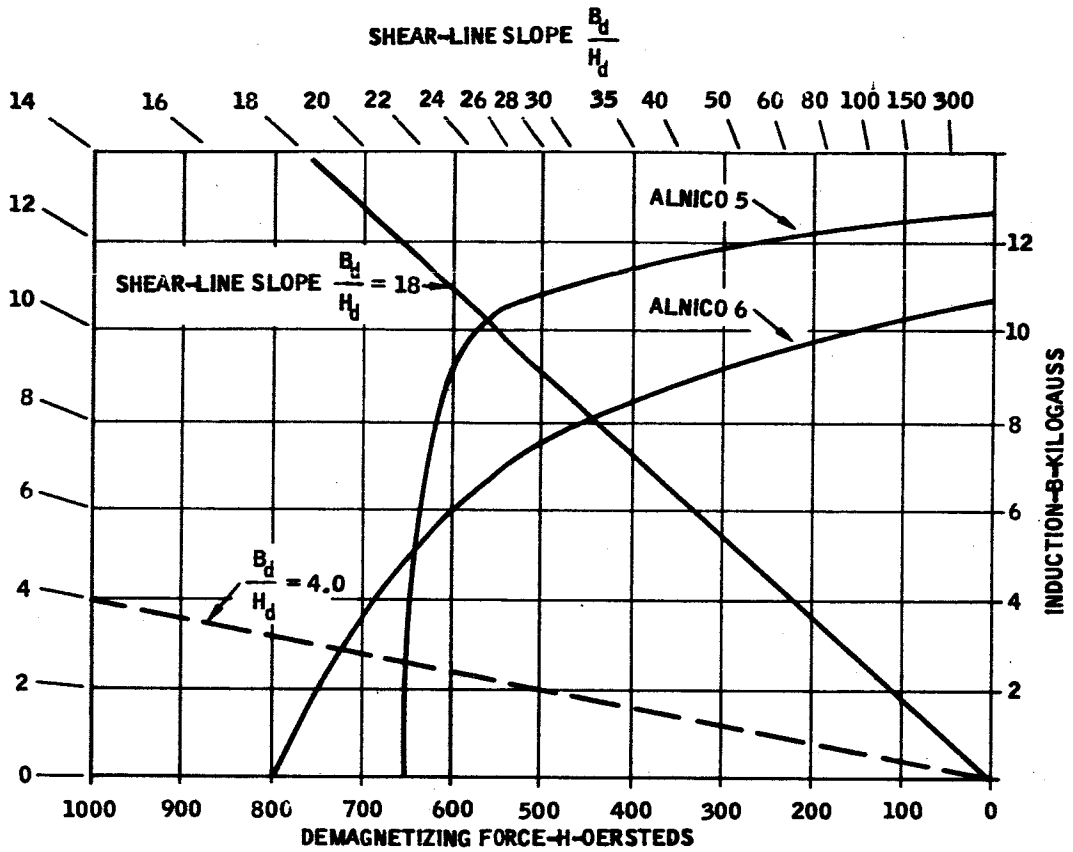
SHEAR-LINE SLOPE $\frac{B_d}{H_d}$
14
16
18
20
22
24
26
28
30
35
40
50
60
80
100
150
300
12
10
8
6
4
2
0
ALNICO 5
ALNICO 6
SHEAR-LINE SLOPE $\frac{B_d}{H_d} = 18$
$\frac{B_d}{H_d} = 4.0$
1000
900
800
700
600
500
400
300
200
100
0
DEMAGNETIZING FORCE-H-OERSTEDS
INDUCTION-B-KILOGAUSS

FIGURE A-3

Because of this similarity, a preliminary estimate of the weight can be made by scaling the double focusing magnet down to the required dimensions of the single focusing instrument. The ratio of pole face areas is

$$\frac{6.31}{11.8} = 0.535$$

The ratio of gaps is

$$\frac{0.537}{1.6} = 0.298$$

Then, the ratio of volumes is

$$0.535 \times 0.298 = 0.159$$

where approximately the same gap flux densities are assumed.

Hence, the weight of the double focusing magnet, 5 pounds, times 0.159 will yield 0.8 pound for single focusing magnet. Utilizing this approximation, a design goal of 1 pound will be set for the magnet.

Proceeding with the design, there are a few constraints that will be imposed. Certain dimensional guidelines have been provided by a parallel effort in package design. Also, Alnico V appears to be the optimum magnetic material.

Now, applying Equation 12,

$$\frac{L_m}{L_g} = \frac{B_g \times f}{H_d}$$ where f is a reluctance factor for the air gaps in the magnetic circuit, taken as 1.1 for these calculations. To achieve 4000 gauss in the gap, a value of L_m of

$$L_m = \frac{4000 \times 1.3 \times 0.537}{0.640} = 4.37 \text{ cm. is required}$$

where B_g and H_d are simultaneous values found on the B-H curve for Alnico V, Figure A-3. However, this factor takes only gap length and magnet length into account. Next the magnet leakage factor must be considered. This is the ratio of the total magnet flux to the useful air gap flux.

To start an iterative design of the magnet, a configuration that takes advantage of the fact that the shear-slope line passes through the B-H curve near the knee, at the maximum energy point, will be used. A shear-line slope of 20 should then be used. Using Equations 4 and 5 and assuming a magnet length of 10.6 cm for a 0.537 cm gap, allows changing the magnetic material

to 11,600 gauss. In addition, 0.3 cm thick pole faces of Armco iron are desirable to achieve a uniformity of field not attainable with the porous Alnico V material. This information then allows other data to be inserted.

Assume that the magnet in question can be approximated as shown in Figure A-4. In this case, the field in the material is given by

$$B = \frac{B_g A_g F}{A_m} .$$

Operation at B_d = 10,600 gauss can be tolerated by assuming the ratio $L_m : L_g$ above, and then F could be approximately 2 for equal pole and magnet areas. F, a leakage factor equal to the ratio between the total flux in the magnetic circuit and the useful gap flux, can now be more accurately determined.

By Equation 24,

$$F = 1 + \frac{A_g}{L_g} = \left[C \left(\frac{1.6(D + d) - A_g}{D + d + 3 L_g} \right) \right]$$

From the estimation of F, assumptions can be made about the magnet dimensions that have not as yet been constrained.

Again utilizing Figure A-3, the intermediate values for the iterative process can be determined.

Assume a circular flux path and almost circular cross sections. Then, the mean path diameter is 3.75 cm. Add 1 cm + and - for the pole diameter to find the major and minor diameters. This then gives D = 3.75 + 2 - 5.75 cm. Now, d = 3.75 -2 = 1.75 cm. This gives C an effective diameter of 2 cm. Assuming the rectangular cross section similar to the pole pieces, choose the area of the magnet at C to be 2 x 2.25 = 4.5 cm^2 with a circumference, C, of 8.5 cm. Having all necessary quantities,

$$F = 1 + \frac{0.537}{10.6} \left[8.5 \left(\frac{1.6 \ (5.75 + 1.75) - 0.537}{5.75 + 1.75 + 1.611} \right) \right] = 1.53$$

which is better than assumed.

Substituting, then, into the magnet area equation (Equation 5) gives

$$B_d = \frac{A_g B_g F}{A_m} = \frac{6.3 \times 4000 \times 1.53}{4.5} = 8600 \text{ gauss}$$

which is well within the constraints of the initial assumptions.

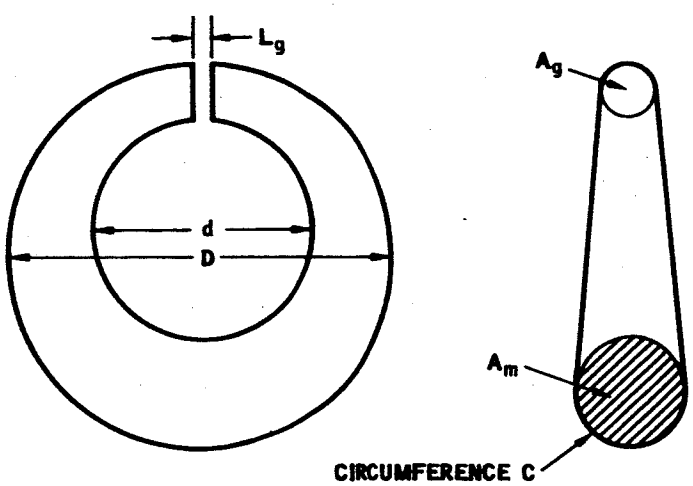

FIGURE A-4
Ideal Magnet Configuration used for Calculations

Now applying the above determined quantities to the geometrical constraints of the analyzer envelope and packaging requirements, the design in Figure A-1 was arrived at. For this configuration,

$A_g = 6.31\ cm^2$

$L_g = 0.537\ cm$

$L_m = 11.8\ cm$

$A_m = 4.25\ cm \quad 4.55\ cm^2$

$C_{equivalent} = 8.0\ cm$ (assumes rectangular cross section is approximately a circle of the same area)

Then,

$$F = 1 + \frac{0.537}{6.31}\left[8.0\left(\frac{1.6\ (5.75 + 2.25) - 0.537}{5.75 + 2.25 + 1.611}\right)\right] = 1.88$$

Now,

$$B_d = \frac{(6.31)\ (4000)\ (1.88)}{4.55} = 10{,}400 \text{ gauss.}$$

From

$$\frac{L_m}{L_g} = \frac{B_g}{H_d} f$$

the following constraint on B_g and H_d, i.e.,

$$\frac{B_g}{H_d} = \frac{11.8}{0.537 \times 1.1} = 20$$

which is the shear-line slope.

This shear-line slope, coupled with the B-H curve shows that, for Alnico V, B_d can be made high as 11,000 gauss, which is close to the calculated requirement for 10,400 gauss and appears to be an adequate design margin.

Complexity of basic magnetic circuit analysis equations have led to iterative design procedures for magnets. The next step in the iterative process should now be construction of models that approximate the present design to substantiate the equations used, perhaps generating correction factors for the equations that will allow a more accurate design to be formulated (accurate to the extent that no excess weight of material is used).

While Alnico V has been used as the magnetic material here, other alternatives were considered. Columax (a high energy, high residual induction material), Placovar (a high energy material for small length to gap ratios) and ceramic materials (for weight savings) were checked for their suitability to this application.

Columax falls into the Alnico family, but derives much of its qualities from the fact that it is cast in the presence of a magnetic field, lining up the magnetic domain to a very high degree. This limits the shape to straight segments only. Its characteristics do not warrant the additional design or cost for this application.

Placovar could provide the necessary field, by fabricating thick pole pieces of the material and utilizing a small cross section Armco yoke. Placovar could be machined to shape and pole faces ground without too much difficulty. For this application, however, where the long path is available. i.e., the magnet yoke, the use of Placovar is not warranted. Being 75% by weight platinum and twice as dense as Alnico, it possessed no advantage over Alnico V that is not offset by its weight.

Ceramic materials, while possessing a distinct weight advantage (almost 2:1 lighter than Alnico V) has the disadvantage of being a very low energy material (five times lower than Alnico V) useful only at low magnetic field strengths (much less than 2000 gauss).

Notwithstanding the development of new magnetic materials, the above design utilizing Alnico V with Armco iron pole faces appears to be an optimum magnet design. A net weight of approximately 0.9 pounds is estimated for the configuration proposed.

APPENDIX B

Design of a Perfect Imaging Ion Source

The initial constraints placed upon the design of this perfect imaging system are that the ion source must have a magnification, M, of 1.75, and an injection energy of 225 v in order to comply with the analyzer. For a perfect imaging system, this can be expressed by

$$V_I = f_1E_1 + \left(f_1 + f_2\right) E_2 + f_2E_3 = \text{injection energy}$$

where

V_I = injection energy of the ions

f_1 = focal length of the accelerator

f_2 = focal length of the focusing lens

E_1 = gradient between the repeller and accelerator

E_2 = gradient between the accelerator and the focusing lens

E_3 = gradient between the focusing lens and the final exit slit.

As an aid to the following discussion Figure B-1 is given which shows the parameters which are important to the design.

For an emersion type lens, which is the most practical type to consider:

$$f_1 = \frac{4V_o}{E_2-E_1} \tag{1}$$

and that for perfect imaging:

$$f_2 = 1.75\ f_1 \tag{2}$$

From these equations, it is shown that

$$f_1 = \frac{4V_I}{330\ E_1} \tag{3}$$

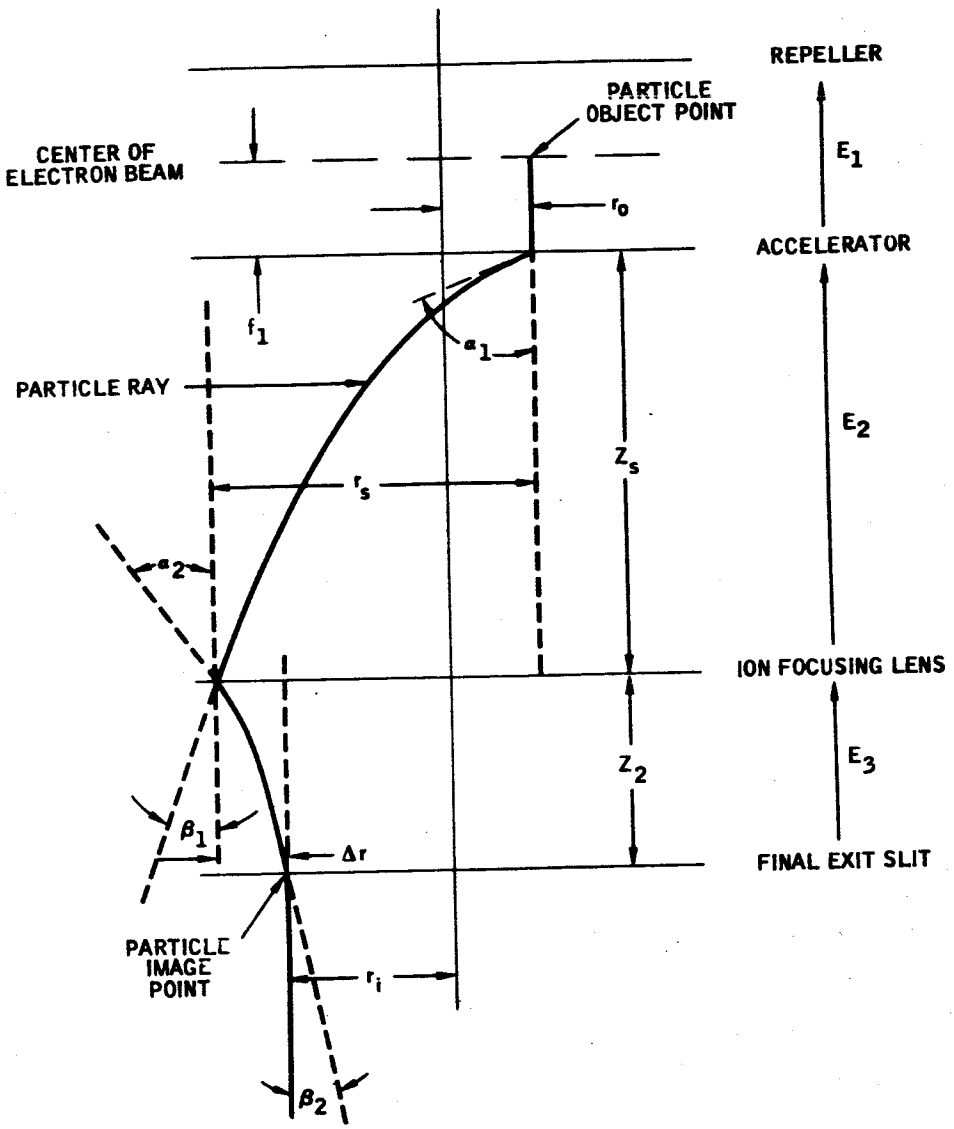

FIGURE B-1
Ion Focusing Parameters

and since $V_o = E_1 f_1$, then

$$V_I = \frac{330}{4} V_o \tag{4}$$

so that for $V_I = 225$ v, then

$$V_o = 2.73 \text{ v}$$

or that $\Delta V_{RA} = 5.46$ v

where

$$\Delta V_{RA} = V_{REPELLER} - V_{ACCELERATOR}$$

and

f_1 = 0.050 in. for the electron beam in the center of the ionizing region.

These calculations, however, do not take into account the bending of a charged particle in the focusing field. This bending can be approximated by the parabolic equation:

$$Z_s = a_1 r_s + b_1 r_s + c_1 \tag{5}$$

where

$$a_1 = \tfrac{1}{4}\left(\frac{E_2}{V_o}\right)\left(\frac{1}{\sin^2 \alpha_1}\right)$$

$$b_1 = \frac{1}{\tan \alpha_1} - \tfrac{1}{2}\left(\frac{E_2}{V_o}\right)\left(\frac{r_o}{\sin^2 \alpha_1}\right)$$

$$c_1 = Z_o - \frac{r_o}{\tan \alpha_1} + \tfrac{1}{4}\left(\frac{E_2}{V_o}\right)\left(\frac{r_o^2}{\sin^2 \alpha_1}\right)$$

For the case of interest, it can be assumed that there is a negligible initial energy on the particles at ionization, thus reducing Z_o and r_o to zero. For an ion source exit slit height, h equal to 0.0614 cm, we find that

$$r_s = 2.75\, r_o \tag{6}$$

$$\tan \alpha_1 = \frac{r_o}{f_1} = 0.138$$

where

$$r_o = \frac{h}{2}\left(\frac{1}{M}\right) \tag{7}$$

such that $\alpha_1 = 7.87°$.

For $f_1 = .050$, then

$$\frac{E_2}{V_o} = 100,$$

$$Z_s = .1855,$$

which is the actual distance to place the ion focusing lens in order to obtain a magnification of 1.75. The effective f_2 to give this magnification is then foung by

$$f_2 = r_s \cot\beta_1 \tag{8}$$

where β is the angle such that

$$\cot\beta_1 = \frac{dZ_s}{dr_s} \quad . \tag{9}$$

This gives an effective $f_2 = .2335$, and Z_2, the distance from the focusing lens to the final exit slit can then be expressed by the equation

$$Z_2 = f_2 \frac{\left[V_I - V_o\left(1 + 100\ Z_s\right)\right]}{4V_o\ (1 + 100\ Z_s + 25\ f_2)} \tag{10}$$

which is only valid for $f_1 = .050$.

Therefore, if $f_2 = .2335$, $Z_s = .1855$, and $V_I = 225$ v, Z_2 can be calculated solely as a function of V_o.

However, there will exist a divergent focusing action at the final slit of the source due to the gradient difference on each side of the slits. The focal length of the slit, f_3, is found by

$$f_3 = \frac{4V_I}{E_4 - E_3} \tag{11}$$

where E_4 is the gradient in the analyzer region and is 0 V/in. Thus f_3, for $V_o = 5$ v, is calculated to be

$$f_3 = -0.414 \text{ in.}$$

and

$$\tan\beta_2 = \frac{h}{2f_3} = -\frac{hE_3}{8V_I} \tag{12}$$

so that $\beta_2 = 1.675°$

This change in exit angle into the analyzer is significant and must be corrected by use of the focus lens.

Consequently, it is desirable to overfocus the ray of the particle by some Δr in region between the accelerator and the focus lens such that the particle will enter the analyzer region with no divergent focusing angle, and yet retain a magnification of 1.75. Equation (6) then becomes

$$r_s = r_i + r_o + \Delta r$$

where

$$\frac{r_i}{r_o} = 1.75$$

or

$$r_s = 2.75\, r_o + \Delta r. \tag{13}$$

This is illustrated in Figure B-1.

Application of the parabolic approximation to the particle in the distance, Z_2, between the focusing lens and the slit yields

$$Z_2 = a_2 \Delta r^2 + b_2 \Delta r + c_2 \tag{14}$$

where

$$a_2 = \tfrac{1}{4}\left(\frac{E_3}{V_2}\right)\left(\frac{1}{\sin^2 \alpha_2}\right)$$

$$b_2 = \frac{1}{\tan \alpha_2}$$

$$c_2 = 0$$

Differentiating with respect to Δr, it is seen that

$$\frac{dZ_2}{d(\Delta r)} = 2a_2 \Delta r + b_2 = \cot \beta_2$$

or

$$\Delta r = \frac{\cot \beta_2 - b_2}{2a_2} \tag{15}$$

The value of V_2 in the expression for a_2 can be found by

$$V_2 = V_o + Z_s E_2$$

$$= V_o \left[1 + Z_s \frac{5}{f_1}\right]$$

$$= V_o \left(1 + 100 Z_s\right) \qquad (16)$$

for the case where $f_1 = .050$.

Substituting V_2, a_2, and b_2 into Equation (15) gives the equation

$$E_3 = \frac{2 V_o \left(\cot \beta_2 - \cot \alpha_2\right) \left(\sin^2 \alpha_2\right) \left(1 + 100 Z_s\right)}{\Delta r} \qquad (17)$$

However, Z_s was defined in Equation (5), so that by substituting Equation (13) for Equation (6), a value for Z_s may be obtained. From this substitution it follows that

$$Z_s = .1855 + 12.29 \ \Delta r + 133 \ \Delta r^2 \qquad (18)$$

Inserting Equation (18) into (17) yields

$$E_3 = \left(\frac{2V_o}{\Delta r}\right) \left(\cot \beta_2 - \cot \alpha_2\right) \left(\sin^2 \alpha_2\right) \left(19.55 + 1229 \ \Delta r + 13300 \Delta r^2\right) \qquad (19)$$

The focal length, f_2, of the focusing lens is defined by the following relationship from geometrical optics:

$$\frac{1}{f_2} = \frac{1}{u} + \frac{1}{v}$$

where

$$\frac{1}{u} = \frac{\tan \beta_1}{r_s - r_o}$$

$$\frac{1}{v} = \frac{\tan \alpha_2}{r_s - r_o}$$

$$\text{or } \tan \alpha_2 = \frac{r_s - r_o}{f_2} - \tan \beta_1 \qquad (20)$$

However,

$$\cot \beta_1 = \frac{dZ_s}{dr_s} = 2a_1 r_s + b_1$$

or

$$\tan \beta_1 = \frac{1}{266\ \Delta r + 12.29} \tag{21}$$

and

$$r_s - r_o = 1.209 \times 10^{-2} + \Delta r \tag{22}$$

Also, we know that

$$f_2 = r_s \cot \beta_1$$

$$= 266\ \Delta r^2 + 17.34\ \Delta r + .2335 \tag{23}$$

Combining Equations (21), (22), and (23) with Equation (20), it follows that

$$\tan \alpha_2 = \Delta r \left[\frac{1.209 \times 10^{-2} + \Delta r}{(266\ \Delta r^2 + 17.34\ \Delta r + .2335)} - \frac{1}{(266\ \Delta r + 12.29)} \right] \tag{24}$$

Evaluating Equation (14), it is found that

$$Z_2 = \left[\frac{r^2}{4V_o}\right]\left[\frac{1}{\sin^2 \alpha_2}\right]\left[\frac{E_3}{19.55 + 1229\ \Delta r + 13300\ \Delta r^2}\right] + \left[\frac{\Delta r}{\tan \alpha_2}\right] \tag{25}$$

And from Equation (12) it is seen

$$\cot \beta_2 = -\frac{8V_I}{hE_3} = \frac{-330\ .5\ V_I}{E_3} \tag{26}$$

Combining Equation (26) with (19) and solving for E_3, it is obvious that

$$E_3 = -\left[\frac{V_o\ \alpha_2}{\Delta r}\ (13{,}300\ \Delta r^2 + 1229\ \Delta r + 19.55)\right]$$
$$\pm \left\{ \left[\frac{V_o\ \alpha_2}{\Delta r}\ (13{,}300\ \Delta r^2 + 1229\ \Delta r + 19.55)\right]^2 \right.$$
$$\left. - \left[\frac{2V_o \alpha^2}{\Delta r}\ (330.5\ V_I)\ (13{,}300\ \Delta r^3 + 1229\ \Delta r + 19.55)\right] \right\}^{1/2} \tag{27}$$

where the approximation that

$$\alpha_2 \approx \sin \alpha_2 \approx \tan \alpha_2$$

has been made since α_2 is assumed to be a very small angle. The other relationship that can then be applied to the source focusing is

$$V_I = V_o + Z_s E_2 + Z_2 E_3 \qquad (28)$$

Thus, if V_o and V_I are constant and by substituting for Z_s, E_2, Z_2, and E_3, then we solve Equation (28) for Δr. This was accomplished by use of a computer program iteration, and the following results were obtained for $V_o = 4$ v, $V_I = 225$ v, and $f_1 = 0.050$ in.

$$Z_s = 0.50443 \text{ in.}$$

$$Z_2 = 0.0408 \text{ in.}$$

$$E_3 = 471.193 \text{ v./in.}$$

$$E_2 = 400 \text{ v./in.}$$

ΔV_{RA} is defined by

$$\Delta V_{RA} = 2 V_o$$

$$= 8 \text{ v.}$$

This set of values defines the ion source focusing parameters required to obtain a magnification of 1.75 and a V_I of 225 v.

Appendix C

PRELIMINARY STRESS ANALYSIS

Three critical areas of the mechanical packaging were reviewed from the stress analysis point of view. Computations were made with respect to relative displacements and rotations between the object slit and the collector planes, deformation of the analyzer envelope, and rigidity of the analyzer mounting bracket. The results of the stress analysis showed that the preliminary mechanical packaging is mechanically rigid and structurally sound.

A list of symbols used in the following analysis is given in Table C-1.

TABLE C-1

List of Symbols

r = radius	τ = shear stress
t = thickness	a = length of panel
ρ = density	I = second moment of area
W = weight per unit length	θ = angular displacement
ℓ = length	S = displacement
M = moment	T = torsion
σ = normal stress	α = rotation
Q = shear load	G = shear modulus
V = volume	R = form factor
K = buckling stress coefficient	p = pressure
E = elastic modules	η = function of lateral displacement
b = panel width	X = vibrational acceleration in g's
τ_{cr} = buckling stress	

Consider the externally projecting pump out tube which is rigidly clamped to the analyzer mounting bracket at one end and free at the other.

Weight per unit length of projecting tube is

$$W = 2\pi rtp = 0.39$$

and the bending moment at the root is

$$M = \frac{1}{2} W \ell^2 = 6.3 \text{ in-lb.}$$

The corresponding bending stress is

$$\sigma = 132 \frac{\text{lb}}{\text{in}^2\text{-g}}$$

Assume that the structure is subject to inertia forces of X g's together with a superimposed factor of 1.25 then

$$\frac{M}{X} = 6.32 \frac{\text{in-lb}}{\text{g}}$$

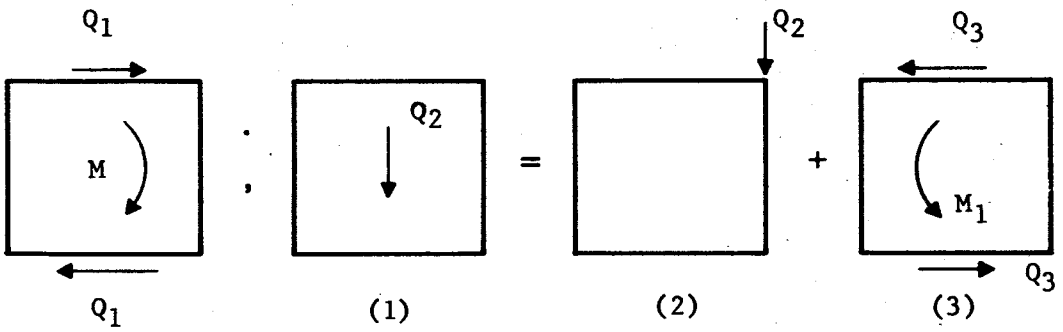

The moment "M" is reacted by a couple formed by shear Q_1 in panels (1) and (3).

$$\frac{Q_1}{X} = \frac{M}{7} = 0.901 \text{ lbs/g}$$

The interial load of the pump out line is

$$\frac{Q_2}{X} = pV = 0.590 \text{ lbs/g}$$

This load is equivalent to a shearing load Q_2 reacted along panel (2) together with a moment M_1 reacted by a couple formed by shear Q_3 in panels (3) and (1)

$$M_1 = 0.5\, Q_2 = 0.295 \text{ lbs/g}$$

so that

$$Q_3 \frac{M_1}{7X} = 0.0421 \text{ lbs/g}$$

Thus the effective shear due to the inertia load acting on the pump out line is 0.859 lbs per g on panels (1) and (3) in the direction of Q_1, and 0.590 lbs per g along panel 2.

When these values are multiplied by the expected acceleration levels the bending stresses are found to be very small and neither failure or instability due to bending will occur[1].

The intertia force acting on the combined analyzer and magnet is

$$\frac{P_1}{X} = PV = 2.02 \text{ lbs/g}$$

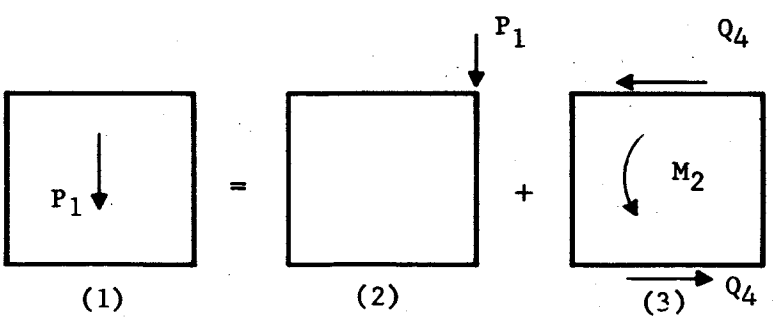

(1) "Thin Walled Circular Beams" by H.D. Tabuakman, Machine Design, March 19, 1959.

This load is equivalent to a shearing load P_1 reacted along panel (2) together with a moment M_2 reacted by a couple formed by shear Q_4 in panels (1) and (3).

If the center of gravity of the analyzer and magnet lies in a plane 1.5 inches from panel (2) then

$$M_2 = 1.5\ P_1$$

and

$$\frac{Q_4}{X} = \frac{1.5P}{7X} = 0.438 \text{ lbs/g}$$

The overall effective shear due to intertia forces acting on the pump out line, magnet and analyzer are

$$\frac{1}{X}(P_1 + Q_2) = 2.61 \text{ lbs. per g along panel (2)}$$

$$\frac{1}{X}(Q_1 - Q_3 - Q_4) = 0.438 \text{ lbs per g along panels (1) and (3) in the direction of } Q_1.$$

Consider the effect of inertia loading P_2 which is coplanar with P_1, taken to act in the direction of Q_1. The supporting structure S_1 may be treated as a simply supported beam.

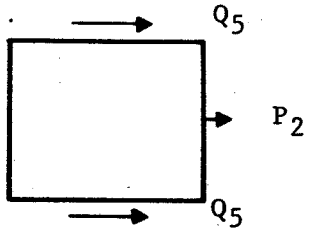

$$\frac{P_2}{X} = PV = 2.61 \text{ lbs/g}$$

This load is reacted in shear Q_5 in panels (1) and (3).

$$\frac{Q_5}{X} = 1.30 \text{ lbs./g}$$

and shear in panel (3) due to simultaneous loading P_1 and P_2 is

$(Q_1 - Q_3 - Q_4 - Q_5)$ = occurs in the narrow of the analyzer mounting bracket S_1.

The bending moment at the section referred to is

$$\frac{M}{X} = \frac{1}{2}\left(\frac{P_2}{2X} \times 3.5\right) = 2.27 \text{ in-lb/g}$$

The second moment of area I of the cross section is

$$I = 1/12 \times 0.25 \times 0.25^3 + (0.032 \times 0.5) \times 0.125^2$$

$$= 0.000575 \text{ in}^4$$

the bending stress is

$$\frac{\sigma}{X} = \frac{M}{I} \times \frac{0.125}{X} = 505 \text{ lb/in}^2 - g$$

which is low when evaluated at the expected acceleration levels.

Consider the mode of loading which acts normal to the plane of the analyzer magnet and of magnitude

$$\frac{P_3}{X} = 2.6 \text{ lbs./g}$$

This load is reacted by the upper lobe of the analyzer mounting bracket which is rigidly attached to the circular plate of 1/8 inch thickness forming the base of the cylindrical element of the analyzer (Plane I) and reacted in shear by panel (2). This shear acts in a direction normal to that of P_1 in the same panel.

The analyzer is subject to a moment M_3, left handed with respect to the direction of P_2.

$$\frac{M_3}{X} = \frac{2P_3}{X} = 5.2 \text{ in-lb/g}$$

The moment M_3 is reacted by a couple as shown in the adjacent sketch:

$$\frac{Q_6}{X} = \frac{5.2}{1.375} = 3.8 \text{ lbs/g}$$

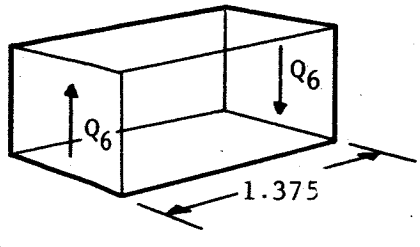

Q_6 is reacted in shear in panel (2) forming a couple reacted by shear Q_7 in panels (1) and (3).

$$\frac{Q_7}{X} = \frac{1.25}{7X} = 1.4 \text{ lbs.}$$

Consider the stability of the panels due to shear. Fixing attention on panel (3) the maximum shear due to combined action of P_1, P_2, and P_3 is

$$\frac{1}{X}\left(Q_1 - Q_3 - Q_4 + Q_5 + Q_7\right) = 2.46 \text{ lbs.}$$

Assume the edge conditions as simply supported. The critical shearing stress is given by

$$\tau_{cr} = KE \left(\frac{t}{b}\right)^2$$

For panel (3),

$$E = 10^7 \text{ lb/in}^2$$

$$t = 0.032 \text{ in.}$$

$$b = 5.0 \text{ in.}$$

For a panel whose $\frac{t}{b} = \frac{5}{6}$ and all edges simply supported

$$K = 7$$

thus

$$\tau_{cr} = 2800 \text{ lb/in}^2$$

Since $\tau_{cr} > T$ no buckling will occur.

For panel (2), the maximum shear is Q_6, for

$$\frac{b}{a} = \frac{1.375}{7} = 0.195$$

and $K = 5$.

Then

$$\tau_{cr} = 5 \times 10^7 \frac{(0.032)^2}{1.375} = 27{,}000 \text{ lbs/in}^2$$

as compared with an actual shear stress of

$$\frac{\tau}{X} = \frac{3.8}{7 \times 0.032} = 16.85 \text{ lb/in}^2\text{-g}$$

Next the relative displacement between the object slit and the collector planes is considered.

The object slit plane is assumed fixed. Assume the center of gravity of all components attached to the object slit plane to be at the magnet and have an effective weight of 1.5 lbs. The inertia force in the direction of P_1 is

$$\frac{P_1}{X} = 1.5 \text{ lbs./g}$$

The line of action of this load is such that no bending occurs and consequently no displacement or rotation takes place.

Consider now an inertia force in the direction P_2. The bending at the root is

$$\frac{M_2}{X} = 1.5 \times 1.5$$

and the second moment of area at the root is

$$I = (1/12 \times 0.2 \times 0.5^3)$$

and the bending stress

$$\frac{\sigma_2}{X} = \frac{1.5 \times 1.5 \times 9.25 \times 12}{0.2 \times 0.5^3} = 37.2 \text{ lb/in}^2\text{-g.}$$

The displacement in the direction of P_2 is given by

$$\frac{\sigma_2}{X} = 1/3 \frac{1.5 \times 1.5^3 \times 12}{30 \times 10^6 \times 0.2 \times 0.5^3} = 2.55 \times 10^{-5} \text{ in/g}$$

and the corresponding rotation

$$\frac{\theta 2}{X} = 1/2 \frac{1.5 \times 1.5^2 \times 12}{30 \times 10^6 \times 0.2 \times 0.5^3} = 0.274 \times 10^{-4} \text{ rad/g}$$

The inertia force in the direction of P_3 contributes to both bending and torsion.

The bending moment at the root is

$$\frac{M_3}{X} = 1.5$$

The corresponding second moment of area is

$$I_3 = 1/12 \times 0.5 \times 0.2^3$$

and the bending stress:

$$\frac{\sigma_3}{X} = \frac{1.5 \times 1 \times 12}{0.5 \times 0.2^3} = 455 \text{ lb/in}^2\text{-g}$$

The displacement in the direction of P_3 is

$$\frac{\sigma_3}{X} = 1/3 \frac{1.5 \times 1.5^2 \times 12}{30 \times 10^6 \times 0.5 \times 0.23} = 1.69 \times 10^{-4} \text{ in/g.}$$

and the corresponding rotation is

$$\frac{\theta_3}{X} = 1/2 \frac{1.5 \times 1.5^2 \times 12}{30 \times 10^6 \times 0.5 \times 0.23} = 1.66 \times 10^{-4} \text{ rad/g.}$$

Consider the effect of torsion at the root

$$\frac{T_3}{X} = 1.5 \text{ in-lb/g}$$

Treat T_3 as an applied torque. The rotation is given by

$$\alpha = \frac{T_3}{RG}$$

where

$$R = ab^3\left(\frac{16}{3} - 3.36\,\frac{b}{a}\right) = 0.8 \times 10^{-3} \text{ in}^4$$

$$\ell = 1.25 \text{ in}$$

$$G = 12 \times 10^6 \text{ lb/in}^2$$

$$\alpha = \frac{1.25 \times 1.5}{12 \times 10^6 \times 0.8 \times 10^{-3}} = 0.00019 \text{ rad/g.}$$

All of the above values can be shown to be well within tolerable limits when evaluated at the appropriate acceleration level.

The analyzer envelope is subject to an external pressure of 14.7 lb/in^2. Maximum displacement of the wall of the tube will occur at its widest cross section.

Treat the tubular element as part plate subject to a pressure normal to its surface with edges simply supported. The maximum displacement normal to the surface is given by *

$$\sigma = \frac{\beta p b^4}{E t^3}$$

take

$$b = 1.0$$

$$t = 0.032 \text{ in}$$

$$E = 30 \times 10^6$$

$$\beta = 0.14$$

$$p = 14.7 \text{ lb/in}^2$$

thus

$$\sigma = \frac{0.14 \times 14.7 \times 1}{30 \times 10^6 \times 0.032^2} = 0.0021 \text{ in}$$

The maximum bending is given by

$$M = \frac{Pb^2}{8} \psi(u)$$

where

$$u = \frac{\pi}{2} (\eta) \frac{1}{2}$$

and the value "η" is given by the equation

$$\eta(1 + \eta)^2 = \frac{3\sigma^2}{t^2}$$

Substituting for σ and t and solving for "η"

$$\eta = 1.26$$

Substituting in the expression for u

$$u = \frac{\pi}{2} (1.26)\frac{1}{2} = 1.65$$

and

$$\psi(u) = 0.5 **$$

* Theory of Plates and Shells., S. Timoshenko 1940 Edition, p.133.
** Strength of Materials - Part II, S. Timoshenko; 1943 Edition Table 3, p.43

the maximum bending stress is

$$\sigma = \frac{6\ M\ max}{t^2} = \frac{6 \times 14.7 \times 1 \times 0.5}{0.032^2 \times 8} = 5600\ lb/in^2$$

The natural frequency for the various mechanical packaging components have not been evaluated. A first approximation as to what the natural frequency of the total integrated package follows:

Assume the package to be flush mounted in a cantilever position with respect to a rigid supporting wall. It is also assumed that the total weight of the package is uniformly distributed along its length of 7.5 inches and is equal to a total of 6.2 pounds.

The fundamental frequency is obtained from the flexural beam vibration relationship for a uniformly loaded cantilever beam.

$$f = \frac{3.66}{2\pi l^2}\sqrt{\frac{EI}{4}}$$

E = Young's modules = 10^7 PSI

I = 2nd moment of area = 3.066 IN^4

l = length of beam = 7.5 cm

μ = mass per unit length = $\frac{6.2}{7.5\ (384)} = 2.15 \times 10^{-3}\ \frac{\#\ Sec^2}{In^2}$

f = 1230 CPS

This value is considered low because of the conservative assumptions, and therefore the actual value should be high enough to avoid problems.

APPENDIX D

QUADRUPOLE MASS SPECTROMETER FOR ENERGETIC PARTICLE MEASUREMENTS

L. G. Hall and M. R. Ruecker

SPACE SCIENCES LABORATORY

ABSTRACT

Analytical expressions are developed which define the initial conditions for 100% transmission of a Quadrupole analyzer and which enable combination with equations for the focal properties of an ion source. The equation for the combined properties can be used to calculate the ion current intensity of the system as a function of the gas density, parameters of the mass spectrometer and upper limits of acceptance of initial energy and initial angle. It is shown that the measurement of density is, in principle, independent of the initial energy and initial angle at the time of ionization within the established upper limits. The equations are particularly useful in design of instruments for measurement in the upper atmosphere.

This work supported by the Jet Propulsion Laboratory and by Goddard Space Flight Center of the National Aeronautics and Space Administration.

QUADRUPOLE MASS SPECTROMETER
FOR ENERGETIC PARTICLE MEASUREMENTS

INTORDUCTION

In terms of optimum performance, the design of any mass spectrometer considers the initial conditions under which the ions enter the analyzer. The initial condition of the ions, in turn, relates to the ion source properties. It is the purpose of this paper to present a means of analytically relating the quadrupole[1] analyzer with an ion source in one of two modes of focusing. For this purpose it is necessary to provide analytical expressions for both the analyzer and ion source operation.

QUADRUPOLE ANALYZER

The discussion of the quadrupole analyzer is limited to operation of the quadrupole in conditions of 100% transmission. This choice is dictated by a desire to: 1) obtain a more accurate absolute value for the ion current as related to gas density in the ion source; and 2) obtain "flat-topped" ion intensity peaks which can be measured by stepping from peak-to-peak. This method of measurement may be useful in space applications, where time or information capacity is limited and where the peak intensity must be independent of small changes in voltage or frequency. The discussion that follows thus treats the top width of the peak and the top to base ratio as important parameters of the operation.

The functional characteristics of the quadrupole analyzer have been adequately described by Paul, Reinhard, V. Zahn[1], and Brubaker[2]. Their work is not extensively reviewed here.

It has been shown[1] that the maximum amplitudes of motion are inversely proportional to the stability parameters $(1 - \beta_x)$ and β_y. Paul, Reinhard, and V Zahn have also computed the stability requirements as a function of entering phase angle under conditions 1) that the initial transverse velocity is zero or 2) that the initial position is zero. Since here we require an analytical expression with all initial conditions (i.e., position, x_o, y_o, transverse velocity, $\dot{x}_o$, $\dot{y}_o$,

and phase angle, ϕ) as variables, by retaining only the first few and important terms, the following approximate expressions for x and y motion are derived (see Appendix I):

$$x \approx A_x \left\{ c_o \sin\left(\frac{\beta_x \omega t}{2} + \delta_x\right) - \left(c_{-2}\right)_x \sin\left[\left(1 - \frac{\beta_x}{2}\right)\omega t - \delta_x\right]\right\} \qquad (1)$$

and

$$y \approx A_y \sin\left(\frac{\beta_y \omega t}{2} + \delta_y\right)\left[c_o + 2\left(\overline{c_2}\right)_y \cos\left(\omega t + \phi\right)\right] \qquad (2)$$

where

$$A_x, \delta_x = f\left(x_o, \dot{x}_o, \phi\right)$$

$$A_y, \delta_y = f\left(y_o, \dot{y}_o, \phi\right)$$

ϕ = Initial phase angle

$$c_o = 1, \left(\overline{c_2}\right)_y = \frac{c_2 + c_{-2}}{2} = 0.168 \neq f\left(\beta_y\right)$$

$$\left(c_{-2}\right)_x = f\left(\beta_x\right), \quad 0.8 < \left(c_{-2}\right)_x < 1.0$$

It is noted in Equation (1) that when β_x is nearly 1 the arguments $\frac{\beta_x}{2}$ and $1 - \frac{\beta_x}{2}$ are nearly the same and since the coefficients[1] are of similar magnitude one obtains an amplitude modulated wave without carrier which is centered about the angular frequency $\frac{\omega}{2}$. On the other hand, when β_y is small the y motion is the low frequency wave $\sin\frac{\beta_y \omega t}{2}$, with superimposed fine motion $(1 + 0.336 \cos \omega t)$. Brubaker has shown the trajectories for both motions computed with specific conditions and has also derived the elements of Equation (2) by the integration of incremental forces on the ion. We differ from his value for $2\left(c_2\right)_y$ only in obtaining 0.336 instead of 0.353.

From Equations (1) and (2) one can obtain values from the maximum amplitude of motion in each plane as a function of initial conditions. Since the y motion is simpler we use this for an example as follows:

From (2),

$$y = A_y \sin\left(\frac{\beta_y \omega t}{2} + \delta_y\right)\left[1 + 0.336 \cos(\omega t + \phi)\right] \tag{3}$$

and we first observe that $(y_{max}) = 1.336\, A_y$. (4)

Evaluation of (3) and its time derivative at $t = 0$ gives:

$$y_o = A_y f_1 \sin \delta_y \tag{5}$$

and

$$\dot{y}_o = A_y \left(f_1 \frac{\beta_y \omega}{2} \cos \delta_y - f_2\, \omega \sin \delta_y\right), \tag{6}$$

where

$$f_1 = (1 + 0.336 \cos \phi) \qquad \text{and}$$

$$f_2 = 0.336 \sin \phi \ .$$

Solving for A_y:

$$A_y^2 = \frac{1}{f_1^2}\left\{y_o^2 + \frac{4}{\beta_y^2}\left(\frac{\dot{y}_o}{\omega} + y_o \frac{f_2}{f_1}\right)^2\right\} \ .$$

Substituting in (4) gives:

$$\left|y_{max}\right| = \frac{1.336}{f_1}\left\{y_o^2 + \frac{4}{\beta_y^2}\left(\frac{\dot{y}_o}{\omega} + y_o \frac{f_2}{f_1}\right)^2\right\}^{\frac{1}{2}} . \tag{7}$$

It can be easily shown that for resolution better than $\frac{m}{\Delta m} = 10$

The term y_o^2 can be neglected. Consequently,

$$\left|y_{max}\right| = \frac{2.672}{\beta_y f_1}\left|\frac{\dot{y}_o}{\omega} + y_o\frac{f_2}{f_1}\right| \tag{8}$$

where the absolute signs are obtained in the process of taking the square root.

By the method employed by Paul[1] an approximate equation for

$\left|x_{max}\right|$ evaluated at $\beta_x = 0.92$ is;

$$\left|x_{max}\right|_{\beta = 0.92} = 16.35\left(f_3 x_o^2 + f_4\frac{x_o\dot{x}_o}{\omega} + f_5\frac{\dot{x}_o^2}{\omega^2}\right)^{\frac{1}{2}} \tag{9}$$

where

$$f_3 = 0.40 - 0.20\cos\phi - 0.20\cos 2\phi,$$

$$f_4 = 0.93\sin\phi + 0.26\sin 2\phi \text{ , and}$$

$$f_5 = 1.63 + 1.86\cos\phi + 0.26\cos 2\phi \text{ .}$$

The variable ω may be eliminated with the following substitutions:

$$\dot{y}_o = \left(\frac{2eV_I}{m}\right)^{\frac{1}{2}}\sin\alpha \tag{10}$$

where eV_I is the injection energy and α the entrance half-angle. Using the quadrupole equation:

$$\frac{e}{m} = \frac{q\omega^2 r_o^2}{4V_{ac}} \tag{11}$$

and letting

$$\gamma = \left(\frac{V_I}{V_{ac}}\right)^{\frac{1}{2}} \sin \alpha \,, \tag{12}$$

equation (10) becomes:

$$\frac{\dot{y}_o}{\omega} = \left(\frac{q}{2}\right)^{\frac{1}{2}} r_o \gamma \tag{13}$$

In the region of the apex of the stability diagram q = 0.706.

Thus dividing y_{max} by y_o in Equation (8) and substituting Equation (13):

$$\frac{|y_{max}|}{y_o} = \frac{2.672}{\beta_y f_1} \left| \frac{0.595\, r_o \gamma}{y_o} + \frac{f_2}{f_1} \right| \tag{14}$$

Similar substitutions may be made for $|x_{max}|$.

From these equations we can now show examples of combined initial position and angle in Figure 1 where (x_{max}) and (y_{max}) are plotted as a function of initial phase angle, ϕ, with γ as a parameter. The value $\frac{r_o}{r_e} = 30$ is used where $r_e = x_o = y_o$ is the radius of a round entrance aperture.

Comparison with the curves which Paul has computed[3] for x_o, $y_o = 0$ or $\dot{x}_o$, $\dot{y}_o = 0$ indicate that the approximate solutions are in good agreement in the x - z plane where maxima are within 7% and the same shaped curve is obtained. In the y - z plane, ion motion reaches a maxima for a phase somewhat shifted from Paul's, however, maxima agree to better than 2%. It appears that one may use the approximate expressions with less error than 10% in the maxima of the curves.

By comparing the $|x_{max}|$ and $|y_{max}|$ curves it is seen that for equal values of γ, $|y_{max}| > |x_{max}|$.

It should be noted that the maximum amplitude in y - z plane occurs in the useful region between $127° > \phi > 142°$. A study was made over a variety of conditions where it was found that for equal initial conditions in the two planes, nominal worst case condition is at $\phi = \frac{3\pi}{4}$ in the y - z plane. At most, a small percentage error will occur, which is in a direction to reduce previous differences.

Consequently, the following generalizations are made:

For 100% transmission $\left|y_{max}\right|_{\phi = 3\pi/4} \leq r_o$,

thus

$$\frac{r_o}{y_o} = \frac{r_o}{r_e} \geq \frac{2.672}{\beta_y f_1} \left| 0.595 \frac{r_o \gamma}{r_e} + \frac{f_2}{f_1} \right|_{\phi = \frac{3\pi}{4}}$$

where

$$\left(f_1\right)_{3\pi/4} = 0.763 \, , \quad \left(f_2\right)_{3\pi/4} = 0.238 \, .$$

Thus letting $\frac{r_o}{y_o} = \frac{r_o}{r_e}$ and evaluating (14) at $\theta = \frac{3\pi}{4}$ gives

$$\frac{r_o}{r_e} \geq \frac{1.09}{\beta_y} \left| 1 + 1.9 \left| \gamma \right| \frac{r_o}{r_e} \right|$$

or solving explicitly for $\frac{r_o}{r_e}$ in the limiting case:

$$\frac{r_o}{r_e} = \frac{1.09}{\beta_y - 2.07 \left|\gamma\right|_{max}} \tag{15}$$

This equation asks: What is the largest value of γ entering at any phase and for given β_y which will just reach r_o, the position of the rod.

Referring to Figure 2, the enterpretation is as follows: As the scan line passes through the stability diagram, β_y is at first very small.

Consequently only low angle ions contained in low values of $\gamma = \left(\frac{V_I}{V_{ac}}\right)^{\frac{1}{2}} \sin \alpha$ are transmitted within a given $\frac{r_o}{r_e}$ ratio. As β_y increases, larger angles are accepted and transmitted by the analyzer with consequent increase in collected current until one of two conditions become predominant. If, by some means, γ is limited, a region of 100% transmission occurs with a resultant constant collected current or "flat-topped" peak. If γ is unlimited the x stability takes over at a position where $\beta_y = 1-\beta_x$ and by the same mechanism ions are lost to the x poles as $\beta_x \longrightarrow 1$. In this condition, a pointed peak is produced.

While one could easily plot families of curves relating to specific values of $\frac{r_o}{r_e}$ and γ and match these to an ion source, this relationship can be obtained more explicitly. Therefore, we proceed to examine ion sources.

ION SOURCES

When reduced to their elements, most ion sources can be typified as focusing in one of two modes. Figure 3 shows the most common method wherein the source ion current is peaked up by producing the smallest line or point "image" and thus the highest density. However, it is noted that given some thermal distribution in the gas being ionized, those with higher side velocity are not transmitted. If only a specific side velocity $\pm\dot{y}_1^o$ is present such as encountered in satellite motion the line spectra are not transmitted at all.

An alternative mode of focusing is shown in Figure 3b where an image of the ion object is produced. In this case each position in the image correlates with a position in the object. Also, up to a limit determined by the lens aperture sizes, the position in the image is independent of initial energies of the ions. It is noted then that the distribution of initial energies lies in the angular distribution.

Since this mode of focusing is more appropriate for energetic particle measurements, we may proceed to describe the ion density more analytically. For a magnification, M the ion density at the image plane is $\frac{J_o^+}{M^2}$ for J_o^+ current per unit area produced is the ionizing beam. Thus the source current is

$$I_s^+ = \pi r_e^2 \frac{J_o^+}{M^2} \quad , \tag{16}$$

where r_e is the radius of a round aperture.

From Abbe's law[4], the bundle of rays produced within an included angle θ_o, at a point in the object plane, fall within an included angle θ_i at the image plane by the relationship;

$$y_o V_o^{\frac{1}{2}} \sin \theta_o = y_i V_i^{\frac{1}{2}} \sin \theta_i, \tag{17}$$

where eV_o is the initial ion energy and eV_i the total ion energy at the image plane.

Letting $\theta_o = \frac{\pi}{2}$ to include a worst case angle and since $\frac{y_i}{y_o} = M$,

$$\sin \theta_i = \left(\frac{V_o}{V_i}\right)^{\frac{1}{2}} \left(\frac{1}{M}\right) . \tag{18}$$

From (18), for a given value of $(V_o)_{max}$, we note that $\sin \theta_i$ can be kept within some upper limit acceptable for transmission by the analyzer by adjusting the magnification and thus from (16) the ion source current becomes established. If the value chosen for r_e is also sufficiently small for 100% transmission then the collected current for the mass spectrometer becomes,

$$I_c^+ = \pi r_e^2 \frac{J_o^+}{M^2} \tag{19}$$

Consequently for this mode of focusing we find that the measurement of partial density is, in principle, independent of initial conditions up to a maximum initial energy $(eV_o)_{max}$. It remains to establish r_e and $\sin \theta_I$ such that the maximum ion current is collected under the restraints of 100% transmission and limited initial energy.

Combining ((19) and (20) yields

$$I_c^+ = \pi r_e^2 \, J_o^+ \left(\frac{V_I}{V_o}\right)_{max} \sin^2 \alpha_I \qquad (20)$$

in which the injection voltage V_I is used for the image plane energy V_i, and the maximum injection angle α_I is substituted for θ_i. In Equation (20), M is an implicit variable used to limit $\sin^2 \alpha$ as $(V_o)_{max}$ is chosen. Since this equation contains r_e and $\sin \alpha$ it may be solved simultaneously with the quadrupole equation.

Combined Quadrupole and Ion Source

By substituting for γ in (15) and solving for $V_I \sin^2 \alpha_{max}$, one obtains

$$V_I \sin^2 \alpha_{max} = 0.233 \, V_{ac} \left(\beta_y - 1.09 \frac{r_e}{r_o}\right)^2, \qquad (21)$$

where α_{max} is the largest acceptable angle for given values of β_y and $\frac{r_e}{r_o}$.

Angles less than this will be transmitted. Further, one may conclude for given α_I and $\frac{r_e}{r_o}$ that the collectable current, I_c^+, reaches a peak when $\alpha_{max} = \alpha_I$ and remain constant when $\alpha_{max} > \alpha_I$

Substituting in (20),

$$I_c^+ = \frac{0.233 \, V_{ac} \, \pi r_e^2 \, J_o^+}{(V_o)_{max}} \left(\beta_y - 1.09 \frac{r_e}{r_o}\right)^2, \qquad (22)$$

where we note that $I_c^+ = o$ at $r_e = o$ and at $1.09 \frac{e}{r_o} = \beta_y$.

These conditions represent zero aperture and zero acceptable angle respectively. Zero angle in turn implies infinite manification and thus zero current density.

By differentiating for a maximum, one finds that α_I and $\frac{r_e}{r_o}$ contribute equally to the "beam width" when

$$\left(\frac{r_e}{r_o}\right)^2_{max} = 0.211 \ \beta_y^2 \tag{23}$$

and from (21)

$$V_I \sin^2 \alpha_{max} = 0.0583 \ V_{ac} \beta_y^2. \tag{24}$$

With reference to Figure 2, for "flat topped" peaks the ion current arrives at a maximum before the scan line reaches the $\beta_y = 1 - \beta_x$ intercept. If the base width, B, of the peak is defined to be that portion of the scan line within the stability diagram (i.e., the theoretical base width); and the top width, T, that portion lying between lines of $\beta_y = 1 - \beta_x$ (not at the intercept) and where the ion current is at its maximum value, then by calculation of the intercepts,

$$\left(\beta_y^2\right) = \left(1 - \beta_x\right)^2 = 0.164 \ \frac{dm}{m} \left(1 - \frac{T}{B}\right). \tag{25}$$

Equation (25) describes the β_y and β_x intercepts with the scan line which are required to produce the resolution $\frac{dm}{m}$ for a top to base ratio, $\frac{T}{B}$. Iso - $\frac{T}{B}$ lines may be constructed by inspection.

We now require that the ion current reach maximum value at the above β_y - scan line intercept. This consequently defines the values of $\left(\frac{r_e}{r_o}\right)$ and $\sin^2 \alpha_{max}$ for

maximum ion current as:

$$\left(\frac{r_e}{r_o}\right)^2_{max} = 0.0346 \frac{dm}{m}\left(1 - \frac{T}{B}\right) \tag{26}$$

and

$$V_I \sin^2 \alpha_{max} = 0.00955 V_{ac} \frac{dm}{m}\left(1 - \frac{T}{B}\right) \tag{27}$$

From (22), (23) and (26),

$$I_{c\,max}^{+} = 3.15 \times 10^{-4} \frac{V_{ac}}{(V_o)_{max}} \pi r_o^2 J_o^{+} \left(\frac{dm}{m}\right)^2 \left(1 - \frac{T}{B}\right)^2. \tag{28}$$

Throughout the T region then $I_{c\,max}^{+}$ is constant at this value since

$$\alpha_{max} > \alpha_I.$$

Thus, with given limits on the initial conditions and choice of the quadrupole parameters one may calculate the expected current of mass peaks meeting criteria of shape and resolution. The interesting result is that, for this mode of ion source focusing, the collected current is, in principle, a measure of partial density in the ionizing region independent of the initial energies up to $(V_o)_{max}$.

An instrument for atmospheric studies has been constructed along these lines having r_o = 7.5 mm, r_e = 0.25 mm and length ℓ = 22 cm. While the ion current exceeds that expected, an accurate confirmation of Equation (28) has not been made. This is partially due to the difficulty of obtaining a rectangular energy distribution and partially as discussed later to a method of biasing the quadrupole rods.

A check on Equation (27) was made however, to determine the validity of injection angle versus resolution and $\frac{T}{B}$ ratio. Figure 4 shows two partial spectra typical

of those used to calculate the apparent injection angle, given measurements for the other variables. V_{ac} was the independent variable while $\frac{T}{B}$ was the primary dependent variable. The theoretical base width was used (i.e., without tails) measured by extending the peak sides. Figure 5 gives the apparent angle vs V_{ac} where the inset shows the directly measured angular distribution. The apparent angle is approximately constant over the range of V_{ac} however, with the density distribution less than the measured angle by a factor of ~ 1.5. This contraction in apparent angle is believed to be due to the effect of quadrupole biasing.

Quadrupole Biasing

The length of the quadrupole rods is required to have a certain minimum value which depends upon the values of several parameters. von Zahn[5] stated this relationship in the simple form:

$$n \geq 3.5 \sqrt{\frac{m}{\Delta m}} \tag{29}$$

where n = number of cycles of the r.f. voltage which occur while the ion is in the quadrupole field. This equation implies that if a half height resolution of $\frac{m}{\Delta m}$ is required then n cycles must occur in order that the peak tails do not make an appreciable contribution to the width of the peak. By relating n to the axial ion energy, V_z, and using the quadrupole equation one obtains:

$$\frac{\ell}{r_o} = K \sqrt{\frac{13.9\ V_z}{V_{ac}}\ \frac{\Delta m}{m}} \tag{30}$$

where ℓ is the length of the quadrupole rods, and K is a constant which depends upon the exact criterion used to measure the resolution and the contribution of the tails to the peak base width. If von Zahn's criterion is used, $K = 3.5$. For one percent peak height resolution $K \approx 7$.

In normal quadrupole operation the ion source injection voltage is equal to the axial kinetic energy of the ions in the quadrupole, i.e., $V_I = V_z$. When an ion source is required to capture and focus energetic particles which have an

appreciable angle of incidence, the injection voltage, V_I, must be large. This implies that the length of the quadrupole rods will be excessive. It was found, however, that by placing a bias voltage V_B between the ion source and the quadrupole rods the mass spectrometer may be successfully operated in a mode where:

$$V_z = V_I - V_B \tag{31}$$

A schematic representation of this technique, along with an approximate axial potential distribution, is shown in Figure 6. The effect of the quadrupole bias voltage is shown in Figure 7. As the bias voltage is raised the peak tails are diminished. There is no observable decrease in sensitivity as V_B is increased until the point at which the injection energy of the least energetic ions is exceeded in which case they are cut off. Even though the reduction in the size of the tails is not considered, the $\frac{T}{B}$ ratio apparently improves as the bias is applied. This may indicate that the field around the entrance nozzle is causing a contraction of the effective angle of injection.

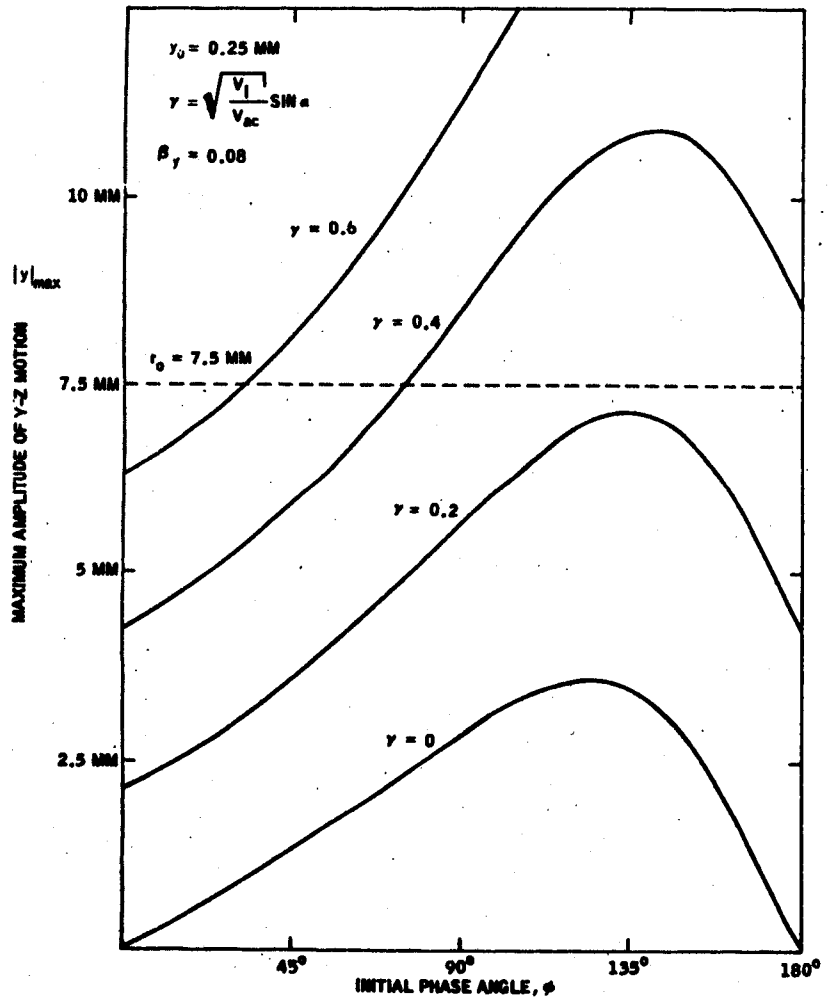
y_0 = 0.25 MM
$\gamma = \sqrt{\frac{V_1}{V_{ac}}} \sin\alpha$
β_y = 0.08
10 MM
7.5 MM
5 MM
2.5 MM
$|y|_{max}$
MAXIMUM AMPLITUDE OF Y-Z MOTION
γ = 0.6
γ = 0.4
γ = 0.2
γ = 0
r_0 = 7.5 MM
45°
90°
135°
180°
INITIAL PHASE ANGLE, ϕ

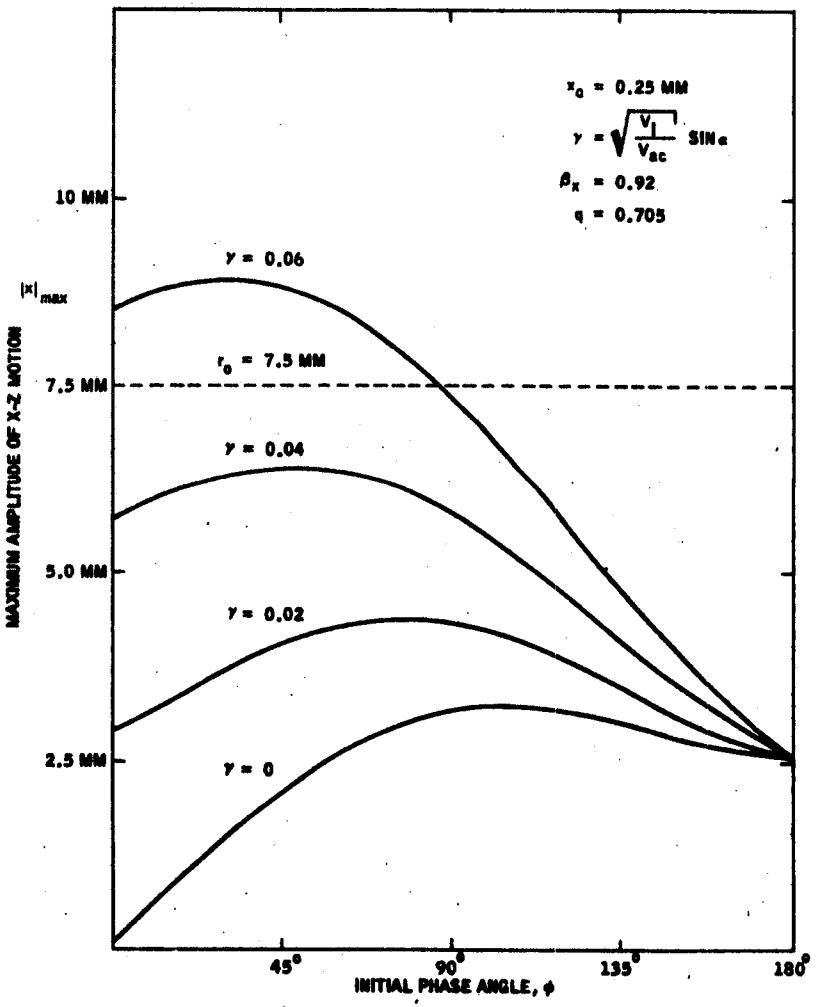
x_0 = 0.25 MM
$\gamma = \sqrt{\frac{V_1}{V_{ac}}} \sin\alpha$
β_x = 0.92
q = 0.705
10 MM
7.5 MM
5.0 MM
2.5 MM
$|x|_{max}$
MAXIMUM AMPLITUDE OF X-Z MOTION
γ = 0.06
γ = 0.04
γ = 0.02
γ = 0
r_0 = 7.5 MM
45°
90°
135°
180°
INITIAL PHASE ANGLE, ϕ

FIGURE 1

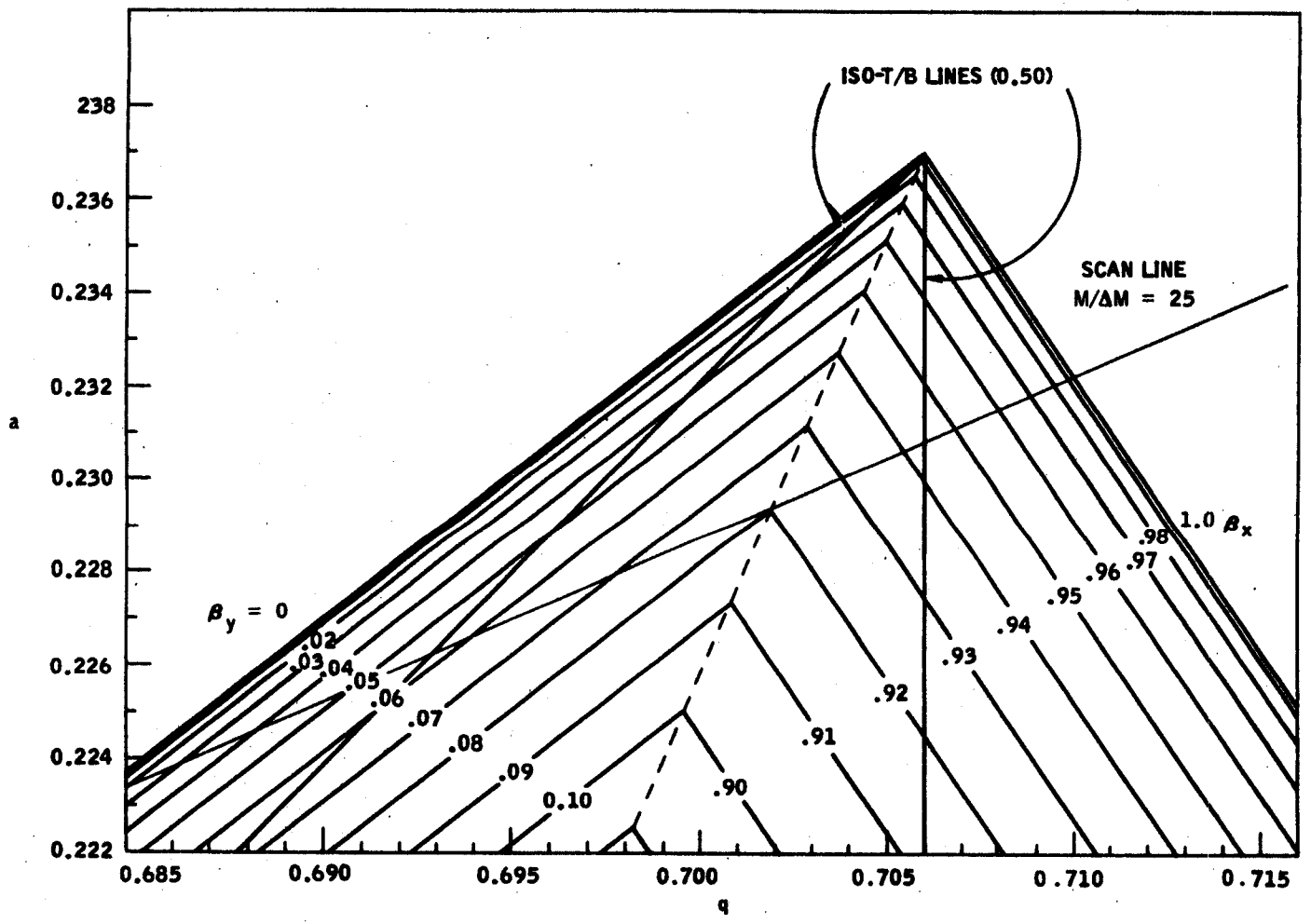
ISO-T/B LINES (0.50)
SCAN LINE
M/ΔM = 25
1.0 β_x
β_y = 0
.02
.03
.04
.05
.06
.07
.08
.09
0.10
.90
.91
.92
.93
.94
.95
.96
.97
.98
238
0.236
0.234
0.232
0.230
0.228
0.226
0.224
0.222
a
0.685
0.690
0.695
0.700
0.705
0.710
0.715
q

FIGURE 2

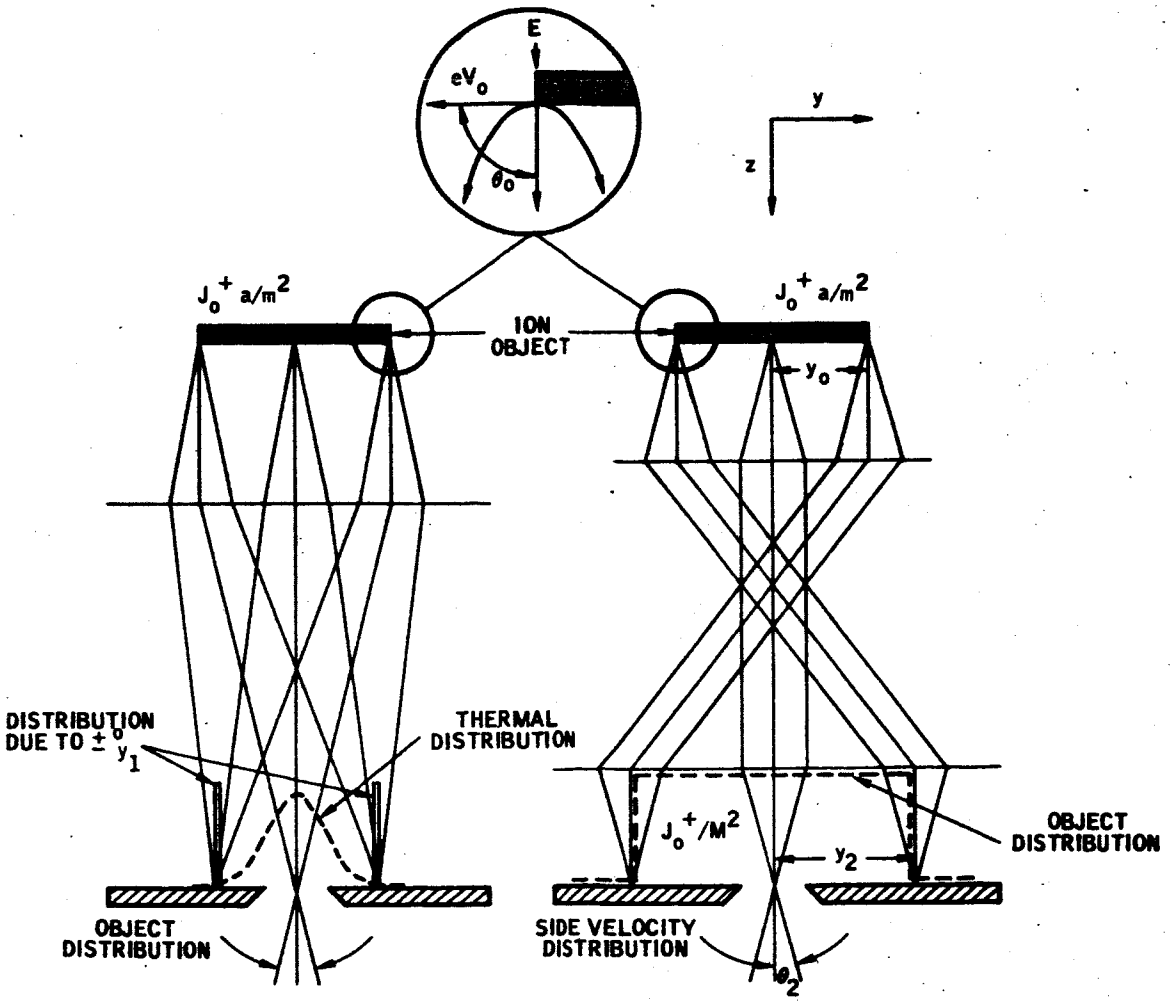

(a) THERMAL IMAGING SOURCE

(b) OBJECT IMAGING SOURCE

FIGURE 3

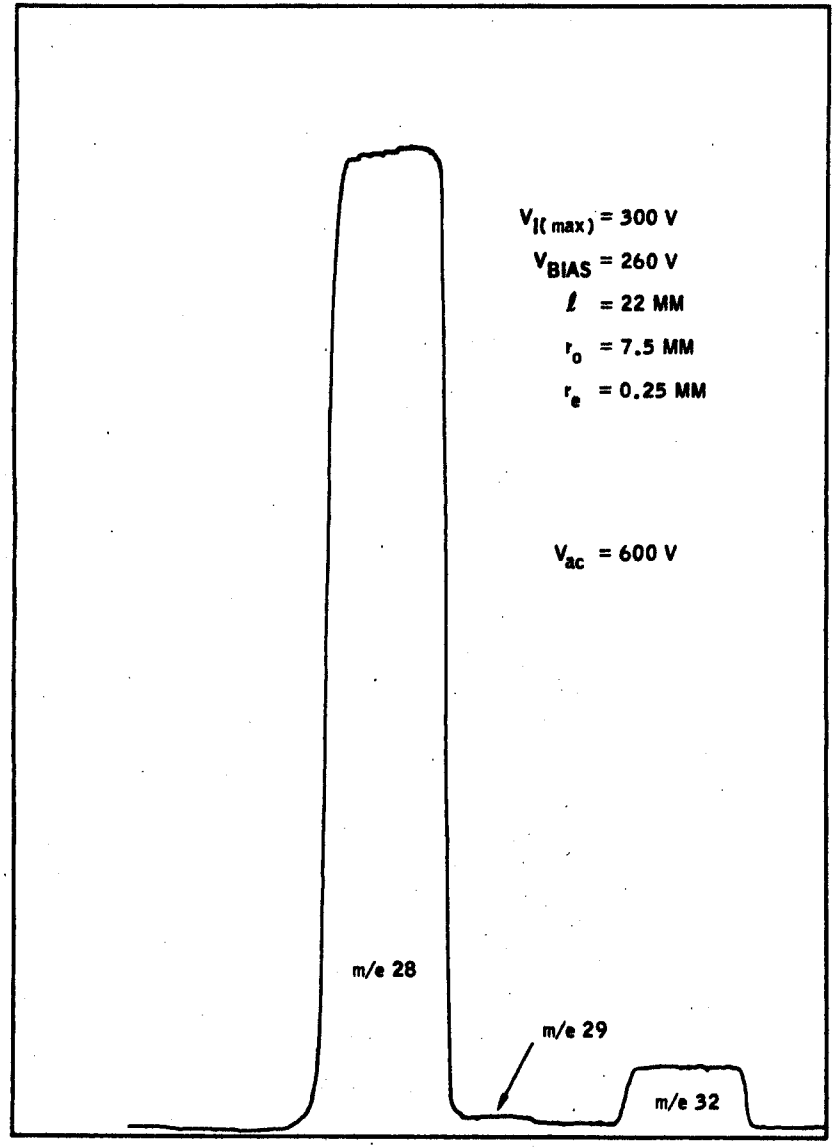
$V_{I(max)}$ = 300 V
V_{BIAS} = 260 V
ℓ = 22 MM
r_o = 7.5 MM
r_e = 0.25 MM
V_{ac} = 600 V
m/e 28
m/e 29
m/e 32

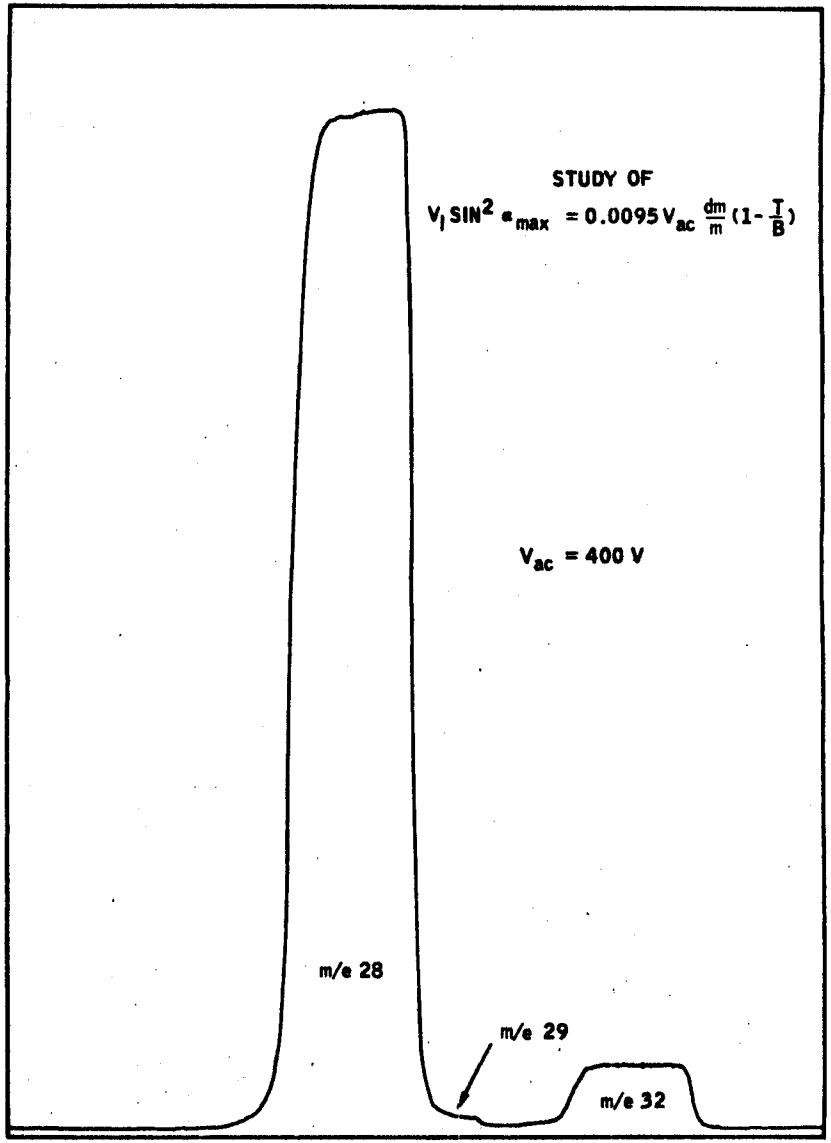
STUDY OF
$V_I \sin^2 \alpha_{max} = 0.0095 V_{ac} \frac{dm}{m} (1 - \frac{I}{B})$
V_{ac} = 400 V
m/e 28
m/e 29
m/e 32

FIGURE 4

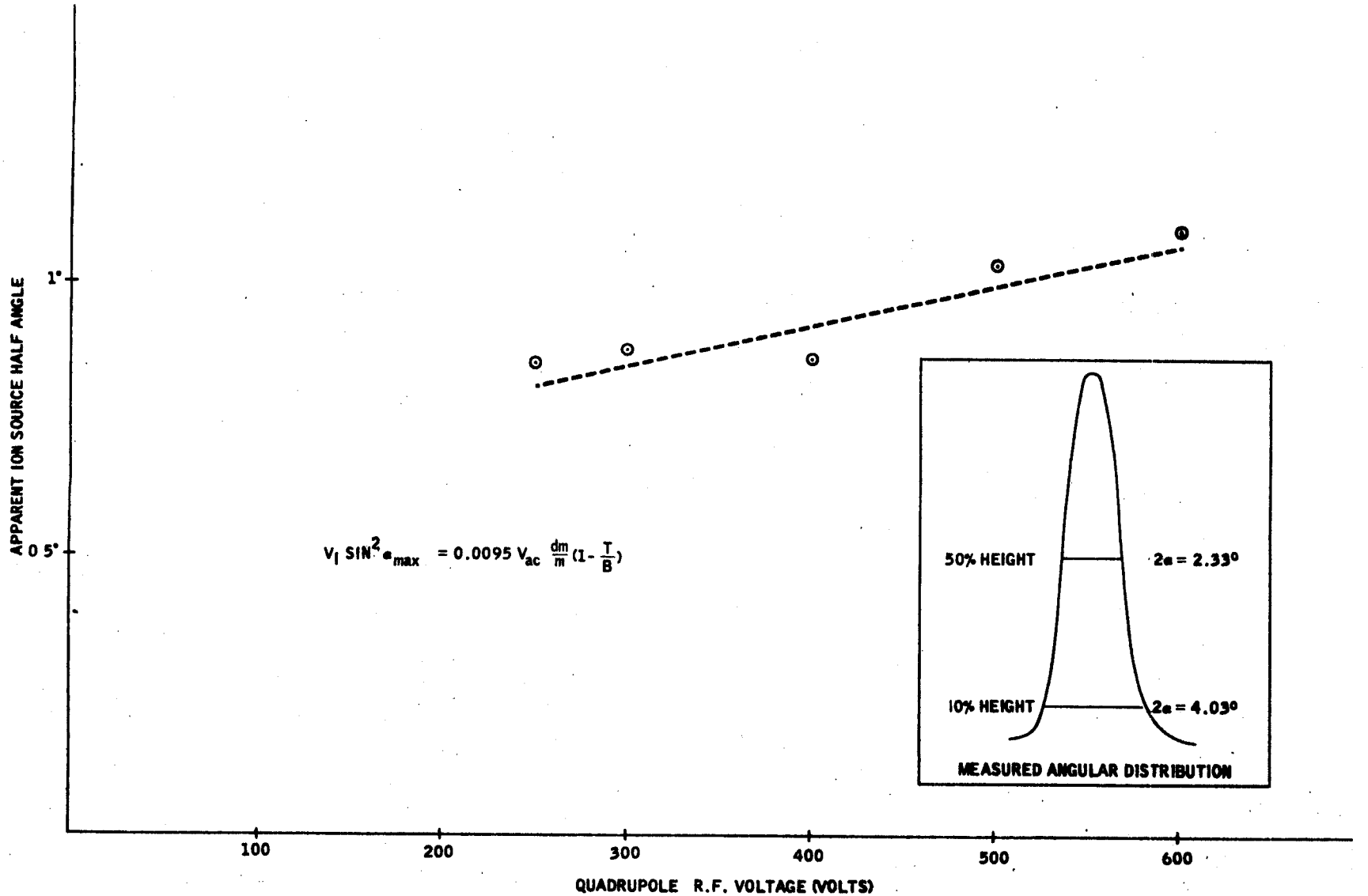
APPARENT ION SOURCE HALF ANGLE
1°
0.5°
$V_I \sin^2 \theta_{max} = 0.0095 V_{ac} \frac{dm}{m}(1 - \frac{T}{B})$
50% HEIGHT
2α = 2.33°
10% HEIGHT
2α = 4.03°
MEASURED ANGULAR DISTRIBUTION
100
200
300
400
500
600
QUADRUPOLE R.F. VOLTAGE (VOLTS)

FIGURE 5

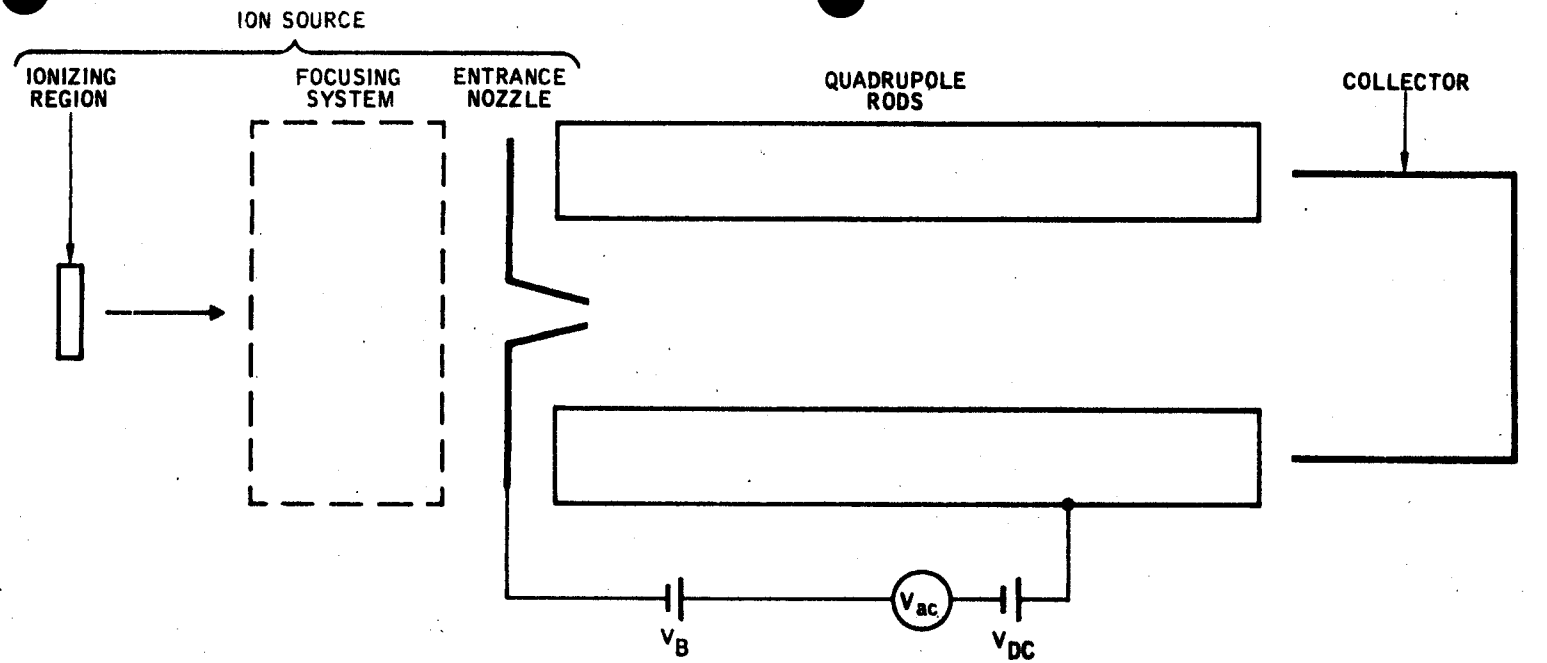

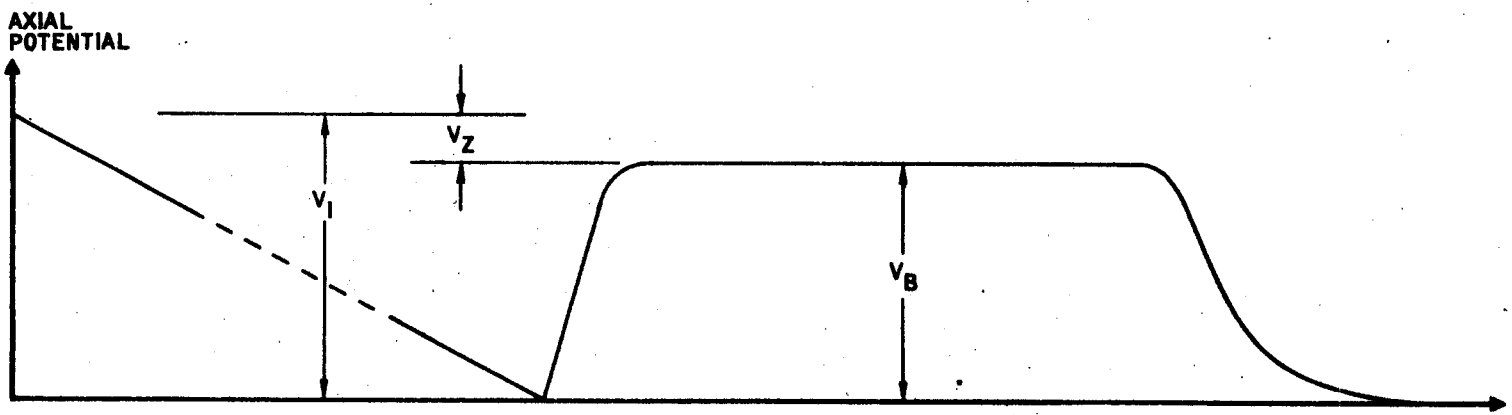

QUADRUPOLE MASS SPECTROMETER SCHEMATIC AND AXIAL POTENTIAL DISTRIBUTION.

FIGURE 6

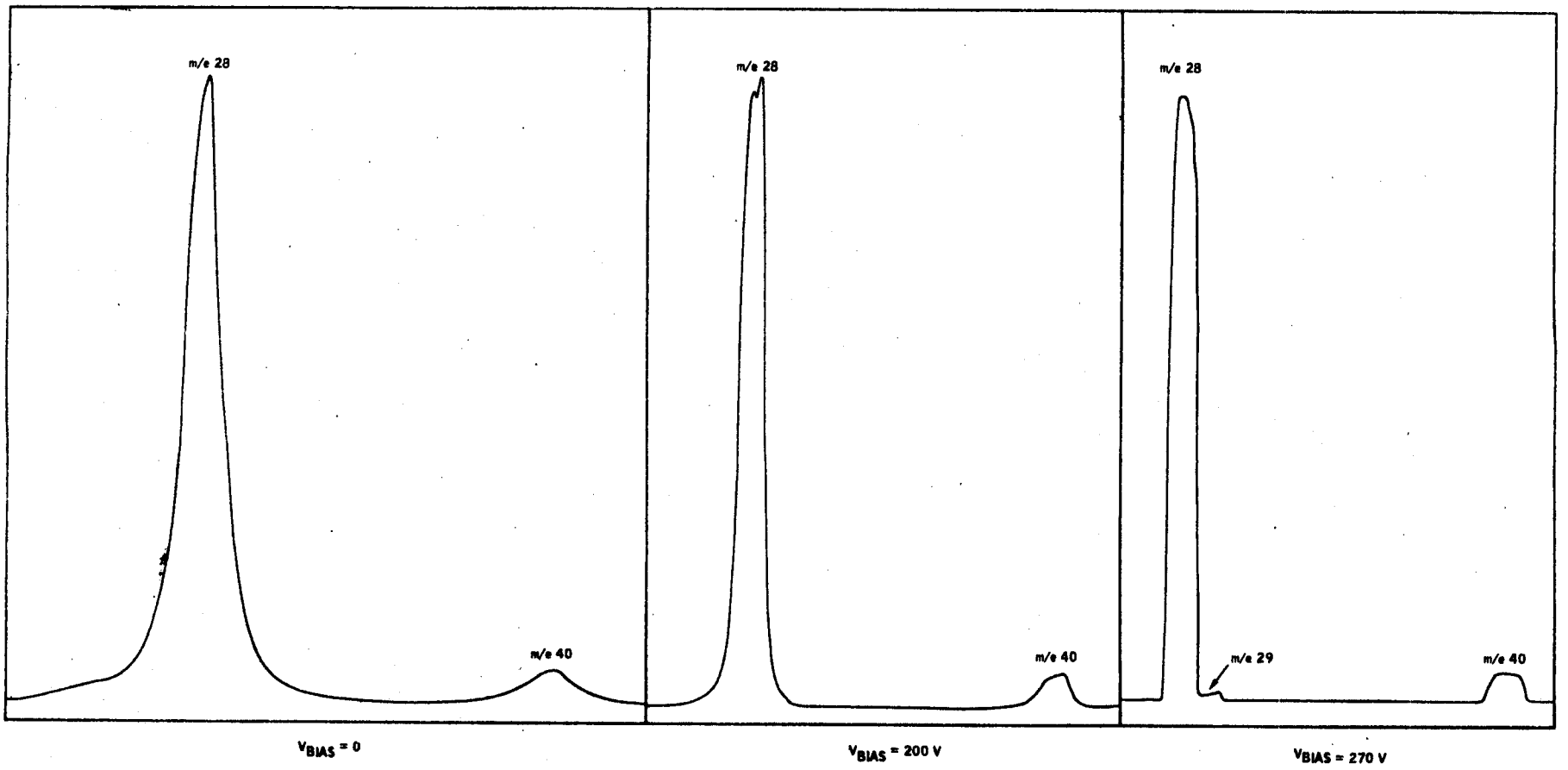

EFFECT OF THE QUADRUPOLE BIAS VOLTAGE ON PEAK TAILS

ℓ = 22 CM, r_o = 7.5 MM, $V_{I_{max}}$ = 300 V, AND V_{ac} = 400 V.

FIGURE 7

REFERENCES

1. W. Paul, H. P. Reinhard and V. von Zahn; Z. Physik 152, 143 (1958).

2. W. M. Brubaker; Neuvieme Colloq. Spectroscopicum Intern., Lyon, France, 1961.

3. Reference 1, Fig. 4.

4. c.f.: Klemperer; Electron Optics, Cambridge University Press, 1953, p 14.

5. U. v. Zahn: Diplomarbeit Bonn, 1956 (unpublished).

*Appendices in preparation.

APPENDIX E

Electronic Reliability Analysis

FOREWORD

This report is grouped into two separate yet mutually inclusive areas.

The first deals with the projection of a goal (.90) for the equipment; thence assessing the design to determine the failures (unreliability) to be expected using selected components during the complete 2880 hour mission. Thus, a standard is used (the projected goal) against which the present conceptual design is evaluated. As part of the above components of known reliability were used to evaluate the drawings presented.

The second part shows the specific requirements necessary in a program of this nature, with respect to specifications, specification control drawings and selection of manufacturers. In this second part, specific examples are given, with respect to components, their electrical characteristics and preferred manufacturer.

Part I

Reliability Analysis

1.0 Purpose

The purpose of this assessment is: (1) to apportion among the various subsystems and components a projected 0.90 spectrometer system reliability goal, and (2) assess the design to determine whether or not individual subsystems or components meet their apportioned goals.

2.0 Logic Diagram

The logic diagrams shown in Figures 1, 2, 3, and 4 represent the reliability equation of the spectrometer system. The logic diagram is based on the following assumptions and restrictions:

- Each functional subsystem or component must function in order that the system function, i.e., the subsystems are functionally dependent. A failure of any functional component or subsystem will cause failure of the system.

- The reliability of the system is based on the exponential distribution: $R = e^{-\lambda t}$

where R = Reliability of the system, subsystem, or component.

λ = The failure rate of the system, subsystem, or component expressed in failures per hour.

t = The time in hours that the system, subsystem, or component must function, i.e., the mission time.

a. The turn-on switches and malfunction sensors were assigned a numerical reliability goal of 0.99999 on the fact that the items are furnished by NASA and detailed knowledge is gained with respect to each of these components the numerical goal may have to be revised. As a result of this revision the reliability goals of the remaining subsystems and components would also have to be revised.

b. The reliability goal of the SDS subsystems (R_CP through R_C, (R_{CP-C}) was derived as follows:

$$Rs = (R_{CP-C})$$

$$0.90 = R_{CP-C}$$

c. The reliability goal of 0.90 was apportioned among the various SDS subsystems as shown in Table 1.

d. The subsystem reliabilities shown in the last column, when combined, approximate the 0.9 goal, i.e.,

$$R_{CP}XR_AX\ R_BX\ R_C$$

$$\geq .86$$

Substituting the subsystem reliabilities back into the reliability equation (logic diagram) the system reliability goal of 0.9 is nearly achieved as shown in Figures 1, 2, 3, and 4, as well as Table I.

e = The base of natural logarithms.

- The mission time of the system is four months (2880 hours).
- The reliability goal of the system is 0.90.
- The logic diagram represents the reliability equation (mathematical model) of the system, not the system functional block diagram.

3.0 Apportionment

The logic diagrams shown in Figures 1, 2, 3, and 4 are based on the knowledge of how the system functions from a reliability viewpoint. The attempt made to determine a present state-of-the-art numerical reliability values (reliability estimate) was based upon sources shown in Section 4.0. Although at this time the internal system temperatures are unknown, the estimates are based upon only a 50% stress level. Therefore, the apportionment, the subject of this section, only apportions the numerical reliability goal of 0.90 among the various subsystems on a part count and engineering judgment basis, not on a detailed stress analysis basis. A detailed apportionment based on a calculated stress will be performed if deemed necessary.

3.1 Apportionment Procedure

The reliability goal of the spectrometer is 0.90. This goal is apportioned among the various subsystems according to the logic diagram by the following sequence:

4.0 Reliability Estimate

Based upon FARADA, PRINCE and IDEP data, the reliability goal of .90 is virtually assured , if careful care is given to adequate component specification, purchasing, handling, and maintenance procedures.

5.0 Recommended specifications control, qualified vendors, and a few components are shown in this section, which has been published as a separate document.

TABLE I

RELIABILITY APPORTIONMENT

SUBSYSTEM	ASSESSED UNRELIABILITY BASED UPON PART COUNT, STRESS LEVEL AND USAGE	APPORTIONED SUBSYSTEM RELIABILITY GOAL	RELIABILITY DESIGN ASSESSMENT
1. Common multivation, bridge, and regulator	.0179	.989	.982
2. Filament Leg	.064	.967	.952
3. Analyzer Leg	.056	.970	.962
4. Detector	.067	.965	.950

The subsystem reliabilities shown in the last column when combined approximate the 0.90 goal*, i.e.,

$$R_{CP} X R_A X R_B X R_C \backsim 0.86$$

*Due to small errors in interpolation of the exponential tables, the reliability values when multiplied do not exactly equal .90.

Part II

Preferred Parts, their Specification and Selection, with preferred manufactures

SDS

Reliability Preferred Parts, Specification - Guided Lines and Specifications

SECTION I

PART SPECIFICATION GUIDELINES

1. Procurement Specifications

1.1 Procurement specifications including appropriate mechanical, electrical, and environmental requirements, quality assurance provisions, failure rate verification requirements, identification and traceability requirements, packing and packaging requirements, and notes shall be written for each electronic and electro-mechanical part used in airborne equipment, except where specifications are in existence for identical parts as a result of prior usage.

1.2 Part specifications may be of one type: The Specification Control Drawings (SCD).

2. Applicable Documents

NASA 200-1

200-2

200-3

200-4

250-1

3. Definitions

3.1 Specification Control Drawings

A Specification Control Drawing (SCD) shall exist, or be written, for each part, or for each group of similar parts, specifying individual part requirements.

1. Scope
2. Applicable Documents
3. Requirements

3.1 Mechanical Requirements

4. Specification Requirements

4.1 Requirements which should be contained in the "Specification Control Drawings" are specified herein.

4.2 Traceability - Where traceability is required, the part specification shall require the part manufacturer to maintain adequate records to identify all of the types of materials, types of piece parts, and types of processes utilized in the production of the end item and such other traceability requirements appropriate to the part as detailed in SDS Specifications.

4.3 Radiographic Inspection - As appropriate, part specifications for parts, not encased in transparent materials (glass), shall include requirements for radiographic inspection (X-Ray) under "Mechanical Requirements." Details of the Radiographic Inspection information to be included in the specification are available from SDS upon request.

4.4 Environmental - As a minimum, each part specification shall require that the parts conform to the specification requirements during and following exposure to the environmental conditions compatible with the applicable subsystem requirements.

4.5 Life - In general, life test requirements shall be for 1000 hours. Appropriate measurements shall be required at 100, 250, 500, and 1000 hours. Appropriate modifications to the life test requirements shall be made for mechanical and electromechanical parts and for parts whose maximum usage dissipation is extremely low, such as, low level filters with inputs of 100 milliwatts or less.

4.6 Qualification Inspection - Qualification test requirements shall be contained in the specification.

4.6.1 It is recommended that contents and sequence of qualification testing requirements of the various groups and subgroups be consistent between specifications, regardless of part category, with the notation "N/A" where a test is not applicable to a given part or part category. If screening is to apply prior to qualification testing, it shall be specified.

4.6.2 The total number of samples and allowable number of defective samples for each test shall be subject to review by SDS at the time the specification is submitted.

4.7 Lot Acceptance Inspection - Acceptance inspection shall consist of (1) screening and (2) acceptance tests and shall be conducted on each production lot. Screening tests shall be designed such that potential early failures are removed and parameters of the remaining units stabilized by the screening process. Screening tests are defined as tests wherein all deliverable parts are exposed to an environment or environments that are selected as critical to the particular part category, such as, temperature cycling, high temperature operation, or vibration, etc. Screening tests shall not be designed to overstress parts beyond specification limits such that accumulated stress history would jeopardize the usage of the parts in the subsystem equipments. It is recommended that, where practicable, an allowable percentage of defective parts in excess of this percentage being cause for rejection of the lot.

4.7.1 For consistency of specification format, the following presentation of requirements is recommended. Acceptance tests consist of Groups A, B, and C inspection. Group A inspection consists of 100% electrical tests of critical parameters. These may include measurements used as final measurements during screening although these tests need not be repeated if no significant time delay exists between final screening measurements and initiation of Group A inspection.

4.7.2 Group B inspection consists of additional electrical tests to be performed on a random sampling basis. If no additional electrical tests are required, the notation "N/A" is used for Group B inspection. Group C inspection consists of subgroups for

4.7.2 various environmental and mechanical tests and life testing to be performed on a random sampling basis. The subgroupings should be consistent between parts and part categories with the use of the notation "N/A" made, as appropriate. Surviving units from Groups A and B testing can be delivered, but units subjected to Group C testing cannot be delivered. Semiconductors which have been subjected to screening and no more than 1000 hours operating life are also considered deliverable.

4.7.3 Number of samples and allowable number of defective parts for each test shall be subject to review by SDS at the time the part specification is submitted.

4.8 Failure Rate Verification - Part specifications shall require that the failure rate of parts covered shall not exceed a given failure rate level. The specification shall also state the degree of confidence to which the failure rate has been established. Terms such as "failure rate goal" or "failure rate objective" shall not be used unless they are accompanied by some information such as date, indicating when such a "goal" or "objective" is to be reached. Details regarding the methods to be used to incorporate failure rate verification into the specifications are given in SDS SCD's.

4.9 Failure Reporting, Analysis, and Corrective Action - The specification shall require the manufacturer to report part failures in qualification testing and acceptance testing to the subcontractor/supplier and to subsequently submit a report of failure analysis and proposed corrective action to the subcontractor/supplier. The subcontractor/supplier shall, in turn, submit these reports to SDS.

4.10 Documentation - Part specifications shall require that an acceptance inspection procedure be submitted and approved by the subcontractor/supplier prior to initiation of acceptance inspection. Part specifications shall also require that each shipment of parts be accompanied by screening test data (variables data recordings) identifiable to the lot from which shipment was made. The Acceptance Test Summary (if a summary is submitted) shall contain, but shall not be limited to, the following:

1. Test performed
2. Specified limit or tolerance
3. Number tested
4. Number failed
5. Range of readings

The part manufacturer shall also be required to maintain screening and acceptance test data on file.

4.10.1 When part qualification tests are required, part specifications shall require that a qualification test procedure be submitted and approved prior to initiation of qualification and that a final report, including a summary of results and all test data, be submitted upon completion of qualification testing.

4.11 Preparation for Delivery - Part specifications shall include a requirements for adequate packing and packaging by referencing an appropriate military or industry packing and packaging specification, or by detailing the vendor's proposed packing and packaging when such has been determined to be satisfactory.

4.12 Notes - Notes shall include information and requirements which are pertinent to the part use, manufacture, and testing, but which do

4.12 not logically appear elsewhere on the specification. Minimum required information shall be as follows:

1. Design and process change approval requirements.
2. A statement of caution to avoid physical damage, particularly to plating of leads or terminals, resulting from the abnormal amount of handling necessary for high reliability processing such as repeated insertions and withdrawals from test fixtures.

The following list represents MIL-specifications acceptable to SDS categorized by part types. Generally, parts that are purchased to meet the requirements of these military specifications will conform with the Quality Assurance and Reliability requirements of SDS. The latest issue of the specification shall be used. This listing does not, however, preclude the subcontractor/supplier's selection of parts covered by other military specification providing the Quality Assurance and Reliability criteria established by the definitions of SDS are fulfilled.

PART TYPE	MILITARY SPECIFICATION NO.	NOMENCLATURE
Capacitor	MIL-C-5	Mica
Capacitor	MIL-C-20	Ceramic - Temperature conpensating
Capacitor	MIL-C-25	Paper - DC, hermetically sealed in metallic case
Capacitor	MIL-C-3965	Tantalum - foil or wet slug
Capacitor	MIL-C-11015	Ceramic - general purpose
Capacitor	MIL-C-11272	Glass
Capacitor	MIL-C-11693	Feedthrough capacitors, radio interference reduction, hermetically sealed in metallic case
Capacitor	MIL-C-14157	Paper/Plastic, hermetic sealed, metallic case, Established Reliability
Capacitor	MIL-C-18312	Metalized paper or Mylar, hermetically sealed in metallic case
Capacitor	MIL-C-19978	Plastic or paper plastic, hermetically sealed in metallic case
Capacitor	MIL-C-23269	Glass - Established Reliability
Capacitor	MIL-C-26655	Solid tantalum
Capacitor	MIL-C-27287(USAF)	Plastic DC, non-metallic case (film wrap)
Capacitor	MIL-C-39001	Mica - Established Reliability
Capacitor	MIL-C-39003	Tantalum, Solid-Electrolyte, Established Reliability

PART TYPE	MILITARY SPECIFICATION NO.	NOMENCLATURE
Capacitor	MIL-C-39006	Tantalum Nonsolid Electrolyte, (foil and slug) Established Reliability
Capacitor	MIL-C-39011	Feedthrough, R F reduction, AC and DC, Hermetically sealed in metallic case Established Reliability
Capacitor	MIL-C-39014	Ceramic, fixed, general purpose, Established Reliability
Capacitor	MIL-C-39022	Metallized paper, (or polyester film) dielectric, DC, hermetically sealed in metal cases. Established Reliability
Coil	MIL-C-15305	Radio Frequency
Connector	NAS 1599	Cylindrical, signal, high temperature
Fuse	MIL-F-23419	Instrument, miniature
Potentiometer	MIL-R-27208	WW Trimmer
Potentiometer	MIL-R-39015	WW Trimmer, Established Reliability
Potentiometer	MIL-R-22097	Non WW Trimmer
Potentiometer	MIL-R-19	WW Low Temperature
Potentiometer	MIL-R-12934	WW Precision
Relay	MIL-R-39016	Relays, Electromagnetic Established Reliability
Relay	MIL-R-5757	Control, Miniature
Relay	MIL-R-6106	Power Control Miniature
Resistor	MIL-R-55182	Resistors, Fixed Film, Established Reliability

PART TYPE	MILITARY SPECIFICATION NO.	NOMENCLATURE
Resistor	MIL-R-10509	Film
Resistor	MIL-R-39005	Resistors, Fixed, WW (Accurate) Established Reliability
Resistor	MIL-R-39007	Resistors, Fixed, WW, (power type) Established Reliability
Resistor	MIL-R-39008	Resistors, Fixed, Composition (insulated) Established Reliability
Semiconductor	MIL-STD-750	- - - -
Switch	MIL-S-8805	Pushbutton
Switch	MIL-S-8834	Toggle
Switch	MIL-S-3786	Rotary
Transformer	MIL-T-27	Audio, Power, and Pulse
Transformer	MIL-T-21038	Pulse, Power, Low

SECTION II

RELIABILITY PREFERRED

PARTS

SDS RELIABILITY PREFERRED PARTS

TRANSISTORS

PART TYPE POLARITY MATERIAL	PART NUMBER	SUPPLIER	POWER, WATTS		BV_{CBO}	BV_{CBO}	BV_{EBO}	$R_{sat.}$	I_C	f_t	HFE at		$\frac{VCF}{I_C}$	C_{ob}	NF	t_{on}	t_{off}
			25°C AMB	25°C CASE	V_{dc}	V_{dc}	V_{dc}	Ohms Max.	Max.	mc Min.	Min.	Max.		pf	db	nsec	nsec
General																	
NPN - Silicon	2N1893	Raytheon	0.8	3.0	120	80	7	10	500mA	60	40	120	$\frac{10V}{150mA}$	18	12		
PNP - Silicon	2N1132	Motorola	0.6	2.0	50	35	5	10	500mA	40	35	110	$\frac{10V}{10mA}$	40	20		
Switching																	
NPN - Silicon	2N2369A	Fairchild Semi-Conductor	0.36	1.2	40	15	4.5	10	200mA	500	40	120	$\frac{1V}{10mA}$	4		12	18
PNP - Silicon	2N2907A	Motorola	0.4	1.8	60	60	5	3	500mA	200	100	300	$\frac{10V}{150mA}$	8		45	200
Low Level																	
NPN - Silicon	2N2484	Fairchild Semi-Conductor	0.36	1.2	60	60	6	350	50mA	60	100	500	$\frac{5V}{10\mu A}$	6	2		
PNP - Silicon	2N3251A	Motorola	0.36	1.2	60	60	6	25	200mA	300	100	300	$\frac{1V}{10mA}$	6	6		
Power																	
NPN - Silicon	2N1724	Texas Instruments	3.0	50	-	80	10	1.0	5A	10	20	90	$\frac{15V}{2A}$	550			
PNP - Germanium	2N1358A	Texas Instruments	-	20	80	60	60	0.1	15A	0.005	25	50	$\frac{2V}{2A}$	-			

SDS RELIABILITY PREFERRED PARTS

RESISTORS, FIXED

PART TYPE	PART NUMBER	SUPPLIER	POWER-WATTS		RANGE-OHMS		TOL	VOLTS	TC	REMARKS
			25°C	125°C	FROM	TO	± %	MAX	PPM	
CARBON FILM (SEALED)	C-1H	Mepco	1/10*		10.0 Ω	301 K	1.0	200	-500	These resistors are recommended for use where good stability is required and where relatively large temperature coefficients can be tolerated. All have established failure rates.
	C-170N	Mepco	1/8 *		5.11 Ω	1.00M	1.0	250	-500	
	C-173C	Mepco	1/4 *		10.0 Ω	2.00M	1.0	300	-500	
* Ambient = 70°C	C-173BN	Mepco	1/2 *		10.0 Ω	4.99M	1.0	350	-500	
	C-177AN	Mepco	1.0 *		10.0 Ω	10.0M	1.0	500	-500	
	C-177BN	Mepco	2.0 *		30.1 Ω	20.0M	1.0	750	-500	
METAL FILM (MOLDED OR CONFORMALLY COATED)	MF4	Electra Mfg Co		1/10	30.1 Ω	301 K	1.0	200	± 25	These resistors are recommended for use where good stability and relatively low temperature coefficients are required. All have established failure rates.
	MF5	Electra Mfg Co		1/8	30.1 Ω	499 K	1.0	250	± 25	
	MF6	Electra Mfg Co		1/4	51.1 Ω	1.00M	1.0	300	± 25	
	MF7	Electra Mfg Co		1/2	51.1 Ω	1.50M	1.0	350	± 25	
	MF8	Electra Mfg Co		1.0	51.1 Ω	2.00M	1.0	500	± 25	
	MF9	Electra Mfg Co		2.0	100 Ω	5.11M	1.0	750	± 25	
METAL FILM (SEALED) * Ceramic Cased ** Glass Cased	SHRM 1/8	Electra Mfg Co		1/8	10.0 Ω	301 K	1.0	100	± 50	See comments for "METAL FILM (MOLDED OR CONFORMALLY COATED) except for temp. coefficient
	XLT **	International Resistance Corp		1/8	10.0 Ω	200 K	1.0	100	± 100	

SDS RALIABILITY PREFERRED PARTS

DIODES, COMPUTER & RECTIFIER TYPES

PART TYPE	COM'L NUMBER	SUPPLIER	P_{IV}	I_F		I_R		REMARKS
			VOLTS	AMPS	VOLTS	μAMPS	VOLTS	
SWITCHED (Glass)	1N3064	Fairchild Semiconductors	50	0.20	1.0	0.10	50	Trr = 4 nsec , C = 4 pf
GENERAL (Glass)	1N645	TRW Semi-Conductor, Inc	225	0.40	1.0	0.025	225	
PURPOSE								
(Glass)	1N3549	General Electric	600	0.60	1.0	0.200	600	
(Ceramic)	1N3868	SEMTECH, Inc	600	1.00	1.1	0.100	600	
RECTIFIER								
STUD (10-32)	1N1204B	General Electric	400	10.0	1.0	50.0	400	-0001 is reverse polarity
(1/4-28)	1N2158	General Electric	400	25.0	1.0	1.0mA	400	-0001 is reverse polarity

SDS RELIABILITY PREFERRED PARTS

RESISTORS, FIXED

PART TYPE	PART NUMBER	SUPPLIER	POWER-WATTS 25°C	POWER-WATTS 125°C	RANGE-OHMS FROM	RANGE-OHMS TO	TOL ± %	VOLTS MAX	TC PPM	REMARKS
POWER WIREWOUND	RS-2A	Dale Electronics Inc	2.0		0.10	39.2 K	1.0	100	± 20	These resistors are reoommended for use where stability is required and where relatively high "hot" spot" temperatures (in the order of +275°C can be tolerated. All level "PP-1" parts have established f failure rates.
* Chassis Mounted	RS-5	Dale Electronics Inc	5.0		0.10	75.0 K	1.0	250	± 20	
	RS-10	Dale Electronics Inc	10.0		0.10	237 K	1.0	650	± 20	
	HG-10*	Dale Electronics Inc	10.0		1.00	5.62 K	1.0	250	± 20	
	HG-25*	Dale Electronics Inc	25.0		1.00	12.4 K	1.0	450	± 20	
	HG-50*	Dale Electronics Inc	50.0		1.00	39.2 K	1.0	1100	± 20	
	MRS-1/2	Dale Electronics Inc	1/2		1.00	4.42 K	1.0	20	± 20	
	G-1	Dale Electronics Inc	1.0		1.00	2.94 K	1.0	25	± 20	
	G-2	Dale Electronics Inc	1.5		1.00	4.42 K	1.0	35	± 20	
	G-5	Dale Electronics Inc	4.0		0.10	20.0 K	1.0	112	± 20	

LOGIC DIAGRAM TO FILAMENT AND ANODE

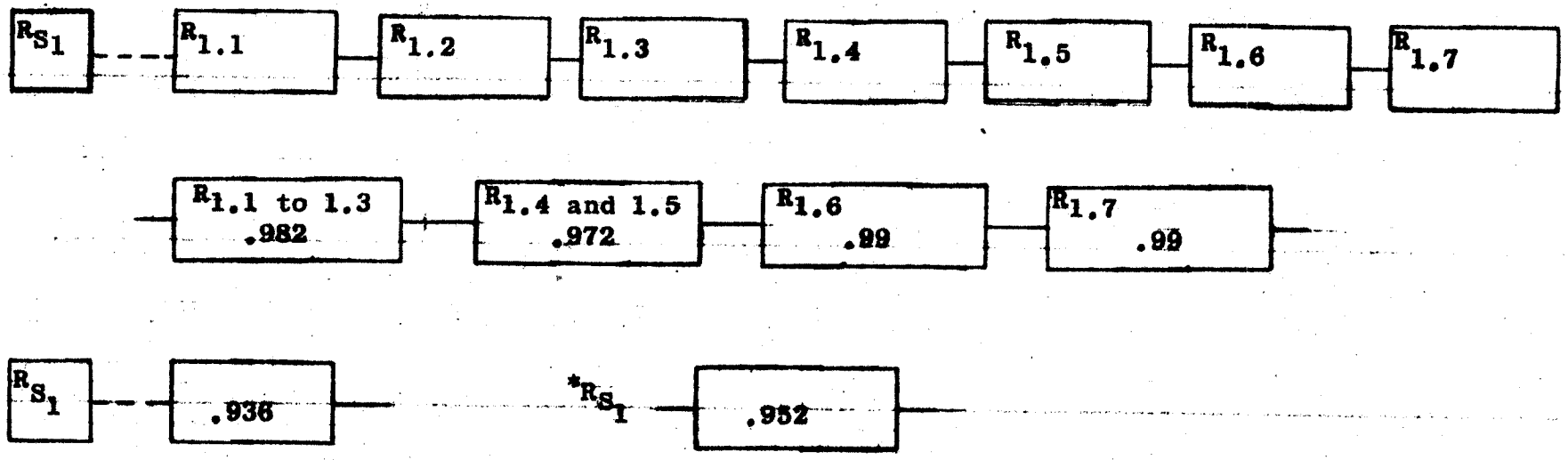

KEY:

$R_{1.1}$ = Reliability Goal of Multivibrator
$R_{1.2}$ = Reliability Goal of Bridge
$R_{1.3}$ = Reliability Goal of Regulator
} Combined

$R_{1.4}$ = Reliability Goal of Multivibrator
$R_{1.5}$ = Reliability Goal of Regulator
} Combined

$R_{1.6}$ = Reliability Goal of Filament (Probability)

$R_{1.7}$ = Reliability Goal of Anode and Associated Power Supply (Probability)

$*R_{S_1}$ - with $R_{1.1}$ to $R_{1.3}$ removed.

FIGURE 1

(Showing this portion as separate subsystem)

LOGIC DIAGRAM TO ANALYZER ELECTRODES

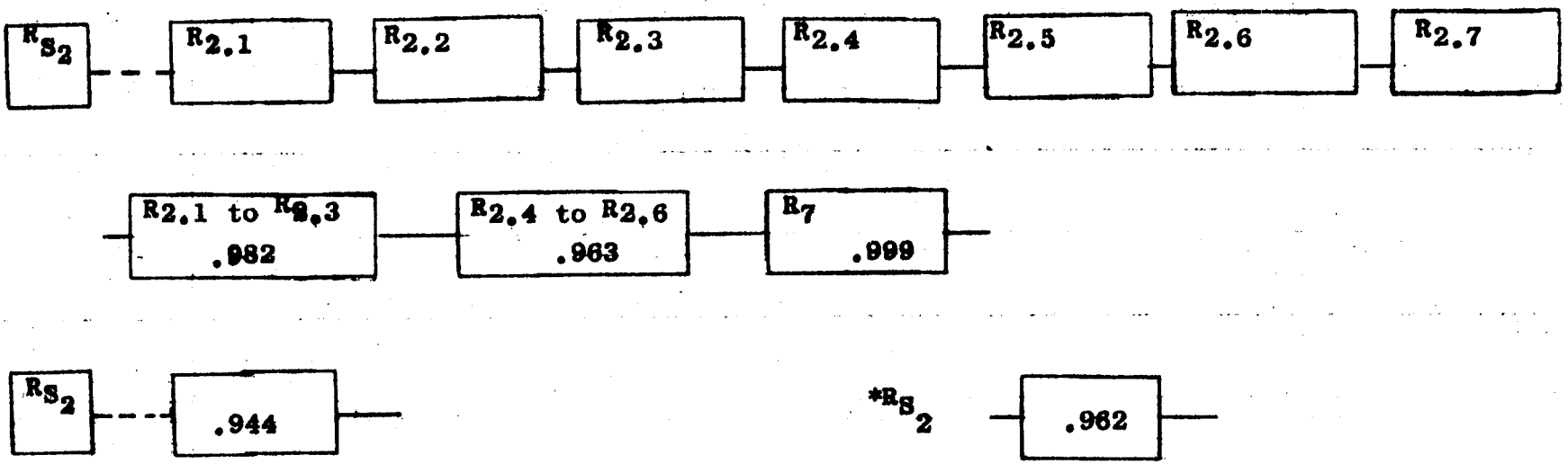

KEY:

$R_{2.1}$ = Reliability Goal of Multivibrator
$R_{2.2}$ = Reliability Goal of Bridge
$R_{2.3}$ = Reliability Goal of Regulator
} Combined

$R_{2.4}$ = Reliability Goal of Multivibrator
$R_{2.5}$ = Reliability Goal of Regulator
$R_{2.6}$ = Reliability Goal of Bridge
} Combined

$R_{2.7}$ = Reliability Goal of Analyzer Electrodes (Probability)

$*R_{S_2}$ - with $R_{2.1}$ to $R_{2.3}$ removed.

FIGURE 2

(Showing this portion as a separate subsystem)

LOGIC DIAGRAM TO DETECTOR

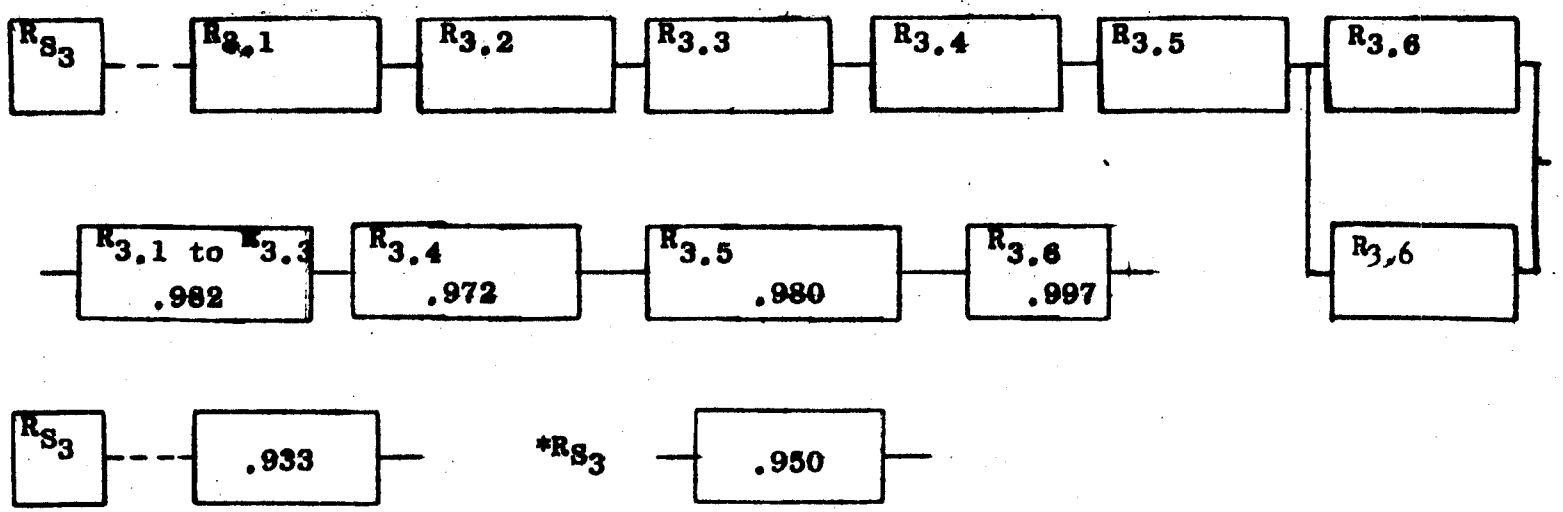

KEY:

$R_{3.1}$ = Reliability Goal of Multivibrator

$R_{3.2}$ = Reliability Goal of Bridge

$R_{3.3}$ = Reliability Goal of Regulator

$R_{3.4}$ = Reliability Goal of Multivibrator

$R_{3.5}$ = Reliability Goal of Bridge and Regulator

$R_{3.6}$ = Reliability Goal of Detector

$*R_{S_3}$ - with $R_{3.1}$ to $R_{3.3}$ removed.

FIGURE 3

(showing this portion as a separate subsystem)

LOGIC DIAGRAM - COMBINED SYSTEM

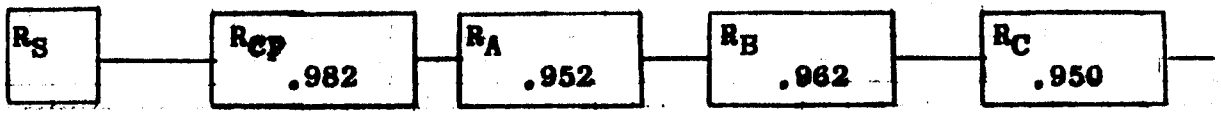

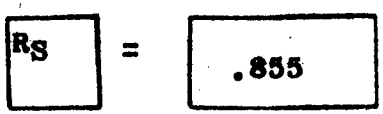

KEY:

R_{CP} = Achievable Reliability Goal of Common Multivibrator, Bridge and Regulator

R_A = Achievable Reliability Goal of Filament Subsystem

R_B = Achievable Reliability Goal of Analyzer Electrode

RC = Achievable Reliability Goal of Detectors

FIGURE 4

APPENDIX F

Quadrupole Stability Requirements

The basis for understanding the operation of the quadrupole mass spectrometer is the stability diagram shown in Figure F-1. The parameters a and q are defined by the equations:

$$a = \frac{8eV_{dc}}{mr_o^2\omega^2} \quad \text{and} \quad q = \frac{4eV_{ac}}{mr_o^2\omega^2} \tag{1}$$

For the second of equation (1) it may be obtained by differentiation:

$$\frac{\Delta q}{q} = \frac{\Delta V_{ac}}{V_{ac}} - \frac{2\Delta f}{f} \tag{2}$$

$$\frac{\Delta m}{m} = \frac{\Delta V_{ac}}{V_{ac}} - \frac{2\Delta f}{f} \tag{3}$$

From (2) and (3):

$$\frac{\Delta m}{m} = \frac{\Delta q}{q} \tag{4}$$

By operating at a resolution of 1/30 and a peak top width to base width ratio of 0.5 then from equation (4) it is found that the allowable variation in q which will keep the operating point on top of the peak is:

$$\Delta q = 1/2 \, \frac{t}{b} \, q_o \, \frac{1}{R} \tag{5}$$

which evaluated becomes:

$$\frac{\Delta q}{q_o} = \pm 0.833\%$$

Then from equation (2) the allowable voltage and frequency variations are:

$$\left| \frac{\Delta V_{ac}}{V_{ac}} \right| + \left| \frac{2\Delta f}{f} \right| = 0.833\% \tag{6}$$

where the voltage and frequency variations are assumed to be uncorrected and hence absolute value signs are used.

If the V_{dc}/V_{ac} ratio varies, then the percentage shown above will also change. In order to investigate the situation more thoroughly, an investigation of the apex region of the stability diagram is necessary.

In the region of the apex of the stability diagram, the boundaries of the stable region can be approximated by the equations:

$$q = q_1 + a/s_1 \qquad q = q_2 - a/s_2 \tag{6}$$

where:

$$s_1 = 0.631 \qquad q_1 = 0.330$$
$$s_2 = 1.1564 \qquad q_2 = 0.911$$

The equation for the locus of operation (called the scan line) is:

$$q = a/s \tag{7}$$

The width of the base of a mass peak is determined by the intersection of the scan line with the boundaries:

$$q_{yb} = \frac{q_1}{1-s/s_1} \qquad q_{xb} = \frac{q_2}{1+s/s_2} \tag{8}$$

Where the peak base width is:

$$\Delta q_b = q_{xb} - q_{yb} \tag{9}$$

then from equations (4), (8), and (9):

$$R = \frac{m}{\Delta m} = \frac{q_o}{\frac{q_2}{1+s/s_2} - \frac{q_1}{1-s/s_1}} \tag{10}$$

By assuming that a mass spectrometer is designed to give a particular resolution R at $S = S_R$ and that the ion source and quadrupole parameters give a mass peak top width to base width ratio $(t/b)_R$, then the width of the top of a mass peak is given by:

$$q_t = q_{xt} - q_{yt} \tag{11}$$

Where:

$$q_{yt} = q_{yb} + q_y \tag{12}$$

$$q_{xt} = q_{xb} - q_x \tag{13}$$

In the region of interest the slope of the scan line changes very slightly and, therefore, it shall be assumed that Δq_x and Δq_y are independent of S. These considerations are shown in Figure F-2. The line which defines the centers of the mass peaks is the line where $\beta_y = 1 - \beta_x$ and in the region of the apex of the stability diagram is given by Brubaker as:

$$q = 0.706 - 0.468(0.237 - a) \tag{14}$$

Then:

$$S_3 = 2.137$$

By use of the law of sines and some other proportionalities it is found that:

$$\frac{\Delta q_x}{\Delta q_y} = \frac{\sin(\alpha_1 - \alpha_o)}{\sin(\alpha_2 + \alpha_o)} \quad \frac{\sin(\pi - \alpha_3 - \alpha_2)}{\sin(\alpha_3 - \alpha_1)} \tag{15}$$

For R = 30, which implies $S_R = 0.3277$, equation (15) gives:

$$\Delta q_x / \Delta q_y = 0.446$$

Then from equation (4) and the definition of the peak top width to base width ratio it is found that:

$$\Delta q_x + \Delta q_y = \frac{q_o}{R} \left[1 - (t/b)_R\right] \tag{16}$$

For R = 30 and $(t/b)_R = 0.5$

$$\Delta q_x = 0.003633 \text{ and } \Delta q_y = 0.008133 \tag{17}$$

By evaluating the expression for Δq_t:

$$\Delta q_t = \frac{0.911}{1 + s/1.1564} - \frac{0.330}{1 - s/0.631} - 0.011767 \tag{18}$$

Equation (17) is evaluated in Figure F-3 along with values for other $(t/b)_R$ ratios. This graph shows the interaction of the stability requirements on V_{ac}, f and V_{dc}/V_{ac} in addition to the change in resolution with V_{dc}/V_{ac}. In order to convert $\%\Delta q$ to $\%\Delta V_{ac}$ and $\%\Delta f$, equation (2) is employed.

An important consideration of quadrupole operation which relates to the stability requirements is the type of mass scan which is employed. It is readily seen from equation (1) that a mass scan may be accomplished either by a voltage or frequency variation. L. Hall has developed an equation relating ion source and quadrupole parameters for the case of 100% transmission. From Project Note #14 of 0569:

$$\frac{V_I \sin^2 \alpha}{V_{ac}} \leq \frac{0.00955(1 - t/b)}{R} \tag{19}$$

In the present case, the quantity V_I and $\sin^2 \alpha$ is a constant ion source parameter. Then, assuming the limiting case:

$$V_{ac} = \frac{kR}{1-t/b} \tag{20}$$

It is apparent that if a frequency scan is used there is no change in the t/b ratio. However, if a voltage scan is employed, the t/b ratio must change, provided that R is held constant, i.e., provided V_{dc}/V_{ac} is held constant.

By considering two voltage points V_{ac1} and V_{ac2} for which there are two corresponding t/b ratios then:

$$\frac{V_{ac1}}{V_{ac2}} = \frac{1-(t/b)_2}{1-(t/b)_1} \tag{21}$$

This function is plotted in Figure F-4. The requirements of the Martian Mass Spectrometer include a mass scan from 12 to 44 which is approximately a 4-1 mass ratio. From equation (1) this can be seen to imply a 4-1 voltage range. Looking at Figure F-4, it is evident that an initial t/b ratio of 0.75 is required if pointed peaks are to be avoided over the mass range. Actually, this is not sufficient. An initial t/b ratio of about 0.85 would be required to give a final t/b of 0.4. It can further be found that to obtain a 0.85 t/b ratio, the initial V_{ac} must be increased by a factor of 3.33, since the present design is for a 0.5 t/b ratio. Since the present V_{ac} level is 250 v, this implies an initial voltage of over 800 v which is definitely prohibitive. It can therefore be concluded that a voltage scan is not feasible.

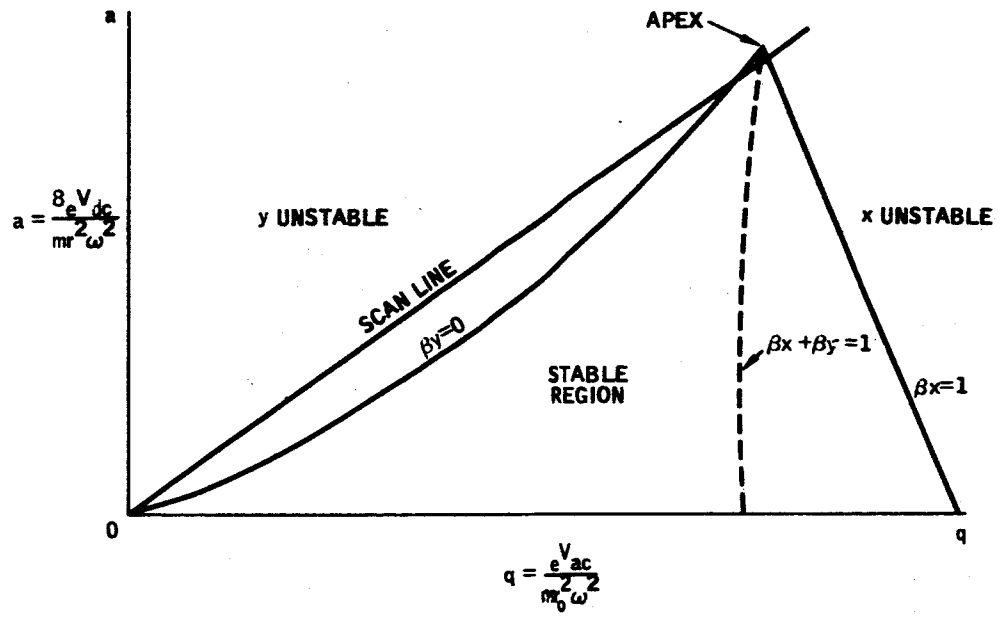

FIGURE F-1
Stability Diagram

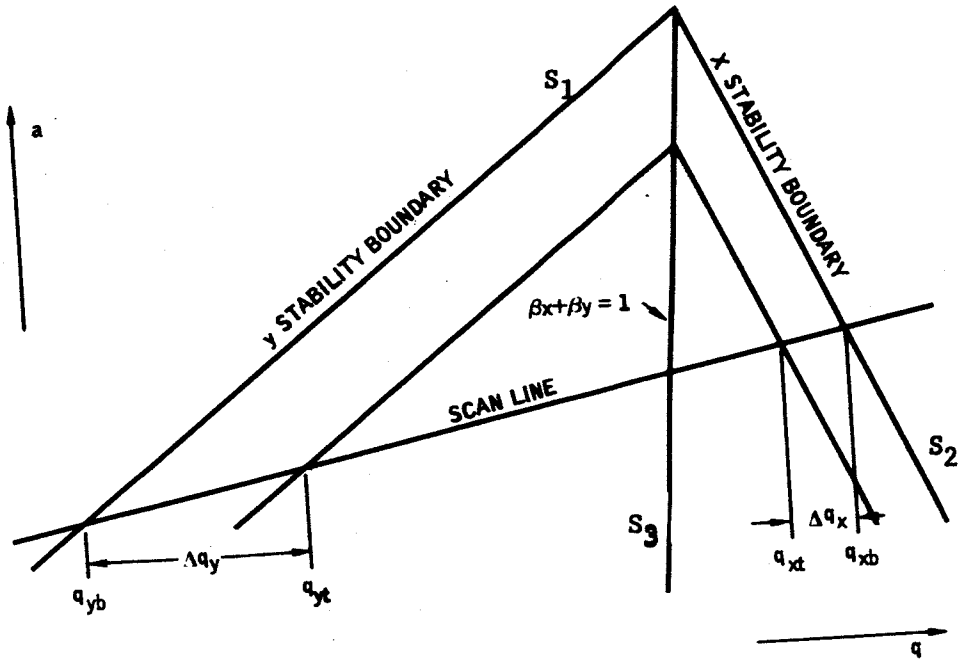

FIGURE F-2
Apex Region of the Stability Diagram

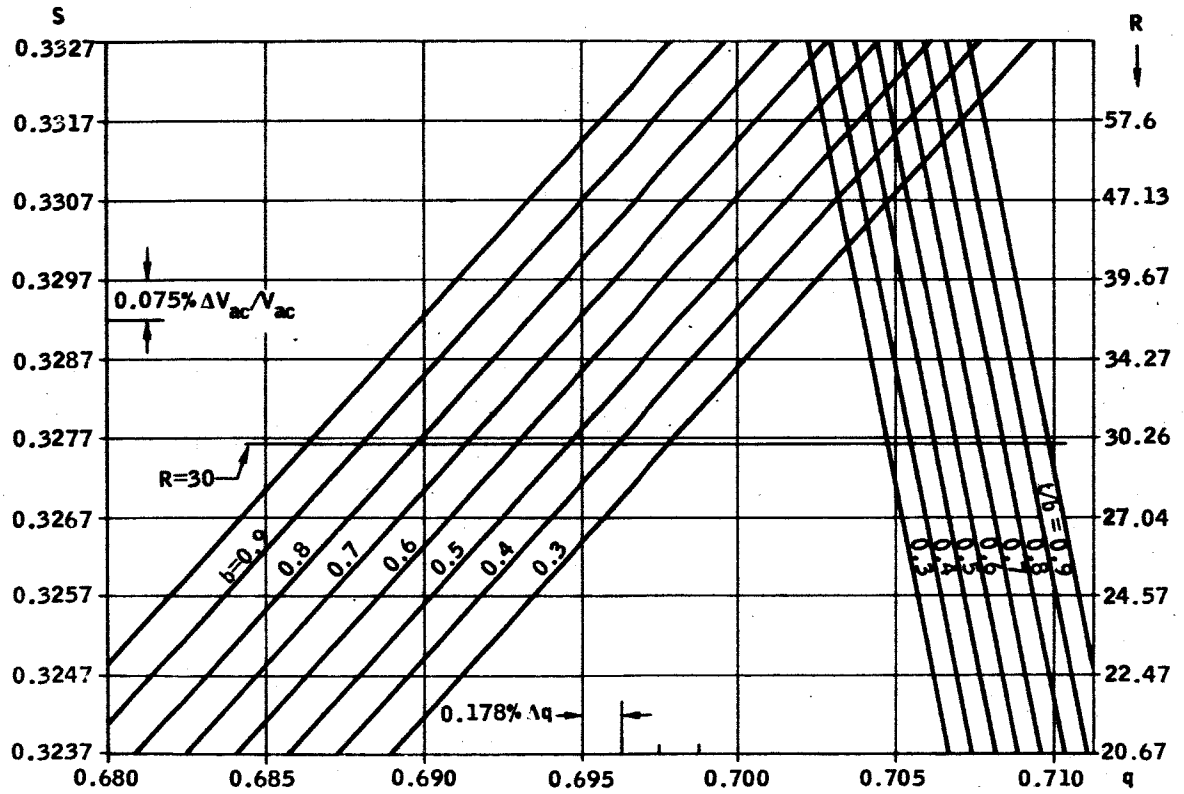

FIGURE F-3
Quadrupole Stability Requirements

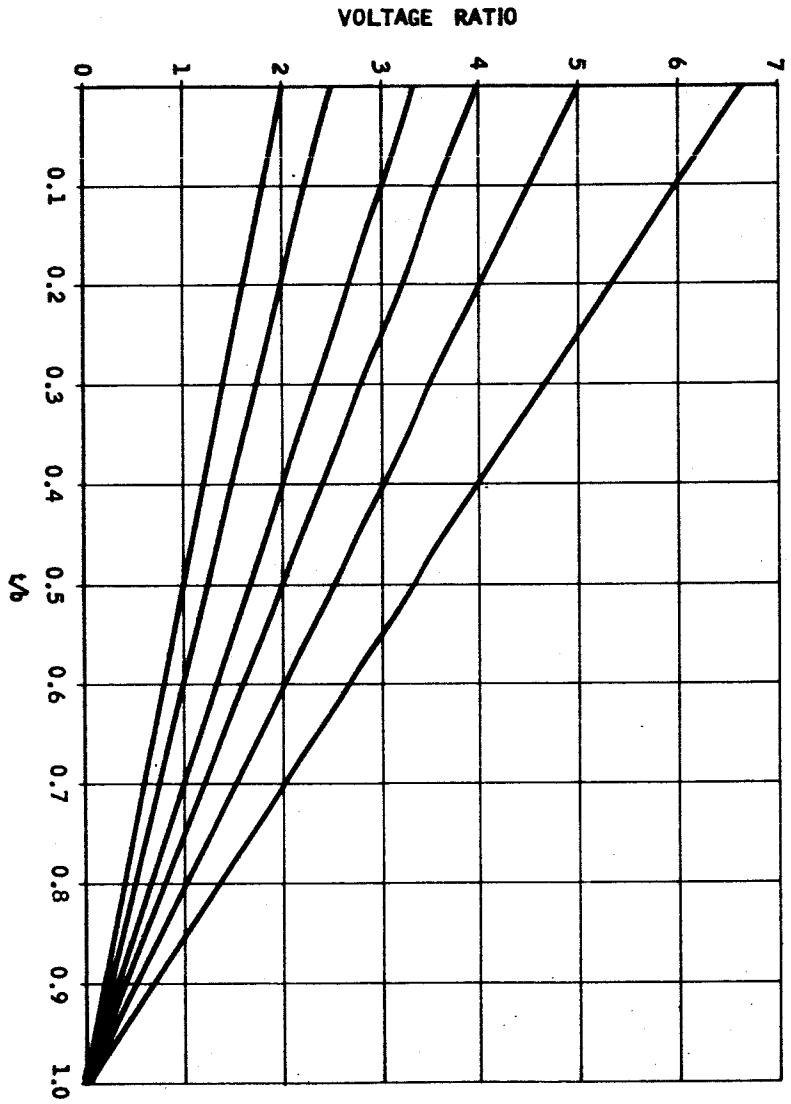

FIGURE F-4
Variation in Peak Top to Base Ratio When Voltage is Scanned

APPENDIX G

Apex Angles For Optic Axis In A Triangular Magnetic Field

The formula of Johnson and Nier, presented in Project Report Number 7, is valid for radii of entry and exit which differs only slightly from the optic axis. Since the path of a charged particle influenced by a magnetic field is determined only by the entry point, entry angle, and exit point, the Johnson and Nier formula need only be modified for the ϕ dependence for a normal heterogeneous beam.

By reference to Part C of Project Note Number 4,

$$R = \Delta \cos 2\theta + \sqrt{\Delta^2 \cos^2 2\theta - 2\Delta\bar{r} + \bar{r}^2}$$

where R is the exit point on the wedge shaped field of apex angle 2θ, and

$$\Delta = \bar{r} - \rho,$$

the difference between the field entry point, $\bar{r}$, and the radius of curvature of the ion, ρ. As can be seen in Figure G-1, ϕ, the apex angle for a magnetic wedge that has the ion entering and exiting normally, may be expressed as

$$\phi = \sin^{-1} \frac{R}{\rho} \sin 2\theta.$$

As an example, assume a field of $2\theta = 60°$, and $\bar{r} = 2.7$ cm. Find the value of for ρ's of 2.03, 2.52, 2.70, and 3.16. The following table shows the results.

ρ	Δ	R	ϕ
2.03	0.67	2.29	77.7°
2.52	0.18	2.62	64.1°
2.70	0	2.70	60.0°
3.16	-0.46	2.91	52.9°

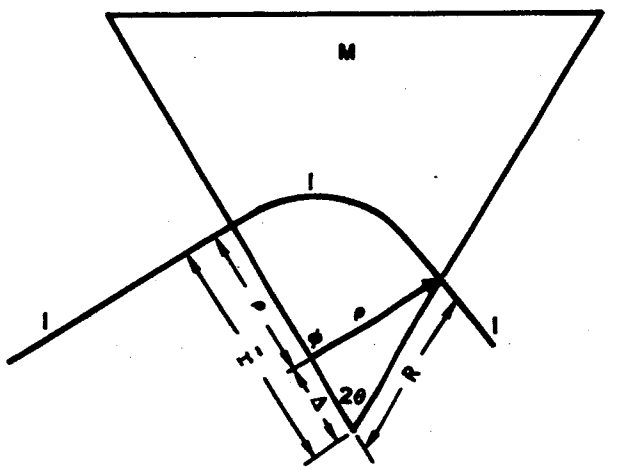

FIGURE G-1

APPENDIX H

Z Axis Focusing By Non-Normal Entry Into a Pole Piece

There are two methods of solving this problem. The first method, which will not be pursued, was the classical derivation of Herzog (Acta Physica Austriaca, V.4, p. 413; 1950). This fringe field is approximated by the leading term of a Taylor Series. The force is calculated as the product Bev. The orthogonal velocity is obtained by integrating the force equation in respect to time, and using the Taylor Series expansion and velocity, v, to change the variable of integration from time ranging from infinity to zero, to differential field (dB) from zero to B. When the expression for the radius of curvature of an ion is substituted into the resulting equation, the angular deviation is obtained. However, Herzog's final result is in terms of a focal length and this technique will be discussed in a future project note.

A more mechanical solution integrates the force equation and uses the solenoidal nature of the field to obtain the result in terms of the beam reflection, half beam height, and obliqueness of beam entry into the uniform magnetic field.

The force acting of an ion is $m\,\bar{a} = e\,(\bar{v} \times \bar{B})$, which is best expressed as,

$$e/m\,(v_y B_z - v_z B_y) = \ddot{x}$$

$$e/m\,(v_x B_z - v_z B_x) = -\ddot{y}$$

$$e/m\,(v_x B_y - v_y B_x) = \ddot{z}$$

It is assumed that $B_x = 0$. The equation of interest is $\ddot{z} = v_x B_y\ e/m$.

By reference to Figure H-1, it can be seen that

$$v_x = \dot{y} \tan \epsilon', \text{ so}$$
$$\dot{z} = \left(\frac{e}{m}\right) \tan \epsilon' \int_{\infty}^{o} B_y dy.$$

To calculate the value of the integral, a closed path, shown in Figure H-1 will be used. Since,

$$\int B ds = 0$$

$$\int_{\infty}^{o} B_y dy + \int_{z}^{o} B_z dz + \int_{o}^{\infty} B_y dy + \int_{o}^{z} B_z dz = 0$$

It is assumed that the field in the neighborhood of the source (or sink) is negligible. Hence B_y at y = a is zero. In the symmetric plane (z = 0), $B_y = 0$. Hence,

$$\int_{\infty}^{o} B_y dy = Bz$$

and

$$\dot{z} = \frac{e}{m} \tan \epsilon' \, Bz.$$

The angle of deflection is,

$$\alpha'_z = \dot{z}/v_o = \frac{eB}{mv_o} \, z \tan \epsilon', \text{ so}$$

$$\alpha'_z = \frac{z \tan \epsilon'}{\rho}$$

A beam entering the field, experiences a change in half beam height of $\alpha'_z c$, where c is the arc length in the beam. The net beam half-height at exit is $z - \alpha_z c$.

The beam deflection angle at the exit is then

$$\alpha''_z = \frac{\left(z - \alpha'_z c \tan \epsilon'\right)}{\rho}$$

The image size in the z direction is

$$\Delta z = \alpha''_z \, l_o$$

where l_o is the image distance.

Application:

For this problem, assume normal entry. In this case $\alpha'_z = 0$, so

$$\alpha''_z = \frac{z \tan \epsilon''}{\rho}$$

where

z = half beam height,

ϵ'' = difference in exit beam angle from optic axis beam,

ρ = radius of curvature,

α''_z = beam convergence.

If it is required that the z component focus to a point,

$$\tan \epsilon''_z = z/l_i.$$

By reference to Project Note Number 10, Table H-1 has been created.

TABLE H-1

ρ(cm)	ℓ(cm)	α''_z	ϵ''
2.03	2.62	10.8°	38°
2.52	7.94	3.6°	17.6°
2.70	9.76	3.0°	15.4°
3.16	53.2	0	3.4°

$z = 0.5$ cm

If the entry angle ϵ', is made 10°, then

$$\alpha'_z = (0.5)\ (0.17)/\rho.$$

Table H-2 gives the value of exit angle for a z focus at the x, y focal point. The value of z' is the beam half-height before exit.

TABLE H-2

ρ	α'_z	c	z'	ϵ''
2.03	0.042	2.76	0.38	38°
2.52	0.034	2.83	0.40	17.6°
2.70	0.31	2.83	0.41	15.4°
3.16	0.27	2.93	0.42	3.4°

The exit angle remains the same because the decrease in z means the beam is closer to the symmetric plane where B_y is less.

Note: The angle ϵ is positive if the ion beam falls on the same side of the normal to the magnet as the center of curvature.

APPENDIX I

Perturbation of the Focal Point Caused By Non-Normal Exit

The principal of this derivation lies in the concept of impulse commonly used in nuclear force scattering problems. The momentum change resulting from this impulse permits one to calculate the scattering coefficient, or the angular change of the projectile.

The force ($F = Bev$), acting for a short period of time (Δt), causes a change in momentum (Δmv).

$$Bev\ \Delta t = m\Delta v$$

The time interval the force acts depends on the size of the force field, a, and the velocity of the projectile, v.

$$\frac{Be\ a}{m} = \Delta v$$

The force field length, a, may be considered to be equal to the maximum deviation, δ, from the optic axis times, the sine of the angle between the normal to the magnetic surface and the exit beam on the optic axis. This angle is ϵ.

$$a = \delta \sin \epsilon$$

The maximum derivation, δ, may be considered as consisting of two factors. The first factor is the spread resulting from a divergent beam incident on the pole force; this has a maximum value of

$$\delta_1 = \alpha l_o$$

where l_o is the distance from pole force to object. The second factor is the beam spread in the field resulting from the energy dispersion. This has a maximum value of

$$S_2 = \rho \Delta V/V$$

where V is the accelerating potential and ρ is the radius of curvature of the ion. Therefore,

$$\Delta v = B(e/M)\ \ (\alpha l_o + \rho \Delta V/V) \sin \epsilon .$$

If the focal point is l_i from the pole face, then the change in the image projection, Δy, is $\Delta v \; l_i \sqrt{\frac{M}{2eV}} = \Delta y$.

If the change in beam angle is of interest, then

$$\gamma = \frac{\Delta y}{l_i} = \Delta v \sqrt{\frac{M}{2\ eV}} \quad .$$

Finding the expression for Δy,

$$\Delta y = (l_i/\rho) \quad (\alpha l_o + \rho \, \Delta V/V) \text{ sine } \epsilon ,$$

where

$$\rho = \sqrt{\frac{2VM}{eB^2}} \quad .$$

It will be observed that, if ϵ is small, this is a second order correction.

Using the information from Project Note Number 10, Table 2, the maximum corrections are listed in Table I-1.

TABLE I-1

Aberration from Non-Normal Exit

ρ (cm)	l_i (cm)	$\epsilon°$	$\Delta y(\epsilon)$
2.03	2.62	-17.7	0.052 cm
2.52	7.94	-4.1	0.032 cm
2.70	9.76	0	0.0
3.16	53.2	7.1	0.35 cm
α = 0.0314 radius			
l_o = 2.7 cm			
$\Delta V/V$ = 0.023			

In all cases, the aberration caused by non-normal exit is less than the Johnson and Nier aberrations.

APPENDIX J

Fringe Field Pre and Post Bending

The fringe field is characterized by changing values of the magnetic field. Actually, two forces contribute to the equations of motion in the fringe field. The first force results from the inhomogeneous magnetic field acting on the magnetic moment of an ion beam (the Stern-Gerlach Experiment). The second force, of primary interest here, is the Lorentz force (e v x H). The result being sought is the net deflection of an ion resulting from its velocity and environmental magnetic field before and after passage through the uniform field. The method of solution is direct. The deflection is calculated at each point in the field and the net deflection is the sum of the individual deflections. In the limit, the technique uses integral calculus.

In a prior report, the z axis deflection was calculated. Here, the interest is in

$$\ddot{x} = e\, B(y)\, \dot{y}/m$$

and

$$\ddot{y} = e\, B(y)\, \dot{x}/m$$

where

$$v_o^2 = \dot{y}^2 + \dot{x}^2 \quad .$$

The assumption, in contradiction to the report on z focusing, is z = 0. Note that B(y) is actually B_z at y. Phenomenologically, the x, y deflection causes z axis defocusing; this effect will not be evident here.

The key to the solution is the creation of a unit vector field coordinate, h(y) so that $B(y) = B_o h(y)$.

The above equations are therefore

$$\dot{x} = \frac{v_o}{\rho} \int h(y)\, dy$$

and

$$\dot{y} = \pm \frac{v_o}{\rho} \left[\rho^2 - \left(\int h(y)\, dy \right)^2 \right]^{1/2}$$

so

$$\frac{dx}{dy} = \frac{\int h(y)\, dy}{\left[\rho^2 - \left(\int h(y)\, dy\right)^2\right]^{1/2}} \quad .$$

The function, h(y), is plotted in Figure J-1. (It is best to experimentally find h(y), but for design purposes, Figure J-1 may be helpful.) For simple construction, let

$$d = \int_0^y h(y)\, dy \quad .$$

In the geometry of a circle

$$p^2 + q^2 = \rho^2 \quad .$$

Since

$$\frac{dp}{dq} = -\frac{q}{\left[\rho^2 - q^2\right]^{1/2}} \quad ,$$

this means an incremental change in the coordinate q, results in an orthogonal change of $(\rho^2 - q^2)^{1/2}$. In the fringe field, a penetration d causes an orthogonal change of $(\rho^2 - d^2)^{1/2}$. It may be concluded that d is the additional increase in the magnet boundary required to compensate for the existence of a fringe field.

The value of the actual magnet boundary may be increased by d to obtain an equivalent boundary. The values of d are plotted in Figure J-2. Also included in Figure J-2 is the displacement of the beam at the magnet face for a radius of curvature of 10 times the gap width. For example, if the source and collector are symmetrically placed 4 cm from a pole piece with a 0.4 cm gap, the effective magnet boundary is 1.2 x 0.4 cm wider than the physical boundary. If the radius of curvature is 4 cm, the displacement (Δx) is 0.3 x 0.4 = 0.12 cm.

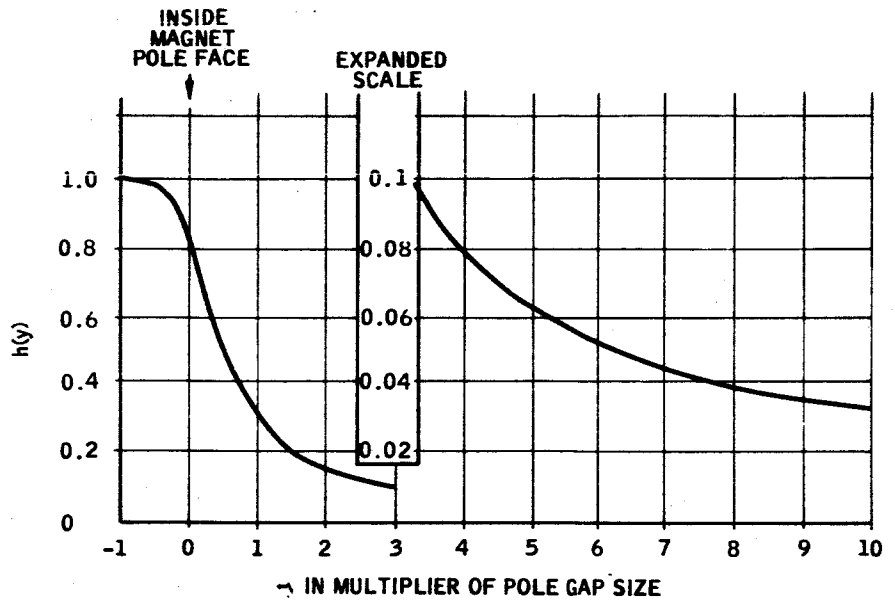

FIGURE J-1

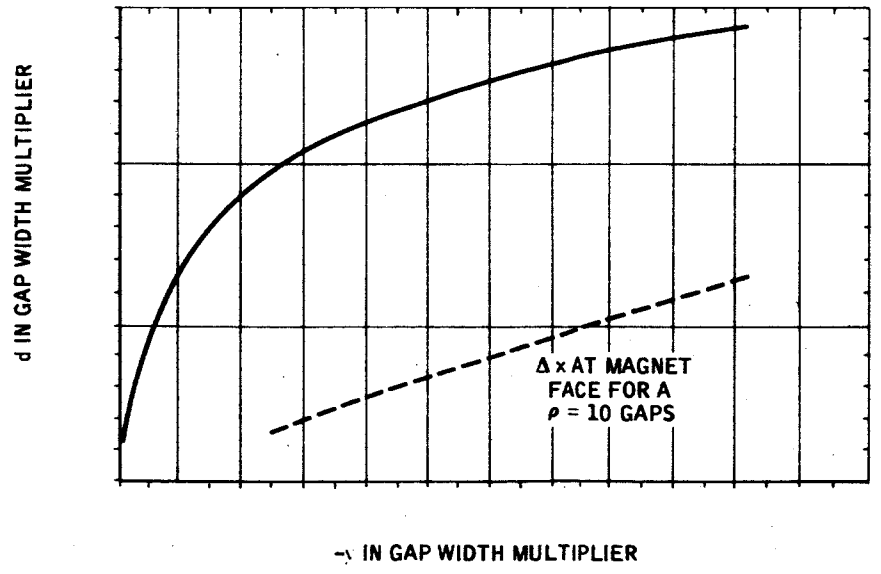

FIGURE J-2

APPENDIX K

Analysis of Tails on Mass Peaks in a Quadrupole Mass Filter

Here an attempt is made to put the subject of tails on a more quantitative basis. In the unstable region to the left of the y stability boundary, the solution of Mathieu's differential equation is given by:*

$$y(z) = Ae^{\mu z}\left\{\rho_o + \sum_{r=1}^{\infty} \rho_{2r} \cos\left(2rz + \phi_{2r}\right)\right\}$$

$$+ Be^{-\mu z}\left\{\rho_o + \sum_{r=1}^{\infty} \rho_{2r} \cos\left(2rz - \phi_{2r}\right)\right\} \qquad (1)$$

y = ion trajectory amplitude

z = $\frac{1}{2}\omega t$

A and B = arbitrary constants

r = integer

m = stability parameter and is a function of a and q

ρ = parameters determined in the solution of the differential equation

As the operation point approaches the stability boundaries, the above expression may be approximated by:

$$y(z) = \left[Ae^{\mu z} + Be^{-\mu z}\right] ce_o\ (z,q) \qquad (2)$$

where $ce_o\ (z,q)$ is a series which has been computed and represents the solution on the stability boundary where $\mu = 0$. In order to get an approximate idea of what is happening, this series can be represented by its first two terms:

$$ce_o(z,q) \approx 1 - \tfrac{1}{2}q \cos 2z$$

The trajectory is then given by

$$y = \left[1 - \tfrac{1}{2}q \cos \omega t\right]\left[Ae^{\frac{1}{2}\mu\omega t} + Be^{-\frac{1}{2}\mu\omega t}\right] \qquad (3)$$

where the substitution for z has been made.

First, two special cases are examined. In the first case, let $y'_o = 0$ and $\omega t_o = 0$. Then it is found that

$$y = y_o \frac{\left[1 - \tfrac{1}{2}q \cos \omega t\right]}{1 - \tfrac{1}{2}q} \cos \tfrac{1}{2}\mu\omega t$$

*. Theory and Application of Mathieu Functions, by M.W. McLacklan, Oxford

where the coefficient A and B have been evaluated in terms of the initial displacement y_o.

In the region of interest $q = 0.7$. Also, this expression is to be evaluated at the time when the ion has reached the end of the rod. Further, it is only the envelope function which is of interest. Under these conditions, the result is:

$$y(L) \text{ envelope} \approx 2y_o \cos\left(\tfrac{1}{2}\mu\omega L\sqrt{\frac{m}{2e\ V_z}}\right) \tag{4}$$

where L is the rod length and V_z is the axial ion energy.

The mass to charge ratio, m/e, may be eliminated from this expression by making use of the relation for q which is:

$$q = \frac{4e\ V_{ac}}{m r_o^2 \omega^2} \tag{5}$$

This expression is given in any reference of quadrupole mass spectrometers.

Then

$$y(L) \text{ envelope} = 2y_o \cos\left(\tfrac{1}{2}\mu\frac{L}{r_o}\sqrt{\frac{2V_{ac}}{q\ V_z}}\right) \tag{6}$$

Next, the stability parameter μ must be eliminated in favor of more meaningful parameters. To do this, an approximate expression is found relating to q on the scan line. This is found to be:

$$q = \frac{q_1 S_1 - \mu^2}{S_1 - S}$$

Where $q_1 = 0.330$, $S_1 = 0.631$ and S = slope of scan line = a/q.

This expression was found from an inspection of the stability diagram referenced earlier and the use of an approximate expression developed in a paper on quadrupole stability requirements found in Appendix F.

Then Δq_t, the width of the tail in terms of q, can be expressed:

$$\Delta q_t = \frac{\mu^2}{S_1 - S_o}$$

where the approximation $S = S_o$ has been made.

$$S_o = a_o/q_o \qquad a_o = 0.237 \qquad q_o = 0.706$$

S_o is the scan line slope when it passes through the apex of the stability diagram.

The fundamental base width of the peak can be expressed

$$\Delta q_b = a/R_o$$

where R_o is the fundamental resolving power. It is then useful to define R_t as the contribution to the resolving power due to the tail width.

In which case $\Delta q_t = q/R_t$. Then

$$\mu = 0.544(q/R_t)^{\frac{1}{2}} \tag{7}$$

Making this substitution gives:

$$y(L) \text{ envelope} = 2y_o \cosh \left(0.384 \frac{L}{r_o}\sqrt{\frac{V_{ac}}{R_t V_z}}\right) \tag{8}$$

This equation must now be related to transmission efficiency. At z = L, an ion will be transmitted if $y < r_o$. Setting y(L) equal to r_o in the above equation and solving for y_o, and substituting into the equation below:

$$\theta = \frac{2 y_o r_e}{\pi r_e^2} = \frac{\text{transmission area}}{\text{total beam area}} = \frac{2 y_o}{\pi r_e} = \text{transmission efficiency}$$

The result is:

$$\theta = \frac{r_o}{r_e} \frac{1}{\left(\cos 0.384 \frac{L}{r_1}\sqrt{\frac{V_{ac}}{R_t V_z}}\right)} \tag{9}$$

This result gives the transmission efficiency for the special case in which all ions enter with zero phase and zero angle (or transverse velocity). If this result is checked with some experimental results, it is found to give numbers which are too large by a factor of 4 to 10. One reason for this is that most of the ions will have some side energy which on the average will tend to increase the y amplitude and therefore decrease the transmission efficiency.

Briefly considering the case in which $y_o = 0$ and y'_o has a non-zero value (for $\omega t_o = 0$) the result is:

$$y(L) \text{ envelope} = \frac{4 y'_o}{\mu\omega} \left(\sinh \tfrac{1}{2}\mu\omega L \sqrt{\frac{m}{2e V_z}}\right) \tag{10}$$

where similar methods have been used as in the derivation of Equation (8).

It can be shown that (1):

$$\frac{\dot{y}_o}{\omega} = \frac{q}{2}\sqrt{\frac{V_I}{V_{ac}}}\, r_o \sin\alpha \qquad (11)$$

where $\sin\alpha$ = half angle of entry of the ion.

Then:

$$y(L) \text{ envelope} = 5.2\, r_o \sin\alpha \frac{R_t V_z}{V_{ac}} \sinh\left(0.384 \frac{L}{r_o}\sqrt{\frac{V_{ac}}{R_t V_z}}\right) \qquad (12)$$

Evaluation of this expression under conditions similar to those which were applied for $\dot{y}_o = 0$ shows that non-zero values for $\dot{y}_o$ are likely to have a considerable effect upon the transmission efficiency and hence upon tail size.

At this point, it must be recalled that all solutions are for zero initial phase angle. Other values of phase angle will give different values for y(L). Carrying out the general solution including non-zero values of y_o, y'_o, and ωt_o and keeping only predominant terms.

$$y(L) \text{ envelope} = 1.35\left[0.5\, y_o + \frac{0.84}{\sin\omega t_o} r_o \sin\alpha\sqrt{\frac{V_I}{V_{ac}}}\right]\exp\left(0.384 \frac{L}{r_o}\sqrt{\frac{V_{ac}}{R_t V_z}}\right) \qquad (13)$$

Several points should be noted about this equation. First, neither of the terms in the coefficient multiplying the exponential are the same as those found separately for $y_o \neq 0$ and $y'_o \neq 0$. This is due to the nature of the approximations which have been made in eliminating the less important ωt_o dependencies. Second, the denominator of the sin α term can go to zero causing that term to go to infinity. Actually, the denominator is $\mu/q + \sin\omega t_o$, but the μ/q term was dropped since it does not appreciably affect the transmission. Third, the cosh and sinh factors which appeared in the earlier expressions have been replaced by the positive exponential. This is allowable since, in the region of interest, the decaying exponential term is negligible.

The next question is to determine the proper distributions over y_o, α, and ωt_o. Clearly the distribution versus ωt_o is uniform from zero to 2π. In view of the limited information concerning the other distributions, it seems only reasonable to assume independent and uniform distributions over y_o and α with y_o ranging from $-r_e$ to $+r_e$ and α ranging from $-\alpha|_{max}$ to $+\alpha|_{max}$. Then these distributions are applied to Equation (21). The transmission efficiency is determined by finding the percentage of ions for which:

$$r_o \leq y(L)_{\text{envelope}} \leq -r_o.$$

APPENDIX L
Typical Series Regulator Power Consumption

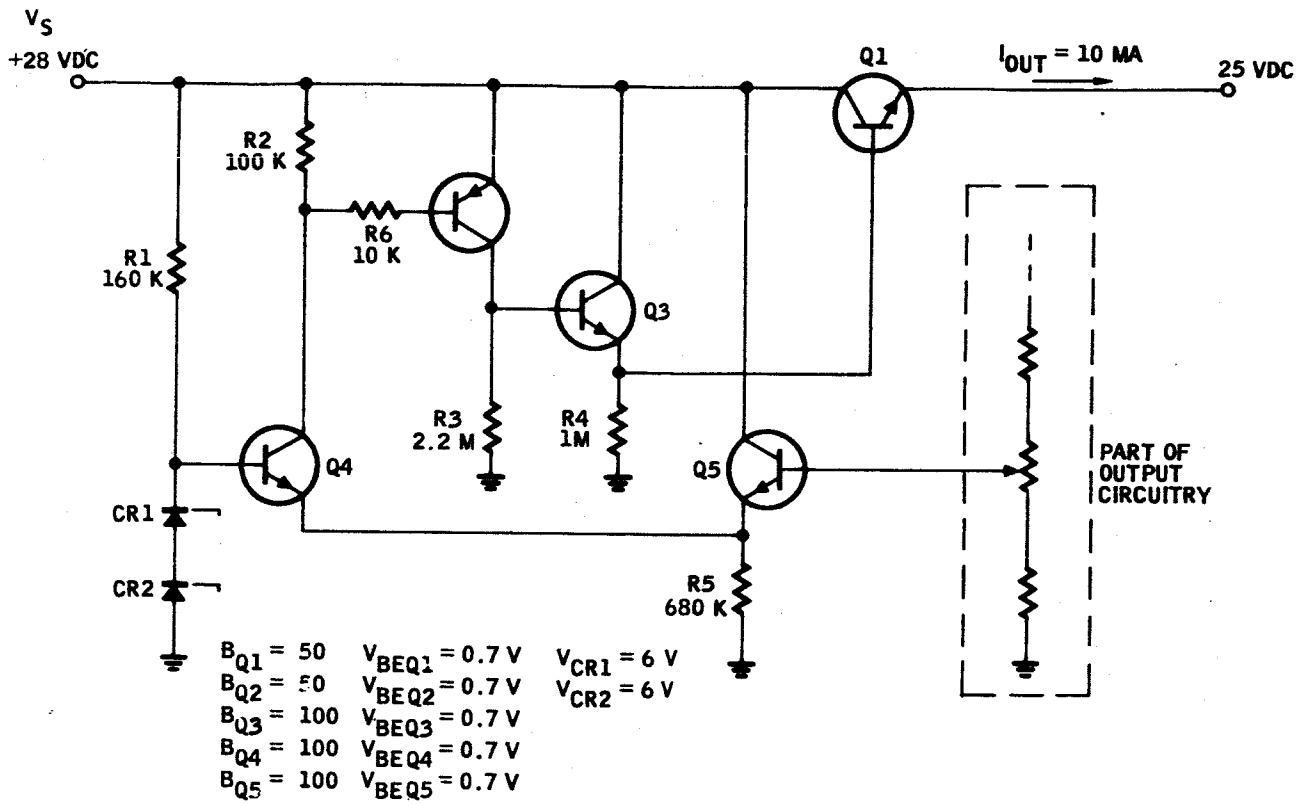

(1) $I_{CQ1} = I_{OUT} = 1 \times 10^{-2}$ AMPERES

(2) $V_{CEQ1} = VS - V_{OUT} = 28 - 25 = 3$ V

(3) $P_{Q1} = V_{CEQ1}\ I_{CQ1} = (3)(1 \times 10^{-2}) = 3 \times 10^{-2}$ WATTS — P_{Q1} = 30 MW

(4) $I_{BQ1} = \frac{I_{CQ1}}{B_{Q1}} = \frac{1 \times 10^{-2}}{50} = 2 \times 10^{-4}$ AMPERES

(5) $V_{EQ3} = V_{OUT} - V_{BEQ1} = 25 - 0.7 = 24.3$ V

(6) $P_{R4} = \frac{(V_{EQ3})^2}{R4} = \frac{(24.3)^2}{1 \times 10^6} = 5.9 \times 10^{-4}$ WATTS — P_{R4} = 0.59 MW

(7) $I_{R4} = \frac{V_{EQ3}}{R4} = \frac{24.3}{1 \times 10^6} = 2.43 \times 10^{-5}$ AMPERES

(8) $I_{CQ3} = I_{BQ1} + I_{R4} = 2 \times 10^{-4} + 2.43 \times 10^{-5} = 2.24 \times 10^{-4}$ AMPS

(9) $V_{CEQ3} = V_S - V_{EQ3} = 28 - 24.3 = 3.7$ V

(10) $P_{Q3} = V_{CEQ3}\ I_{CQ3} = (3.7)(2.24 \times 10^{-4}) = 8.3 \times 10^{-4}$ WATTS — P_{Q3} = 0.83 MW

11-863

(11) $V_{BQ3} = V_{EQ3} - V_{BEQ3} = 24.3 - 0.7 = 23.6$ V

(12) $V_{CQ2} = V_{BQ3} = 23.6$ V

(13) $P_{R3} = \frac{(V_{CQ2})^2}{R3} = \frac{(23.6)^2}{2.2 \times 10^6} = 2.5 \times 10^{-4}$ WATTS — $P_{R3} = 0.25$ MW

(14) $I_{R4} = \frac{V_{CQ2}}{R4} = \frac{23.6}{2.2 \times 10^6} = 1.1 \times 10^{-5}$ AMPERES

(15) $I_{bQ3} = \frac{I_{CQ3}}{BQ3} = \frac{24 \times 10^{-6}}{1 \times 10^2} = 2.4 \times 10^{-7}$ AMPERES

(16) $I_{CQ2} = I_{R4} + I_{bQ3} = 1.1 \times 10^{-5} + 2.4 \times 10^{-7} = 1.12 \times 10^{-5}$ AMPS

(17) $V_{CEQ2} = V_S - V_{CQ2} = 28 - 23.6 = 4.4$ V

(18) $P_{Q2} + I_{CQ2} V_{CEQ2} = (1.12 \times 10^{-5})(4.4) = 5 \times 10^{-5}$ WATTS — $P_{Q2} = 0.05$ MW

(19) $I_{bQ2} = \frac{I_{CQ2}}{BQ2} = \frac{1.12 \times 10^{-5}}{50} = 2 \times 10^{-7}$

(20) $P_{R6} = (I_{BQ2})^2 R6 = (2 \times 10^{-7})^2 1 \times 10^4 = 4 \times 10^{-14}$ W ≈ 0 — $P_{R6} \approx 0$

(21) $V_{R6} = I_{BQ2} R6 = (2 \times 10^{-7})(1 \times 10^4) = 2 \times 10^{-3}$ V ≈ 0

(22) $V_{CQ4} = V_S - V_{BEQ2} - V_{R4} = 28 - 0.7 - 0 = 27.3$ V

(23) $V_{R2} = V_S - V_{CQ4} = 28 - 27.3 = 0.7$ V

(24) $P_{R2} = \frac{(V_{R2})^2}{R2} = \frac{(0.7)^2}{1 \times 10^5} = 4.9 \times 10^{-6}$ WATTS ≈ 0 — $P_{R2} \approx 0$

(25) $I_{R2} = \frac{V_{R2}}{R2} = \frac{0.7}{1 \times 10^5} = 7 \times 10^{-6}$ AMPERES

(26) $I_{CQ4} = I_{R2} + I_{BQ2} = 7 \times 10^{-6} + 2 \times 10^{-7} = 7.2 \times 10^{-6}$ AMPERES

(27) $V_{BQ4} = V_{CR1} + V_{CR2} = 6 + 6 = 12$ V

(28) $V_{CQ4} = V_S - V_{R2} = 28 - 0.7 = 27.3$ V

(29) $V_{EQ4} = V_{BQ4} - V_{BEQ4} = 12 - 0.7 = 11.3$ V

(30) $V_{CEQ4} = V_{CQ4} - V_{EQ4} = 27.3 - 11.3 = 16.0$ V

(31) $P_{Q4} = V_{CEQ4}\, I_{CQ4} = (16)\,(7.2 \times 10^{-6}) = 1.15 \times 10^{-4}$ WATTS

$P_{Q4} = 0.12$ MW

(32) $V_{EQ5} = V_{EQ4} = 11.3$ V

(33) $P_{R5} = \frac{(V_{EQ5})^2}{R5} = \frac{(11.3)^2}{6.8 \times 10^5} = 1.88 \times 10^{-4}$ WATTS

$P_{R5} = 0.19$ MW

(34) $I_{R5} = \frac{V_{EQ5}}{R5} = \frac{11.3}{6.8 \times 10^5} = 1.7 \times 10^{-5}$ AMPERES

(35) $I_{EQ4} \approx I_{CQ4} = 7 \times 10^{-6}$ AMPERES

(36) $I_{CQ5} \approx I_{R5} - I_{EQ4} = 1.7 \times 10^{-5} - 7 \times 10^{-6} = 1.0 \times 10^{-5}$ AMPERES

(37) $V_{CEQ5} = V_S - V_{EQ5} = 28 - 11.3 = 16.7$ V

(38) $P_{Q5} = V_{CEQ5}\, I_{CQ5} = (16.7)\,(1 \times 10^{-5}) = 1.67 \times 10^{-4}$ WATTS

$P_{Q5} = 0.17$ MW

(39) $V_{R1} = V_S - V_{BQ4} = 28 - 12 = 16$ V

(40) $P_{R1} = \frac{(V_{R1})^2}{R1} = \frac{(16)^2}{1.6 \times 10^5} = 1.6 \times 10^{-3}$ WATTS

$P_{R1} = 1.6$ MW

(41) $I_{R1} = \frac{V_{R1}}{R1} = \frac{16}{1.6 \times 10^{-5}} = 1 \times 10^{-4}$

(42) $P_{CR1} = P_{CR2} \approx V_{CR}\, I_{R1} = (6)\,(1 \times 10^{-4}) = 6 \times 10^{-4}$ WATTS

$P_{CR1} = 0.6$ MW

$P_{CR2} = 0.6$ MW

(43) $P_{TOTAL} = P_{Q1} + P_{Q2} + P_{Q3} + P_{Q4} + P_{Q5} + P_{R1} + P_{R2} + P_{R3} + P_{R4} + P_{R5} + P_{R6} + P_{CR1} + P_{CR2}$

$= 30 + 0.05 + 0.83 + 0.12 + 0.17 + 1.6 + 0.0 + 0.25 + 0.59 + 0.19 + 0.0 + 0.6 + 0.6 = 35.00$ MW

$P_{TOTAL} \approx 35$ MW

APPENDIX M

Typical DC to DC Converter Power Consumption

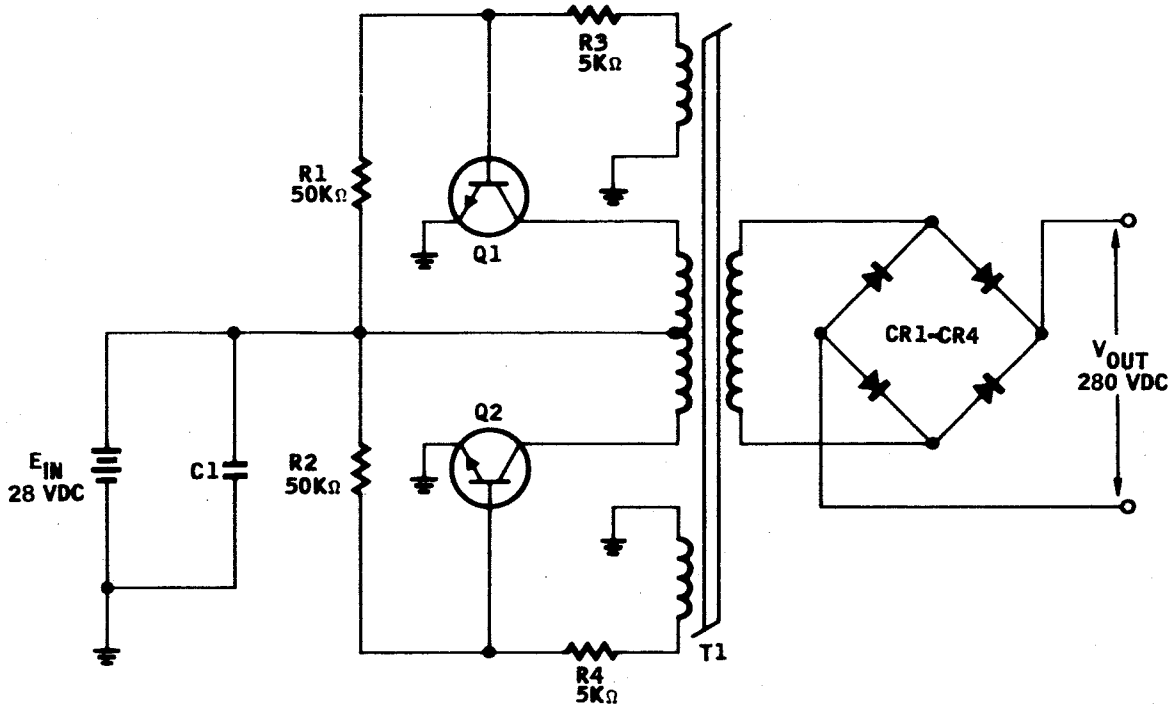

$P_{OUT} = 1 \times 10^{-1}$ WATTS
$\eta_{T1} = 0.80$
$F = 2 \times 10^{3}$ HZ
$T = 0.5 \times 10^{-3}$ SECONDS
$V_{peak} = 56$ V
$T \gg tr$
$T \gg tf$

Q1 = Q2
$SV_{CE} = 0.2$ V
$t_{rise} = 200 \times 10^{-9}$ SECONDS
$t_{fall} = 300 \times 10^{-9}$ SECONDS
$I_{co} = 1 \times 10^{-6}$ AMPERES
$\beta = 10$

CR1 = CR2=CR3=CR4
$SV_{CR} = 0.7$ V

$$P_{T1} = \left(P_{OUT}\right)\left(\frac{1-\eta_{T1}}{\eta_{T1}}\right) = 1 \times 10^{-1}\left(\frac{1-0.8}{0.8}\right) = 2.5 \times 10^{-2} \text{ W}$$

$P_{T1} = 25$ MW

$$I_{peak} = \frac{P_{OUT} + P_{T1}}{E_{IN}} = \frac{1.25 \times 10^{-1}}{28} = 4.5 \times 10^{-3} \text{ AMPERES}$$

USE 5×10^{-3} AMPERES

$$P_{on\ Q1} = P_{on\ Q2} = FI_{peak}\, SV_{CE}\left(\frac{T}{2}\right) \text{for } T \gg t_r$$
$$= \left(2 \times 10^{3}\right)\left(5 \times 10^{-3}\right)\left(0.2\right)\left(2.5 \times 10^{-4}\right)$$
$$= 5 \times 10^{-4} \text{ AMPERES}$$

$P_{on\ Q1} = P_{on\ Q2} = 0.5$ MW

11-1055

$$P_{off_{Q1}} = P_{off_{Q2}} = FI_{co} V_{peak} \left(\frac{T}{2}\right) \text{ for } T \gg t_f$$
$$= (2 \times 10^3)(1 \times 10^{-6})(56)(2.5 \times 10^{-4})$$
$$= 2.8 \times 10^{-5} \text{ USE } 3.00 \times 10^{-5} \text{ WATTS}$$

$P_{off_{Q1}} = P_{off_{Q2}} = 0.03$ MV

$$P_{SWQ1} = P_{SWQ2} = \frac{F\, I_{peak} (V_{peak} + 25V_{CE})(t_f + t_r)}{6}$$
$$= \frac{(2 \times 10^3)(5 \times 10^{-3})(56 + 0.4)(5 \times 10^{-7})}{6}$$
$$= 4.70 \times 10^{-5} \text{ WATTS}$$

$P_{SW}Q1 = P_{SW}Q2 = 0.05$ MW

$$P_{TQ1} = P_{TQ2} = P_{on} + P_{off} + P_{SW}$$
$$= 0.5 \text{ MW} + 0.03 \text{ MW} + 0.05 \text{ MW}$$

$P_{TQ1} = P_{TQ2} = 0.6$ MW

$$P_{R1} = P_{R2} = \frac{(E_{IN})^2}{R} = \frac{(28)^2}{5 \times 10^4} = \frac{784}{5 \times 10^4} = 15.7 \times 10^{-3} \text{ WATTS}$$

$P_{R1} = P_{R2} = 16$ MW

$$I_b = \frac{I_{peak}}{\beta} = \frac{5 \times 10^{-3}}{10} = 5 \times 10^{-4} \text{ AMPERES}$$

$$P_{R3} = P_{R4} = I_b{}^2 R = (5 \times 10^{-4})^2\ 5 \times 10^3 = 1.25 \times 10^{-3} \text{ WATTS}$$

$P_{R3} = P_{R4} = 1.25$ MW

$$I_{OUT} = \frac{P_{OUT}}{E_{OUT}} = \frac{1 \times 10^{-1}}{2.8 \times 10^2} = 3.57 \times 10^{-4} \text{ AMPERES}$$

$$P_{CR1} = P_{CR2} + P_{CR3} + P_{CR4} = SV_{CR}\, I_{OUT}\, F \left(\frac{T}{2}\right)$$
$$= (0.7)(3.56 \times 10^{-4})(2 \times 10^3)$$
$$(2.5 \times 10^{-4}) = 1.25 \times 10^{-4} \text{ WATTS}$$

$P_{CR1} = P_{CR2} = P_{CR3} = P_{CR4} =$ 0.125 MW

$$P_{TOTAL} = P_{TQ1} + P_{TQ2} + P_{R1} + P_{R2} + P_{R3} + P_{R4} + P_{T1} + P_{CR1} + P_{CR2} + P_{CR3} + P_{CR4} = 0.6 + 0.6 + 16 + 16 + 1.25 + 1.25 + 25 + 0.125 + 0.125 + 0.125 + 0.125$$

$P_{TOTAL} = 61.2$ MW

APPENDIX N

Derivation of Radial Probability Distribution

The initial ion velocities arise from the thermal energies of the molecules before they are ionized. It can be shown that the change in energy due to the electron interaction and resulting ionization process is small. Therefore the initial energies can be represented by Maxwell-Boltzman statistics.

In order to find the percentage of ions with radial velocity components less than or equal to

$$\frac{2}{m}\left(\frac{3kT}{e}\right) \tag{1}$$

To do this one must begin by finding the density distribution dn/dv_r, i.e., the distribution of radial velocities over the total ion population. This distribution is not readily available and therefore it must be developed from one that is. We choose the Maxwell-Boltzman distribution for dn/dv_x which is given in Sproull [1].

$$\frac{dn}{dv_x} = N\left(\frac{m}{2\pi kT}\right)^{\frac{1}{2}} \exp\left(\frac{-mv_x^2}{2kT}\right) \tag{2}$$

where

dn = ions with x directed velocity in the range v_x to $v_x + dv_x$

N = total ions under consideration (dn and N can be expressed as ion densities)

m = molecular mass

K = Boltzman's constant

T = temperature

Let us convert this to a probability density distribution by normalization with respect to N and simplify the notation:

$$p_x(v_x) = K \exp\left\{-\left(v_x/v_o\right)^2\right\} \tag{3}$$

---

[1] Modern Physics, Robert L. Sproull, Wiley (1956), Page 33

The probability distribution for $p_y(v_y)$ is identical. Making use of the relationship

$$v_r^2 = v_x^2 + v_y^2 \tag{4}$$

and the fact that $p_x(v_x)$ and $p_y(v_y)$ are statistically independent probability distributions, then the probability that v_r is less than some value V_r can be found by integrating the product of the independent distributions over the appropriate velocity space. The expression is:

$$P(v_r < V_r) = 2 \int_{-v_r}^{+v_r} \int_{o}^{+\sqrt{V_r^2 - v_x^2}} p_x(v_x)\, p_y(v_y)\, dv_x dv_y \tag{5}$$

Instead of directly evaluating this expression let us convert it from a probability function for $v_r < V_r$ to a probability density distribution for v_r, i.e., $p_r(v_r)$. This is done by use of the following expression:*

$$p_r(v_r) = \frac{dP}{dV_r} \quad (v_r < V_r) \tag{6}$$

and

$$\frac{d}{dt} \int_k^{g(t)} f(x)dx = f(g)\, \frac{dg}{dt} \tag{7}$$

the result is:

$$p_r(v_r) = 2 \int_{-v_r}^{+v_r} p_x(v_x)\, p_y\left\{\sqrt{v_r^2 - v_x^2}\right\} \frac{v_r\, dv_x}{\sqrt{v_r^2 - v_x^2}} \tag{8}$$

Substituting Equation (3) and a similar expression for p_y into Equation (8) gives:

$$p_r(v_r) = 4\, K^2\, v_r \exp -(v_r/v_o)^2 \int_o^{v_r} \frac{dv_x}{\sqrt{v_r^2 - v_x^2}} \tag{9}$$

* Probability relationships can be found in any standard text book. For example: "Random Signals and Noise", by W. Davenport and W. Root. McGraw Hill (1958)

From 320.01 in Dwight (Third Edition) the result of this integration is:

$$p_r(v_r) = 2K^2 \pi v_r \exp^{-(v_r/v_o)^2} \tag{10}$$

Substitution for K and v_o gives:

$$p_r(v_r) = \frac{m}{kT} v_r \exp\left(\frac{-mv_r^2}{2kT}\right) \tag{11}$$

For the problem at hand it is necessary to integrate the probability density over v_r from zero to V_r:

$$P(v_r < V_r) = \int_o^{V_r} p_r(v_r)\, dv_r \tag{12}$$

Using the substitution $u = mv_r^2/2kT$, then

$$P(u < U) = \int_o^U \exp^{-u} du \tag{13}$$

$$= 1 - \exp^{-U} \tag{14}$$

For the case of interest U = 3 [See expression (1)].